

INFORMATION TO USERS

This manuscript has been reproduced from the microfilm master. UMI films the text directly from the original or copy submitted. Thus, some thesis and dissertation copies are in typewriter face, while others may be from any type of computer printer.

The quality of this reproduction is dependent upon the quality of the copy submitted. Broken or indistinct print, colored or poor quality illustrations and photographs, print bleedthrough, substandard margins, and improper alignment can adversely affect reproduction.

In the unlikely event that the author did not send UMI a complete manuscript and there are missing pages, these will be noted. Also, if unauthorized copyright material had to be removed, a note will indicate the deletion.

Oversize materials (e.g., maps, drawings, charts) are reproduced by sectioning the original, beginning at the upper left-hand corner and continuing from left to right in equal sections with small overlaps.

Photographs included in the original manuscript have been reproduced xerographically in this copy. Higher quality 6" x 9" black and white photographic prints are available for any photographs or illustrations appearing in this copy for an additional charge. Contact UMI directly to order.

**ProQuest Information and Learning
300 North Zeeb Road, Ann Arbor, MI 48106-1346 USA
800-521-0600**

UMI[®]

**REACTION DYNAMICS AND CHEMICAL SPECIATION OF
PHOSPHORUS AND ARSENIC (III AND V) AT THE METAL OXIDE-
WATER INTERFACE AND IN SOILS**

by

Yuji Arai

A dissertation submitted to the Faculty of the University of Delaware in
partial fulfillment of the requirements for the degree of Doctor of Philosophy in Plant
and Soil Sciences

Spring 2002

© 2002 Yuji Arai
All Rights Reserved

UMI Number: 3046603

UMI[®]

UMI Microform 3046603

**Copyright 2002 by ProQuest Information and Learning Company.
All rights reserved. This microform edition is protected against
unauthorized copying under Title 17, United States Code.**

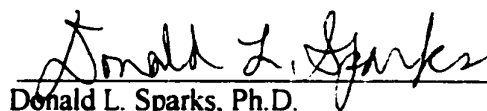
**ProQuest Information and Learning Company
300 North Zeeb Road
P.O. Box 1346
Ann Arbor, MI 48106-1346**

**REACTION DYNAMICS AND CHEMICAL SPECIATION OF
PHOSPHORUS AND ARSENIC(III AND V) AT THE METAL OXIDE-
WATER INTERFACE AND IN SOILS**

by

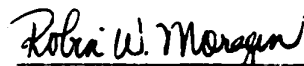
Yuji Arai

Approved:



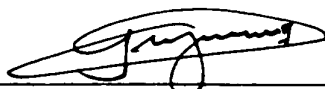
Donald L. Sparks, Ph.D.
Chair of the Department of Plant and Soil Sciences

Approved:



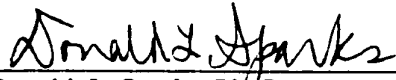
Robin Morgan, Ph.D.
Acting Dean of the College of Agriculture and Natural Resources

Approved:



Conrado M. Gempesaw II, Ph.D.
Vice Provost for Academic Programs and Planning

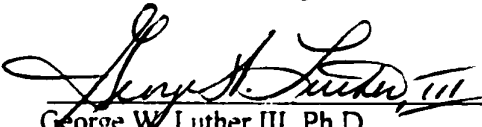
I certify that I have read this dissertation and that in my opinion it meets the academic and professional standard required by the University as a dissertation for the degree of Doctor of Philosophy.

Signed: 
Donald, L. Sparks, Ph.D.
Professor in charge of dissertation

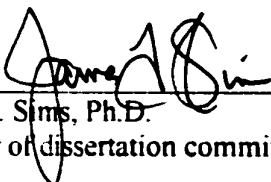
I certify that I have read this dissertation and that in my opinion it meets the academic and professional standard required by the University as a dissertation for the degree of Doctor of Philosophy.

Signed: 
Robert G. Ford, Ph.D.
Member of dissertation committee

I certify that I have read this dissertation and that in my opinion it meets the academic and professional standard required by the University as a dissertation for the degree of Doctor of Philosophy.

Signed: 
George W. Luther III, Ph.D.
Member of dissertation committee

I certify that I have read this dissertation and that in my opinion it meets the academic and professional standard required by the University as a dissertation for the degree of Doctor of Philosophy.

Signed: 
James T. Sims, Ph.D.
Member of dissertation committee

ACKNOWLEDGEMENTS

Achieving my doctoral degree at the University of Delaware has been challenging and an exciting experience. I am grateful to have received wonderful support and encouragement from my research committee members, family, friends, and collaborators. I would like to thank: my advisor Dr. Donald L. Sparks for accepting me into his prestigious graduate program and for his continuous support and guidance during my life in Delaware. Dr. J.T. Sims for teaching me the importance of applied research, Dr. George Luther for teaching me the fundamental aspects of inorganic chemistry and their importance, Dr. Robert Ford for helping to train me as a researcher in geo/soil chemistry, and members of 1997-2002 University of Delaware environmental soil chemistry group including K. Staats and Jerry Hendricks for their support. I would also like to thank research scientists/collaborators from the National Synchrotron Light Source and Advanced Photon Source for helping with X-ray Fluorescence and X-ray absorption spectroscopic measurements. These include Wolfgang Caliebe and Lisa Miller at beamline X-19A, Kumi Pandya and Larry Ferrari at beamline X-11A, Tony Lanzarotti and Bill Rao at beamline X-26A (National Synchrotron Light Source), and Steve Sutton and Matt Newville at the Sector-13 (Advanced Photon Source). I would

like to acknowledge the support of James A. Dyer (DuPont Engineering Technology), Tom A. Ei (DuPont Corporate Remediation Group), Ronald B. Wesley (URS Corporation), and David C. Shelton (DuPont Legal) for assisting in my arsenic contaminated soil research, Rich B. Maynard (DuPont central research and development) for BET surface area analyses on soil minerals, Steve Dentel for allowing me to use the zeta meter, Brian McCandless for helping with XRD analyses, Ken Livi from Johns Hopkins University for assistance with electron microprobe analyses, University of Delaware soil testing laboratory staff for assistance with the ICP and physicochemical soil analyses, and departmental secretaries for providing me with a cheerful/comfortable work environment to pursue my graduate work.

Finally, I would like to acknowledge the United States Geological Survey (USGS), and College of Agriculture and Natural Resources for granting me a research assistantship, and the DuPont Co. and USGS for financially supporting my research.

TABLE OF CONTENTS

LIST OF TABLES	xi
LIST OF FIGURES	xii
ABSTRACT	xvii

Chapter

1 INTRODUCTION	1
1.1 Introduction	1
1.2 Phosphorus in the Environments	3
1.3 Arsenic in the Environments	5
1.4 Phosphorus Chemistry	8
1.5 Arsenic Chemistry	9
1.6 Phosphorus (P) and Arsenic (As) Adsorption on Soils and Soil Components	10
1.6.1 Adsorption Theory	10
1.6.2 Phosphorus and Arsenic Adsorption on Soils (Empirical and Modeling Approaches)	13
1.6.3 Phosphorus and Arsenic Retention as Effected by Physicochemical Properties of Soils	15
1.6.4 pH Effects on P and As Adsorption on Variable Charged Minerals	18
1.6.5 Phosphate and Arsenate Adsorption on Metal Oxides	19
1.6.6 Phosphate and Arsenate Adsorption on Phyllosilicate Minerals	20
1.6.7 Arsenite Adsorption on Soil Components	21
1.6.8 Temperature Effects on P and As adsorption on Soils and Soil Components	21
1.6.9 Ionic Strength Effects on P and As Adsorption Rates	24
1.6.10 Ionic Strength Effects on P and Adsorption Surface Complexation	26
1.7 Phosphorus and Arsenic Surface Complexation on Soil Components	27

1.7.1 Empirical Approaches	28
1.7.2 Electrophoretic Mobility Measurement Studies.....	29
1.7.3 <i>Ex situ</i> Spectroscopic Studies.....	30
1.7.4 <i>In Situ</i> Spectroscopic Studies	32
1.8 Phosphorus and Arsenic Desorption from Soils and Soil Components....	34
1.8.1 Desorption Theory.....	34
1.8.2 Phosphate Desorption and Kinetic Models	37
1.9 Redox Effects on Phosphorus Retention/Release on Soils and Soil Components	39
1.10 Redox Effects on Arsenic Retention/Release on Soils and Soil Components	40
1.11 Residence Time Effects on P and As Adsorption/Desorption from Soils and Soil Components	42
1.11.1 Residence Time Effect Theory	42
1.11.2 Solid-State or Inter- and Intra Particle Diffusion	46
1.11.3 Surface Precipitation.....	50
1.11.4 High Energy Binding Through Chemical Reconfiguration.....	55
1.12 Research Justification	56
1.13 Objectives of Research	58
1.14 References.....	60
2 ATR-FTIR SPECTROSCOPIC INVESTIGATION OF PHOSPHATE ADSORPTION MECHANISMS AT THE FERRIHYDRITE-WATER INTERFACE	97
2.1 Abstract	97
2.2 Introduction.....	98
2.3 Materials	101
2.4 Method	101
2.4.1 Ionic Strength Effects on P Adsorption Envelopes.....	101

2.4.2	Electrophoretic Mobility Measurements	102
2.4.3	Sample Preparation for the ATR-FTIR Analysis	103
2.4.4	ATR-FTIR Analyses	104
2.5	Results and Discussion	105
2.5.1	Ionic Strength Effects on P Adsorption Envelopes	105
2.5.2	Electrophoretic Mobility Measurements	108
2.5.3	ATR-FTIR Analyses	111
2.5.3.1	Theoretical IR vibrations of Phosphoric Acid.....	111
2.5.3.2	pH Effect on P Adsorption Complexes at pH 4-9	117
2.5.3.3	Loading Level Effects on P Adsorption Complexes at pH \geq 7.5	120
2.5.3.4	Loading Level Effects on P Adsorption Complexes at pH $<$ 7.5	126
2.6	Conclusion	134
2.7	References	136
3	X-RAY ABSORPTION SPECTROSCOPIC INVESTIGATION ON ARSENITE AND ARSENATE ADSORPTION MECHANISMS AT THE ALUMINUM OXIDE-WATER INTERFACE.....	146
3.1	Abstract	146
3.2	Introduction	147
3.3	Materials and Reagents	150
3.3	Methods.....	151
3.4.1	Adsorption Envelopes	151
3.4.2	Electrophoretic Mobility Measurements	152
3.4.3	Synchrotron XAS Data.....	153
3.5	Results and Discussion	156
3.5.1	Adsorption Envelopes	156
3.5.2	Electrophoretic Mobility Measurements	160
3.5.3	Arsenic XANES Analyses	162
3.5.4	Arsenic K-edge EXAFS Analyses	168
3.6	Conclusion	175

	3.7 References	176
4	RESIDENCE TIME EFFECTS ON PHOSPHATE SURFACE SPECIATION AT FERRIHYDRITE-WATER INTERFACE	182
	4.1 Abstract	182
	4.2 Introduction	183
	4.3 Materials	186
	4.4 Methods	187
	4.4.1 Batch Adsorption Experiments	187
	4.4.2 Phosphate Desorption Experiments	188
	4.4.3 ATR-FTIR Analyses	189
	4.4.4 Theoretical IR Vibrations of Phosphoric Acid	190
	4.4.5 Phosphorus K-edge XANES Analyses	192
	4.5 Results and Discussion	194
	4.5.1 Phosphate Adsorption Envelope Kinetics	194
	4.5.2 Residence Time Effects on Phosphate Desorption	197
	4.5.3 ATR-FTIR Analyses	203
	4.5.4 Phosphorus K-edge XANES Analysis	208
	4.6 Conclusion	217
	4.7 References	219
5	RESIDENCE TIME EFFECTS ON ARSENATE SURFACE SPECIATION AT ALUMINUM OXIDE-WATER INTERFACE	232
	5.1 Abstract	232
	5.2 Introduction	233
	5.3 Materials	236
	5.4 Methods	236
	5.4.1 Batch Adsorption Experiments	236
	5.4.2 Batch Desorption Experiments	237
	5.4.3 Arsenic K edge EXAFS Analyses	238
	5.5 Results and Discussion	240
	5.5.1 Arsenate Adsorption Kinetics	240

	5.5.2 Arsenate Desorption.....	243
	5.5.3 Arsenic K edge EXAFS Analyses.....	248
	5.6 Conclusion	260
	5.7 References.....	262
6	MULTI-SCALE SPECTROSCOPIC INVESTIGATION ON ARSENIC SOLID STATE SPECIATION IN INDUSTRIALLY CONTAMINATED SOILS	274
	6.1 Abstract	274
	6.2 Introduction	275
	6.3 Materials and Site History.....	278
	6.4 Methods.....	280
	6.4.1 Bulk-X-ray Diffraction Analyses	280
	6.4.2 <i>In situ</i> Microfocused SXRF Analyses	280
	6.4.3 <i>In situ</i> Microfocused XANES Analyses.....	282
	6.4.4 <i>In situ</i> bulk-EXAFS Analyses	283
	6.5 Results and Discussion	284
	6.5.1 Bulk XRD Analyses	284
	6.5.2 Bulk XANES Analyses	286
	6.5.3 <i>In situ</i> μ -SXRF Analyses.....	289
	6.5.4 <i>In Situ</i> Microfocused-XANES Analyses.....	290
	6.5.5 <i>In Situ</i> Bulk-EXAFS Analyses	299
	6.5 Conclusion	310
	6.6 References.....	313
7	SUMMARY AND CONCLUSIONS	319

LIST OF TABLES

Table 2.1	Position of IR peak maxima of phosphoric acid, and adsorption complexes on iron oxides.....	115
Table 2.2	Position of IR peak maxima of ferric phosphate solution complexes	116
Table 3.1	Structural parameters from EXAFS analysis for As(III and V)/ γ -Al ₂ O ₃ , adsorption and As(III and V) solution samples.....	173
Table 4.1	Position of IR peak maxima of phosphoric acid and P adsorption complexes at the ferrihydrite-water interface	193
Table 4.2	Phosphate desorption experimental conditions and total desorbed P after 24 h of desorption.....	198
Table 5.1	As(V) desorption experimental conditions and As(V) remaining after 25 days of desorption.....	247
Table 5.2	Structural parameters from EXAFS and XRD analysis for aged reacted aluminum oxide and aluminum arsenate reference compounds.....	252
Table 6.1	Structural parameters for dussertite and conichalcite derived from the best-fit results of EXAFS experimental data	302
Table 6.2	Structural parameters for sample A and B derived from the best-fit results of EXAFS experimental data.....	305
Table 6.3	Reported structural parameters for As adsorption complexes on aluminum and iron oxides and orpiment from the best-fit results of EXAFS experimental data	306

LIST OF FIGURES

Figure 2.1	Ionic strength effects on P adsorption envelopes at the ferrihydrite-water interface	106
Figure 2.2	Electrophoretic mobility measurements on ferrihydrite with/without 25 and 50 μmol sodium P solution.....	110
Figure 2.3	ATR-FTIR spectra of phosphoric acid at different pHs.....	114
Figure 2.4	ATR-FTIR spectra: pH effects (4-9) on the P adsorption complexes ($\Gamma = 0.38 \mu\text{mol m}^{-2}$) at the ferrihydrite-water interface.....	119
Figure 2.5	ATR-FTIR spectra: loading level effect ($\Gamma = 0.38\text{-}2.69 \mu\text{mol m}^{-2}$) on the P adsorption complexes at pH 7.5 at the ferrihydrite-water interface.....	121
Figure 2.6	ATR-FTIR spectra of P adsorption complexes at pH/pD 7.5 at the ferrihydrite-water interface	123
Figure 2.7	ATR-FTIR spectra: loading level effect ($\Gamma = 0.38\text{-}2.42 \mu\text{mol m}^{-2}$) on the P adsorption complexes at pH 4 at the ferrihydrite-water interface	125
Figure 2.8	ATR-FTIR spectra of P adsorption complexes at pH/pD 4 at the ferrihydrite-water interface	129
Figure 2.9	ATR-FTIR spectrum of monodentate mononuclear Fe-P (aq) complex. The spectra show raw data and deconvoluted peaks in solid line and the fitted profiles in dotted line	130
Figure 2.10	Possible molecular configurations (C_{2v} or lower) of protonated P inner-sphere complexes at the ferrihydrite-water interface. a) monoprotonated bidentate mononuclear(C_1), b) diprotonated bidentate mononuclear(C_{2v}), c) monoprotonated monodentate mononuclear(C_{2v}), d) diprotonated monodentate mononuclear (C_{2v}), e) nonprotonated monodentate mononuclear	

	hydrogen-bonded with the hydroxyl group of the FH(C ₁), f) monoprotated monodentate mononuclear hydrogen-bonded with the hydroxyl group of the FH(C ₁), and g) diprotated monodentate mononuclear hydrogen-bonded with the hydroxyl group of the FH(C ₁).....	131
Figure 3.1	Ionic strength effects on As(III and V)/ γ -Al ₂ O ₃ adsorption envelopes.....	157
Figure 3.2	Electrophoretic mobility measurements on γ -Al ₂ O ₃ with and without 0.1mM As(III or V). All systems contained 0.1 M NaNO ₃	159
Figure 3.3	XANES spectra of the As(III)- γ -Al ₂ O ₃ and sodium As(III) solution samples.....	163
Figure 3.4	XANES spectra of the As(V)- γ -Al ₂ O ₃ and sodium As(V) solution samples.....	164
Figure 3.5	Results of linear combination (LC) of XANES profile fit for As(III)/ γ -Al ₂ O ₃ adsorption sample (pH 8, I = 0.01). The solid line is the experimental data and the open circles represent the LC fit.....	167
Figure 3.6	k ³ weighted normalized χ -functions for As(III)(aq) and As(III)/ γ -Al ₂ O ₃ adsorption samples	169
Figure 3.7	k ³ weighted normalized χ -functions for As(V)(aq) and As(V)/ γ -Al ₂ O ₃ adsorption samples	170
Figure 3.8	Fourier transforms (RSF) of the χ -functions of As(III)/ γ -Al ₂ O ₃ adsorption samples. The solid lines are the experimental data and the dotted lines represent the theoretical multishell fit to the data	171
Figure 3.9	Fourier transforms (RSF) of the χ -functions of As(V) / γ -Al ₂ O ₃ adsorption samples. The solid lines are the experimental data and the dotted lines represent the theoretical multishell fit to the data.....	172
Figure 4.1	Phosphate adsorption kinetics at the ferrihydrite-water interface as a function of pH.....	195

Figure 4.2	Residence time effects on P desorption from ferrihydrite at pH 4.0.....	199
Figure 4.3	Residence time effects on P desorption from ferrihydrite at pH 7.5.....	200
Figure 4.4a	ATR-FTIR spectra of P adsorbed ferrihydrite at pH 4 as a function of residence time. The raw spectra are shown with solid lines, the deconvoluted peaks with dotted lines, and the fitted curve with open circles.....	204
Figure 4.4b	ATR-FTIR spectra of P adsorbed ferrihydrite at pH 7.5 as a function of residence time. The raw spectra shown with solid lines and the deconvoluted peaks with dotted lines, and the fitted curve with open circles.....	205
Figure 4.5	Phosphorus adsorption reaction steps at the ferrihydrite-water interface at $\text{pH}_{\text{bulk}} \leq \text{PZSE}$, Step I = Formation of outer-sphere complex, Step II = Formation of monodentate mononuclear complex, Step III = Formation of monodentate mononuclear complex hydrogen Bonded with the hydroxyl group of the FH, Step IV = Formation of Bidentate binuclear complex, and Step V = Formation of bidentate mononuclear complex.....	207
Figure 4.6a	P K-edge XANES spectra of synthetic amorphous strengite, crystalline strengite, barbosalite and rockbrigitte.....	210
Figure 4.6b	P K-edge XANES spectra of P reacted ferrihydrite at pH 4.0 as a function of residence time.....	211
Figure 4.6c	P K-edge XANES spectra of P reacted ferrihydrite at pH 7.5 as a function of residence time.....	212
Figure 4.7	First derivative of P XANES spectra in Figs. 4.6a-c.....	216
Figure 5.1	Arsenate adsorption kinetics at the aluminum oxide-water interface at pH 4.5 and 7.8.....	242
Figure 5.2	Residence time effects on As(V) desorption from aged As(V) reacted aluminum oxide at pH 4.5.....	245
Figure 5.3	Residence time effects on As(V) desorption from aged As(V) reacted aluminum oxide at pH 7.8.....	246

Figure 5.4a	k^3 -weighted normalized χ functions for aged As(V) reacted aluminum oxide and reference Al-As(V) compounds.....	250
Figure 5.4b	Fourier transforms of the χ functions (uncorrected for phase shift) for aged As(V) reacted aluminum oxide and reference Al-As(V) compounds. The solid lines are the experimental data and the opened circles represent the theoretical fit to the data.....	251
Figure 5.5a	Magnified XANES spectra of aged As(V) sorption samples and mansfieldite.....	256
Figure 5.5b	Results of linear combination (LC) of XANES profile fit for a 11 m aged sample at pH 4.5 and a 1 yr aged sample at pH 7.8. The solid lines are the experimental spectra and the open circles represent the LC fit in which 3d at pH 4.5 or pH 7.8 and mansfieldite spectra were used as components.....	257
Figure 6.1	X-ray diffraction patterns of sample A and B. Peak labels: A = albite, B = barite, C = calcite, G = gypsum, H = hematite, and Q = quartz	285
Figure 6.2a	Bulk XANES spectra of sample A and B.....	287
Figure 6.2b	First derivative of the bulk XANES spectra shown in Fig 6.1a.....	288
Figure 6.3a	Microfocused SXRF elemental map images of sample A.....	291
Figure 6.3b	Microfocused SXRF elemental map images of sample B.....	292
Figure 6.4	Microfocused (18 μm resolution) XANES spectra at region 1-6 of sample A and B shown in Figs. 6.3a and 6.3b.....	293
Figure 6.5	Microfocused (100 μm resolution) XANES spectra of sample A and B shown in Figs. 6.3a and 6.3b.....	293
Figure 6.6	Bulk XANES spectra of reference minerals and As adsorption complexes	297
Figure 6.7	First derivative of the XANES spectra shown in Figs. 6.5 and 6.6....	298
Figure 6.8a	Non-linear least-square fits to normalized k^3 -weighted EXAFS spectra of the reference compounds and the sample A and B. Raw data and fits are shown in solid lines and open circles, respectively. See Tables 6.1 and 6.2 for fit parameters.....	300

Figure 6.8b Non-linear least-square fits to Fourier transforms (FT) of the reference compounds and the sample A and B. Raw data and fits are shown in solid lines and open circles, respectively. See Tables 6.1 and 6.2 for fit parameters301

ABSTRACT

Understanding the molecular scale reaction mechanisms and speciation of oxyanions at the soil mineral-water interface provides significant insights and predictions on their fate and transport and bioavailability in soil-water environments. In this research, phosphate, arsenite, and arsenate adsorption and desorption mechanisms on ferrihydrite and bayerite surfaces were investigated as a function of reaction time, pH, and ionic strength. An array of techniques were employed including equilibrium and kinetic studies, electrophoretic mobility (EM) measurements, attenuated total reflectance Fourier transform infrared spectroscopy (ATR-FTIR), X-ray absorption near edge structure spectroscopy (XANES) and extended X-ray absorption fine structure spectroscopy (EXAFS). To expand on the knowledge gained from the reaction dynamics and the surface speciation in the model component systems, arsenic solid-state speciation and reactivity were further investigated in real-world materials (i.e., industrially contaminated landfill materials). Traditional chemical extraction/digestion, novel microfocused *in situ* X-ray fluorescence (XRF) and X-ray absorption spectroscopies, and electron microprobe spectroscopy were employed to understand the complex chemical speciation in the natural materials.

Phosphate adsorption on ferrihydrite was dependent on pH and independent of ionic strength. The rate of adsorption increased with decreasing pH, and the adsorption kinetics were initially rapid followed by slow P uptake after 24 h at pH 4-9.5. Inner-sphere adsorption complexes (nonprotonated bidentate binuclear species ($\equiv\text{Fe}_2\text{PO}_4$) at $\text{pH} \geq 7.5$ and protonated inner-sphere complexes at pH 4-6 at loading levels between 0.38 and $2.69 \mu\text{mol m}^{-2}$) were observed using the ATR-FTIR and EM measurements. Reversibility of adsorbed P decreased with increasing aging times (2d-1 yr) at pH 4 and 7.5, and the C_{2v} and/or C_1 molecular symmetry of the inner-sphere complexes remained the same regardless of aging time (3 d-1 yr) and pH (4 and 7.5). An enhancement in the P K-edge XANES pre-edge feature (i.e., a signature for the inner-sphere Fe(III) octahedral and P tetrahedral linkage) with aging indicated an increase in P-O-Fe linkages. Rearrangement of surface complexes resulted in higher energy bindings was suggested as a cause of increased irreversibility.

In the As(III and V)-bayerite study, As(III and V) adsorption was pH dependent and changes in ionic strength influenced As(III) adsorption, but not As(V) adsorption. Results from the EM measurements indirectly suggested the formation of outer-sphere complexes for As(III) and inner-sphere complexes for As(V). However, the EXAFS analyses indicated the presence of As(III) and As(V) inner-sphere bidentate binuclear complexes. Additional XANES analyses showed that the formation of As(III) outer-sphere and inner-sphere complexes were pH and ionic strength dependent. Biphase As(V) adsorption kinetics were observed at pH 4.5 and 7.8. The longer the residence time (3 d-1 yr), the greater the irreversibility of sorbed

As(V) at both pHs. EXAFS analyses showed the formation of bidentate binuclear bonding environments in all of the aged samples (3 d to 1yr) at pH 4.5 and 7.8. Interestingly, XANES features suggested some changes in the local chemical structure of the adsorbed As(V) with aging. Surface transformations such as: 1) a rearrangement of surface complexes, and/or 2) a conversion of surface complexes into aluminum arsenate-like precipitates might be important chemical factors responsible for the decrease in As(V) reversibility with aging.

Arsenic solid-state speciation in landfill materials from oxidized and reduced sites was also investigated using novel *in situ* microfocused XRF and XANES (μ -XRF and μ -XANES, respectively), bulk-XAS, and XRD techniques. Simultaneous μ -XANES and μ -XRF measurements revealed that As(V) was highly associated with Ba, Ca, and Fe in the stagnant sample, and that As(III) was not strongly distributed with these elements. Similarly, the oxidized sample also contained both As (III and V) oxidation states, and the As(V) valence state was predominant at the region where Fe concentration was elevated. Bulk EXAFS analyses of the reduced sample suggested the formation of As(V) bidentate binuclear/bidentate mononuclear adsorption complexes most probably on amorphous iron oxyhydroxides, and amorphous orpiment (AsS) like minerals. In addition, the presence AsO₄ substituted barite (BaSO₄) and gypsum (CaSO₄) and or adsorption complexes on these minerals were also suggested as possible species, evidenced by the As(V)-Ba/Ca shell fit (4.26 and 3.68 Å, respectively). However, the oxidized sample contains the predominant

As(V) bidentate binuclear surface species most probably adsorbed on amorphous iron oxyhydroxides.

Chapter 1

INTRODUCTION

1.1 Introduction

Oxyanions are ubiquitous in soil/water environments. Important plant nutrients (i.e., phosphate, nitrate and molybdate), naturally abundant carbonate species, and potentially toxic metals/metalloids (i.e., arsenite, arsenate, borate, chromate, selenite and selenate) are commonly found oxyanions due to natural geological settings and anthropogenic inputs. Oxyanions in the soil/water environment greatly affect natural biogeochemical cycling and ecological and human health. Over the past few decades, excessive levels of nutrients and toxic metals/metalloids in surface and ground water have become a serious environmental issue in the U.S.

The phosphorus (P) fertility status of the Atlantic Coastal Plain soils has been greatly affected by intensive animal based agriculture. Decades of animal waste and inorganic fertilizer amendments to the soils have resulted in excessive accumulations of P. Seasonal P release via surface runoff, soil erosion, and subsurface transport has

been linked to eutrophication and outbreaks of *pfiesteria* (fish killing toxic zoospore) in aquatic environments.

Environmental health has also been jeopardized by arsenic (As) contamination of soil/water environments because of its carcinogenic, phytotoxic and biotoxic characteristics. Long-term anthropogenic inputs (e.g., inorganic and organic arsenical pesticides and defoliants) to agricultural fields have increased total As levels up to about 165 ppm (the average arsenic concentration in uncontaminated soils is 5 ppm) in 12 states. High As concentrations (>50 ppb) have already been detected in ground waters in the Western United States due to hydrogeochemical activities. Interest in As has been recently heightened by the controversy over setting the maximum concentration level of As in drinking water, which was recently set at 10 ppb (USEPA, 2001).

The fate and transport of nutrients and metalloids must be well understood to propose the best strategies for effectively reducing the negative impact of nutrients and contaminants such as P and As in aquatic/terrestrial environments. It is a challenge to understand the fate and transport of contaminants in natural systems because of complex solid-state species and various abiotic and biotic factors (e.g., redox, ionic strength, temperature, and microbial communities) that greatly affect the bioavailability, mobility, and toxicity of contaminants in surface and subsurface environments. Accurate prediction of the environmental fate would require better understanding in the oxyanion solid-state speciation and the reactivity (i.e.,

adsorption/desorption reactions) as a function of environmental conditions (e.g. pH and reaction time) in soils and soil components.

Many soil chemical studies have been conducted using short-term equilibration approaches (ca. 24 h) to understand the interaction of oxyanions at mineral-water interfaces. Using equilibrium expressions to predict the fate and transport of pollutants in a natural system is tenuous, since soils and sediments are nearly always at disequilibrium with respect to ion transformations. Therefore, it is fundamental to study not only the equilibrium processes but also the kinetics (rate and mechanism) of soil chemical reactions as a function of reaction conditions such as pH and ionic strength. Long-term studies are especially important, because contaminant availability can be reduced, or increased in the environment with increasing residence time. These macroscopic studies can be effectively combined with state-of-the-art *in situ* spectroscopic techniques (e.g., Attenuated Total Reflectance-Fourier Transform Infrared Spectroscopy and X-ray Absorption Spectroscopy) to gain better insights for comprehending the overall molecular scale chemical processes (i.e., changes in surface speciation and reactivity) at the soil mineral-water interface.

1.2 Phosphorus in the Environment

Phosphorus is an indispensable element for all living protoplasmic organisms because of its genetic role in ribonucleic acid and as an essential nutrient, along with N, for growth. More than 90% of the total P in the soil-plant-animal system is in soils and less than 10% is in the remaining biological systems (Ozanne, 1980). The P

content is approximately 1200 ppm in the lithosphere and 200 to 5000 ppm (an average of 600ppm) in soils (Lindsay, 1979). In the hydrosphere, typical concentrations of total P in domestic wastewater, agricultural drainage, and lake surface waters are 3-15 ppm, 0.05-1ppm, and 0.01-0.04 ppm, respectively (Snoeyink and Jenkins, 1980).

In the last few decades, excess P has been recognized as a nonpoint-source pollutant throughout the world due to long-term anthropogenic inputs (i.e. synthetic and animal based fertilizer, and waster water)(Ryden et al., 1973; Vaithyanathan and Correll, 1992). In 1996 the USEPA reported that more than 50% of fresh water eutrophication is attributed to agricultural nutrients such as P and N.

In the Southern Delaware inland watershed, which consists of sandy soils, gentle slopes, and shallow water tables, soils contain an excessive amount of P (Andres, 1991; Sims and Ritter, 1993). About 75 % of agricultural soils contain high levels of P as a result of more than three decades of poultry manure application. High soil P is agronomically defined as either 1) >25ppm P by the Bray and Kurtz extraction (0.025M HCl + 0.03 M NH₄F) or 2) >28ppm P by the Mehlich 3 extraction (0.2M CH₃COOH, 0.2M NH₄Cl, 0.015M NH₄F and 0.012M HCl) (Tisdale et al., 1993). One of the original reasons to apply poultry manure was to meet the N requirement for crops and to mitigate nitrate leaching and ground water contamination. However, P accumulation was escalated due to the high N/P uptake ratio (8/1-3/1) of crops (Edwards and Daniel, 1992; Sharpley and Robinson, 1996) and the strong retention of P on soils. Annually applied poultry manure has increased

both total and bioavailable P in surface and subsurface soil horizons (Cooked et al., 1958; Kuo and Baker, 1982; Sharpley et al., 1984). In addition, seasonal P release through surface runoff, erosion, and channeling processes has caused serious problems in surrounding aquatic environments.

In the fresh water environment, seasonal total P concentrations in Southern Delaware ditch water samples fluctuate between 0.04 to 1.14 mg L⁻¹, and these values are above eutrophication inducible levels (as low as 0.02 – 0.035 mg L⁻¹) (Brookes et al., 1997; Sims et al., 1996). Eutrophication causes problems in recreational, industrial and drinking water supplies due to over-growth of algae and cyanobacteria and their decomposition, leading to a dissolved oxygen shortage (Kotak et al., 1993; Sharpley and Rekolainen, 1997). Consumption of such water, containing cyanobacteria, can be a serious health hazard to livestock and humans due to its neuro- and hepato-toxic effects (Lawton and Codd, 1991).

The nutrient (inorganic phosphorus) rich surface runoff in the Delaware and Chesapeake Bays has been linked to the growth of the toxic microorganism, *Pfiesteria* (Burkholder and Glasgow Jr., 1997). This microscopic organism produces a toxin, killing various lower food chain marine organisms (fish and crustaceans). The toxin is also harmful to humans because it is known to cause symptoms such as nausea, migraine headaches, skin sores, acute loss of learning and memory problems in laboratory rats (Levin et al., 1997)

1.3 Arsenic in the Environments

Arsenic(As) in soil/water environments can threaten both human and ecological health. because of its carcinogenicity, phytotoxicity and biotoxicity (DaCosta, 1972; Sheppard, 1991). Arsenite (As(III)) is more toxic than arsenate (As(V)) due to its preferential reaction with sulfhydryl groups in mammalian enzymes (Faust and Aly, 1981). Labile As(III) as arsenious oxide (As_2O_3) is absorbed through the lungs and intestines, and biochemically acts to coagulate proteins, form complexes with coenzymes, and inhibit the production of the essential enzyme adenosine triphosphate(ATP) in metabolic processes (Manahan, 1994).

The average total As content in uncontaminated soils is approximately 5 ppm (Colburn et al., 1975; Voigt and Brantley, 1996). On the other hand, volcanic soils may contain up to 20ppm total As (Faust and Aly, 1981). Due to the application of arsenic containing pesticides and defoliants, the As content of contaminated soils ranges from 5 to 2.553 ppm (Walsh and Keeny, 1975). The average As level in agricultural soils in 12 states was approximately 165ppm (Woolson et al., 1971).

In aquatic environments, typical concentrations of total As in domestic water, sea water, precipitation and river water are 0.01 to 1 ppm, 3ppm, 1ppb, and 1.7ppb respectively (Onishi, 1969; People, 1975; Westcot et al., 1993; Whitacre and Pearse, 1974). High As concentrations (>50ppb) already have been detected in ground water in the Western United States (Gao et al., 1997). The current standard maximum concentration level (MCL) of total As in drinking water is 50ppb. In the future, however, the expected new standard could be 2 ppb. This raises a serious concern regarding protection of human and ecological health (Whitacre and Pearse, 1974).

Sources of As in soil/water environments are due to: 1) indigenous sources (volcanic eruptions and weathering) and 2) anthropogenic inputs (mining, industrial processes, and pesticide application). Naturally occurring As is found in about 245 mineral species including alloys, arsenides, sulfides, sulfosalts, and oxidation products such as oxides, arsenites, and arsenates. These are generally associated with basin-filled deposits of alluvial-lacustrine origin, and volcanic deposits. (Gao et al., 1997; Subcommittee on Arsenic, 1977). Naturally occurring As-S minerals are arsenopyrite (FeAsS), enargite (Cu_3AsS_4), orpiment (As_2S_3), and realgar (AsS). In the terrestrial environment, inorganic forms are generally predominant over organic forms. The speciation of the inorganic forms (arsenite and arsenate) is highly affected by pH and redox conditions. Most of the organic fractions are associated with methyl groups ($-\text{CH}_3$) such as methanearsonic acid (MAA) and dimethylarsinic acid (DMAA) (Braman, 1983). Approximately 40% of DMAA and 15% of MAA have been speciated in agricultural evaporation ponds (Tanji and Dalgren, 1993). Eventually organic As species are converted into either CO_2 and inorganic As by oxidative degradation or volatile As compounds or arsine (AsH_3) by reduction and further methylation. Due to the low solubility of the volatile compounds, they complex with atmospheric particulates and are deposited on the ground (Gao et al., 1997).

The anthropogenic sources are 1) industrial processes such as smelting of As containing ores and by-products of fossil fuel combustion (e.g., flycoal ash), and 2) agricultural uses including insecticides, herbicides, fungicides, algacides, sheepdips,

wood preservatives, deworming agents for livestock, and vaccination for poultry and swine (Adriano, 1986). The total inputs are classified into a) inorganic (i.e., calcium arsenate, sodium arsenate, and lead arsenate) and b) organic arsenicals (i.e., mono- and di-sodium methanearsonates, cacodylic acid, and sodium cacodylate). Since the mid 1970's the use of inorganic arsenic compounds has decreased, and organic arsenicals are primarily used (Gao et al., 1997).

1.4 Phosphorus Chemistry

Phosphorus(P) belongs to the Group VA in the periodic table with its electronic configuration of $([\text{Ne}] 4s^2 4p^3)$. It is stable in the pentavalent state to form an orthophosphate anion that retains a near tetrahedral complex surrounded by four oxygens. To satisfy classical valency requirements, the structure (PO_4^{3-}) contains a $\text{O}=\text{P}$ double bond.

In most soil/water environments, H_2PO_4^- and HPO_4^{2-} are the thermodynamically favorable species ($\text{pK}_{a1}=2.1$, $\text{pK}_{a2}=7.2$, and $\text{pK}_{a3}=12.3$). There are several other forms of P containing compounds (polyphosphates, metaphosphates, and organic P). The condensed forms of inorganic P (polyphosphate and metaphosphates) are formed with two or more orthophosphate groups. Whereas polyphosphates are linear O-P-O linkages, the metaphosphates are cyclic.

The organic P percentage of total soil P can range from 20 to 80 % (Dalal, 1977). Several forms of organic P have been identified in soils. They are inositol phosphate, nucleic acids, and phospholipids. Inositol phosphate (phytic acid) makes

up more than 50% of the total organic P due to its high stability in soils whereas the phospholipid content is as little as 0.5 to 7 % of total organic P (Dalal, 1977). Nucleic acid, which originates from the decomposition of microbes, plants and animal remains, is the smallest (less than 3%) fraction of the total organic P (Dalal, 1977).

P forms complex minerals with a wide variety of elements. About 150 P-minerals are known (Cathcart, 1980). According to Povarennykh's structural classification, P minerals can be placed into four groups. They are framework, insular, chain, and layer minerals. A majority of the P minerals belong to insular minerals including the apatite group, $\text{Ca}_2\text{Ca}_3(\text{PO}_4)_3(\text{OH}, \text{F})$ and wavellite, $\text{Al}_3(\text{PO}_4)_2(\text{OH})_3 \cdot 5\text{H}_2\text{O}$.

P solubility products are generally controlled by pH, the concentration of P, and divalent (i.e., Ca^{2+} , Mg^{2+} , and Fe^{2+}) and trivalent cations (i.e., Fe^{3+}) in bulk solutions. Where these cations are less available, P solubility is strongly controlled by adsorption onto clays and clay minerals in subsurface horizons. In reduced soil environments, P solubility can be increased due to the reductive dissolution of iron containing adsorbents like iron oxides and ferric P minerals (Diaz et al., 1993; Gale et al., 1992; Shapiro, 1957).

1.5 Arsenic Chemistry

Arsenic (As) belongs to the Group VA elements in the periodic table. The electron configuration is $[\text{Ar}]3d^{10} 4s^2 4p^3$, and it has four major oxidation states (+5, +3, 0, and -3). In the soil/water environment, inorganic As is mainly present in two

oxidation states (+3 and +5). Arsenite (As(III)) commonly exist as arsenious acid (As(OH)_3) in the reduced environment ($\text{Eh} = -200\text{mV} < +300\text{mV}$ over a pH range of 4 to 8) (Gao et al., 1997). It has weak acid characteristics similar to boric acid. $\text{As(OH)}_3 + \text{H}_2\text{O} = \text{As(OH)}_4^- + \text{H}^+$, $\log K = -9.29$. A fully protonated form is expected to be predominant in reduced soil environments due to the high pK values ($\text{pK}_1 = 9.22$, and $\text{pK}_2 = 12.13$). Conversely, an oxidized environment ($\text{Eh} > +300\text{mV}$) contains more arsenate(As(V)) as arsenic acid. Dissociation constants of arsenic acid ($\text{pK}_1 = 2.20$, $\text{pK}_2 = 6.97$, and $\text{pK}_3 = 13.4$) predict deprotonated forms (H_2AsO_4^- and HAsO_4^{2-}) in acidic to neutral environments. As(III) is more soluble than As(V).

Arsenic can form precipitates with calcium, aluminum, sulfur, and iron in the soil/water environment. The average solubility constant values (K_{sp}) for iron and aluminum arsenates are smaller compared to that of calcium arsenate (10^{-11} and 10^{-5} , respectively), indicating that iron and aluminum control the availability of As in soils (Walsh and Keeny, 1975).

In general, the solubility of inorganic As increases in reduced environments (i.e., ground water and sediments). Adsorbed As can be released through reductive dissolution of the adsorbent, for example, conversion from the ferric ion to the ferrous ion. A direct reduction of As(V) to As(III) also increases the solubility of total As due to the weak As(III) adsorption on soil components.

1.6 Phosphorus(P) and Arsenic(As) Adsorption on Soil Components

1.6.1 Adsorption Theory

Adsorption is defined as the accumulation of adsorbate at an interface between the adsorbents and the bathing solution (Sparks, 1995b). Adsorption is often confused with absorption which includes solute molecule retention, surface complexation, surface precipitation, coprecipitation, and solid state- and particle-diffusion. Adsorption is largely considered to result in two-dimensional molecular arrangements at the mineral/water interface whereas precipitation is considered to result in a three-dimensional molecular structure (Sposito, 1989). Oxyanions can be attached on the surfaces of metal oxides and phyllosilicate minerals in soils via different adsorption mechanisms.

Adsorption can be categorized into specific and non-specific. Specific adsorption (inner-sphere complexation) occurs via ligand exchange whereas non-specific adsorption (outer- sphere complexation and diffuse ion) arises via electrostatic interaction. An inner-sphere complex does not have any water molecules between surface functional groups and adsorbate ions due to ionic and covalent bonding mechanisms. In the case of oxyanions, chemisorption can occur on variable charged mineral surfaces as evidenced by 1) OH⁻ release into the bulk solution, 2) a high degree of specificity shown toward particular oxyanions, 3) almost nonreversible processes, and 4) a lowered point of zero charge due to an increased negatively charged surface density (McBride, 1994a). Conversely, an outer-sphere complex forms mainly by electrostatic interactions in which there is an intervening water molecule between the adsorbate and adsorbent functional groups (Sposito, 1989). If

an adsorbate ion is fully dissociated from the surface functional groups of the adsorbent (delocalization), it is referred to as a diffuse ion (Sposito, 1989).

Adsorption is a thermodynamically favorable process. A state function (G : Gibbs free energy), which is derived by combining the first and second laws of thermodynamics (energy is conserved and entropy monotonically increases), indicates the direction (forward or backward) of the reaction. The Gibbs free energy of products must be lower than that of the reactants to induce the forward reaction (adsorption processes). If the adsorption reaction spontaneously occurs, dG is always less than zero.

Such adsorption complexes (inner- or outer-sphere), and bonding environments (e.g., monodentate mononuclear and bidentate binuclear) can be identified and studied using macroscopic, microscopic, and spectroscopic techniques. Microelectrophoretic mobility (EM) measurements, ionic strength (I) effects on the adsorption envelope, and sorption-proton balance data can be used to indirectly distinguish predominant surface complexes at mineral/water interfaces. Extended X-ray absorption fine structure spectroscopy (EXAFS), and Attenuated Total Reflectance Fourier Transform Infrared (ATR-FTIR) spectroscopy are two powerful techniques that can be employed to directly identify not only the types of surface complexes (inner- or outer-sphere), but also the bonding mode at mineral/water interfaces under in-situ conditions.

1.6.2 Phosphorus and Arsenic Adsorption on Soils (Empirical and Modeling Approaches)

The retention of P and As in soil/water environments has received much attention in soil chemical studies due to their important biogeochemical roles. It is often found that P adsorption in soils increases with decreasing pH (Sanchez and Uehara, 1980). P adsorption reactions on acidic soils are typically biphasic, characterized by an initial rapid reaction followed by a much slower reaction (Barrow, 1985; Parfitt, 1978). The slow and continuous P and As(V) adsorption on soils and soil components has been reported by many researchers (Barrow and Shaw, 1975; Fuller et al., 1993; Munns and Fox, 1976; van der Zee and van Riemsdijk, 1988; van Riemsdijk and de Haan, 1981). Researchers have attempted to understand P adsorption phenomena using macroscopic approaches (e.g., adsorption isotherms and envelopes) coupled with empirical and surface complexation models.

In the past, P adsorption isotherm curves have been extensively fitted using the Langmuir equation to describe different adsorption sites. These sites are defined by the multiple linear portions of the Langmuir plot (Fried and Shapiro, 1956; Muljadi, 1966; Olsen and Watanabe, 1957; Ryden et al., 1977b). Some investigators used a two-site Langmuir equation to describe the low and high energy sites in the adsorption reaction. A P adsorption reaction at pH \approx 7 on nineteen Vertisols (clay rich soils) was described using a two-site Langmuir equation. The maximum adsorption values from the two site model were highly correlated with the calcite content for high energy sites and dithionate-citrate-bicarbonate (DCB) extractable iron for low

energy sites (López-Pineiro and Navarro, 1997). Since the Langmuir equation can equally well describe both adsorption and precipitation reactions (Veith and Sposito, 1977), such empirical equations can not be used to interpret any particular adsorption mechanisms, or even if adsorption, as opposed to precipitation, actually has occurred (Sposito, 1989).

The lack of mechanistic information obtained from empirical approaches has led to the use of surface complexation models (SCM) to describe adsorption phenomena. SCM are chemical models that are based on the molecular description of the electric double layer using equilibrium-derived data (Goldberg, 1992). The constant capacitance model (CCM) is one of many SCM and has been successfully used to describe an array of chemical reactions on mineral surfaces. These include adsorption, desorption, and dissolution reactions on soil components. For instance, the CCM has been used to quantitatively describe P adsorption on 44 noncalcareous soils over a wide range of pH (4.9 - 7.6) (Goldberg and Sposito, 1984). Using the derived parameters (intrinsic surface protonation dissociation constants, capacitance density, P packing area parameters), the CCM could accurately describe the adsorption envelopes and isotherms. Arsenic adsorption on soil components has also been successfully modeled using the CCM, the triple layer model, and the two-layer model (Benjamin and Bloom, 1981; Dzombak and Morel, 1990; Goldberg, 1986; Hsia et al., 1992).

Results of well modeled equilibrium data using the SCM must be carefully interpreted because 1) assumed surface complexation does not always indicate the

actual adsorption mechanisms. because high degrees of freedom in the adjustable parameters allows one to describe any material balance data very well, and 2) the majority of SCM do not include surface precipitation and other nonadsorption phenomena as part of the model description and prediction (Sparks. 1995b).

1.6.3 Phosphorus and Arsenic Retention as Effected by Physicochemical Properties of Soils

The retention of P and As on soils is highly dependent on the physicochemical properties of the soils. for example the crystalline and amorphous iron and aluminum oxide, organic matter, clay and calcium contents. Many researchers have shown a correlation between these parameters and adsorption and chemical extraction data.

Long-term (256 d) P adsorption on twelve Oxisols (well-weathered soils) was investigated by Barron and Torrent (1995). In their experiments, the adsorption maximum from the Freundlich and Langmuir equations suggested that slow adsorption was highly correlated with the ratio of the organic matter (OM) content and the specific surface area of the solids. High P retention in a high OM soils (i.e., an aluminum substituted woody peat) was also observed (Bloom, 1981; López-Hernandez and Burnhan, 1974).

Several researchers have reported that P and As(III and V) retention in various soils (i.e., Andisols, Entisols, and Gelisols and Oxisols) are highly associated with ammonium oxalate extractable iron (Fe_{ox}) and/or aluminum (Al_{ox}) and DCB extractable iron and/or aluminum (Bloom, 1981; Jacobs et al., 1970; Livesey and

Huang, 1981; López-Hernandez and Burnhan, 1974; Sakata, 1987). Arsenic (in acidic fly ash leachate) partitioning reaction in fly ash matrix was linked to the hydroxylamine extractable iron which is operationally defined as an amorphous iron oxyhydroxide fraction (Van der Hoek and Comans, 1996).

High P and As(V) retention in calcium rich soils and soil components at $\text{pH} > 7$ has also been reported. Kuo and Lotse (1972) observed strong P retention on calcite and Ca-kaolinite, and a second-order rate equation was fitted to obtain the rate coefficient. The coefficient was 30,000 times higher for calcite than for Ca-kaolinite. A similar correlation was also observed for P adsorption on calcite-rich Vertisols (López-Pineiro and Navarro, 1997) and for As(V) adsorption on calcareous soils (Goldberg and Glaubig, 1988).

While many macroscopic studies have shown a strong correlation between P and As retention and specific soil properties, they have not provided any information on the spatial distribution of P and As in heterogeneous systems. Several microscopic techniques have been applied to investigate P and As retention phenomena in heterogeneous systems.

P fixation in P fertilizer amended soils ($\text{pH} \approx 7$) was investigated using scanning transmission electron microscopy (TEM) along with energy dispersive X-ray spectroscopy (EDX) (Pierzynski et al., 1990b). In the separated clay fractions, it was observed that discrete P rich particles were highly associated with Al and Ca in the highest density separated fraction ($< 2.2 \text{ Mg m}^{-3}$). Furthermore, the EDX model calculations, using elemental ratios (cations/phosphorus), also showed an Al and Ca

enrichment associated with P. These results were later supported by a P solubility equilibrium study which predicted the formation of varicite (aluminum phosphate) like solids at $\text{pH} < 6.8$ and calcium phosphate like solids at $\text{pH} > 6.8$.

(Pierzynski et al., 1990a).

The P mineralogy of Florida soils derived from phosphoric deposits was investigated using XRD, thermal analysis, and selective dissolution (Wang et al., 1991). The XRD data showed the presence of carbonate-fluoroapatite ($\text{Ca}_{10}(\text{PO}_4)_6\text{F}_{2-3}$), wavelite ($\text{Al}_3(\text{PO}_4)(\text{OH})_3 \cdot 5\text{H}_2\text{O}$) and crandallite ($\text{CaAl}_3(\text{PO}_4)_2(\text{OH})_5 \cdot \text{H}_2\text{O}$). The oxalate extractable P (P_{ox}) was associated with Al_{ox} in the surface horizons. Endothermic differential scanning calorimetry peaks (90-100°C), which originated from dehydration of amorphous Al and Fe-P minerals, were eliminated by oxalate extraction. This suggests that P might associate with amorphous Al and Fe minerals.

A similar study was conducted on manure-derived surface soils and sediments ($\text{pH} 6.9-9.5$) (Harris et al., 1994). Amorphous apatite and ferrous P minerals (vivianite) were detected by XRD in stream sediment samples. The lack of crystalline Ca-P minerals suggest that the manure components might inhibit the crystallization of Ca-P minerals.

Arsenate retention in the clay fraction of Australian acid soils was assessed by autoradiography using arsenate-73 and an electron microprobe. Arsenate was strongly retained in the iron oxide fraction, with much less being present in titanium oxides and gibbsite (Fordham and Norrish, 1979). The reactivity of arsenate in an Australian

podzol was also investigated using an electron microprobe, XRD, and selective dissolution methods. The data showed that Al substituted goethite and titanium oxides strongly competed for As uptake (Norrish and Rosser, 1983).

1.6.4 pH Effects on P and As Adsorption on Variable Charge Minerals

Oxyanion adsorption on soil minerals is greatly influenced by the pH of the bulk solution. Metal oxides and phyllosilicate minerals in soils contain surface functional groups (unsatisfied bonds with respect to the repeated bonding of the unit cells). Examples include 1) the siloxane surface associated with the plane of oxygen atoms bound to the silica tetrahedral layer of phyllosilicate minerals, and 2) hydroxyl groups that are associated with the edges of inorganic minerals such as phyllosilicates, metal oxides, oxyhydroxides, and hydroxides (Sparks, 1995a). When the mineral is hydrated, the metal ion (Lewis acid) sites are occupied with water molecules, and the association is with Lewis base sites (hydroxylated surface) because of the dissociative chemisorption of the water molecules. The surface sites can be protonated and deprotonated depending on the pH of the bulk fluid. Therefore they are often called variable charge (pH dependent charge) mineral surfaces.

The speciation of the oxyanions is also influenced by pH. The dissociation constant (equilibrium constant), K_a , for the oxyanions refers to the reaction in which an acid donates a proton to water. The larger the K_a value, the higher the tendency to donate protons to water molecules.

Therefore oxyanion adsorption on soil components is a function of both the net surface charge density of the adsorbent and the chemical speciation of the adsorbate which in turn are dependent on the pH of the bulk fluid (pH_b). In general, anion adsorption on inorganic minerals increases with decreasing pH_b due to 1) the negatively charged chemical species (i.e., $H_2PO_4^-$ and $HAsO_4^{2-}$) and 2) the positively charged mineral surfaces, when $pH_b < pH_{PZC}$ of the solids (Hingston et al. 1972).

1.6.5 Phosphate and Arsenate Adsorption on Metal Oxides

Phosphate(P) and arsenate(As(V)) pH dependent speciation are similar. The first dissociation constant of P and As(V) is approximately 2.2, this is followed by constants of ≈ 7 and ≈ 12.8 . At most environmental pH's (4-8), the species are predominantly in deprotonated forms (negatively charged species), and the charge properties of metal oxides are positive due to the PZC of the solids (i.e., 6.5-8.5 for iron oxides, 8.2-9.1 for aluminum oxides, an exception is manganese oxides (e.g., Birnessite) ≈ 2.8). Therefore, P and As(V) are expected to adsorb on metal oxide surfaces strongly via electrostatic interaction when $pH_b - pH_{PZC}$ is less than zero, and to predominantly adsorb via ligand exchange when $pH_b - pH_{PZC}$ is greater than zero. Hingston and co-workers reported that P adsorption increased with decreasing pH (Hingston et al., 1967). The P adsorption envelope on goethite showed inflection points near pK values of phosphoric acid (Hingston et al., 1967). Nilsson et al. investigated the intrinsic constants of adsorbed P on goethite using the constant capacitance model with the aid of the FITEQL program (Nilsson et al., 1992). The

intrinsic constants, which are approximately 2.16, 7.93, and 12.68, are shifted from the dissociation constants of the solution species.

A similar pH dependent adsorption behavior has been observed for P and As(V) on ferrihydrite, hematite, α -Al₂O₃, boehmite; γ -AlOOH, and amorphous Al(OH)₃ (Anderson et al., 1976; Bleam et al., 1991; Chen et al., 1973; Pierce and Moore, 1982; Shang et al., 1992; Xu et al., 1988).

1.6.6 Phosphate and Arsenate Adsorption on Phyllosilicate Minerals

While the metal oxides exhibit a strong affinity of P and As(V) at acidic pHs, the phyllosilicate minerals show a different adsorption capacity. In general, the PZC of clays is lower than that of iron and aluminum oxides (i.e., 4.6 for kaolinite and 2.5 for montmorillonite) (Sparks, 1995a). Therefore the pH dependent edge sites of phyllosilicate minerals are generally negatively charged at most environmental pH (4-8). If there is any oxyanion adsorption at the latter pH range, the oxyanions usually specifically adsorb onto edge sites via ligand exchange.

Phosphate and As(V) adsorption on illite, kaolinite and montmorillonite gradually increase from pH 3 to 5, and then the adsorption decreases with increasing pH (Chen et al., 1973; Edzwald et al., 1976; Goldberg and Glaubig, 1988; Xu et al., 1988). As(V) adsorption on montmorillonitic soils increases with increasing pH up to 10 (Goldberg and Glaubig, 1988). Conversely, the As(V) adsorption envelope on quartz shows no significant adsorption (less than 15% of net adsorption) between pH 2.8 to 9.5 even after 3d of reaction time (Xu et al., 1988).

1.6.7 Arsenite Adsorption on Soils and Soil Components

The adsorption of P and As(V) on metal oxides and phyllosilicate minerals is highly dependent on the relation between pH of the bulk solution and the PZC of solids. However, As(III) adsorption is more dependent on its speciation. At most environmental pHs (4-8), arsenite (as $\text{As}(\text{OH})_3$) does not have any charge and negative charge increases with increasing pH due to its weak acidity ($\text{pK}_1 = 9.22$, and $\text{pK}_2 = 12.13$). As(III) adsorption on metal oxides and phyllosilicate minerals increases with increasing pH.

The As(III) adsorption envelope and isotherm on kaolinite and montmorillonite was investigated using landfill leachate containing As(III) (Frost and Griffin, 1977). As(III) adsorption on montmorillonite and kaolinite increased with increasing pH up to 6.5, and then gradually decreased. Montmorillonite exhibits more than a three-fold greater adsorption capacity than kaolinite due to its higher surface area. Pierce and Moore studied the As(III) adsorption envelope on ferrihydrite using a wide range of initial As(III) concentration of 1.33-334 $\mu\text{mol L}^{-1}$ (Pierce and Moore, 1982). Overall adsorption increased with increasing initial As(III) concentration and with increasing pH. A similar pH dependent behavior in As(III) adsorption has also been observed on goethite and arid soils which have high (> 4000 mg kg^{-1}) DCB extractable iron (Manning et al., 1998).

1.6.8 Temperature Effects on Phosphorus and Arsenic Adsorption on Soil

Components

Temperature may have two distinct effects on a chemical reaction. These are: 1) the rate of reaction, and 2) the equilibrium end point (Barrow, 1987). The reaction at high temperature results in an increase in the reaction rate, and a decrease in the subsequent desorption if the reaction involves activated complexes (intermediate or high-energy states) (Barrow, 1979b).

The effect of temperature on the chemical reaction can be explained using the transition state theory (Eyring reaction rate theory). The schematic reaction flow is



where A and B are the reactants and AB^\ddagger is the activated complex.

Using transition state theory, the elementary reaction process can be expressed as 1) the total molecular partition functions per unit volume (q_i) for the reactant species and for the activated complexes (q^\ddagger), and 2) the difference in zero-point potential energies between the activated complex and reactants (E_0):

$$k = [(k_B T)/h] [q^\ddagger / (q_A \cdot q_B)] \cdot \exp(-E_0 / (k_B T)),$$

where k = elementary rate constant, k_B = Boltzmann's constant, T = absolute temperature, and h = Planck's constant (Stumm and Morgan, 1995b).

The previous equation can be thermodynamically re-expressed as

$k = [(k_B T)/h] \cdot K^\ddagger \cdot (\gamma_A \cdot \gamma_B / \gamma^\ddagger) \cdot \exp(-\Delta G^\ddagger / (R T))$, where K^\ddagger = thermodynamic formation constant, and γ = activity coefficient. The Linearized Arrhenius empirical rate law, $\ln k = \ln A + [-E_a / (RT)]$, (where A = the pre-exponential factor, E_a = activation energy, R = the ideal gas constant, and T = temperature) is also commonly

used. Combining the transition state theory and the above thermodynamic expression gives $A = [(k_B T)/h] \cdot \exp(-\Delta S^\ddagger/R)$ and $E_a = \Delta H^\ddagger + R \cdot T$ assuming the activity coefficients are all unity. If an endothermic adsorption reaction (positive enthalpy) is observed, one can estimate the apparent activation energy of the reaction. A linear plot between $\ln k$ Vs $1/T$ allows one to obtain the value of the slope ($-E_a / R$). The reaction is diffusion limited when $E_a < 42 \text{ kJ mole}^{-1}$, whereas a chemically controlled reaction is suggested when $E_a > 42 \text{ kJ mole}^{-1}$ (Sparks, 1995b).

Various results have been reported on temperature dependent P adsorption/desorption on soils and soil components. In acid soils, P adsorption increases with increasing temperature and desorption is subsequently reduced, suggesting that the reaction involves activated complexes. (Barrow, 1979b; Barrow and Shaw, 1977; Chien et al., 1982; Sheppard and Racz, 1984). Van Riemsdijk and Lykema reported that P adsorption on gibbsite at pH 5 increased with increasing temperature (2, 12, 22, and 45°C). An estimated activation energy of $63 \pm 4 \text{ kJ mole}^{-1}$ was determined, suggesting that the reaction was controlled more by chemical than by physical processes (van Riemsdijk and Lykema, 1980). With goethite, however, P adsorption increased with decreasing temperature from 68°C to 25°C. This indicated an exothermic temperature dependent reaction, and non-activated complex formation (Madrid and Posner, 1979).

Temperature dependent P desorption kinetics from desert soils were studied using an anion-exchange resin (Evans and Jurinak, 1976). The energy of activation was estimated from the data based on 4h of desorption. An activation energy of less

than 42 kJ mole⁻¹ in all soils was determined, suggesting that P release might depend on diffusion processes. Conversely, Barrow(1979) found that the activation energy for the P adsorption (forward) reaction was similar to that of the desorption (backward) reaction (Barrow, 1979b). The values for both steps were approximately 80 kJ mole⁻¹, which suggested that the rate-limiting steps for both reactions were not diffusion-controlled.

Bar-Yosef and Kafkafi estimated activation energies for initial rapid and slow P desorption processes from kaolinite of 67.8 kJ mole⁻¹ and 20.8kJ mole⁻¹, respectively (Bar-Yosef and Kafkafi, 1978). This suggested that chemically-controlled desorption was followed by diffusion-controlled desorption.

1.6.9 Ionic Strength Effects on Reaction Rate

Ionic strength (I) can have an influence on both the rate of the elementary reaction and the type of surface complexation (inner- and/or outer-sphere complexation) (Hayes et al., 1988; Stumm and Morgan, 1995b).

The mathematical equation described in the previous section 2.5.8, $k = [(k_B T)/h][(q^\ddagger / q_A \cdot q_B) \cdot \exp (-E_o/(k \cdot T))]$ can be used to explain the ionic strength effect on the reaction rate (Stumm and Morgan, 1995b). The simplified equation is, $k = k_o \cdot (\gamma_A \cdot \gamma_B / \gamma^\ddagger)$, where k_o is the value of the second rate coefficient in the reference state. This refers to a system in an infinitely diluted solution in which the ion activity coefficients are all unity. Under the assumption that the charge of the activated complex is the sum of the charges of the reactants, each ion activity coefficient can be

estimated using the Davies equation. Since the ion activity coefficient decreases with increasing I, the rate of the elementary reaction decreases.

The rate can also be influenced by changes in the acidity constant, which is affected by I. Three expressions (i.e., an equilibrium expression, and mass balance and the proton balance expressions) are used to determine the acidity constants. The equilibrium expression only changes when I is accounted for. Using the Debye-Hückel theory and the Güntelberg approximation, one can derive

$pK^* = pK + \{ [0.5 \cdot (z_{HB}^2 - z_B^2) \cdot I]^{1/2} / (1 + I^{1/2}) \}$ where pK^* is the corrected acidity constant and pK is the acidity constant valid at infinite dilution (Stumm and Morgan, 1995b). For example, the first acidity constant (pK_1) of phosphoric acid (H_3PO_4) decreases to

$pK^* = pK_1 - 0.07$ when I decreases from a 10 mM Na_2SO_4 solution to a <1 mM Na_2SO_4 solution. The valency change of the reactants in the elementary reaction can affect the rate of the reaction. For instance, if like-charge species increase, the rate of the reaction will also increase.

Gupta and co-workers investigated effects of I (water and sea water) on As(III and V) adsorption kinetics on activated alumina (surface area: $210 \text{ m}^2 \text{ g}^{-1}$) (Gupta and Chen, 1978). As(V) adsorption kinetics ($pH \approx 6.6$) showed that an initial adsorption rate in sea water was much slower than that in water, however, the same adsorption maximum ($\approx 25 \text{ } \mu\text{mol g}^{-1}$) was reached in both media after 3000 min. In the case of As(III) adsorption ($[As(III)]_0 = 12.4$, $pH \approx 8$), the adsorption rate in seawater was

slower than that in water. Furthermore, the final adsorption value in water was ≈ 1 $\mu\text{mol g}^{-1}$ higher than that in seawater.

1.6.10 Ionic Strength Effects on Surface Complexation

Oxyanions adsorb onto variable charge mineral surfaces by both inner-sphere (via ligand exchange) and outer-sphere complexation (via electrostatic interaction) (McBride, 1989). These surface complexes can be hypothesized by studying the ionic strength (I) effect on the degree of adsorption (Hayes et al., 1988). Inner-sphere complexes (i.e., selenite) are insensitive to changes in I due to ligand exchange adsorption mechanisms, while the outer-sphere complexes (i.e., selenate) are sensitive to the changes in I because of competition with counter anions in the indifferent electrolytes.

Many macroscopic studies have investigated the theoretical I dependent oxyanion adsorption behavior on clays and clay minerals. There is an exception to this theory. P adsorption could increase with increasing I on soils (New Zealand loamy soils) and soil components (kaolinite, montmorillonite, illite, and goethite) (Barrow et al., 1980; Edzwald et al., 1976; Helyar et al., 1976a; Helyar et al., 1976b; Ryden et al., 1977b). Two theories have been suggested to explain this unique adsorption behavior. They are 1) the quadruple-layer model theory and 2) the diffuse double layer thickness theory. Barrow's data has been successfully fitted using a quadruple-layer adsorption model (Bowden et al., 1980). Such complex model applications are generally not subject to direct confirmation by experiments because

they employ several fitting parameters that can not be analytically measured (McBride, 1997). Decreased double layer thickness (DLT), due to increased I, allows the oxyanions to approach close to the negatively charged surface, and then they adsorb via ligand exchange. The inner-sphere adsorption, however, should not be influenced by either the DLT or the repulsion force because the specific adsorption is in direct coordination with discrete surface metal cations (McBride, 1997). Therefore the model and DLT are inappropriate to describe the above P adsorption behavior. McBride used the simple mass action principle to explain the adsorption phenomena. This approach is similar to the constant capacitance model described by Goldberg and Sposito (Goldberg and Sposito, 1984). It ignores, however, the surface electrical potential correction term, ψ , by assuming that any inner-sphere, and outer-sphere counter ions are adsorbed to balance the surface charge created in the process. In the case of high I, the negatively charged surfaces created by inner-sphere P adsorption are likely to be neutralized by co-adsorption of cations (i.e., Na^+) from indifferent electrolytes maintaining the charge balance. This mass action principle favors such reactions when a higher concentration of indifferent electrolyte is present. No spectroscopic evidence, however, is available to support this theory.

1.7 Phosphorus and Arsenic Surface Complexation on Soil Components

While numerous macroscopic studies have investigated adsorption behavior by developing isotherms and envelopes, they have not provided any information on

adsorption mechanisms (i.e., surface complexation) at the molecular scale. Recent empirical and modeling approaches (proton balance measurements, and SCM), microscopic (EM measurements) and spectroscopic (FTIR and XAS) studies have provided better insight at the molecular scale on oxyanion adsorption mechanisms.

1.7.1 Empirical Approaches

Surface complexation can be indirectly suggested using adsorption data coupled with the SCM and proton balance measurements. Hsia and co-workers modeled As(V) adsorption on ferrihydrite using a triple layer model (Hsia et al., 1992). The data suggested inner-sphere complexation surface species ($\equiv\text{Fe}(\text{H}_2\text{AsO}_4)$, $\equiv\text{Fe}(\text{HAsO}_4)^-$, and $\equiv\text{Fe}(\text{AsO}_4)^{2-}$) were formed at the ferrihydrite / water interface. Using proton balance measurements during P adsorption on aluminum oxides, Rajan suggested that the predominant surface complexation was a binuclear bidentate complex (Rajan, 1976).

Proton balance data for As(III and V) adsorption on ferrihydrite shows that net H^+ and OH^- release per mole of adsorbed As varies with As surface coverage. This indicates types of surface complexes are a function of loading level (Jain et al., 1999). In addition, pH dependent bonding modes are suggested. Firstly, with As(III) adsorption at low pH(4.6), the oxygen of the Fe-O-As bond is partially protonated as Fe-OH-As, and monodentate mononuclear adsorption increases with increasing pH (< 8). Secondly, the As(V) adsorption complex is predominantly a bidentate mononuclear inner-sphere, but monodentate complexes increase with increasing pH

and loading level. Interestingly, these findings contradict the findings of the EXAFS investigation by Fendorf et al. (Fendorf et al., 1997).

1.7.2 Electrophoretic Mobility Measurement Studies

The Microelectrophoretic Mobility (EM) measurement is a useful microscopic technique not only for determining the isoelectric point (IEP) of pure components but also for obtaining information that can be used to indirectly distinguish bulk surface complexes at colloidal/water interfaces. Non-specific ion adsorption of indifferent electrolyte at the outside of shear plane (i.e., formation of outer-sphere complexes via van der Waals forces) generally do not affect the IEP but it could cause shifts in the value of EM if present at high concentration (Hunter, 1981). The shear plane is at the outer edge of the inner part of the double layer and near the outer Helmholtz plane or the Stern layer, depending on the models to describe the interface (Hunter, 1981). Inner-sphere complexes, however, cause shifts in both EM and IEP due to specific ion adsorption inside the shear plane (Hunter, 1981). In some cases, however, inner-sphere adsorption does not cause shifts in EM (Hunter, 1981). In other words, oxyanion inner-sphere adsorption does increase the net negative charge on the surface. With this knowledge, one can indirectly distinguish the predominant surface complexes on pure colloidal materials using the EM measurements.

There are EM data suggesting predominant inner-sphere P and As(V) complexes on metal oxides. Microelectrophoretic mobility measurements of P adsorbed on goethite and boehmite (γ -AlOOH) have shown that inner-sphere complexes form due to

charge reversal and a lower IEP with increasing P loading level (Anderson and Malotky, 1979; Bleam et al., 1991; Hansmann and Anderson, 1985; Tejedor-Tejedor and Anderson, 1990).

As(V) adsorption also causes a large shift in IEP on ferrihydrite and amorphous Al(OH)₃ with increasing As(V) loading level (Anderson et al., 1976; Suarez et al., 1998).

As(III) adsorption, however, does not seem to alter the surface charge properties of the adsorbents greatly. Suarez reported that As(III) adsorption caused a slight shift in the IEP of amorphous aluminum oxide (Suarez et al., 1998), which suggests predominant outer-sphere adsorption of As(III).

1.7.3 *Ex situ* Spectroscopic Studies

Ex situ spectroscopic techniques have been extensively utilized to directly distinguish the adsorption mechanisms of P and As(III and V) on clays and clay minerals.

Parfitt investigated P adsorption complexation on iron oxides (ferrihydrite, goethite, lepidocrocite and hematite) using *ex situ* IR spectroscopy (Parfitt et al., 1975). The IR spectra of P adsorbed on iron oxides shows the replacement of two singly coordinated surface hydroxyls, suggesting the formation of bidentate binuclear species. Using the same IR technique, Atkinson and co-workers compared the ν_3 vibrations of P adsorption complexes on goethite and other model systems (e.g., Co(III)P solution complexes). They suggested that the shift in ν_3 bands of the

adsorption complex was due to binuclear bidentate species (Atkinson et al., 1974). Nanzyo and Watanabe (1982) utilized Diffuse reflectance Fourier transform infrared (DRIFTIR) spectroscopy to investigate P adsorption complexes on goethite over a wide pH range of 3.3-11.9. Goethite background subtracted IR spectra showed that 1) the surface complexes at the same pH did not change with increasing loading level up to 197 mol g⁻¹, and 2) bidentate bridging complexes were present throughout all pHs based on the IR bands assigned by Parfitt.

Diffuse reflectance infrared Fourier transform spectroscopy was also utilized to re-investigate P adsorption surface complexation on goethite (Persson et al., 1996). Using the symmetry rule arguments of P ν_3 bands, Persson suggested that the monodentate surface complex predominantly formed between pH-3-12.8, but at intermediate pH, a bidentate complex could not be ruled out. *Ex situ* DRFTIR was also used to investigate IR bands of surface hydroxyl groups on goethite after As(III and V) adsorption (Sun and Doner, 1996). With both arsenic species, the replacement of two surface hydroxyls was observed, suggesting the formation of an inner-sphere bidentate binuclear complex.

Lumsdon and co-workers investigated As(V) surface complexation on goethite at pH 2.2 using *ex situ* IR (Lumsdon et al., 1984). AsOH bending frequencies were examined comparing the IR spectra of adsorbed As(V) and the surface hydroxyls in D₂O. Inner-sphere bidentate binuclear species were suggested due to the replacement of singly coordinated surface OH groups by ligand exchange.

Martine and co-workers utilized X-ray photoelectron spectroscopy (XPS) to investigate phosphate adsorption complexation on goethite at pH 3 and 12, with high initial P concentrations ($[P]_0=5$ mM and 50mM) (Martine and Smart, 1987). They observed that the replacement of two A-type surface hydroxyls via a ligand exchange reaction suggested bidentate binuclear adsorption.

While *ex situ* spectroscopic studies have strongly suggested a specific P adsorption (inner-sphere complexes) on iron and aluminum oxides, the results have been questioned by many researchers because of the creation of experimental artifacts (i.e., a structural alternation by vacuum pressure and or bulk precipitates by drying residual adsorbates) under dry and severely evacuated sample conditions.

Colloidal/water interfaces in natural settings are usually under near atmospheric pressure. Analyzing samples near environmental conditions (*in situ*) is more appropriate to obtain accurate information on environmental samples (Goldberg and Sposito, 1985).

Accordingly, in the past decade, with the development of *in situ* molecular scale techniques such as XAFS and ATR-FTIR, one can directly determine oxyanion reaction mechanisms on minerals under environmental conditions that are representative of field settings.

1.7.4 *In situ* Spectroscopic Studies

Parfitt and Atkinson combined in-situ IR spectroscopy and potentiometric titration experiments to examine P adsorption complexation at the goethite/water

interface at pH 3.6 or 5.1 (Parfitt and Atkinson, 1976). They suggested that binuclear bidentate complexes are predominantly formed at both pHs.

Tejedor-Tejedor and Anderson used in-situ cylindrical internal reflection-FTIR (CIR-FTIR) to investigate P adsorption complexation on goethite between pH 4-8. Comparing the spectra of ferric phosphate solutions with that of adsorption complexes on goethite, the formation of protonated and non-protonated bidentate binuclear, and nonprotonated monodentate mononuclear complexes were suggested (Tejedor-Tejedor and Anderson, 1990).

Magic angle spinning Nuclear Magnetic Resonance (NMR) spectroscopy coupled with the constant-capacitance model was utilized to investigate the hydrolysis of adsorbed P molecules on boehmite (γ -AlOOH) (Bleam et al., 1991). An inner-sphere complex was suggested between the pH range of 4 to 11, and a fully deprotonated P surface complex was also reported at pH > 9 (Bleam et al., 1991).

Waychunas and co-workers (1993) investigated As(V) adsorption complexes on ferrihydrite, and iron polymorphs (goethite, lepidocrocite, and akagenite) at pH 8. Extended X-ray Absorption Fine Structure (EXAFS) analysis showed that As(V) formed a primary inner-sphere bidentate binuclear species on all the iron oxides. The adsorption complexes attach to the adjacent apices of edge-sharing iron octahedrals, and the As(V)-Fe distance is $3.28 \pm 0.01 \text{ \AA}$ in iron polymorphs and $3.25 \pm 0.02 \text{ \AA}$ in ferrihydrite. The loading level affected As(V) surface complexation in ferrihydrite. Monodentate mononuclear species ($\text{As(V)-Fe} = 3.60 \pm 0.03 \text{ \AA}$) were observed in

approximately 30% of the total As-Fe correlation, and decrease with increasing total loading level. Monodentate adsorption sites were postulated at structural defect sites.

A similar relation between the As(V) bonding environment on goethite has also been reported by EXAFS and pressure(p)-jump relaxation studies (Fendorf et al., 1997; Grossl and Sparks, 1995). Both studies showed the formation of an inner-sphere bidentate binuclear surface complex at the goethite water interface, however, an EXAFS investigation also showed that the types of surface complex changed from monodentate to bidentate mononuclear, and then to bidentate binuclear with increasing loading level of As(V) on goethite (Fendorf et al., 1997).

As(III) adsorption and stability on goethite at $\text{pH} \approx 7.5$ was investigated using batch adsorption and XAS (Manning et al., 1998). EXAFS gave an average As(III)-Fe interatomic distance of $3.378 \pm 0.014 \text{ \AA}$, which is indicative of bidentate binuclear complexation. Application of the surface complexation model (constant capacitance model) with data about surface complexes, determined by XAS, provided excellent agreement with the batch adsorption data.

1.8 Phosphorus and Arsenate Desorption on Soils and Soil Components

1.8.1 Desorption Theory

While adsorption has been extensively studied, few studies have been performed examining desorption of metals and metalloids. An understanding of desorption phenomena is extremely important to predict the fate and transport of contaminants in soil/water environments.

Desorption processes are generally categorized as either reversible or irreversible processes. Oxyanion desorption phenomena on variable charge mineral surfaces can be predicted by estimating enthalpy (ΔH) of a reaction energy during adsorption. When the shared charge value (the positive charge of the central atom (oxyanion) divided by the number of bonded O atoms) of the oxyanion (i.e. $\text{NO}_3^- = 1.67$) is greater than that of the surface hydroxyls ($\text{OH}^- = 1$), it is difficult for the oxyanion to compete with the hydroxyls to form strong bonds. As a result, the electrostatic interaction is weak with small adsorption reaction energy (ΔH) (McBride, 1994a). The small reaction energy is easily overcome by counter anions in the bulk solution, resulting in reversible reactions. If on the other hand, the surface hydroxyls are displaced by incoming oxyanions forming a strong chemisorption (inner-sphere complexes), a large reaction energy (ΔH) is generated. When the large reaction energy cannot be fully overcome, an irreversible reaction (i.e., hysteresis, nonsingularity, and residence time (aging) effects) results. The chemisorbed oxyanions can, however, be desorbed by strong desorption agents, and/or when the bulk solutions have high or low pHs. Several desorption mechanisms have been suggested to explain the release of the chemisorbed oxyanions. These mechanisms are categorized into two groups, 1) direct oxyanion desorption and 2) indirect oxyanion desorption.

Direct oxyanion desorption involves a) oxyanion desorption through competitive desorption of the adsorbate with counter oxyanions and b) direct reduction of the adsorbate with incoming reductants (e.g., ascorbate reduction of

adsorbed As(V)). As discussed earlier, the shared charge of the counter oxyanion (desorbing agent) controls the release of the adsorbed oxyanion. If the shared charge of the counter oxyanion is less than that of the adsorbed oxyanion, it competes readily with the adsorbed oxyanions at the adsorption (metal coordinated) sites. As a result, the adsorbed oxyanion will be released. Effective P desorption on goethite under higher pH (hydroxy promoted dissolution of adsorbent) was reported (Madrid and Posner, 1979). The reduction of adsorbed oxyanions with any electron donor ligands could facilitate desorption. For instance, adsorbed As(V) on aluminum oxides could be released as As(III) due to the electron-transfer reaction between adsorbed As(V) and the reductant (e.g., ascorbate).

Indirect oxyanion desorption includes a) a pH effect (proton and hydroxyl promoted adsorbent dissolution), and b) non-reductant and reductant promoted adsorbent dissolution. At low pH, the protonation of the surface ligands polarizes the interatomic bonds near the central surface ions, which causes the release of cation surface groups. Similarly at high pH, hydroxyl adsorption can also weaken the bond of the anionic groups causing dissolution. The non-reductants (e.g., EDTA, siderophores, and pyrophosphate), which form inner-sphere complexes, can lower (polarize) the Lewis acidity of the coordination center. The metal ions can be released as well as adsorbed oxyanions due to weakened metal-oxygen bonds. Indirect oxyanion desorption through the reductant promoted dissolution of adsorbents will be reviewed in later chapters (redox effects on P retention/release and redox effects on As retention/release).

1.8.2 Phosphate Desorption and Kinetic Models

Many researchers utilizing batch techniques (e.g., dilution method) to observe short-term (< 24 h) P desorption processes from soils and soil components have reported that the process was often biphasic (a fast initial desorption followed by slow desorption). Two studies examined P desorption (>120 h) on synthetic goethite and ferrihydrite using batch dilution techniques (diluting the reacted samples at a constant ionic strength) (Madrid and Posner, 1979; Ryden and Syers, 1977). Desorption phenomena were biphasic, a fast reaction for a few hours followed by a slow reaction for over 100h (Madrid and Posner, 1979; Ryden and Syers, 1977). Biphasic P desorption phenomena were also observed for kaolinite using a similar batch technique (Bar-Yosef and Kafkafi, 1978). Overall, the desorption process was divided into a rapid and a slow first-order reaction, and the rate coefficient for the rapid reaction was about four times higher.

The traditional batch technique is not usually suitable to investigate desorption processes due to 1) possible re-adsorption of reaction products due to their accumulation in the bulk solution, 2) pH fluctuation during desorption, and 3) establishment of a different equilibrium in each dilution step. Flow systems and batch techniques that employ a "sink" for the desorbed species (e.g., ion exchange resin) prevent the build-up of the reaction products in the bulk solution, and are better kinetic methods for studying the apparent desorption behavior for long time periods (> 24 h).

An assessment of P release from iron oxide (i.e., ferrihydrite, goethite, and hematite) coated silica was investigated using a flow-through reactor containing a ferrihydrite coated sand as a sink (Freese et al., 1999). After 4400 min of desorption at pH 4, the relative amount of desorbed P = $P_{\text{desorb}} / P_{\text{sorb}}$ on the iron oxides was found to be of the order of ferrihydrite < goethite < hematite.

A proton promoted long term (> 500 h) P desorption study ($\rho = 400 \text{ g L}^{-1}$) from manure amended sandy soils was conducted using a synthetic ferrihydrite in a dialysis membrane tube as a dynamic sink to recover the reaction products (Freese et al., 1995). P in bulk solution never reached a desorption plateau after desorption periods >500 h. These data indicate that desorption would continue at considerable rates for much longer than 500 h. The same P desorption technique was applied to observe much longer desorption (> 1500 h) at lower suspension density (62.5 g L^{-1}) (Lookman, 1995). The results showed (even after 1600 h) that the amount of labile P increased with increasing P saturation index of the soils. $\alpha_o = P_{\text{ox}} / (\text{Fe}_{\text{ox}} + \text{Al}_{\text{ox}})$ (where $_{\text{ox}}$ indicates ammonium oxalate extractable value). A maximum of 70% ammonium oxalate extractable P was released after 1600h (Lookman, 1995). These two studies showed irreversibly fixed P in long-term manure amended soils.

Several kinetic models have been used to successfully describe biphasic P desorption processes on soils and soil components. These include zero-order (Onken and Matheson, 1982), first-order (Griffin and Jurinak, 1973), second-order (Kuo and Lotse, 1973), third-order (Onken and Matheson, 1982), parabolic diffusion (Evans and Jurinak, 1976), and Elovich (Atkinson et al., 1970; Chen, 1977; Chen and

Clayton, 1980). One of the reasons a single kinetic model is highly applicable to describe biphasic reactions is that experimental conditions (i.e., length of experimental periods associated with disequilibrium) are often appropriate for the assumptions of the model (Sparks, 1989). Aharoni and Suzin used heterogeneous diffusion models to describe segments of kinetic processes (initial, intermediate, and long term) (Aharoni and Suzin, 1982). Their expression was approximated by a sequence of parabolic, Elovich, and exponential equations.

1.9 Redox Effects on Phosphorus Retention/Release on Soils and Soil Components

In high P environments, P release occurs not only by simple P desorption from adsorbents but also by the dissolution of adsorbent materials. During the wet season, poor drainage can easily lead to long-term saturation of soil profiles. Such anaerobic conditions can greatly affect the retention/release of P from soil components.

Increased P solubility in saturated soils has been reported by many researchers (Diaz et al., 1993; Gale et al., 1992; Shapiro, 1957). This phenomenon may be explained by the reductive dissolution of iron in Fe-P fractions in soils (i.e., ferric phosphate solubility products (strengite), and/or adsorbed P on Fe oxides). Labile ferrous ions from both amorphous and crystalline Fe-P fractions could facilitate the P release (Margerum, 1978). The reduction of the ferric ion can also be enhanced by various organic reducing agents (ascorbate, hydroquinone, and oxalate) and microbial catalysts (Lovley, 1991). The reductive dissolution reactions of iron oxides have been

well documented using different reductants. for example. ascorbate (Afonso et al., 1990; Postma, 1993), H₂S (Afonso and Stumm, 1992), phenolic reductants (LaKind and Stone, 1989) and dithionite (Torrent et al., 1987).

1.10 Redox Effects on Arsenic Retention/Release on Soils and Soil

Components

The influence of redox potential and pH on arsenic speciation is important in the soil/water environment. In neutral oxygenated aquatic systems, As(III) oxidation has been reported to have a half-life of one year (Tallman and Shaikh, 1980) and no oxidation occurred over a 37 day period in distilled deionized water (Eary and Schranke, 1990). Arsenite oxidation in a 0.0005 M NaCl solution is stable below pH 9 after 72 h (Manning and Goldberg, 1997).

In the soil environment, As solubility is controlled not only by the redox potential but also by the types of adsorbent (i.e. Fe(III) and Mn(IV) hydr oxides) and As minerals. In general, reduced conditions and or the presence of reductants readily promote adsorbent dissolution causing the release of adsorbed As. Increased As solubility in reduced soils has been reported by many researchers (Deuel and Swoboda, 1972; Masscheleyn et al., 1991a; Masscheleyn et al., 1991b; McGeeham and Naylor, 1994), however, decreased As solubility in long-term flooded soils has also been observed (McGeeham and Naylor, 1994; Onken and Hossner, 1995). Re-adsorption of As on solids (Onken and Adriano, 1997) and co-precipitation of

$Mn_3(AsO_4)_2$ like phases (Masscheleyn et al., 1991b) might decrease As solubility under long-term and moderately reduced conditions (0 – 100 mV).

The influence of the redox potential on As solubility from several metal-arsenate minerals was investigated in a Santa silt loam soil from northern Idaho using an equilibrium thermodynamic study coupled with XANES analysis of arsenic oxidation. (Rochette et al., 1998). Arsenic solubility decreased in the phases under oxidized conditions ($Ca_3(AsO_4)_2 = Na_2AsO_4 > AlAsO_4 > Mn_3(AsO_4)_2 > Fe(AsO_4)_2$), however, under anoxic conditions (< 0 mV) ($Fe(AsO_4)_2 > Ca_3(AsO_4)_2 = Na_2AsO_4 > AlAsO_4 > Mn_3(AsO_4)_2$). X-ray Absorption Near Edge Structure analysis showed that aluminum arsenate is rapidly converted to solid phase arsenite, indicating the most susceptible metal-arsenate phase in the reduced condition.

Arsenite(As(III)) can be oxidized to As(V) at the mineral surface and the mineral/water interface either by surface catalysis or direct surface oxidation. The oxidized As(V) interacts more with mineral surfaces due to higher negative charge, resulting in strong retention.

Foster and co-workers observed photo-and non-photo-catalyzed As(III) oxidation at the surface of Georgia kaolinite and Wyoming smectite due to Ti and Mn impurities (Foster et al., 1998). The rate of oxidation was proportional to the length of the equilibration time, light exposure and the concentration of oxygen. An XANES study showed As(III) oxidation at goethite surfaces (Initial pH 7, and $\Gamma=150\mu\text{mol/g}$) after 15d of aging in air (Sun and Doner, 1998). The amount of As(V) increased with increasing time, up to 30d. Since the samples were aged in air, the authors could not

suggest the specific oxidant which could include Fe(III), oxygen, and microbial processes.

Arsenite oxidation/retention on birnessite and Mn-containing natural materials was investigated by many researchers. The uptake of As(III) by synthetic birnessite increased with decreasing pH, and oxidation products (i.e., As(V)) were released faster than Mn(II) at a pH of 4 – 8.2 (Scott and Morgan, 1995). The reaction, which was independent of oxygen concentration, indicated that birnessite acted as a direct oxidant for As(III). The reaction rate was positively correlated to the molar ratio of $\text{MnO}_2/\text{As(III)}$, and the respective reaction order was 1.5 (Driehaus et al., 1995). In a heterogeneous system (i.e., Mn(IV) oxide containing Canadian lake sediments), As(III) oxidation was observed (Oscarson et al., 1980). An XANES spectroscopy study showed that As(III) oxidation increased with increasing amounts of Mn substitution from 0% to 10% (Sun et al., 1999). This reaction was more sensitive to temperature than to pH. The authors suggested that the surface of the Mn-substituted goethite might act like a semiconductor to delocalize electrons within the mineral structure, facilitating the oxidation of inner-sphere complexes at mineral/water interfaces.

1.11 Residence Time Effects on P and As Adsorption/Desorption from Soils and Soil Components

1.11.1 Residence Time Effects Theory

In environmental settings, it is important to consider the residence time (aging) effect on contaminant bioavailability, transport, and remediation. Soils and sediments are nearly always at disequilibrium with respect to ion transformations (Sparks, 1987). The rate of bioavailability can be reduced or increased in the environment with increasing time (Pignatello and Xing, 1995). The residence time effect has also been described as irreversible, hysteretic, and nonsingular reactions, and can be suggested by the observation of two slow reaction processes: 1) a continuous slow sorption of the adsorptive onto the adsorbent with increasing time and 2) a slow desorption of the adsorptive from the adsorbent with increases in time.

A slow adsorption process usually occurs after an establishment of quasi-equilibrium following an initial rapid reaction for a few hours. In thermodynamics, the definition of slow desorption is that it is difficult for the desorptive to overcome the total activation energy created during adsorption. In other words, the activation energy of desorption is less than the sum of the activation energy for adsorption and the formed energy during adsorption ($E_{\text{desorption}} \ll E_{\text{adsorption}} + \Delta H$, where $E_{\text{desorption}}$ = activation energy for desorption, $E_{\text{adsorption}}$ = activation energy for adsorption (≥ 0), and ΔH = formed energy during adsorption)(McBride, 1991). Formation of inner-sphere complexes via ligand exchange and or the transformation of amorphous to crystalline materials generate a greater ΔH , increasing the value of the total activation energy. The slow adsorption/desorption phenomena are attributed not only to chemical factors (chemisorption) but also to physical factors (diffusion). Ions trapped in meso-pores (inter-particle) between aggregates and micro-pores (intra-particles)

within an individual particle fissure are difficult to extract/desorb with any desorptive (e.g., pore water). Continuous slow adsorption of P and As on soils and soil components (i.e., amorphous $\text{Al}(\text{OH})_3$, natural allophane, ferrihydrite, hematite, goethite, $\alpha\text{-Al}_2\text{O}_3$ and kaolinite) were reported by many researchers over different time scales (hours to months) (Anderson et al., 1976; Barron and Torrent, 1995; Barrow, 1974; Barrow, 1985; Beek and van Riemsdijk, 1982; Black, 1942; Colemann, 1944; Edzwald et al., 1976; Fuller et al., 1993; Hingston et al., 1974; Hsu and Rennie, 1962; Kafkafi et al., 1967; Madrid and Posner, 1979; Okajima et al., 1983; Parfitt, 1979; Parfitt, 1989; Ryden and Syers, 1977; van Riemsdijk et al., 1977; Willett et al., 1988).

In early P research, Australian researchers have compared P adsorption and desorption processes on soils and soil components, investigating the hysteresis effect, in which an adsorption isotherm curve does not coincide with a desorption isotherm curve. Using a batch equilibrium study (< 24 h), Barrow showed the slight shifts between adsorption and desorption isotherm curves on an Australian sandy loam (Barrow, 1983b). Ryden and Syers utilized the same experimental approaches to compare the P hysteresis effect on soils and ferrihydrite. Desorption isotherm curves on the soils and ferrihydrite were greatly shifted from adsorption isotherm curves, and ferrihydrite showed greater irreversibility than the soils (Ryden and Syers, 1977). The concentration effect on hysteresis was also investigated. A wide range of initial P ($[\text{P}]_0 = 0.001\text{-}1\text{ mM}$) was reacted with kaolinite, and then the desorption was

investigated using isotopic exchange (Kafkafi et al., 1967). A hysteresis effect was observed over all concentration ranges.

Incubation time highly influences the reversibility of adsorbed P and As(V) from soils and soil components. Barrow reported that P desorption from Australian soils was rapid when aging time was short (< 24 h), but the desorption process became much slower when aging time was longer (> 24 h) (Barrow, 1979a; Barrow and Shaw, 1975). Madrid observed similar irreversible P desorption from goethite (Madrid and Posner, 1979). P desorption decreased with increasing aging time from 1h to 23h. Aging effects on the As(V) fraction of three different Maryland soils (silty clay loam, sandy loam, and fine sand) were investigated (Woolson et al., 1973). Moist soils were spiked with 100-1.667 $\mu\text{g As(V) g}^{-1}$ soil for up to 36 weeks. 1M NH_4Cl extractable As(V) decreased with increasing aging time in all soils. Lin and Puls also reported that irreversible As(V) on the clay mineral surfaces (halloysite, kaolinite, illite, montmorillonite, and chlorite) (Lin and Puls, 2000). The As(V) recovery decreased with increasing aging time from 1 to 75d, and the effects were most pronounced in halloysite and kaolinite. A similar study was also conducted on a synthetic goethite and Australian clay loam using longer desorption experiments (> 96 h) and varying incubation time. The irreversibility was enhanced with increasing aging time (Barrow, 1979a; Madrid and Posner, 1979). The irreversibility could also occur within a short adsorption reaction (< 15 sec). The pressure-jump relaxation study showed that the rate constants for the As(V) adsorption reactions on goethite

exceeded those for desorption, indicating that the desorption of As(V) from the goethite surface was the rate-limiting process (Grossl and Sparks, 1995).

The mechanisms responsible for the residence time effect are not clearly defined, however, they have been ascribed to, 1). Solid-state diffusion, or intra- and inter-pore diffusion, 2). Surface precipitation and 3). Higher energy binding on surface structures through chemical reconfiguration (Beek and van Riemsdijk, 1982; Fendorf et al., 1992; Pignatello and Xing, 1995).

1.11.2 Solid-state, Inter-, and Intra-particle Diffusion

In situ soil chemical reactions between ions and solids are ultimately limited by the process of diffusion (McBride, 1994b). For example, if the initial oxyanion reaction on soil materials is quickly completed, then the unreacted oxyanions build up in solution until the rate of diffusion of oxyanions in the adsorbents equals the overall reaction rate. Fast chemisorption (i.e., inner-sphere complexation) takes place at external sites where ions in the bulk fluid can easily access the sites. The slow adsorption processes occur at sites within soil particle aggregates, and are often controlled by diffusion processes. Four different diffusion processes have been proposed: film, meso-pore (≈ 2 nm), micro-pore (< 2 nm), and solid state diffusion (Pignatello and Xing, 1995). Film diffusion involves the transport of an ion or molecule through a boundary layer or film (water molecules) that surrounds the particle surface (Sparks, 1995a). Meso-pore (inter-particle) diffusion takes place between aggregates. Micro-pore (intra-particles) diffusion involves ion penetration at

the inside of an individual particle fissure. Solid-state diffusion involves diffusion in the solid, and it can be a rate-limiting step for all diffusion processes. The rate of these diffusion processes is dependent on the size and chemical properties of the diffusant, and the size, shape, tortuosity, and discontinuity of the particle pores (Pignatello and Xing, 1995).

One way to investigate the diffusion process is to model slow adsorption processes using models accounting for diffusion reactions.

Several modeling studies have indirectly suggested P solid-state meso-pore and micro-pore diffusion processes in natural materials (Barrow, 1983a; Enfield et al., 1981; van Riemsdijk et al., 1984). In an early P adsorption modeling study, Barrow developed a mechanistic model to describe slow P adsorption processes on soils (Barrow, 1983a). The model had three components 1) the reaction between phosphate ions and variable charge mineral surfaces, 2) the assumption that soils consisted of an assemblage of elements each with different values for the binding constant and or initial electrostatic potential, and 3) the assumption that the solid-state diffusion processes are driven by the gradients of electrical and chemical potentials at the adsorbent surface (Manning, 1968; Rickert, 1982). As a result, the model closely described P adsorption processes as influenced on concentration, pH, temperature, and reaction time. It suggested that long-term (≈ 90 d) P adsorption is predominantly attributed to P penetration into the soil particles. In a later study Bolan (1985) utilized Barrow's mechanistic model to describe slow P adsorption processes on soil components (i.e., amorphous iron and aluminum oxides) (Bolan et al., 1985). Models

that fit the data well. indirectly suggested that a slow uptake of P was caused by redistribution of P into the interior of amorphous metal oxide particles by solid-state diffusion. A similar model successfully described the continuous P sorption on ferric hydroxide gel (Ryden et al., 1977a). While Barrow's mechanistic model has been extensively used to describe oxyanion adsorption phenomena, other models have also been utilized to investigate slow adsorption processes.

The slow As(V) adsorption kinetics on ferrihydrite at pH \approx 8 was modeled using a diffusion-limited adsorption model (Pore-space diffusion model) described by Curtis (Curtis, 1991; Fuller et al., 1993). The adsorption data were fit well suggesting that the rate limiting processes were due to As(V) diffusion to adsorption sites with ferrihydrite aggregated particles. The slow reaction was not due to surface precipitation as only two-dimensional surface complexes were evident by XAFS analysis (Waychunas et al., 1993). Other researchers applied a multiple site first-order-model to describe an initial fast reaction step followed by a slower diffusion (assuming the reaction is transport-limited) on reaction for sorption of organic chemicals on soils (Ball and Roberts, 1991; Pignatello et al., 1993; Steinberg et al., 1987).

While these modeling approaches indirectly suggest a diffusion controlled reaction, they do not provide any information on what soil physical properties (e.g., crystallinity of adsorbents) are associated with slow adsorption. Several researchers have pointed out that slow adsorption processes could be affected by crystallinity and particle morphology.

P adsorption on goethite and lepidocrocite was compared using a batch adsorption technique (Cabrea et al., 1981). Lepidocrocite exhibited more pronounced continuous slow sorption than goethite, and adsorbed P was more irreversible in lepidocrocite. Cabrea suggested that the enhanced slow reaction and irreversibility were attributed to P micro-pore diffusion into the less crystalline nature of lepidocrocite particles. Parfitt (1989) also indirectly suggested that P particle diffusion was caused by poor crystallinity and the greater porosity of metal oxides (Parfitt, 1989). A comparison of 1d and 30d P sorption isotherm experiments showed that slow P sorption was observed in only amorphous goethite and ferrihydrite and not in highly crystalline goethite (Parfitt, 1989). Later Torrent and co-workers (1992) conducted experiments that supported the above findings. The slow P adsorption on 10 goethite rich soils was described using a modified Freundlich equation including a rate term (Torrent et al., 1992). The study showed that the extent of the slow continuous reaction was correlated to the ratio between micropore surface area and total surface area, as well as impurities due to amorphous Fe oxides (ammonium oxalate extractable iron). Willet and co-workers (1988) found 1) long-term (> 200 d) adsorption and 2) rapid (< 24 h) migration of phosphate (meso-pore diffusion) into the aggregated particles of ferrihydrite using electron microprobe analyses (Willet et al., 1988). Long-term P adsorption kinetics at pH 4 showed an initial fast reaction followed by slow sorption up to 260d, and a maximum sorption capacity of approximately 1.2 mM g^{-1} . The distribution of P moved toward the core of ferrihydrite aggregate particles as time increased from 1h to 1d.

Recent electron microscopic studies have also showed that the crystalline morphologies of goethite are related to P irreversibility (Torrent et al., 1990). After sequential acid (5 M HCl and 0.5 M H₂SO₄) / base (0.1 M KOH) extractions of adsorbed P from 31 different goethite, the amount of nonextractable P (P was adsorbed at pH 6 for 24 h) was correlated to the observation of solid morphologies [thin, multidomainic laths (V-shaped interdomainic grooves) and slit-shaped macropores of multidomainic laths].

The diffusion control reaction can also be suggested by a low energy of activation (< 42 kJ mol⁻¹). E (Sparks, 1989). The result of a temperature dependent sorption/desorption reaction can be applied to the Arrhenius equation ($k = A e^{-E/RT}$) to obtain E (Sparks, 1989). The activation energy of the slow reaction between phosphate and different morphologies of goethite was investigated (Torrent, 1991). The slow sorption was described by a modified Freundlich equation including time and activation energy (E) terms. Activation energy values ranged from 38 to 80 kJ mol⁻¹ suggesting the P sorption reaction might involve a penetration of P into the different crystalline matrices.

1.11.3 Surface Precipitation

Whereas an adsorption complex has a two-dimensional surface structure, surface precipitates involve a three-dimensional growth of the adsorbate on the adsorptive surface. The magnitude of the precipitation growth is a function of the saturation of the adsorbate in the bulk fluid. When the adsorbate is supersaturated

with respect to the precipitate in the bulk fluid, a bulk precipitate forms rapidly. However, when the system is even undersaturated with respect to the bulk precipitate, precipitates could still form. Such a precipitate is called a surface precipitate.

Surface precipitates are categorized into one of three groups based on formation mechanisms. They are 1) Polymerization of the adsorptive at the surface, 2) Coprecipitation which forms between dissolved coions and the adsorbate in the bulk fluid, and 3) Precipitates composed of ions from the bulk fluid (e.g., hydrolysis products) (Chisholm-Brause et al., 1990; Farley et al., 1985). Polymerization occurs as the result of continued chemisorption. Newly created sites, by monolayer coverage of the adsorbate, facilitates the formation of the precipitates (multilayer surface coverage). Coprecipitation processes can also be facilitated by an increase in the surface coverage of adsorbent, and then the precipitation of adsorbate ions form with dissolved coions of the solids (Sparks, 1995b).

Several hypotheses have been suggested to describe the formation of surface precipitates on clays and clay minerals.

The first theory states that the dielectric constant of the solution near the surface is less than that of the bulk fluid because the mineral surfaces are polar due to the dipole moment of adsorbed water molecules (O'Day et al., 1994). Since the activity of the ions in the bulk fluid is inversely proportional to the dielectric constant of water, the lowered dielectric constant can induce the ion activity products.

The second theory states that the activity of the solid phase is less than unity (Sposito, 1986). The activity of the pure solid (i.e. FePO_4) can be assumed to be one.

however, if a mixed solid ($\text{Fe}_x\text{Al}_{1-x}\text{PO}_4$) is formed, the activity is less than one. $\text{Fe}_x\text{Al}_{1-x}\text{PO}_4$ will precipitate prior to FePO_4 . The following empirical equation describes formation of the surface precipitate which is favored over the pure solubility products. $(\text{IAP})_i = g_i X_i K_i^{so}$ where g_i is the activity coefficient of the solids, X_i is the mole fraction of the solid and K_i^{so} is the bulk precipitate of the pure minerals i (van Riemsdijk and Lyklema, 1980).

The third theory states that sterically similar sites promote further nucleation (McBride, 1991). Sterically similar sites indicate that the crystal lattice have energy barriers which are reduced to facilitate nucleation processes.

While mechanisms and theories have been postulated on the formation of surface precipitates, many researchers have reported indirect (macroscopic data) and direct (spectroscopic data) evidence for aluminum and iron P surface precipitates on metal oxides and clays.

Chen and Stumm (1973) indirectly suggested a nucleation of a new P containing phase (i.e., P surface precipitate) at the kaolinite/water interfaces (Chen et al., 1973). They observed a disequilibrium phenomenon for the P adsorption envelope on kaolinite where the adsorption maximum at pH 4 increased with increasing time from 1d to 23d when P in the bulk solution was undersaturated with respect to aluminum phosphate. Van Riemsdijk and Lykema (1980) also suggested that P adsorption on gibbsite resulted in the formation of a potassium aluminum phosphate precipitate. This was due to 1) the increase in the rate of excess sorption (i.e., beyond monolayer coverage) with increasing supersaturation, 2) enhanced P adsorption with

increasing potassium in the bulk solution. and 3) increased surface area after P adsorption (van Riemsdijk and Lyklema, 1980).

Direct evidence for P surface precipitates have been suggested from microscopic and spectroscopic investigations. Electron microscopy, electron diffraction, and XRD were utilized to investigate long-term (40days) P sorption on amorphous $\text{Al}(\text{OH})_3$ and $\alpha\text{-Al}_2\text{O}_3$ at pH 5. Researchers observed the formation of a new solid aluminum-phosphate mineral (Sterrettite-like) at aluminum oxide surfaces (van Riemsdijk et al., 1977). Nanzyo (1984 and 1986) investigated P adsorption on amorphous aluminum and iron oxides over a wide pH range (approximately 4-9) using diffuse reflectance infrared spectroscopy (Nanzyo, 1984; Nanzyo, 1986). He suggested that the formation of amorphous aluminum phosphate-like and amorphous iron phosphate-like products increased with decreasing pH based on the observation of similar IR spectra between the adsorption complex and synthetic minerals (i.e., aluminum phosphate and iron phosphate). X-ray photoelectron spectroscopy (XPS), scanning transmission electron microscopy (STEM), and X-ray diffraction (XRD) investigations have shown that a mixture of goethite and tincite ($\text{Fe}_4(\text{PO}_4)_4(\text{OH})_6 \cdot 7\text{H}_2\text{O}$) are formed after 18d of P adsorption (25°C and $[\text{P}]_0 = 0.01 \text{ mM L}^{-1}$) at pH 3 (Jonasson et al., 1988). Multi-spectroscopic techniques (Auger, XPS, scanning SIMS, and TEM) have been applied to investigate P adsorption on natural goethite ($[\text{P}]_0 = 1 \text{ mM}$, 90 d, and 60°C) (Martine et al., 1988). The mineral griphite, $(\text{Fe}_3\text{Mn}_2(\text{PO}_4)_{2.5}(\text{OH})_2)$ was found in isolated crystallites. Martine and co-workers suggested that P fixation in soils could be controlled by

precipitation reactions on Fe oxides. Similarly Wang and Tzou (1995) observed a Fe-P precipitate-like compound on a P reacted hematite surface (Wang and Tzou, 1995). *Ex situ* Mössbauer analysis showed quadrupole splitting for P adsorbed hematite ($[P]_0 = 155 \text{ mg g}^{-1}$, pH 3, 24 h, and 298 K). Such splitting resembled the spectra observed for vivianite ($\text{Fe(II)}_3(\text{PO}_4)_2$) and strengite ($\text{Fe(III)}(\text{PO}_4)$) (McCammon and Burn, 1980; Wang, 1987). Since XRD analysis did not detect the mineral phase, the mineral phase is presumed to be amorphous.

Slow P adsorption on allophane with continuous silicon release has been indirectly linked to a precipitation reaction by many researchers. A reaction with P caused a disruption in the allophane structure by displacing structural silicon. Exposed reactive sites might facilitate P precipitation as aluminum phosphate (Nanzyo, 1987; Parfitt, 1989; van Riemsdijk and Lyklema, 1980). Induced silicon release during phosphate adsorption has also been reported on soils and natural clay minerals (i.e., kaolinite, natural allophane, ferrihydrite, goethite and allophanic clay) (Low and Black, 1950; Mattson and Hester, 1935; Parfitt, 1989; Reifenberg and Buckwold, 1954). Rajan observed silicon release during P adsorption on allophanic clay which was pre-treated with selenite to remove labile silicate (Rajan, 1975). Phosphorus isomorphic substitution of structural silicon in allophanic clay has been also suggested. Veith and Sposito (1977) also reported the formation of aluminum phosphate surface precipitates on allophanic materials after P adsorption (Veith and Sposito, 1977). The formation of X-ray amorphous analogs of variscite and Namontebasite were demonstrated by reacting $\text{Al}_2\text{O}_3 \cdot n\text{H}_2\text{O}$, synthetic allophanes, and

allophanic soils with P at varying acidity. The formation of amorphous Al-phosphates was favored by both the large values of the hydration number in $\text{Al}_2\text{O}_3 \cdot n\text{H}_2\text{O}$ and the increase in the acidity of the added P solution. The formation of amorphous Al-phosphate by secondary precipitates has been indicated by 1) An observed slow reaction rate between P and Al-coatings. 2) The immediate and significant increase of silicate in solution when aluminosilicate minerals were reacted. and 3) A significant amount (above monolayer coverage) of P adsorption.

While numerous macroscopic, microscopic, and spectroscopic studies have speculated on the formation of P surface precipitates at mineral surfaces, there are some questions about these findings. These doubts have been raised because: 1) chemical speciation of surface precipitates can not be elucidated by macroscopic data. 2) high (> 1 mM) P concentration might cause a supersaturated condition with respect to bulk precipitates. and 3) *ex situ* conditions in XRD, XPS, SEM, and TEM analyses might create artifacts with residual P in the samples. Macroscopic and microscopic data must be carefully combined with *in situ* spectroscopic techniques to draw better conclusions about the formation of surface precipitates.

1.11.4 Higher Energy Binding through Chemical Reconfiguration

Real soil environments are not in equilibrium and always undergo slow chemical changes to reach equilibrium (Koskinen and Harper, 1990; Steinfield et al., 1989). As the materials become more stable (i.e., lowering solubility or resulting multidentate complexes) with increasing aging time through transformations, the

release of the adsorbate becomes slower, as evidenced by slow desorption phenomena. Lowering the Gibbs free energy with increasing entropy converts the products to more stable compounds. As a result, the activation energy of the desorption phenomena can be expressed as $E_d = E_a + Q$.

This theory can be categorized into two groups. They are 1) a chemical transformation from two-dimensional surface complexes to three-dimensional precipitates and 2) a reconfiguration within two-dimensional surface complexes.

Ostwald-step rule chemical transformation theory proposes that the nucleation process involves the formation of the least stable solid phase (highly soluble amorphous materials) first followed by the formation of a more stable solid phase (insoluble crystalline materials) (Stumm and Morgan, 1995a).

The stability of the surface complexes can be altered from monodentate to multidentate configuration with increasing time. The more that bonds are associated with the surface functional group of the solid, the greater the stability. The chemical transformation from mononuclear to binuclear bridging complexation was suggested to describe the hysteresis phenomena for P adsorption on soils and soil components (Kafkafi et al., 1967; Mengel, 1985), however, there is no molecular scale evidence to support this chemical reconfiguration theory.

1.12 Research Justification:

Arsenic and phosphate are ubiquitous in soil/water environments due to indigenous sources and anthropogenic inputs. Over the past few decades, excessive

levels of P and As in surface and ground water have become serious environmental issues in the U.S. The reactivity and the speciation of P and As in soil/water environments must be well understood to enable one to predict fate and transport. Such an understanding can greatly assist in developing sound remediation strategies and formulating regulations for effectively reducing the impact of P and As in aquatic/terrestrial environments.

In the past, equilibrium macroscopic and *ex situ* (evacuated and dry) spectroscopic investigations have been extensively performed to understand the retention/release of P and As at mineral-water interfaces. Data interpretation based on these studies, however, has not resulted in a precise understanding of the reactivity, adsorbate speciation at mineral-water interfaces, mobility, and bioavailability of P and As due to the following four reasons.

- 1) Adsorption complexes cannot be speciated based solely on macroscopic evidence.
- 2) Short-term (< 24 h) equilibration studies do not often apply to natural systems (e.g., soils and sediments) for predicting the fate of oxyanions because ion transformations at the mineral/water interface are nearly always at disequilibrium with respect to time.
- 3) *Ex situ* experimental conditions do not simulate actual field conditions. It is fundamental to study soil chemical reactions (e.g., determination of surface complexes) under near field conditions (i.e., *in situ*).

4) Lack of adsorption/desorption kinetics measurements. In order to predict the transport of pollutants in a natural system, one must measure the rate of adsorption/desorption over a wide range of reaction times (< 24 h and > 24 h). The residence time (>24 h) effect is especially important, because contaminant availability can be reduced or increased in the environment with increasing time.

In this study, macroscopic, microscopic and spectroscopic studies were effectively combined to investigate the reaction dynamics and surface speciation of P and As(III and V) at the metal oxide-water interface and in soils. This comprehensive approach provided more precise data to understand P and As reactivity in soils than employing only one technique. Novel data obtained from state-of-the-art *in situ* spectroscopic techniques (i.e., Attenuated Total Reflectance-Fourier Transform Infrared Spectroscopy and X-ray Absorption Spectroscopy) provided better insights for comprehending molecular scale chemical speciation at the soil mineral-water interface. Adsorption/desorption kinetic measurements over a wide range of reaction times enable one to better predict the stability of P and As in natural systems. Overall a better understanding of P and As retention/release mechanisms from soils will significantly enhance sustainable agricultural management and the development of effective remediation strategies to improve human and ecological health.

1.13 Research Objectives

The specific systems studies, and the corresponding research objectives were the following:

- 1) To investigate P surface speciation at the ferrihydrite ($\text{Fe}(\text{OH})_3$)-water interfaces using ATR-FTIR and electrophoretic mobility measurements.
- 2) To investigate As(III and V) surface speciation at the bayerite($\text{Al}(\text{OH})_3$)-water interface using EXAFS and electrophoretic mobility measurements.
- 3) To investigate the residence time effect on P adsorption mechanisms and desorption at the ferrihydrite-water interface using ATR-FTIR and P K-edge XANES spectroscopy.
- 4) To investigate the residence time effect on As(V) adsorption mechanisms and desorption at the bayerite-water interface using EXAFS spectroscopy.
- 5) To investigate As solid-state speciation in industrially contaminated landfill materials using multi-scale spectroscopic techniques (X-ray diffraction, synchrotron based *in situ* XRF, microfocused- and bulk-XANES, and bulk EXFAFS).

1.14 References

Adriano, D.C., 1986. Trace elements in the terrestrial environment. Springer-Verlag New York Inc.

Afonso, M.D.S., Morando, P.J., Blesa, M.A., Banwart, S. and Stumm, W., 1990. The reductive dissolution of iron oxides by ascorbate. *Journal of Colloid and Interface Science*, 138(1): 74-82.

Afonso, M.d.S. and Stumm, W., 1992. Reductive dissolution of iron(III) (hydr)oxides by hydrogen sulfide. *Langmuir*, 8: 1671-1675.

Aharoni, C. and Suzin, Y., 1982. Application of the Elovich equation to the kinetics of chemisorption. Part 3. Heterogeneous microporosity. *Journal of Chemical Society Faraday Transaction 1*, 78: 2329-2336.

Anderson, M.A., Ferguson, J.F. and Gavis, J., 1976. Arsenate adsorption on amorphous aluminum hydroxide. *Journal of Colloid and Interface Science*, 54: 391-399.

Anderson, M.A. and Malotky, D.T., 1979. The adsorption of protolyzable anions on hydrous oxides at the isoelectric pH. *Journal of Colloid and Interface Science*, 72(3): 413-427.

Andres, A.S.. 1991. Results of the coastal Sussex county, Delaware ground-water quality survey, 49. 29. Delaware geological survey.

Atkinson, R.J., Hingston, F.J., Posner, A.M. and Quirk, J.P., 1970. Elovich equation from the kinetics of isotopic exchange reactions at isotopic exchange reactions at solid-liquid interfaces. *Nature*, 226: 148-149.

Atkinson, R.J., Parfitt, R.L. and Smart, R.S.C., 1974. Infrared study of phosphate adsorption on goethite. *Journal of Chemical Society Faraday Transaction*, 1, 70: 1472-1479.

Ball, W.P. and Roberts, P.V., 1991. Long-term sorption of halogenated organic chemicals by aquifer material. 2. Interparticle diffusion. *Environmental Science and Technology*, 25: 1237-1249.

Barron, E.A.V. and Torrent, J., 1995. Organic matter delays but does not prevent phosphate sorption by cerrado soils from Brazil. *Soil Science*, 159(3): 207-211.

Barrow, N.J., 1974. The slow reactions between soil and anions. 1. Effects of time, temperature, and water content of a soil on the decrease in effectiveness of phosphate for plant growth. *Soil Science*, 118: 380-386.

Barrow, N.J., 1979a. The description of desorption of phosphate from soil. *Journal of*

Soil Science, 30: 259-270.

Barrow, N.J., 1979b. Three effects of temperature on the reactions between inorganic phosphate and soil. *Journal of Soil Science*, 30: 271-279.

Barrow, N.J., 1983a. A mechanistic model for describing the sorption and desorption of phosphate by soil. *Journal of Soil Science*, 34: 773-750.

Barrow, N.J., 1983b. On the reversibility of phosphate sorption by soils. *Journal of Soil Science*, 34: 751-758.

Barrow, N.J., 1985. Reactions of anions and cations with variable-charge soils. *Advances in Agronomy*, pp. 183-230.

Barrow, N.J., 1987. Reactions with variable-charge soils. *Developments in Plant and Soil Sciences*, Martnus Nijhoff Publishers, Dordrecht / Boston / Lancaster.

Barrow, N.J., Bowden, J.W., Posner, A.M. and Quirk, J.P., 1980. Describing the effects of electrolyte on adsorption of phosphate by a variable charge surface. *Australian Journal of Soil Research*, 18: 395-404.

Barrow, N.J. and Shaw, T.C., 1975. The slow reactions between soils and anions: 2.

Effect of time and temperature on the decrease in phosphate concentration in the soil solution. *Soil Science*, 119(2): 167-177.

Barrow, N.J. and Shaw, T.C., 1977. The slow reactions between soil and anions: 6. effect of time and temperature of contact on fluoride. *Journal of Soil Science*. 124(5): 265-278.

Bar-Yosef, B. and Kafkafi, U., 1978. Phosphate desorption from kaolinite suspensions. *Soil Science Society of America Journal*, 42: 570-574.

Beek, J. and van Riemsdijk, W.H., 1982. Interactions of orthophosphate ion with soil. In: G.H. Bolt (ed.), *Soil chemistry B. Physico-chemical models*. Elsevier Sci. Publ. Co., Amsterdam, pp. 259-284.

Benjamin, M.M. and Bloom, N.S., 1981. Effects of strong binding of anionic adsorbates on adsorption of trace metals on amorphous iron oxyhydroxide. In: P.H. Tewari (ed.), *Adsorption from aqueous solution*. Plenum, New York, pp. 41-60.

Black, C.A., 1942. Phosphate fixation by kaolinite and other clays as affected by pH, phosphate concentration, and time of contact. *Soil Science Society Proceedings*: 123-133.

Bleam, W.F., Pfeffer, P.E., Goldberg, S., Taylor, R.W. and Dudley, R., 1991. A ^{31}P solid-state nuclear Magnetic resonance study of phosphate adsorption at the boehmite/aqueous solution. *Langmuir*, 7: 1702-1712.

Bloom, P.R., 1981. Phosphorus adsorption by an aluminum-peat complex. *Soil Science Society of America Journal*, 45: 267-272.

Bolan, N.S., Barrow, N.J. and Posner, A.M., 1985. Describing the effect of time on sorption of phosphate by iron and aluminium hydroxides. *Journal of Soil Science*, 36: 187-197.

Bowden, J.W., Nagarajah, S., Barrow, N.J., Posner, A.M. and Quirk, J.P., 1980. Describing the adsorption of phosphate, citrate and selenite on the variable charge mineral surface. *Australian Journal of Soil Research*, 18: 49-60.

Bowman, R.A., 1989. A sequential extraction procedure with concentrated sulfuric acid and dilute base for soil organic phosphorus. *Soil Science Society of America Journal*, 53: 362-366.

Braman, R.S., 1983. Environmental reaction and analysis method. In: B.A. Fowler (ed.), *Biological and environmental effects of arsenic*. Ch.3 Topics in environmental health. Elsevier Science Publishers, New York, pp. 141-154.

- Brookes, P.C., Heckrath, G., Smet, J.D., Hofman, G. and Vanderdeelen, J., 1997. Losses of phosphorus in drainage water. In: O.T.C. H. Tunney, P.C. Brookes and A. E. Johnston (ed.), Phosphorus loss from soil to water. CAB International, Wallingford, New York, pp. 253-271.
- Burkholder, J.M. and Glasgow Jr., G.B., 1997. *Pfiesteria piscicida* and other *Pfiesteria*-like dinoflagellates: Behavior, impacts, and environmental controls. *Limnology and Oceanography*, 42(5): 1052-1075.
- Cabrea, F., Arambarri, P.D., Madrid, L. and Toca, C.G., 1981. Desorption of phosphate from iron oxides in relation to equilibrium pH and porosity. *Geoderma*, 26: 203-216.
- Cathcart, J.B., 1980. World phosphate reserve and resources. In: F.E. Khasawneh, E.C. Sample and E.J. Kamprath (eds.), *The Role of Phosphorus in Agriculture*. Soil Science Society of America, American Society of Agronomy, Crop Science Society of America, Madison, Wisconsin, pp. 1-18.
- Chen, S.H., 1977. Dissolution rates of phosphate rocks. *Soil Science Society of America Proceedings*, 41: 656-657.

Chen, S.H. and Clayton. W.R., 1980. Application of Elovich equation to the kinetics of phosphate release and sorption by soils. *Soil Science Society of America Journals*, 44: 265-268.

Chen, Y.R., Butler. J.N. and Stumm. W., 1973. Adsorption of phosphate on almina and kaolinite from dilute aqueous solutions. *Journal of Colloid and Interface Science*, 43(2): 421-436.

Chien. S.H., Savant. N.K. and Mokwunye. U., 1982. Effect of temperature on phosphate sorption and desorption in two acid soils. *Soil Science*, 133(3): 160-166.

Chisholm-Brause. C.J. et al., 1990. Spectroscopic investigation of Pb(II) complexes at the γ -Al₂O₃/water interfaces. *Geochimica et Cosmochimica Acta*, 54: 1897-1909.

Colburn. P., Aloway, B.J. and Tompson. I., 1975. Arsenic and heavy metals in soil associated with regional geochemical anomalies in Southwest England. *Sci. Total Environment Science*, 4: 359-363.

Colemann. R., 1944. The mechanism of phosphate fixation by montmorillonitic and kaolinitic clays. *Soil Science Society of America Proceedings*, 9: 72-78.

Cooked, G.W., G. E. G. Mattingly and Williams, R.J.B., 1958. Changes in the soil of

a long continued field experiment at Saxmundham, Suffolk. *Journal of Soil Science*, 9: 298-305.

Cummings, D.E., F. Caccavo, J., Fendorf, S. and Rosenzweig, R.F., 1999. Arsenic mobilization by the dissimatory Fe(III)-reducing bacterium *shewanella alga* BrY. *Environmental Science and Technology*, 33(5): 723-729.

Curtis, G., 1991. Reductive dehalogenation of hexachloroethane and carbon tetrachloride by aquifer sand and humic acid. Ph.D. Dissertation Thesis, Stanford University.

DaCosta, E.W.B., 1972. Variation in the toxicity of arsenic compounds to microorganisms and the suppression of the inhibitory effects by phosphate. *Applied Microbiology*, 23: 46-53.

Dalal, R.C., 1977. Soil organic phosphorus. *Advances in Agronomy*, 29, pp. 83-117.

Deuel, L.E. and Swoboda, A.R., 1972. Arsenic solubility in a reduced environment. *Soil Science Society of America Proceedings*, 36: 276-278.

Diaz, O.A., Anderson, D.L. and Hanlon, E.A., 1993. P mineralization from histosols of the everglades agricultural area. *Soil Science*, 156: 178-185.

Driehaus, W., Seith, R. and Jekel, M., 1995. Oxidation of arsenate(III) with manganese oxides in water treatment. *Water Research*. 29(1): 297-305.

Dzombak, D.A. and Morel, F.M.M., 1990. Surface complexation modeling: hydrous ferric oxide. Willey, New York.

Eary, L.E. and Schranke, J.A., 1990. Chemical modeling of aqueous systems II. 416. American Chemical Society, Washington, DC. 379-396 pp.

Edwards, D.R. and Daniel, T.C., 1992. Environmental impacts of on-farm poultry waste disposal - a review. *Bioresource Technology*. 41: 9-33.

Edzwald, J.K., Toensing, D.C. and Leung, M.C., 1976. Phosphate adsorption reaction with clay minerals. *Environmental Science and Technology*. 10(5): 485-490.

Enfield, C.G., Phan, T., Wolters, D.M. and R. Ellis, J., 1981. Kinetic model for phosphate transport and transformation in calcareous soils I. and II. *Soil Science Society of America Journal*. 45: 1059-1064.

Evans, R.L. and Jurinak, J.J., 1976. Kinetics of phosphate release from a desert soil. *Soil Science*, 121(4): 205-211.

Farley, K.J., Dzombak, D.A. and Morel, F.M.M., 1985. A surface precipitation model for the sorption of cations on metal oxides. *Journal of Colloid and Interface Science*, 106: 226-242.

Faust, S.D. and Aly, O.M., 1981. *Chemistry of natural waters*. Ann Arbor Science publishers, Inc., Ann Arbor, Michigan.

Fendorf, S., Sparks, D.L. and Fendorf, M., 1992. Surface precipitation reactions on oxide surfaces. *Journal of Colloid and Interface Science*, 148: 295-298.

Fendorf, S.E., Eick, M.J., Grossl, P. and Sparks, D.L., 1997. Arsenate and chromate retention mechanisms on goethite. 1. Surface structure. *Environmental Science and Technology*, 31(2): 315-320.

Fordham, A.W. and Norrish, K., 1979. Arsenate-73 uptake by components of several acidic soils and its implications for phosphate retention. *Australian Journal of Soil Research*, 17: 307-316.

Foster, A.L., G. E. Brown, J. and Parks, G.A., 1998. X-ray absorption fine structure spectroscopy study of photocatalyzed, heterogeneous As(III) oxidation on kaoline and anatase. *Environmental Science and Technology*, 32: 1444-1452.

Freese, D., R. Lookman, R. Merckx and Riemsdijk, W.H.v., 1995. New method for assessment of long-term phosphate desorption from soils. *Soil Science Society of America Journal*, 59: 1295-1300.

Freese, D., Weidler, P.G., Grolimund, D. and Sticher, H., 1999. A flow-through reactor with an infinite sink for monitoring desorption processes. *Journal of Environmental Quality*, 28: 537-543.

Fried, C.R. and Shapiro, G., 1956. Phosphate supply pattern of various soils. *Soil Science Society of America Proceedings*, 20: 471-475.

Frost, R.R. and Griffin, R.A., 1977. Effect of pH on adsorption of arsenic and selenium from landfill leachate by clay minerals. *Soil Science Society of America Journal*, 41: 53-57.

Fuller, C.C., Davis, J.A. and Waychunas, G.A., 1993. Surface chemistry of ferrihydrite: Part 2. Kinetics of arsenate adsorption and coprecipitation. *Geochimica et Cosmochimica Acta*, 57: 2271-2282.

Gale, P.M., Reddy, K.R. and Graetz, D.A., 1992. Mineralization of sediment organic matter under anoxic conditions. *Journal of Environmental Quality*, 21: 394-400.

Gao, S., Tanji, K.K. and Goldberg, S., 1997. Session 1: Potentially toxic trace elements in soils and sediments Paper 4: Reactivity and transformation of arsenic. In Agroecosystems: Sources, control, and remediation of oxyanions. In: L.M. Dudley and J. Guitjens (eds.), Symposium on sources, control, and remediation of oxyanions in agroecosystems. Proc. Symp. . Pacific Div., Am. Assoc. Adv. Sci., San Francisco.

Gee, G.W. and Bauder, J.W., 1986. Particle-size analysis. In: A. Klute (ed.), Method of soil analysis. Part 1. Physical and mineralogical methods-Agronomy monograph no.9. Soil Science Society of America, Madison, WI, pp. 383-411.

Goldberg, S. 1986. Chemical modeling of arsenate adsorption on aluminum and iron oxide minerals. Soil Science Society of America Journals, 52: 1297-1300.

Goldberg, S. 1992. Use of surface complexation models in soil chemical system. Advances in Agronomy, pp. 233-329.

Goldberg, S. and Glaubig, R.A. 1988. Anion sorption on a calcareous, montmorillonitic soil-arsenic. Soil Science Society of America Journals, 52: 1297-1300.

Goldberg, S. and Sposito, G., 1984. A chemical model of phosphate adsorption by

soils:2. Nonclacareous soils. *Soil Science Society of America Journal*. 48: 779-783.

Goldberg, S. and Sposito, G.. 1985. On the mechanism of specific phosphate adsorption by hydroxylated mineral surfaces: A review. *Communication in Soil Sciences and Plant Analysis*. 16(8): 801-821.

Goldberg, S. and Sposito, G.. 1984. A chemical model of phosphate adsorption by soils: 1. Reference oxide minerals. *Soil Science Society of America Journal*. 48: 772-778.

Griffin, E.A. and Jurinak, J.. 1973. Test of a new model for the kinetics of adsorption-desorption processes. *Soil Science Society of America Journal*. 37: 869-872.

Grossl, P.R. and Sparks, D.L.. 1995. Evaluation of contaminant ion adsorption/desorption on goethite using pressure-jump relaxation kinetics. *Geoderma*. 67: 87-101.

Grove, J.H., Fowler, C.S. and Sumner, M.E.. 1982. Determination of the charge character of selected acid soils. *Soil Science Society of America Journal*. 46: 32-38.

Gupta, S.K. and Chen, K.Y.. 1978. Arsenic removal by adsorption. *Journal. Water Pollution Control Federation*. 50: 493-506.

Hansmann, D.D. and Anderson, M.A., 1985. Using electrophoresis in modeling sulfate, selenite, and phosphate adsorption onto goethite. *Environmental Science and Technology*, 19: 544-551.

Harris, W.G., Wang, H.D. and Reddy, K.R., 1994. Dairy manure influence on soil and sediment composition: Implications for phosphorus retention. *Journal of Environmental Quality*, 23: 1071-1081.

Hayes, K.F., Papeis, C. and Leckie, J.O., 1988. Modeling ionic strength effects of anion adsorption at hydrous oxide/solution interface. *Journal of Colloid and Interface Science*, 125(2): 717-726.

He, Z.L., Baligar, V.C., Martens, D.C. and Ritchey, K.D., 1998. Determination of soluble phosphorus in the presence of organic ligands or fluoride. *Soil Science Society of America Proceedings*, 62: 1538-1541.

Helyar, K.R., Munns, D.N. and Burau, R.G., 1976a. Adsorption of phosphate by gibbsite. I. Effects of neutral chloride salts of calcium, magnesium, sodium and potassium. *Journal of Soil Science*, 27: 307-314.

Helyar, K.R., Munns, D.N. and Burau, R.G., 1976b. Adsorption of phosphate by

gibbsite. II. Formation of a surface complex involving divalent cations. *Journal of Soil Science*. 27: 315-323.

Hingston, F.J., Atkinson, R.J., Posner, A.M. and Quirk, J.P., 1967. Specific adsorption of anions. *Nature*. 215: 1459-1461.

Hingston, F.J., Posner, A.M. and Quirk, J.P., 1974. Anion adsorption by goethite and gibbsite. *Journal of Soil Science*. 25: 16-26.

Hsia, T.H., Lo, S.F. and Lin, C.F., 1992. As(V) Adsorption on amorphous iron oxide: Triple layer modeling. *Chemosphere*. 25(12): 1825-1837.

Hsu, P.H. and Rennie, D.A., 1962. Reactions of phosphate in aluminum systems. I. Adsorption of phosphate by x-ray amorphous aluminum hydroxide. *Canadian Journal of Soil Science*. 42: 197-209.

Hunter, R.J., 1981. Zeta potential in colloid science, Principles and Applications. *Colloid science. A series of monographs*. Academic press. San Diego, 219-257 pp.

Jackson, M.L., 1956. Soil chemical analysis-Advanced course. University of Wisconsin, Madison, Wis.

- Jacobs. L.W., Syers. J.K. and Keeney. D.R.. 1970. Arsenic sorption by soils. Soil Science Society of America Proceedings. 34: 750-754.
- Jain. A., Raven. K.P. and Loeppert. R.H.. 1999. Arsenite and arsenate adsorption on ferrihydrite: surface charge reduction and net OH⁻ release stoichiometry. Environmental Science and Technology. 33: 1179-1184.
- Jonasson. R.G., Martin. R.R., Giuliacci. M.E. and Tazaki. K.. 1988. Surface reactions of goethite with phosphate. Journal of Chemical Society Faraday Transaction 1. 84(7): 2311-2315.
- Kafkafi. U., Posner. A.M. and Quirk. J.P.. 1967. Desorption of phosphate from kalolinite. Soil Science Society Proceedings. 31: 348-353.
- Koskinen. W.C. and Harper, S.S.. 1990. The retention process: Mechanisms. In: H.H. Cheng (ed.), Pesticides in the soil environment: Processes, Impacts, and modeling. Soil Science Society of America, Inc., Madison, WI, pp. 51-77.
- Kotak. B.G. et al.. 1993. Occurrence and toxicological evaluation of cyanobacterial toxins in Alberta lakes and farm dugouts. Water Research. 27: 495-506.
- Kuo. S.. 1996. Phosphorus. In: D.L. Sparks (ed.), Method of soil analysis Part 3-

chemical method. Soil Science Society of America, Madison, WI, pp. 896-919.

Kuo, S. and Baker, A.S.. 1982. The effect of soil drainage on phosphorus status and availability to corn in long-term manure amended soils. Soil Science Society of America Journal, 46: 744-747.

Kuo, S. and Lotse, E.G.. 1972. Kinetics of phosphate adsorption by calcium carbonate and Ca-kaolinite. Soil Science Society of America Proceedings, 36: 725-729.

Kuo, S. and Lotse, E.G.. 1973. Kinetics of phosphate adsorption and desorption from hematite and gibbsite. Soil Science, 116: 400-405.

LaKind, J.S. and Stone, A.T., 1989. Reductive dissolution of goethite by phenolic reductants. Geochimica et Cosmochimica Acta, 53: 961-971.

Lawton, L.A. and Codd, G.A., 1991. Cyanobacteria (Blue-green algae) toxins and their significance in UK and European waters. Journal of the Institute of Water Environmental Management, 5: 460-465.

Levin, E.D. et al., 1997. Persisting learning deflects in rats after exposure to *Pfiesteria piscida*. Environmental Health Perspectives, 105(12): 1320-1325.

Lindsay, W.L., 1979. Phosphate. Chemical equilibria in soils. John Wiley, New York. pp. 163-209.

Livesey, N.T. and Huang, P.M., 1981. Adsorption of arsenate by soils and its relation to selected chemical properties and anions. *Soil Science*, 131(2): 88-94.

Lookman, L.D.F., R. Merckx, K. Vlassak, W. M. van Riemsdijk, 1995. Long-term kinetics of phosphate release from soil. *Environmental Science and Technology*, 29: 1569-1575.

López-Hernandez, D. and Burnhan, C.P., 1974. The covariance of phosphate sorption with other soil properties in some British and tropical soils. *Journal of Soil Science*, 25(2): 207-216.

López-Pineiro, A. and Navarro, A.G., 1997. Phosphate sorption in vertisols of Southwestern Spain. *Soil Science*, 162(1): 69-77.

Lovley, D.R., 1991. Dissimatory Fe(III) and Mn(IV) reduction. *Microbiological reviews*, 55: 259-287.

Low, P.F. and Black, C.A., 1950. Reactions of phosphate with kaolinite. *Soil Science*.

70: 273-290.

Lumsdon, D.G., Fraser, A.R., Russell, J.D. and Livesey, N.T., 1984. New infrared band assignments for the arsenate ion adsorbed on synthetic goethite (α -FeOOH). *Journal of Soil Science*, 35: 381-386.

Madrid, L. and Posner, A.M., 1979. Desorption of phosphate from goethite. *Journal of Soil Science*, 30: 697-707.

Manahan, S.E., 1994. Toxicological chemistry of chemical substances. Environmental chemistry. Lewis publishers, Ann Arbor, pp. 675-704.

Manning, B.A., Fendorf, S.E. and Goldberg, S., 1998. Surface structure and stability of arsenic(III) on goethite: Spectroscopic evidence for Inner-sphere complexes. *Environmental Science and Technology*, 32: 2383-2388.

Manning, B.A. and Goldberg, S., 1997. Adsorption and stability of arsenic (III) at the clay mineral-water interface. *Environmental Science and Technology*, 31(7): 2005-2011.

Manning, J.R., 1968. Diffusion kinetics for atoms in crystals. D. Van Nostrand and company, Inc., Princeton, New Jersey.

Margerum, D.W.. 1978. Coordination chemistry Vol. 2. In: A.E. Martell (ed.). ACS Monograph No. 174. ACS, Washington, D. C.

Martine, R.R., Smart, R.S. and Tazaki, K., 1988. Direct observation of phosphate precipitation in the goethite/phosphate system. Soil Science Society of America Journal, 52: 1492-1500.

Martine, R.R. and Smart, R.S.C., 1987. X-ray photoelectron studies of anion adsorption on goethite. Soil Science Society of America Journal, 51: 54-56.

Masscheleyn, P.H., Delaune, R.D. and W. H. Patrick, J., 1991a. Arsenic and selenium chemistry as affected by sediment redox potential and pH. Journal of Environmental Quality, 20: 522-527.

Masscheleyn, P.H., Delaune, R.D. and W. H. Patrick, J., 1991b. Effect of redox potential and pH on arsenic speciation and solubility in a contaminated soil. Environmental Science and Technology, 25(8): 1414-1418.

Mattson, S. and Hester, J.B., 1935. The laws of soil colloidal behavior: XV. The degradation and the regeneration of the soil complex. Soil Science, 39: 75-84.

McBride, M.B., 1989. Reactions controlling heavy metal solubility in soils. In: B.A. Stewart (ed.), *Advances in soil science*, pp. 1-56.

McBride, M.B., 1994a. Ion sorption. *Environmental chemistry of soils*. Oxford university press. New York. pp. 121-168.

McBride, M.B., 1994b. Review of chemical principles. *Environmental chemistry of soils*. Oxford university press. New York. pp. 3-30.

McBride, M.B., 1997. A critique of diffuse double layer models applied to colloid and surface chemistry. *Clays and Clay Minerals*, 45(4): 598-608.

McBride, M.B., 1991. Processes of heavy metal and transition metal sorption by soil minerals. In: G.H. Bolt, M.F.D. Boodt, M.H.B. Hayes and M.M. McBride (eds.), *Interactions at the soil colloid-soil solution interface*. Kluwer academic publishers. Dordrecht, pp. 149-176.

McCammon, C.A. and Burn, R.G., 1980. The oxidation mechanism of vivianite as studied by Mössbauer spectroscopy. *American Mineralogist*, 65: 361-366.

McGeeham, S.L. and Naylor, D.V., 1994. Sorption and redox transformation of arsenite and arsenate in two flooded soils. *Soil Science Society of America Journals*.

58: 337-342.

Mengel, K.. 1985. Dynamics and availability of major nutrients in soils. In: B.A. Stewart (ed.). *Advances in soil science*. Springer-Verlag, New York, Berlin, Heidelberg, Tokyo. pp. 96-105.

Muljadi, D., A. M. Posner, and J. P. Quirk. 1966. The mechanism of phosphate adsorption by Kaolinite, Gibbsite, and Pseudoboehmite. *Journal of Soil Science*. 17(2): 212-229.

Munns, D.N. and Fox, R.L.. 1976. The slow reaction which continues after phosphate adsorption: kinetics and equilibrium in some tropical soils. *Soil Science Society of America Journal*. 40: 46-51.

Murphy, J. and Riley, J.P., 1962. A modified single solution method for the determination of phosphate in natural waters. *Analytical Chimica Acta*, 27: 31-36.

Nanzyo, M., 1984. Diffused reflectance infrared spectra of phosphate sorbed on alumina gel. *Journal of Soil Science*. 35: 63-69.

Nanzyo, M., 1986. Infrared spectra of phosphate sorbed on iron hydroxide gel and the sorption products. *Soil Science and Plant Nutrition*. 32(1): 51-58.

Nanzyo, M., 1987. Formation of noncrystalline aluminum phosphate through phosphate sorption on allophanic soils. *Communication in Soil Science Plant Analysis*, 18(7): 735-742.

Nanzyo, M. and Watanabe, Y., 1982. Diffuse reflectance infrared spectra and ion-adsorption properties of the phosphate surface complex on goethite. *Soil Science and Plant Nutrition*, 28(3): 359-368.

Nilsson, N., Lövgren, L. and Sjöberg, S., 1992. Phosphate complexation at the surface of goethite. *Chemical speciation and bioavailability*, 4(4): 121-130.

Norrish, K. and Rosser, H., 1983. *Mineral phosphate. Soils: an Australian view point.* Academic press, Melbourne.

O'Day, P., Parks, G.A. and Brown, G.E., 1994. X-ray absorption spectroscopy of cobalt (II) multinuclear surface complexes and surface precipitates on kaolinite. *Journal of Colloid and Interface Science*, 165: 269-289.

Okajima, Kubota, H. and Sakuma, T., 1983. Hysteresis in the phosphorus sorption and desorption processes of soils. *Soil Science Plant Nutrition*, 29(3): 271-283.

Olsen, S.R. and Watanabe, F.S., 1957. A method to determine a phosphorus adsorption maximum of soils as measured by the Langmuir isotherm. *Soil Science Society of America Proceedings*, 21: 144-149.

Onishi, H., 1969. Arsenic. *Handbook of geochemistry*. Springer-Verlag, New York.

Onken, A.B. and Matheson, R.L., 1982. Dissolution rate of EDTA-extractable phosphate from soils. *Soil Science Society of America Journal*, 46: 276-279.

Onken, B.M. and Adriano, D.C., 1997. Arsenic availability in soil with time under saturated and subsaturated conditions. *Soil Science Society of America Journal*, 61: 746-752.

Onken, B.M. and Hossner, L.R., 1995. Plant uptake and determination of arsenic species in soil solution under flooded conditions. *Journal of Environmental Quality*, 24: 373-381.

Oscarson, D.W., Huang, P.M. and Liaw, W.K., 1980. The oxidation of arsenite by aquatic sediments. *Journal of Environmental Quality*, 9(9): 700-703.

Ozanne, P.G., 1980. Phosphate nutrition of plants-a general treatise. In: F.E. Khasawneh, E.C. Sample and E.J. Kamprath (eds.), *The role of phosphorus in*

agriculture. Soil Science Society of America. American Society of Agronomy. Crop Science Society of America. Madison, WI. pp. 559-589.

Parfitt, R.L.. 1978. Anion adsorption by soils and soil materials. Advances in Agronomy, pp. 1-50.

Parfitt, R.L.. 1979. The nature of the phosphate goethite (α -FeOOH) complex formed with $\text{Ca}(\text{H}_2\text{PO}_4)_2$ at different surface coverage. Soil Science Society of America Journal. 43: 623-625.

Parfitt, R.L.. 1989. Phosphate reactions with natural allophane, ferrihydrite and goethite. Journal of Soil Science. 40: 359-369.

Parfitt, R.L. and Atkinson, R.J., 1976. Phosphate adsorption on goethite(α -FeOOH). Nature. 264(30): 740-741.

Parfitt, R.L., Atkinson, R.J. and Smart, R.S.C., 1975. The mechanism of phosphate fixation by iron oxides. Soil Science Society of America Proceedings, 39: 837-841.

People, S.A., 1975. Review of arsenical pesticides. In: E.A. Woolson (ed). American Chemical Society, pp. 1-12.

- Persson, P., Nielsson, N. and Sjöberg, S., 1996. Structure and bonding of orthophosphate ions at the iron oxide-aqueous interface. *Journal of Colloid and Interface Science*, 177: 263-275.
- Pierce, M.L. and Moore, C.B., 1982. Adsorption of arsenite and arsenate on amorphous iron hydroxide. *Water Research*, 16: 1247-1253.
- Pierzynski, G.M., Logan, T.J. and Traina, S.J., 1990a. Phosphorus chemistry and mineralogy in excessively fertilized soils: Solubility equilibria. *Soil Science Society of America Journal*, 54: 1589-1595.
- Pierzynski, G.M., Logan, T.J., Traina, S.J. and Bigham, J.M., 1990b. Phosphorus chemistry and mineralogy in excessively fertilized soils: Quantitative analysis of phosphorus-rich particles. *Soil Science Society of America Journal*, 54: 1576-1583.
- Pignatello, J.J., Ferrandino, F.J. and Huang, L.Q., 1993. Elution of aged and freshly added herbicides from a soil. *Environmental Science and Technology*, 27: 1563-1571.
- Pignatello, J.J. and Xing, B., 1995. Mechanisms of slow sorption of organic chemicals to natural particles. *Environmental Science and Technology*, 30(1): 1-11.
- Postma, D., 1993. The reactivity of iron oxides in sediments: A kinetic approach.

Geochimica et Cosmochimica Acta. 57: 5027-5034.

Rajan, S.S.S., 1975. Phosphate adsorption and the displacement of structural silicon in allophane clay. *Journal of Soil Science*. 26(3): 250-256.

Rajan, S.S.S., 1976. Changes in net surface charge of hydrous alumina with phosphate adsorption. *Nature*. 262: 45-46.

Reifenberg, A. and Buckwold, S.J., 1954. The release of silica from soils by the orthophosphate anion. *Journal of Soil Science*. 5(1): 106-115.

Rickert, H., 1982. *Electrochemistry of solids - An introduction*. Springer, Berlin.

Rochette, E.A., Li, G.C. and Fendorf, S.E., 1998. Stability of arsenate minerals in soil under biotically generated reducing conditions. *Soil Science Society of America Journal*. 62: 1530-1537.

Ryden, J.C., McLaughlin, J.R. and Syers, J.K., 1977a. Time-dependent sorption of phosphate by soils and hydrous ferric oxides. *Journal of Soil Science*. 28: 585-595.

Ryden, J.C. and Syers, J.K., 1977. Desorption and isotopic exchange relationship of phosphate sorbed by soils and hydrous ferric oxide. *Journal of Soil Science*. 28: 596-609.

Ryden, J.C., Syers, J.K. and Harris, R.F., 1973. Phosphorus in run off and streams. *Advances in Agronomy*, pp. 1-45.

Ryden, J.C., Syers, J.K. and Mclaughlin, J.R., 1977b. Effects of ionic strength on chemisorption and potential-determining sorption of phosphate. *Journal of Soil Science*, 28: 62-71.

Sakata, M., 1987. Relationship between adsorption of As(III) and boron by soil and soil properties. *Environmental Science and Technology*, 21(11): 1126-1130.

Sanchez, P.A. and Uehara, G., 1980. Management considerations for acid soils with high phosphorus fixation capacity. In: F.E. Khasawneh, E.C. Sample and E.J. Kamprath (eds.), *The role of phosphorus in agriculture*. American Society of Agronomy, Madison, Wisconsin.

Schwertmann, U. and Cornell, R.M., 1991. *Iron Oxides in the Laboratory: Preparation and Characterization*. VCH Publisher, pp.137 .

Scott, M.J. and Morgan, J.J., 1995. Reactions at oxide surface. 1. oxidation of As(III) by synthetic birnessite. *Environmental Science and Technology*, 29(8): 1898-1905.

Shang, C., Stewart, J.W.B. and Huang, P.M., 1992. pH effect on kinetics of adsorption of organic inorganic phosphates by short-range ordered aluminum and iron precipitates. *Geoderma*, 53: 1-14.

Shapiro, R.E., 1957. The effect of flooding on the availability of P and nitrogen. *Soil Science*, 85: 190-197.

Sharpley, A.N. and Rekolainen, S., 1997. Phosphorus in agriculture and its environmental implications.

Sharpley, A.N. and Robinson, J.S., 1996. Reaction in soil of phosphorus released from poultry litter. *Soil Science Society of America Journal*, 60: 1583-1588.

Sharpley, A.N., S. J. Smith and B. A. Stewart, A.C.M., 1984. Forms of phosphorus in soils receiving cattle feedlot waste. *Journal of Environmental Quality*, 13: 211-215.

Sheppard, S.C., 1991. Summary of phytotoxic levels of soil arsenic. *Water, Air, and Soil Pollution*, 64: 539-550.

Sheppard, S.C. and Racz, G.J., 1984. Effects of soil temperature on phosphorus extractability 1. Extractions and plant uptake of soil and fertilizer phosphorus. *Canadian Journal of Soil Science*, 64: 241-254.

Sims, J.T. and Ritter, W.F.. 1993. Development of environmental soil tests and field rating systems for phosphorus in the Inland bays watershed of Delaware.. Dover, DE.

Sims, J.T., S. Andres, J. M. Denver and Gangloff, W.J.. 1996. Assessing the impact of agricultural drainage on ground and surface water quality in Delaware.. University of Delaware.

Snoeyink, V.L. and Jenkins, D.. 1980. Precipitation and dissolution. Water Chemistry. John Wiley & Sons, Inc.. New York, pp. 243-315.

Sparks, D.L., 1987. Dynamics of soil potassium. Adv. Soil Sci.. 6: 1-63.

Sparks, D.L., 1989. Kinetics of Soil Chemical Processes. Academic Press, Inc.

Sparks, D.L., 1995a. Environmental Soil Chemistry. Academic Press, Inc., San Diego.

Sparks, D.L., 1995b. Sorption phenomena on soils. Environmental soil chemistry. Academic press, San Diego, CA. pp. 99-139.

Sposito, G., 1986. Distinguishing adsorption from surface precipitation. In: J.A.

Davis and K.F. Hayes (eds.). Geochemical processes at mineral surfaces.
American chemical society, Washington DC. pp. 217-228.

Sposito, G.. 1989. Soil adsorption phenomena, The chemistry of soils. Oxford
university press, New York, Oxford.

Steinberg, S.M., Pignatello, J.J. and Sawhney, B.L.. 1987. Persistence of 1, 2-
dibromoethane in soils: Entrapment in interparticle micropores. Environmental
Science and Technology, 21: 1201-1208.

Steinfeld, J.I., Francisco, J.S. and Hase, W.L.. 1989. Chemical kinetics and
dynamics. Englewood Cliffs, Prentice hall.

Stumm, W. and Morgan, J.J., 1995a. Aquatic chemistry. Chemical equilibria and
rates in natural water. John Wiley & Sons, Inc. New York.

Stumm, W. and Morgan, J.J., 1995b. Theory of elementary processes, Aquatic
chemistry, Chemical equilibria and rates in natural water. John Wiley & Sons, Inc.
New York. pp. 69-76.

Suarez, D.L., Goldberg, S. and Su, C.. 1998. Evaluation of oxyanion adsorption
mechanisms in oxides using FTIR spectroscopy and electrophoretic mobility. In: D.L.

Sparks and T.J. Grundl (eds.), Mineral-water interfacial reactions kinetics and mechanisms. Am. Chem. Soc., Washington, DC, pp. 136-178.

Subcommittee on arsenic, N.R.C., 1977. Chemistry and distribution of arsenic in the environment, Arsenic , medical and biologic effects of environmental pollutants. National Academy of Science, pp. 4-79.

Sun. X. and Doner. H.E.. 1996. An investigation of arsenate and arsenite bonding structures on goethite by FTIR. Soil Science. 161(12): 865-872.

Sun. X. and Doner, H.E.. 1998. Adsorption and oxidation of arsenite on goethite. Soil Science, 163(4): 278-287.

Sun. X., Doner, H.E. and Zavarin. M.. 1999. Spectroscopy study of arsenite [As(III)] oxidation on Mn-substituted goethite. Clays and Clay Minerals. 47(4): 474-480.

Tallman, D.E. and Shaikh. A.U.. 1980. Redox stability of inorganic arsenic(III) and arsenic(V) in aqueous solution. Analytical Chemistry. 52: 196-199.

Tanji, K.K. and Dalgren, R.A., 1993. Acidification of evaporation ponds to reduce contaminant hazards to wildlife-phase I (Chemical aspects). DWR agreement #:B58194.

Tejedor-Tejedor, M.I. and Anderson, M.A., 1990. Protonation of phosphate on the surface of goethite as studied by CIR-FTIR and electrophoretic mobility. *Langmuir*, 6: 602-611.

Tisdale, L.T., W. L. Nelson, J. D. Beaton and Harlin, J.L., 1993. *Soil fertility and fertilizers*. Macmillan publishing Co.

Torrent, J., 1991. Activation energy of the slow reaction between phosphate and goethite of different morphology. *Australian Journal of Soil Research*, 29: 69-74.

Torrent, J., Barron, V. and Schwertmann, U., 1990. Phosphate adsorption and desorption by goethite differing in crystal morphology. *Soil Science Society of America Journal*, 54: 1007-1012.

Torrent, J., Schwertmann, U. and Barron, V., 1987. The reductive dissolution of synthetic goethite and hematite in dithionite. *Clay Minerals*, 22: 329-337.

Torrent, J., Schwertmann, U. and Barron, V., 1992. Fast and slow phosphate sorption by goethite-rich natural materials. *Clays and Clay Minerals*, 40(1): 14-21.

United States Environmental Protection Agency. 2001. EPA To Implement 10ppb

Standard for Arsenic in Drinking Water. EPA 815-F-01-010.

Vaithyanathan, P. and Correll, D.L.. 1992. The Rode river watershed: Phosphorus distribution and export in forest and agricultural soils. *Journal of Environmental Quality*, 21: 280-288.

van der Zee, S.E.A.T.M. and van Riemsdijk, W.H.. 1988. Model for long -term phosphate reaction kinetics in soil. *Journal of Environmental Quality*, 17: 35-41.

van Riemsdijk, W.H., Boumans, L.J.M. and de Haan, F.A.M.. 1984. Phosphate sorption by soils I. A model for phosphate reaction with metal-oxides in soil. *Soil Science Society of America Journal*, 48: 537-541.

van Riemsdijk, W.H. and de Haan, F.A.M.. 1981. Reaction of orthophosphate with a sandy soil at constant supersaturation. *Soil Science Society of America Journal*, 45: 261-266.

van Riemsdijk, W.H. and Lyklema, J.. 1980. Reaction of phosphate with gibbsite ($\text{Al}(\text{OH})_3$) beyond the adsorption maximum. *Journal of Colloid and Interface Science*, 76(1): 55-66.

van Riemsdijk, W.H., Weststrate, F.A. and Beek, J.. 1977. Phosphate in soils treated with sewage water: III. Kinetics studies on the reaction of phosphate with aluminum

compounds. *Journal of Environmental Quality*. 6(1): 26-29.

Veith, J.A. and Sposito, G., 1977. Reactions of aluminosilicates, aluminum hydrous oxides, and aluminum oxide with *o*-phosphate: The formation of x-ray amorphous of variscite and montebasite. *Soil Science Society of America Journal*. 41: 870-876.

Voigt, D.E. and Brantley, S.L., 1996. Chemical fixation of arsenic in contaminated soils. *Applied Geochemistry*. 11: 633-643.

Walkley, A., 1947. A critical examination of a rapid method for determining organic carbon in soils: Effect of variations in digestion conditions and of inorganic soil constituents. *Soil Science*. 63: 29-38.

Walsh, L.M. and Keeny, D.R., 1975. Behavior and phytotoxicity of inorganic arsenicals in soils. *Arsenical pesticides*. ACS, Washington, DC., 35-52 pp.

Wang, H.D., Harris, W.G. and Yuan, T.L., 1991. Noncrystalline phosphates in Florida phosphatic soils. *Soil Science Society of America Journal*, 55: 665-669.

Wang, M.K., 1987. Synthetic and characterization of iron phosphate and aluminum-substituted iron phosphate compounds. *Journal of Chinese Agricultural Chemical Society*. 25: 398-411.

Wang, M.K. and Tzou, Y.M., 1995. Phosphate sorption by calcite, and iron-rich calcareous soils. *Geoderma*, 65: 249-261.

Waychunas, G.A., Rea, B.A., Fuller, C.C. and Davis, J.A., 1993. Surface chemistry of ferrihydrite: Part 1. EXAFS studies of the geometry of coprecipitated and adsorbed arsenate. *Geochimica et Cosmochimica Acta*, 57: 2251-2264.

Westcot, D.W., Chilcott, J.E. and Smith, G., 1993. Pond water, sediments and crystal chemistry. ASCE National conference on irrigation and drainage engineering. ASCE, New York.

Whitacre, R.W. and Pearse, C.S., 1974. Arsenic and the environment. Colorado school of mines minerals industries bulletin, 17(3).

Willett, I.R., Chartres, C.J. and Nguyen, T.T., 1988. Migration of phosphate into aggregated particles of ferrihydrite. *Journal of Soil Science*, 39: 275-282.

Williams, J.D.H., Syers, J.K., Harris, R.F. and Armstrong, D.E., 1971. Fractionation of inorganic phosphate in calcareous lake sediments., 35: 250-255.

Woolson, E.A., Axley, J.H. and Kearney, P.C., 1971. Correlation between available

soil arsenic, estimated by six methods, and response of corn (*Zea Mays L.*). Soil Science Society of America Proceedings, 35: 101-105.

Woolson, E.A., Axley, J.H. and Kearney, P.C., 1973. The chemistry and phytotoxicity of arsenic in soils: II. Effects of time and phosphorus. Soil Science Society of America Proceedings, 37: 254-259.

Xu, H., Allard, B. and Grimvall, A., 1988. Influence of pH and organic substance on the adsorption of As(V) on geologic materials. Water, Air, and Soil Pollution, 40: 293-305.

Zelazny, L.W., He, L. and Vanwormhoudt, A., 1996. Charge analysis of soils and anion exchange. In: D.L. Sparks (ed.), Methods of soil analysis Part 3-Chemical methods. SSSA Book Series No.5. Soil Science Society of America, Inc., Madison, Wisconsin, pp. 1231-1254.

Chapter 2

ATR-FTIR SPECTROSCOPIC INVESTIGATION ON PHOSPHATE ADSORPTION MECHANISMS AT THE FERRIHYDRITE-WATER INTERFACE

2.1 Abstract

We investigated the P adsorption mechanisms at the ferrihydrite (FH)-water interface as a function of pH, ionic strength (I) and loading level, using a combination of adsorption envelopes, electrophoretic mobility (EM) measurements, and attenuated total reflectance Fourier transform infrared (ATR-FTIR) spectroscopy. The P adsorption envelopes show that; 1) adsorption decreases with increasing pH 3.5-9.5 and 2) adsorption is insensitive to changes in I at pH 4-7.5, but slightly increases with increasing I from 0.01 to 0.8 at pH > 7.5. The EM in 0.1M NaCl decreases with increasing P concentration from 0 to 50 $\mu\text{mol L}^{-1}$ at pH 3-9. The results of these macroscopic studies suggest the formation of inner-sphere complexes. The ATR-FTIR investigation shows that inner-sphere surface complexes are nonprotonated bidentate binuclear species ($\equiv\text{Fe}_2\text{PO}_4$) at pH ≥ 7.5 and could be associated with Na^+

ions at P loading levels $0.38 \mu\text{mol m}^{-2}$. At pH 4-6, protonated inner-sphere complexes are proposed at the loading levels between 0.38 and $2.69 \mu\text{mol m}^{-2}$.

2.2 Introduction

In the last few decades, excess P has been recognized as a nonpoint-source agricultural pollutant throughout the world due to the over-application of both synthetic and animal based fertilizers (Ryden et al., 1973; Vaithyanathan and Correll, 1992). In 1996 the USEPA reported that more than 50% of fresh water eutrophication is attributed to agricultural nutrients such as P. Eutrophication as well as the overgrowth of cyanobacteria due to the excess P in recreational, industrial and drinking water could greatly threaten human and ecological health. Therefore, the fate and transport of P in soil/water environments must be well understood to design effective remediation strategies for reducing negative impacts on aquatic/terrestrial environments. Various abiotic and biotic factors (pH, redox, ionic strength, adsorbent type, % organic matter content, temperature, concentration, competitive adsorbates, solubility product effects, and nonreductive/reductive dissolution of adsorbate) greatly affect the reactivity, speciation, mobility, and bioavailability of P. Because adsorption to mineral surfaces is one of the most important rate-limiting factors controlling P release in subsurface environments, it is vital to study the mechanisms of P adsorption on naturally occurring soil minerals.

Many researchers have investigated P adsorption mechanisms on major soil minerals (e.g., iron oxides) using *in situ/ex situ* FTIR spectroscopy. While the

predominant formation of inner-sphere bidentate binuclear complexes on ferrihydrite, goethite, lepidocrocite and hematite was suggested by several researchers (Atkinson et al., 1974; Nanzyo and Watanabe, 1982; Parfitt, 1976; Parfitt and Atkinson, 1976; Parfitt et al., 1975; Tejedor-Tejedor and Anderson, 1990), the inner-sphere monodentate mononuclear complexes at the goethite surface were later proposed (Persson et al., 1996).

An important factor accounting for the differences in the proposed P surface complexes on iron oxides between the previous studies may lie in the use of 1) different FTIR techniques (e.g., *in situ* versus *ex situ* FTIR spectroscopy) and 2) different data interpretation processes (e.g., molecular symmetry assignment of adsorption complexes based on asymmetric ν^3 vibration or peak position comparison with iron phosphate model complexes). Evidence of inner-sphere complexation in the *ex situ* (dry and severely evacuated sample conditions) studies has been questioned by many researchers due to the possible creation of artifacts (*i.e.*, a structural alteration by drying the residual adsorbate and removal of entrained water). *In situ* spectroscopic investigations are preferred, because the colloidal interfaces in natural settings contain water and are at atmospheric pressure (Goldberg and Sposito, 1985). Comparing the peak position between adsorption complexes and model complexes to assign the type of surface complexes can be problematic because the peak position could often shift due to different reaction conditions (e.g., loading level, pH and moisture content) (Atkinson et al., 1974; Hug, 1997; Parfitt and Atkinson, 1976; Tejedor-Tejedor and Anderson, 1990). The molecular symmetry assignment of adsorption complexes

based on the asymmetric vibration has been preferably used in recent vibrational spectroscopic studies to investigate oxyanion (arsenate, carbonate, phosphate, selenate and sulfate) adsorption mechanisms at the mineral-water interface (Goldberg and Johnston, 2001; Hug, 1997; Peak et al., 1999; Persson et al., 1996; Schulthess et al., 1998; Wijnja and Schulthess, 2000).

The two-line ferrihydrite (FH) (an amorphous hydrous ferric oxide) was chosen in this study because 1) it commonly forms in soils and sediments (Fuller and Davis, 1989; Jackson and Keller, 1970; Schwertmann et al., 1982; Schwertmann and Taylor, 1989) and 2) strong adsorption capacity for P (Parfitt, 1989; Willett et al., 1988) has implications in P aggeochemical cycles in the environment. The presence of P ligands at the FH surfaces are known to retard the transformation of FH into crystalline phases like goethite (Barron et al., 1997; Kandori et al., 1992) and might also inhibit reductive/nonreductive dissolution reactions of the FH. The reductive or nonreductive dissolution inhibitory reactions have been documented for P adsorbed lepidocrocite and goethite surfaces (Biber et al., 1994; Bondietti et al., 1993). Since the P surface speciation on FH surfaces has been only investigated via *ex situ* FTIR spectroscopic analysis (Nanzyo, 1986; Parfitt et al., 1975), the reaction dynamics of P ligand at the FH-water interfacial environments are not clearly understood. Therefore the objective of our study was to investigate P surface speciation (i.e., P surface complexation and the protonation environment) at the FH-water interface using *in situ* ATR-FTIR spectroscopy. Phosphate surface complexes are proposed based on the molecular symmetry assignment via Gaussian profile fit analysis of phosphate ν_3

vibrations. Additionally, the *in situ* spectroscopic analyses were complimented with macroscopic investigations such as adsorption envelopes as a function of ionic strength (I) and electrophoretic mobility (EM) measurements.

2.3 Materials

The two-line ferrihydrite (FH) was synthesized according to Schwertmann and Cornell (Schwertmann and Cornell, 1991). Forty g of ferric nitrate was dissolved in 500 ml deionized water. The pH of the solution was titrated to pH 7.5, and maintained at this pH value for 45 min by addition of 1 M NaOH. The FH precipitate was washed with deionized water and the supernatant was decanted after centrifugation. This was repeated until the nitrate concentration was reduced to below 0.003 mmol. The FH paste was then freeze-dried prior to the adsorption experiments. The five-point Brunauer-Emmett-Teller (BET) surface area was $260 \text{ m}^2 \text{ g}^{-1}$. The Point of Zero Salt Effect (PZSE), as determined by the potentiometric titration method, (Zelazny et al., 1996) was 8. Powder X-ray diffraction (XRD) analysis revealed the diagnostic two broad peaks for two-line ferrihydrite (0.24 and 0.15 nm).

2.4 Methods

2.4.1 Ionic Strength Effects on P Adsorption Envelopes

Phosphate adsorption envelopes were investigated at different solution ionic strengths (0.8, 0.1, and 0.01 M NaCl). A N_2 filled glove box was used to minimize the pH shifts the atmospheric CO_2 partitioning. Twenty ml of FH suspensions ($\rho = 2 \text{ g L}^{-1}$

¹) were transferred to 50 ml Nalgene high speed centrifuge tubes. A total of ten samples were prepared for each value of I. After 2 min of ultrasonification at 60 W, pHs were adjusted to provide a range of 3-10 with addition of 0.1 M HCl or NaOH. The samples were shaken at 150rpm at 25(±1)°C for 24 h. Next, the samples were spiked with 20 ml of 1.4 mmol P stock solution over the same pH range and I to provide an initial P concentration of 0.7 mmol. The samples were shaken on an orbital shaker at 150 rpm for 24 h. The pH was periodically adjusted with 0.1 M HCl or NaOH. After equilibration, the tubes were centrifuged at 1750 g for 10 min. The pH of the supernatant was measured. The filtered supernatants were passed through a 0.2 µm Supor 200™ filter and analyzed for dissolved P using the modified molybdeum blue method (He et al., 1998; Murphy and Riley, 1962).

2.4.2 Electrophoretic Mobility Measurements

To assure accuracy of the EM measurements, a Zeta-Meter 3.0 system (Zeta Meter, Inc. NY) was calibrated by measuring a constant zeta potential (-29 ±1 mV) of Min-U-Sil (*i.e.*, standard colloidal silica) in distilled water. Freeze dried FH (Suspension density (ρ) = 0.4 g L⁻¹) was hydrated in 30 ml of 0.01 M NaCl solution, and ultrasonified for 2 min at 60 W. The pH was adjusted to the desired pH values (4, 4.75, 5.5, 6.25, 7, 7.5, 8.5, and 9.25) by adding 0.1 M HCl and 0.1 M NaOH. After 24 h of equilibration, the mineral suspensions were reacted with 20 ml of sodium phosphate solutions (62.5 or 125 µmol L⁻¹) over the same pHs and I to provide initial

P concentration of 25 and 50 $\mu\text{mol L}^{-1}$. After 48 h of equilibration, approximately 10ml of well-mixed suspensions were inserted into the electrophoretic cell. Tracking time measurements of particle movement were repeated for ten particles. The average value was used to estimate the EM values using the Helmholtz – Smoluchowski equation (Hiemenz and Rajagopalan, 1997).

2.4.3 Sample Preparation for the ATR-FTIR Analysis

Infrared spectra of adsorbed phosphate on the FH surface were studied as a function of 1) pH (4-9) at constant loading level (i.e., $\Gamma = 0.38 \mu\text{mol m}^{-2}$) and 2) the P loading level ($0.38\text{-}2.69 \mu\text{mol m}^{-2}$) at constant pH 4 and pH 7.5. Hydration and pH adjustment of the FH suspensions were accomplished using the method described in the adsorption envelope section. The final suspension density of 1 g L^{-1} and $I = 0.1 \text{ M NaCl}$ were used in all experiments. A monodentate mononuclear iron phosphate (aq) reference complex ($1.5 \text{ M FeCl}_3 \cdot 6\text{H}_2\text{O}$, $0.75 \text{ M Na}_2\text{HPO}_4$ and (Ro et al.,)/[Fe] = 1) was prepared based on the study by Rose et al. (1996)(Rose et al., 1996) to aid in IR spectra data interpretation. The sodium P solution complexes ($0.1 \text{ M Na}_2\text{HPO}_4$ in 1 M NaCl) at different pHs (1.3, 4.8, 8, and 12.8) were also prepared following the method described in the study by Tejedor-Tejedor and Anderson (1990) (Tejedor-Tejedor and Anderson, 1990).

Adsorption samples for pH 4 and 7.5 under the 0.38 and/or $2.69 \mu\text{mol m}^{-2}$ loading level were also prepared in D_2O under the same reaction conditions above.

The preparation of the reagents (0.1 M NaCl and 2 mmol Na₂HPO₄) and the P adsorption experiments in D₂O were performed in the N₂ filled glove box. The FH was hydrated in the 20 ml 0.1 M NaCl in D₂O for 3d. After the hydration, pH of the suspension was adjusted to 4 or 7.5 for 24h with 0.1M DCl and NaOD. The P stock solution (pH 4 or 7.5 and I=0.1 M NaCl) was added to the mineral suspensions, and then the pH was periodically adjusted for 48h. The samples were recovered by the centrifugation method described above, and the paste was recovered in the N₂ glove box. To minimize the partitioning of the atmospheric hydrogen, the paste was quickly loaded on the ATR-FTIR trough and it was continuously purged with N₂ during the FTIR analysis.

2.4.4 ATR-FTIR Analyses

ATR-FTIR data collection was conducted on a Perkin-Elmer 1720x spectrometer equipped with a N₂ purge gas generator and a MCT detector. ZnSe and Ge horizontal crystals (45° angle of incidence) were used for the adsorption samples and the P solution samples (sodium phosphate and iron phosphate solutions), respectively. A total of 500 co-added spectra were collected for the adsorption samples at a resolution of 2 cm⁻¹, and a total of 150 co-added spectra were taken.

All spectra were ratioed against the spectra of an empty cell. Subtraction of the spectra was performed to obtain all final spectra. For example, the final spectra were obtained by subtracting the spectra of the entrained solution and the FH paste or the background solution from the spectra of reacted samples (i.e., P adsorbed iron oxides

or P solution, respectively). All spectra were normalized with respect to the highest absorbance (at $\approx 1020 \text{ cm}^{-1}$) of each sample. Since ATR-FTIR spectra subtraction was done at the slope of the absorption band of the ferrihydrite ($< 1100 \text{ cm}^{-1}$), it is difficult to preserve the P ν_1 vibration at $< 800 \text{ cm}^{-1}$ if present. Therefore the changes in the P ν_3 vibrations are mainly discussed in the "Results and Discussion" section.

2.5 Results and Discussion

2.5.1 Ionic Strength Effects on Adsorption Envelopes

Fig.2.1 shows the effects of ionic strength on P adsorption envelopes. Approximately 70 % ($\approx 1.85 \mu\text{mol m}^{-2}$) of P was removed at $\text{pH} \approx 4$ at all I, and the net adsorption decreased to 30 % ($\approx 0.8 \mu\text{mol m}^{-2}$) with pH increasing up to 9.5 (Fig.1). The P adsorption appears to be insensitive to changes in I between pH 3 and 7.5, whereas the adsorption increases with increasing I at $\text{pH} > 7.5$. Ionic strength independent P adsorption behavior on soils (New Zealand loamy soils) and soil components (kaolinite, montmorillonite, illite, and goethite) have been reported by several researchers (Barrow et al., 1980; Edzwald et al., 1976; Helyar et al., 1976a; Helyar et al., 1976b; Kafkafi et al., 1988; Ryden et al., 1977; Ryden and Syers, 1975).

Oxyanion adsorption onto variable charge mineral surfaces may form inner-sphere complexes (via ligand exchange) and/or outer-sphere complexes (via electrostatic interaction). These surface complexes can be indirectly distinguished by the I effects on the adsorption envelopes (Hayes et al., 1988). Inner-sphere complexes

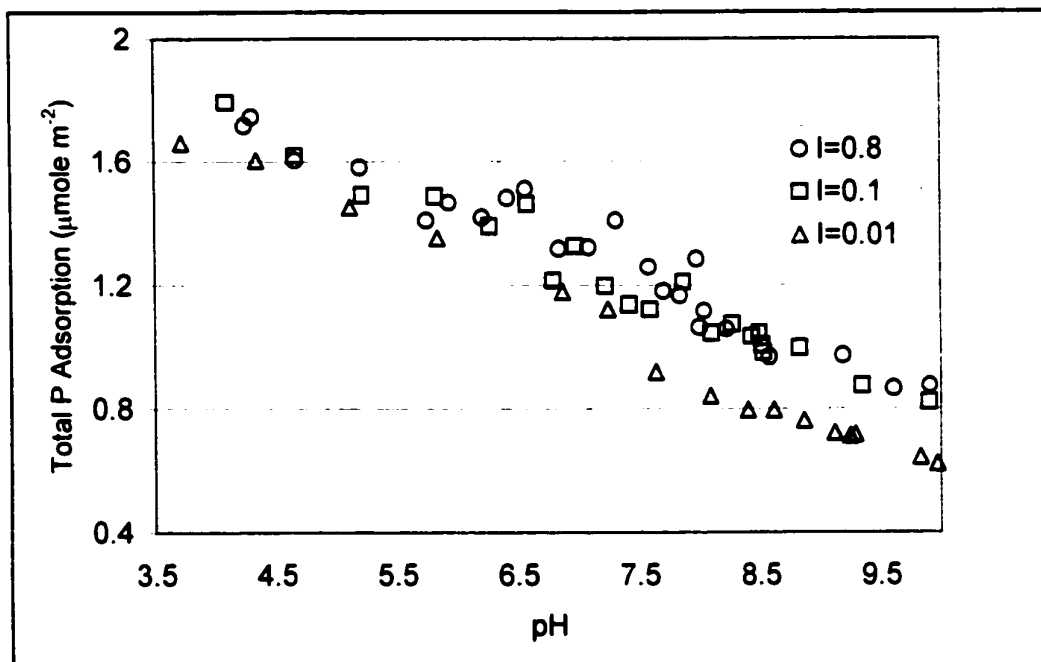
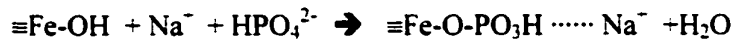


Figure 2.1 Ionic strength effects on P adsorption envelopes at the ferrihydrite-water interface.

(i.e., selenite) are insensitive to changes in I, while outer-sphere complexes (i.e., selenate) are sensitive to the changes in I because of competition with counter anions in the background electrolytes. Based on this argument, we can suggest the formation of P inner-sphere complexes at pH 3-7.5. We, however, do not have a straightforward explanation for the increase in the P adsorption with increasing I observed at pH > 7.5. Barrow (1980) also observed this unique P adsorption phenomena at the goethite-water interface at pH > 4.3 (Barrow et al., 1980). The data were later explained using the quadruple-layer adsorption model (Bowden et al., 1980), but McBride (1997) pointed out that the model is not suited to explain the anion adsorption behavior due to the use of the hypothetical fitting parameters (McBride, 1997). The Diffuse Double Layer theory (DLT) can also be considered. Decreased double layer thickness due to increased I allows the P ions to approach closer to the negatively charged surfaces, where they form inner-sphere complexes via ligand exchange mechanisms. Inner-sphere adsorption, however, should not be influenced by either the thickness of diffuse double layer or the repulsion force because the specific adsorption involves direct coordination to discrete surface metal cations (McBride, 1997). Instead, McBride suggested the simple mass action principle to explain the unique P adsorption phenomena. The principle is similar to the constant capacitance model described by Goldberg and Sposito (1984) (Goldberg and Sposito, 1984). The surface electrical potential correction term is ignored by assuming that any inner-sphere and outer-sphere counter ions are adsorbed to balance the surface charge created in the process. In the case of high I, the negatively charged surfaces created by the inner-

sphere P adsorption are likely to be neutralized by co-adsorption of cations (*i.e.*, Na⁺) from indifferent electrolytes. Therefore, higher electrolyte concentrations may facilitate the P adsorption via the following reaction:



In fact, there is macroscopic evidence to support this theory. Nanzyo (1986) reported that sodium adsorption was significantly enhanced from 0.76 to 1.84 $\mu\text{mol m}^{-2}$ with increasing P adsorption from 0 to 0.8 $\mu\text{mol m}^{-2}$ on iron hydroxide gel at pH \approx 10 (Nanzyo, 1986).

Accordingly, our P adsorption envelope data suggest that P predominantly forms inner-sphere complexes at the FH–water interface at pH 4-9.5. No conclusive statements can be made based on the macroscopic data. We therefore performed the EM measurements and ATR-FTIR analysis of P adsorption at the FH-water interface.

2.5.2 Electrophoretic Mobility Measurements

The EM measurements showed that the presence of 25 and 50 $\mu\text{mol P}$ in 0.1 M NaCl solution lowered the EM between pH 4-10 and shifted the isoelectric point (IEP) of the solid from \approx 8 to $<$ 4.0 (Fig. 2.2). Charge reversals in EM and shifts in IEP due to P adsorption to hematite and goethite have been previously reported (Hansmann and Anderson, 1985; Tejedor-Tejedor and Anderson, 1990).

According to Hunter (1981), the EM measurements are useful not only in obtaining isoelectric points (IEP) for colloidal materials, but also to indirectly distinguish inner-sphere complexes from outer-sphere complexes (Hunter, 1981). Non-specific ion adsorption of indifferent electrolytes outside of the shear plane (i.e., formation of outer-sphere complexes via van der Waals forces) generally does not affect the IEP, but it could cause shifts in the value of EM if the concentrations of indifferent electrolyte are high (Hunter, 1981). The shear plane is at the outer edge of the inner part of the double layer and near the outer Helmholtz plane or the Stern layer, depending on the models used to describe the interface (Hunter, 1981). Inner-sphere complexes generally cause shifts in both IEP and EM due to specific ion adsorption inside the shear plane (Hunter, 1981). In some cases, however, inner-sphere adsorption does not significantly affect the EM and IEP of the pure solid suspension (Hunter, 1981; Suarez et al., 1998).

Based on the information above, our EM measurements suggest the formation of inner-sphere complexes for P at pH 4-9. As mentioned above, EM can be shifted of inner-sphere complexes for P at pH 4-9. As mentioned above, EM can be shifted by physically adsorbed anions such as chloride. Moreover the chloride concentration was same in all EM measurements, so if physical adsorption of chloride is outcompeting the formation of outer-sphere P complexes, we should observe the same EM values for the systems containing 0.1 M NaCl regardless of P being present or not. This is not the case (Fig. 2.2). Therefore, our experimental evidence (shifts in IEP

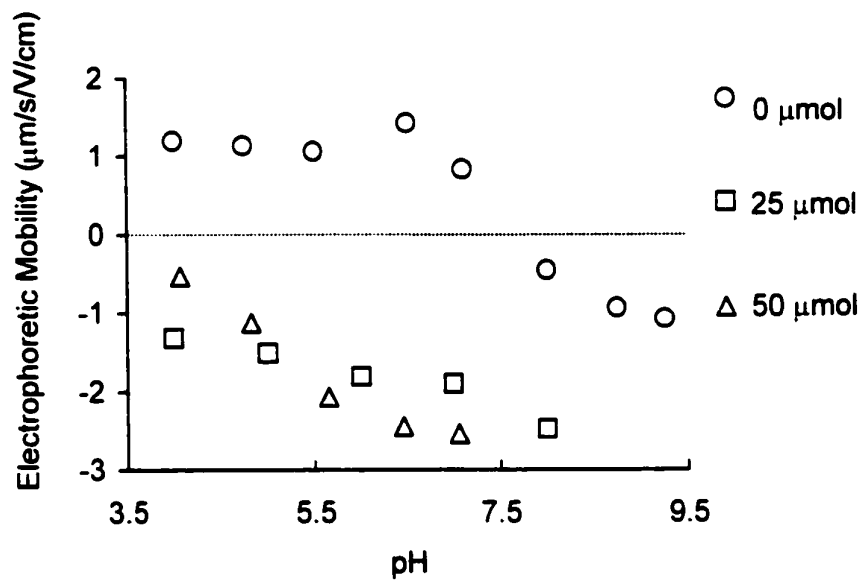


Figure 2.2 Electrophoretic mobility measurements on ferrihydrite with/without 25 and 50 μmol sodium P solution.

and EM with 25 and 50 $\mu\text{mol P}$ and 0.1 M NaCl) suggests that P is specifically adsorbed (*i.e.* forms inner-sphere complexes) at the FH-water interface.

Another explanation for the observed EM shift of the P- FH samples is the formation of iron-phosphate (surface) precipitates, which might alter the charge properties of the FH. However, speciation calculations in MINEQL+ (Schecher and McAvoy, 1998) predict that all samples were undersaturated with respect to $\text{FePO}_4 \cdot 2\text{H}_2\text{O(s)}$.

The EM measurement results are consistent with the result of the I effects on the P adsorption envelopes discussed in the previous section. It is, however, difficult to suggest molecular scale adsorption mechanisms based on our macroscopic data alone (the adsorption envelopes and the EM measurements). We therefore performed ATR-FTIR spectroscopic analyses to investigate the molecular scale P surface speciation at the FH-water interface.

2.5.3 ATR-FTIR Analyses

2.5.3.1 Theoretical IR vibrations of Phosphoric Acid

A tetragonal penta-atomic molecule (*e.g.*, PO_4^{3-}) exhibits four different vibrations; 1) the symmetric stretching (A_1 , ν_1), 2) the symmetric bending (E , ν_2), 3) the asymmetric stretching (F , ν_3) and 4) the asymmetric bending (F , ν_4). The ν_1 (nondegenerate symmetric stretching) and the ν_3 (triply degenerate asymmetric stretching) vibration can be utilized to understand not only the molecular symmetry of the phosphoric acid (P) but also the coordination environments of the P adsorption

complexes on metal oxide surfaces. Infrared spectra of P have been extensively investigated by several researchers (Chapman and Thirlwell, 1964; Nakamoto, 1997; Persson et al., 1996; Tejedor-Tejedor and Anderson, 1990). Phosphate has several pK_a values ($pK_1 = 2.20$, $pK_2 = 7.2$, and $pK_3 = 12.3$) (Snoeyink and Jenkins, 1980), and the protonation significantly affects the P molecular symmetry. In Table 2.1, we have summarized 1) the molecular symmetry and 2) the number and the position of the ν_1 and ν_3 vibrations of the phosphoric acid at different pHs reported in previous studies. Fig. 2.3 shows the IR spectra of P solution species which are reproduced based on Tejedor-Tejedor and Anderson's research (1990).

Fully deprotonated phosphoric acid (PO_4^{3-}) at pH 11 has T_d symmetry. This tetrahedra molecule shows a single ν_3 asymmetrical vibration (F_2) at $\approx 1006\text{ cm}^{-1}$, and there is no activation of the ν_1 vibration (Fig. 2.3). Monoprotonated (HPO_4^{2-}) species has C_{3v} symmetry and the ν_3 vibration splits into two (E and A_1) at ≈ 1077 and 989 cm^{-1} . There is also ν_1 band activation at $\approx 850\text{ cm}^{-1}$. Further protonation results in the formation of diprotonated phosphate (i.e., $H_2PO_4^-$), which leads to a reduction in the symmetry from C_{3v} to the C_{2v} . The ν_3 (E) vibration splits into two bands (B_1 and B_2), therefore, there are a total of three ν_3 bands (B_1 , B_2 and A_1) at ≈ 1060 , 1074 and 940 cm^{-1} . The ν_1 vibration shifts to higher wavenumber at $\approx 870\text{ cm}^{-1}$. At $pH \approx 1.3$, the symmetry of the dominant phosphoric acid species is H_3PO_4 (C_{3v}) and the spectrum shows doublets (E and A_1) of the ν_3 vibration at ≈ 1177 and 1006 cm^{-1} . In summary, the numbers of the ν_3 vibration are two for the C_{3v} symmetry and three for the C_{2v} or

lower (C_1) symmetry. The results of the P IR spectra are in good agreement with the studies by Chapman et al. (1964) and Nakamoto (1997).

The peak positions of several P model compounds and P adsorption complexes at iron oxide-water interfaces based on *in situ* FTIR studies are also summarized in Table 2.1 and 2.2. Although the band positions significantly differ between different P compounds, the numbers of bands with respect to the symmetry are consistent. This is also true for other P model compounds reported in Table 2.1. Atkinson and co-workers (1974) reviewed the ν_1 and ν_3 vibrations of the reference monodentate mononuclear complex $\text{Co}(\text{NH}_3)_5\text{PO}_4$ (C_{3v}), and the reference bidentate binuclear complexes $(\text{CH}_3\text{O})_2\text{PO}_2^-$ (C_{2v}) and $\text{Co}(\text{NH}_2\text{CH}_2\text{CH}_2\text{NH}_2)\text{PO}_4$ (C_{2v}) based on the studies by Kumamoto (1965) and Lincoln and Stranks (1968) (Atkinson et al., 1974; Kumamoto, 1965; Lincoln and Stranks, 1968). The number of the ν_3 vibrations in these complexes is in good agreement with the predicted numbers based on the molecular symmetry (C_{3v} or C_{2v}) (Table 2.1).

We can apply the concept of molecular symmetry as related to changes in the ν_3 and ν_1 vibrations to P adsorption complexes on metal oxide surfaces. If orthophosphate ions (PO_4^{3-}) are coordinated with metal ion(s) at the hydr oxide surface by forming inner-sphere complexes, one should observe a reduction in symmetry with respect to the free aqueous PO_4^{3-} (T_d). As the symmetry lowers from T_d to C_{3v} and to C_{2v}/C_1 , the triply degenerate ν_3 vibration splits into two or three bands, and the nondegenerate ν_1 vibration shifts upon the changes in coordination

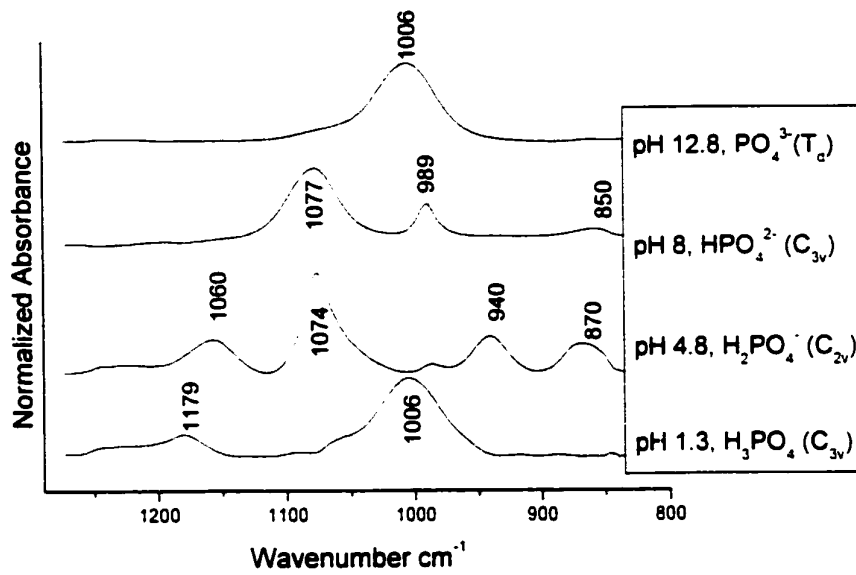


Figure 2.3 ATR-FTIR spectra of phosphoric acid at different pHs.

Table 2.1 Position of IR peak maxima of phosphoric acid and P adsorption complexes on iron oxides.

Species, symmetry and reaction conditions	Infrared active band positions (cm ⁻¹)		
	1100	1000	900
PO ₄ ³⁻ (aq), T _d (This study)		1010(v ₁)	
HPO ₄ ²⁻ (aq), C _{3v} (This study)		1076(v ₁)	989(v ₁) 846(v ₁)
H ₂ PO ₄ ⁻ (aq), C _{2v} (This study)	1155(v ₁)	1076(v ₁)	942(v ₁) 874(v ₁)
H ₃ PO ₄ (aq), C _{3v} (This study)	1174(v ₁)	1007(v ₁)	888(v ₁)
Reference monodentate mononuclear complexes			
Co(NH ₃) ₅ PO ₄ , C _{3v} (Atkinson et al., 1974)		1030(v ₁)	980(v ₁) 934(v ₁)
Reference bidentate binuclear complexes (CH ₃ O) ₂ PO ₂ ⁻ , C _{2v} (Atkinson et al., 1974)	1220(v ₁) 1110(v ₁)	1050(v ₁)	815(v ₁)
Co(NH ₂ CH ₂ CH ₂ NH ₂)PO ₄ , C _{2v} (Atkinson et al., 1974)		1085(v ₁) 1050(v ₁)	915(v ₁) 900(v ₁)
Goethite-P (paste) (Tejedor-Tejedore and Anderson, 1990)			
pH 4.5, 2.35 μmol m ⁻²	1121(v ₁)	1044(shoulder) 1004(v ₁ bands)	Peaks <940 cm ⁻¹ can not be identified due to the absorption bands of goethite
pH 4.5, 1.85 μmol m ⁻²	1095(v ₁)	1044(v ₁) 1004(v ₁)	
pH 4.5, 1.23 μmol m ⁻²	1097(v ₁)	1044 1004(shoulder) (v ₁ bands)	
pH 5-8.4, 1.85-2.35 μmol m ⁻²	≅1100(v ₁)	≅1040(v ₁) ≅1006(v ₁)	
Goethite-P (in suspension) (Partif and Atkinson, 1976)			
pH 3.6-5.1, 1.25-2.5 μmol m ⁻²	≅1100(v ₁) (Not well defined)	≅1000(v ₁) (Not well defined)	
pH 8.1-9.7, 0.63-1.25 μmol m ⁻²		≅1080(v ₁) ≅1040(v ₁)	

Table 2.2 Position of IR peak maxima of ferric phosphate solution complexes.

Species, symmetry and reaction conditions	Infrared active band positions (cm ⁻¹)		
	1100	1000	900
<i>Ferric phosphate monodentate mononuclear solution complexes</i>			
FeH ₂ PO ₄ or FeHPO ₄ (Tejedore-Tejedore and Anderson, 1990) pH 1, 1.4mmol H ₃ PO ₄ , 0.8mmol Fe(ClO ₄) ₃ , 0.1 M HClO ₄ , 0.25 M NaClO ₄	1170(v ₁)	1077(v ₁)	980(v ₁)
pH 1, 1.4mmol H ₃ PO ₄ , 0.8mmol Fe(NO ₃) ₃ , 0.1 M HNO ₃ , 0.25 M NaNO ₃ (Tejedore-Tejedore and Anderson, 1990)	1149(v ₁)	1085(v ₁)	960(v ₁)
Fe(III)-P monodentate mononuclear (This study based on Rose et al., 1997)		1095(v ₁) 1034(v ₁)	986(v ₁)

environment (Nakamoto, 1997). If P ions form outer-sphere complexes, the ν_3 vibration of the free P ions at the same pH should be shifted slightly due to slight distortion in adsorbed P molecules via *van der Waals* forces, but there should be no influence on the number of ν_3 vibrations.

To investigate the P surface complexes at the FH-water interface, we first compared the IR spectra of adsorbed species to the spectrum of the dominant phosphoric acid species at the same pH to distinguish the inner-sphere from the outer-sphere adsorption complexes. Second, we assigned the symmetry of the adsorption complexes based on the number of ν_3 band splitting and/or the presence or absence of the ν_1 vibration. Peak deconvolution and Gaussian profile fitting were performed to reveal the assemblage of multiple ν_3 bands using the PeaksolveTM software package version 1.05 (Galactic Industries Corp.). This molecular symmetry assignment allows us to speculate on the molecular configurations of the surface complexes. Third, the spectra of the adsorption complexes in H₂O were compared with those in D₂O. If there are any shifts in the band position in these spectra, one can suggest that the surface complexes are associated with proton(s). Based on the combined information from these experiments, the final adsorption complexes can be proposed.

2.5.3.2 pH Effect on P Adsorption Complexes at pH 4-9

Fig. 2.4 shows the pH effect on the P surface complexes for samples with the same loading level of $\Gamma = 0.38 \mu\text{mol m}^{-2}$. The highest peak at $\approx 1020 \text{ cm}^{-1}$ for the

sample reacted at pH 4 is slightly shifted to $\approx 1025 \text{ cm}^{-1}$ with increasing pH from 4 to 9. The broad spectrum at pH 4 is an assemblage of three ν_3 vibrations ($\approx 1102 \text{ cm}^{-1}$ and 1020 cm^{-1} , and at $\approx 920 \text{ cm}^{-1}$) (Fig. 2.4), as determined via Gaussian profile fit analysis. This indicates the C_{2v} or lower symmetry for the P adsorption complexes forming at this pH. The position of peak maxima ($\approx 1102 \text{ cm}^{-1}$ and $\approx 1020 \text{ cm}^{-1}$) is similar to the spectra of P on goethite surfaces in previous *in situ* FTIR studies (Table 2.1) (Parfit and Atkinson, 1976; Tejedore-Tejedore and Anderson, 1990), suggesting similar P surface complexes might be forming at the FH/goethite-water interface.

As pH increases, the triplet splitting of the ν_3 vibration becomes well resolved (Fig. 2.4). Interestingly, the spectra at pH 7.5, 8.2 and 9 show a small shoulder at $\approx 890 \text{ cm}^{-1}$ (indicated by arrows in Fig. 2.4) that is probably the nondegenerate ν_1 vibration of the C_{2v} or C_1 symmetry species. The presence of the ν_1 vibration at pH > 7.5 will be discussed later. Overall, there are no significant changes in the IR spectra of the P surface complexes with changing pH, but the molecular symmetry seems to remain C_{2v} or lower (Fig. 2.4). It is clear that the inner-sphere adsorption of P causes the reduction in the molecular symmetry from T_d (PO_4^{3-}) to C_{2v} or lower. If the symmetry reduction is caused only by protonation, as would be the case for outer-sphere adsorption, then the ν_3 vibrations should appear at similar wavenumber for the dominant phosphoric acid species in the pH range studied (4-9) (i.e., H_2PO_4^- and or HPO_4^{2-}). The peak maxima of the ν_3 vibrations of the reacted samples, however, are significantly different from those of the P solution species (Fig. 2.3 and 2.4).

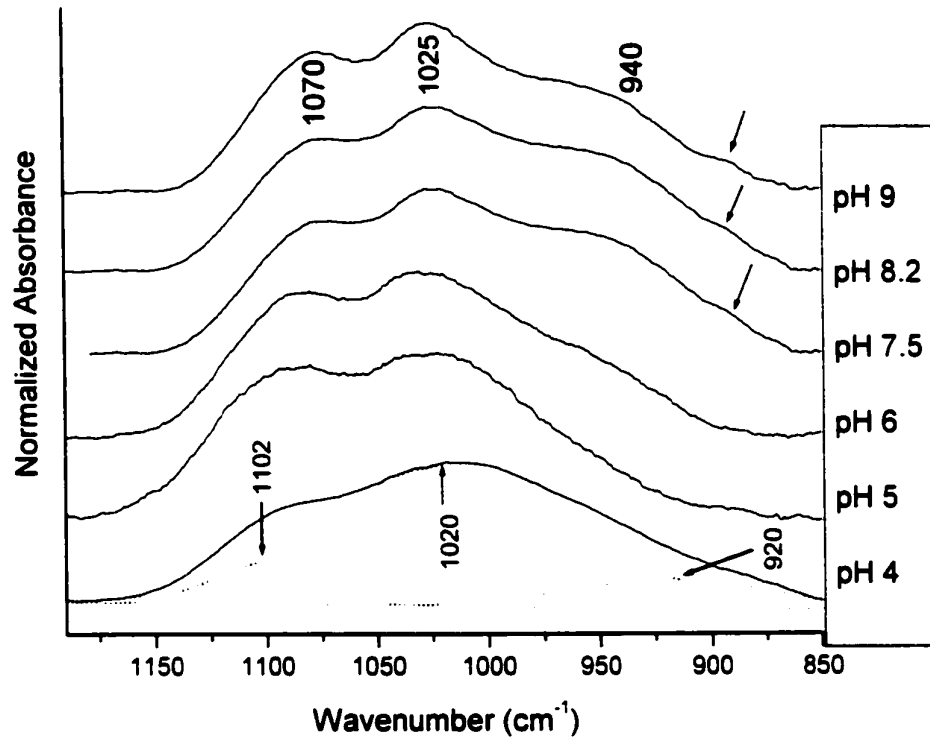


Figure 2.4 ATR-FTIR spectra: pH effects (4-9) on the P adsorption complexes ($\Gamma = 0.38 \mu\text{mol m}^{-2}$) at the ferrihydrite-water interface.

Therefore, the symmetry reduction resulted from the P coordination onto iron octahedral structures at the FH surfaces, indicating the formation of P inner-sphere complexes. This is consistent with the results of the adsorption envelopes and the EM measurements. The type of adsorption complexes will be discussed in the next section.

2.5.3.3 Loading Level Effects on P Adsorption Complexes at pH \geq 7.5

The IR spectra of the P adsorption complexes ($\Gamma = 0.38, 1.15, 1.82,$ and $2.42 \mu\text{mol m}^{-2}$) at pH 7.5 are shown in Fig. 2.5. All spectra show well-resolved triplet splitting of the ν_3 vibration ($\approx 952, \approx 1021$ and $\approx 1088 \text{ cm}^{-1}$) as determined via Gaussian profile fit analysis, indicating C_{2v} or lower symmetry regardless of loading levels. The central peak at $\approx 1021 \text{ cm}^{-1}$ is surrounded by two peaks (≈ 1088 and 952 cm^{-1}) that are of near equal intensity (Fig. 2.5). The distribution and the peak intensity of the triplet splitting resemble those of the IR spectrum for H_2PO_4^- (Fig. 2.3). Possible adsorption complexes can be postulated to be $\equiv\text{FeHPO}_4$ or $\equiv\text{Fe}_2\text{PO}_4$. The similar IR spectra can also be seen in the adsorption samples at pH 8.2 and 9 (Fig. 2.4). To further investigate the coordination and protonation environment of the P surface complexes, we compared the spectra at pH/pD 7.5 with the loading level of $2.42 \mu\text{mol m}^{-2}$ (Fig. 2.6). The spectra show no significant change in the position of the ν_3 vibration at $850\text{-}1175 \text{ cm}^{-1}$ (Fig. 2.6), indicating that the adsorption complexes are not associated with protons. Similar results were obtained in samples with loading levels of $0.38\text{-}1.82 \mu$

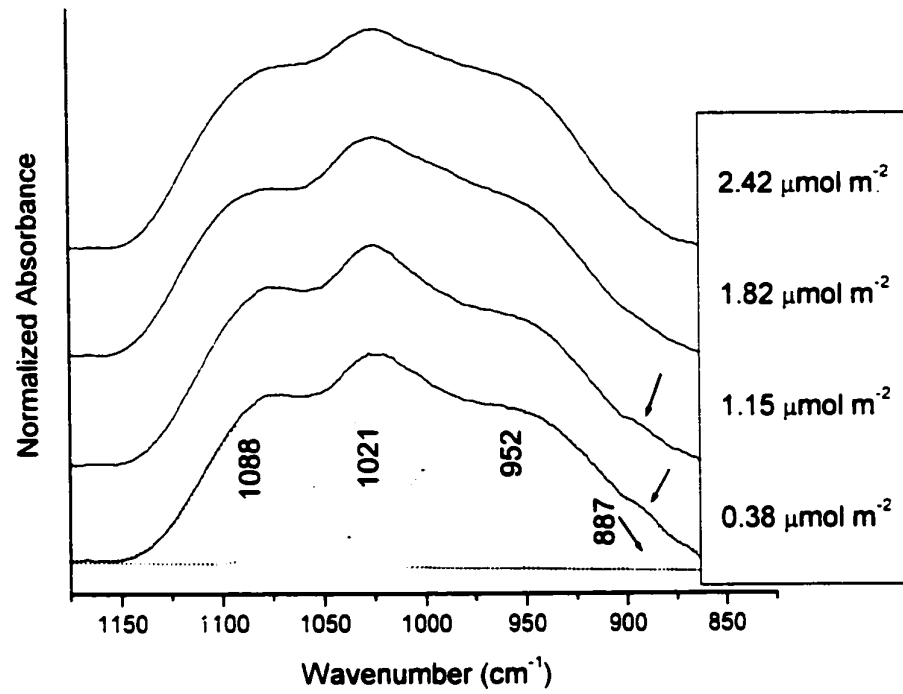


Figure 2.5 ATR-FTIR spectra: loading level effect ($\Gamma = 0.38\text{-}2.42 \mu\text{mol m}^{-2}$) on the P adsorption complexes at pH 7.5 at the ferrihydrite-water interface.

mol m⁻² at pH ≥ 7.5 (not shown). The surface complexes that have the C_{2v} or lower symmetry without proton association are the nonprotonated bidentate binuclear complexes (≡Fe₂PO₄). We, therefore, suggest the predominant formation of the nonprotonated bidentate binuclear species at pH 7.5 at a loading level of 0.38-2.42 μmol m⁻². These data interpretations can be supported by comparing them to arsenate (AsO₄³⁻) adsorption mechanisms at the FH-water interface at pH 8, since arsenate has similar chemical properties (e.g., pK_a) to phosphate. Waychunas and co-workers reported the formation of As(V) bidentate binuclear species based on extended X-ray absorption fine structure spectroscopy (EXAFS) (Waychunas et al., 1993). Previous *in situ* FTIR study also showed similar triplet splitting of the ν₃ vibration in the spectra for P adsorbed goethite surfaces (pH 6-8.3, Γ = 1.85-2.35 μmol m⁻²) (Table 2.1), which was assigned to nonprotonated bidentate binuclear complexes (Tejedor-Tejedor and Anderson, 1990).

Interestingly, there is an activation of the ν₁ vibration at ≈887 cm⁻¹ in the low loading (Γ = 0.38 and 1.15 μmol m⁻²) samples as determined via Gaussian profile fit analysis (Fig. 2.5). In Fig. 2.5, the small ν₁ vibration becomes hidden when the loading level from 0.38 to 2.42 μmol m⁻² due to the shift and the intensification of the ν₃ vibration at ≈950 cm⁻¹. The ν₁ symmetrical vibration is observed in the loading level (Γ = 0.38-1.15 μmol m⁻²) samples reacted at pH ≥ 7.5 (indicated by arrows in Fig. 2.4 and 2.5), but not in the samples reacted at pH < 7.5 (Fig. 2.4 and 2.7). The ν₁ vibration can be possibly explained by 1) the presence of different surface complexes

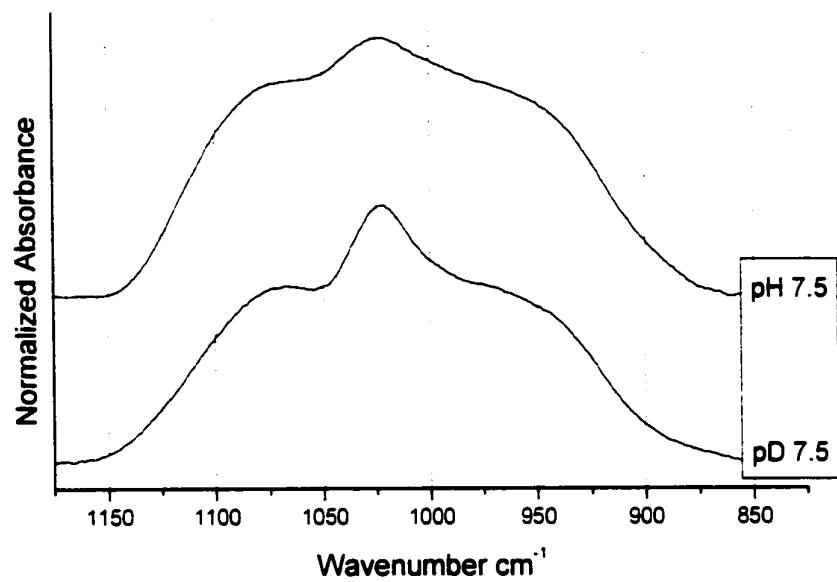


Figure 2.6 ATR-FTIR spectra of P adsorption complexes at pH/pD 7.5 at the ferrihydrite-water interface.

(e.g., monodentate mononuclear complexes) other than the predominant nonprotonated bidentate binuclear complexes and/or 2) further distortion in the molecular symmetry of the predominant nonprotonated bidentate binuclear complexes. A mixture of surface complexes, therefore, might be forming at these pHs and loading levels. In Fig 4, the peak at $\approx 1070 \text{ cm}^{-1}$ becomes more intensified relative to the peak maxima at $\approx 940 \text{ cm}^{-1}$ with increasing pH from 7.5 to 9. The slight changes in the peak intensity in ν_3 vibrations (≈ 940 and 1070 cm^{-1}) at $\text{pH} \geq 7.5$ may suggest that the C_{2v} molecular symmetry is slightly lowered. If one can assume that the same surface species are present between pH 7.5 and 9, the distortion in the C_{2v} molecular symmetry could be caused by complexation with either protons or other ions from the bulk solution. Since the positions of the ν_3 vibrations had no influence after the deuterium exchange, between $850\text{-}1200 \text{ cm}^{-1}$ in the samples at pH 7.5 (Fig. 2.6), the surface complexes are not associated with protons. Association with sodium ions may account for the molecular distortion observed at $\text{pH} \geq 7.5$. As discussed in the adsorption envelope section, the Na^+ ions might be electrostatically attracted to the adsorbed P at the FH-water interface. This mechanism is indirectly supported by Nazyo's macroscopic evidence that Na^+ adsorption onto FH significantly increases from 0 to $\approx 1.12 \mu\text{mol m}^{-2}$ with increasing pH from 4.4 to 10.2 at constant P loading level ($\Gamma \approx 0.29 \mu\text{mol m}^{-2}$) on the FH surface (Nazyo, 1986).

We, therefore, suggest that the nonprotonated bidentate binuclear complexes (Fe_2PO_4 , C_{2v}) predominantly form at $\text{pH} \geq 7.5$ at the FH-water interface under our

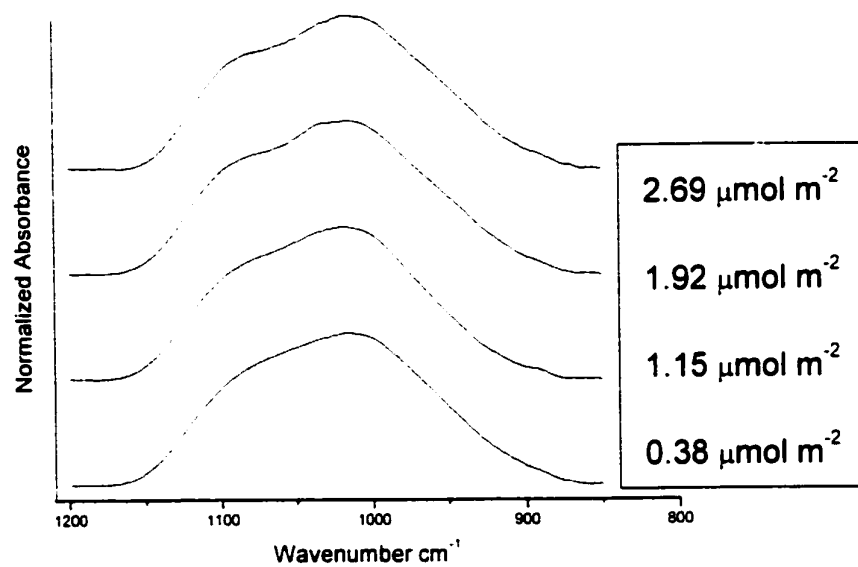


Figure 2.7 ATR-FTIR spectra: loading level effect ($\Gamma = 0.38\text{-}2.69 \mu\text{mol m}^{-2}$) on the P adsorption complexes at pH 4 at the ferrihydrite-water interface.

experimental conditions. However the presence of different surface complexes (e.g., monodentate mononuclear complexes) and/or $\equiv\text{Fe}_2\text{PO}_4\cdots\text{Na}^-$ complexes cannot be excluded.

2.5.3.4 Loading level Effects on P Adsorption Complexes at pH < 7.5

Fig. 2.7 shows the loading level effects on the P surface complexes at pH 4. The loading level does not seem to have a strong influence on the IR spectra, suggesting that the molecular symmetry of the P surface complexes is similar. To deconvolute the assemblage of peaks in these broad spectra, the Gaussian profile fit analyses were performed. The peak fitting analysis in the spectrum at pH 4 with $\Gamma = 0.38 \mu\text{mol m}^{-2}$ revealed that the broad peak was an assemblage of three ν_3 vibrations at $\approx 1102 \text{ cm}^{-1}$ and 1020 cm^{-1} , and $\approx 920 \text{ cm}^{-1}$ (Bottom spectrum in Fig. 2.4), indicating the C_{2v} or lower symmetry. Similar results were obtained in samples at pH 4, 5 and 6 (not shown), indicating these surface complexes have C_{2v} or lower symmetry.

The P adsorption complexes at pH 4 with $\Gamma = 0.38$ and $2.69 \mu\text{mol m}^{-2}$ compared with those at pH 4 show that the peaks at pH 4 are shifted to ≈ 948 and 1077 cm^{-1} (dashed line A and B in Fig. 2.8) after deuterium exchange. These results suggest that the adsorption complexes forming at pH 4 and $\Gamma = 0.38$ - $2.69 \mu\text{mol m}^{-2}$ are associated with proton(s). As pH decreases below 7.5, protonation on the surface complexes can be expected. The protonation further lowers the symmetry of the P

adsorption complexes to C_1 . Based on the IR spectra assignment at $\text{pH} \geq 7.5$ (i.e., nonprotonated bidentate binuclear complexes), we can predict the type of adsorption complexes at $\text{pH} < 7.5$ to be protonated bidentate binuclear complexes. In fact, Tejedore-Tejedore and Anderson (1990) suggested that the nonprotonated bidentate binuclear complexes at $\text{pH} > 6$ becomes monoprotonated bidentate binuclear ($\equiv\text{Fe}_2\text{HPO}_4$) surface complexes with decreasing pH from 6.0 to 3.6 at the goethite-water interface (Tejedore-Tejedore and Anderson, 1990).

It is possible, however, that the protonated monodentate mononuclear complexes ($\equiv\text{FePO}_4\text{H}$ and $\equiv\text{FePO}_4\text{H}_2$) and monodentate mononuclear complexes with hydrogen bonding with hydroxyl groups of the FH surface form, because they all have the C_{2v} or lower symmetry and are associated with proton(s) (Fig. 2.10). We, therefore, compare our IR spectra with the FTIR spectra of Fe-P monodentate aqueous complexes that were well-characterized by *in situ* spectroscopic techniques such as the spectrophotometric method and EXAFS. Wilhelmy et al. (1985) studied the equilibria and kinetics of ferric and phosphate ion complexation at $\text{pH} < 2$ using spectrophotometric and stop-flow techniques (Wilhelmy et al., 1985). They suggested that $\text{FeH}_2\text{PO}_4^{2-}$ species are formed under the specific reaction conditions (0.014 M H_3PO_4 , 0.1 mmol $\text{Fe}(\text{ClO}_4)_3$, 0.1 M HClO_4 , 0.25 M NaClO_4 at pH 1). The IR spectrum of this complex was earlier reported by Tejedore-Tejedore and Anderson (Tejedore-Tejedore and Anderson, 1990). The peak maxima of the triplet splitting of the ν_3 vibrations are reported in Table 2.2, and are consistent with C_{2v} or lower

symmetry. The symmetry is in a good agreement with the three ν_3 band splitting of either diprotonated monodentate mononuclear complexes ($\text{FeH}_2\text{PO}_4^{2+}$, C_1) and/or monoprotated monodentate mononuclear complexes (FeHPO_4^{2-} , C_1).

The phosphorus K edge EXAFS spectroscopic study by Rose and co-workers (1997) also showed the formation of monodentate mononuclear ferric phosphate solution complexes (Rose et al., 1997). They investigated the local structural environment of phosphate during the hydrolysis of FeCl_3 in the presence of phosphate at $\text{pH} < 1$ with $\text{P/Fe} = 0.5$ and $n = [\text{OH}]/[\text{Fe}] = 1$, and found evidence for the formation of monodentate mononuclear Fe-PO_4 (aq) complexes (Rose et al., 1997). We determined the ATR-FTIR spectrum for the P species forming under the same reaction conditions as those of Rose et al. (1997). The broad peak is an assemblage of three ν_3 vibrations positioned at 1100, 1028, and 971 cm^{-1} (Fig. 2.9), indicating C_{2v} or lower symmetry. Whereas EXAFS analysis is not sensitive to reveal the protonation environment of the PO_4 surface complexes, the molecular symmetry identification via FTIR analysis is sensitive to protonation of the P surface complexes. Several molecular symmetries are possible for this Fe-P monodentate mononuclear (aq) complex with C_{2v} or lower symmetry. They are monoprotated monodentate mononuclear (C_1), diprotonated monodentate mononuclear (C_1), nonprotonated monodentate mononuclear with hydrogen bonded with the hydroxyl group of the FH (C_1), monoprotated monodentate mononuclear with hydrogen bonded with the hydroxyl group of the FH (C_1), and diprotonated monodentate mononuclear with

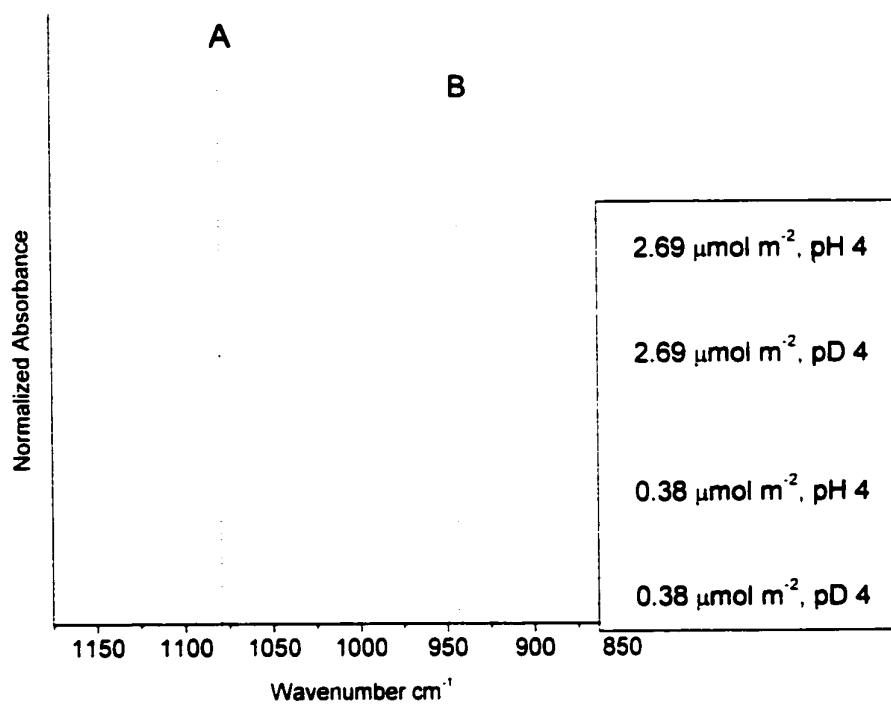


Figure 2.8 ATR-FTIR spectra of P adsorption complexes at pH/pD 4 at the ferrihydrite-water interface.

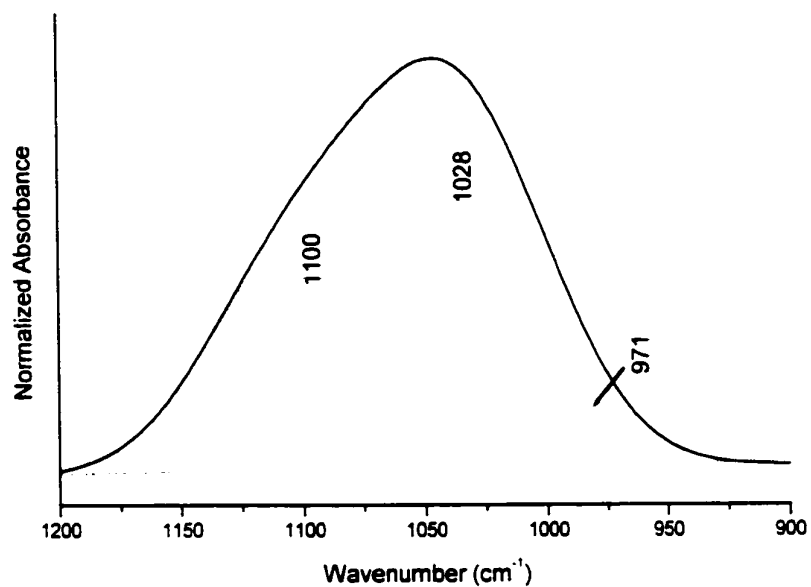


Figure 2.9 ATR-FTIR spectrum of monodentate mononuclear Fe-P (aq) complex. The spectra show raw data and deconvoluted peaks in solid line and the fitted profiles in dotted line.

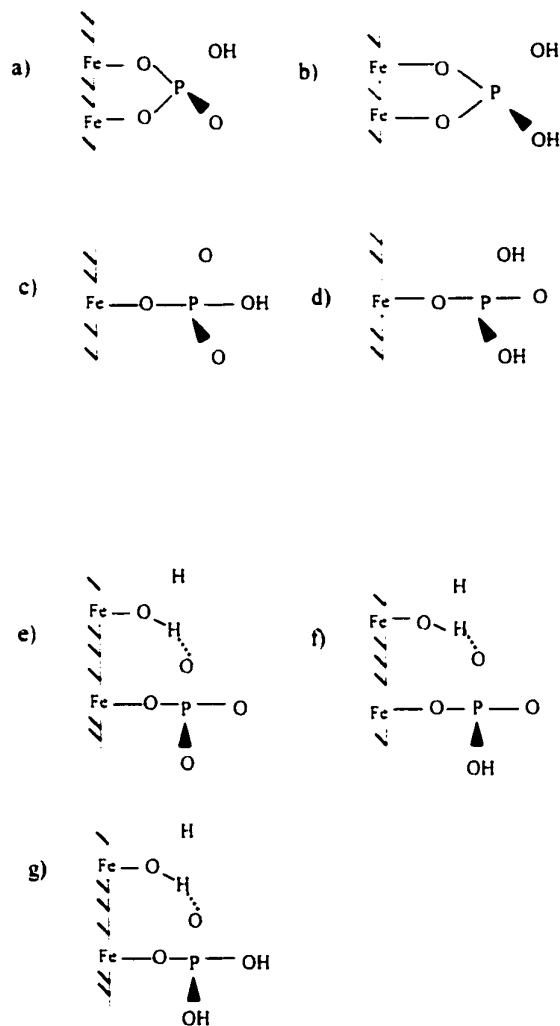


Figure 2.10 Possible molecular configurations (C_{2v} or lower) of protonated P inner-sphere complexes at the ferrihydrite-water interface.

a) monoprotonated bidentate mononuclear (C_1), b) diprotonated bidentate mononuclear (C_{2v}), c) monoprotonated monodentate mononuclear (C_1), d) diprotonated monodentate mononuclear (C_1), e) nonprotonated monodentate mononuclear hydrogen-bonded with the hydroxyl group of the FH (C_1), f) monoprotonated monodentate mononuclear hydrogen-bonded with the hydroxyl group of the FH (C_1), and g) diprotonated monodentate mononuclear hydrogen-bonded with the hydroxyl group of the FH (C_1) (Fig. 2.10 (c)-(g)).

Comparison of the peak positions of the monodentate mononuclear reference complexes to our experimental spectra at $\text{pH} < 7.5$ indicates no similarities. The peak at 920 cm^{-1} is only present in our IR spectra. This dissimilarity might suggest that the predominant complexes forming at $\text{pH} 4$ at the FH–water interface are unlikely to be mono-/di- protonated monodentate mononuclear complexes. Assigning the type of surface complexes based on the band positions of the reference compounds, however, is risky because the position of bands could be shifted due to differences in the reaction conditions (e.g., loading levels, P/Fe ratio and water content). Tejedore-Tejedor and Anderson (1990) reported changes in the peak position with changing P loading levels ($1.23\text{-}2.35 \mu\text{mol m}^{-2}$) at the goethite-water interface at $\text{pH} 4.5$ (Table 2.1) (Tejedore-Tejedor and Anderson, 1990). The band position could be shifted with changing the moisture content. Several researchers have shown that the position and the intensity of the ν_3 vibration of oxyanions (phosphate and sulfate) can be altered by changing drying conditions (air dry, N_2 drying, and evacuation) (Atkinson et al., 1974; Hug, 1997; Parfitt and Atkinson, 1976). Elimination of the entrained water could facilitate transformation from low energy binding (outer-sphere and/or monodentate mononuclear complexes) to higher energy binding (bidentate binuclear) complexes. The IR spectra collected under dry and/or severely evacuated conditions must be carefully interpreted based on the purpose of the study. We, therefore, rely on the number of the ν_3 vibrations and the molecular symmetry of the P surface complexes more than on the positions of bands. In summary, it is possible that the protonated

Comparison of the peak positions of the monodentate mononuclear reference complexes to our experimental spectra at $\text{pH} < 7.5$ indicates no similarities. The peak at 920 cm^{-1} is only present in our IR spectra. This dissimilarity might suggest that the predominant complexes forming at $\text{pH} 4$ at the FH–water interface are unlikely to be mono-/di- protonated monodentate mononuclear complexes. Assigning the type of surface complexes based on the band positions of the reference compounds, however, is risky because the position of bands could be shifted due to differences in the reaction conditions (e.g., loading levels, P/Fe ratio and water content). Tejedore-Tejedor and Anderson (1990) reported changes in the peak position with changing P loading levels ($1.23\text{-}2.35 \mu\text{mol m}^{-2}$) at the goethite-water interface at $\text{pH} 4.5$ (Table 2.1) (Tejedore-Tejedor and Anderson, 1990). The band position could be shifted with changing the moisture content. Several researchers have shown that the position and the intensity of the ν_3 vibration of oxyanions (phosphate and sulfate) can be altered by changing drying conditions (air dry, N_2 drying, and evacuation) (Atkinson et al., 1974; Hug, 1997; Parfitt and Atkinson, 1976). Elimination of the entrained water could facilitate transformation from low energy binding (outer-sphere and/or monodentate mononuclear complexes) to higher energy binding (bidentate binuclear complexes). The IR spectra collected under dry and/or severely evacuated conditions must be carefully interpreted based on the purpose of the study. We, therefore, rely on the number of the ν_3 vibrations and the molecular symmetry of the P surface complexes more than on the positions of bands. In summary, it is possible that the

protonated monodentate mononuclear complexes, nonprotonated monodentate mononuclear complexes with hydrogen bonding, and protonated bidentate binuclear complexes are present at $\text{pH} < 7.5$ (Fig. 2.10).

2.6 Conclusion

The results of the P inner-sphere adsorption mechanisms are consistent based on adsorption envelopes, EM measurements and ATR-FTIR analysis. Based on our IR analysis, the predominant formation of the nonprotonated bidentate binuclear species (Fe_2PO_4) at $\text{pH} > 7.5$ is proposed and the surface complexes might co-exist with different surface species (e.g., monodentate mononuclear) and/or $\equiv\text{Fe}_2\text{PO}_4\text{Na}$ at $\text{pH} \geq 7.5$. The exact identity of the protonated P inner-sphere surface complexes (i.e., protonated monodentate mononuclear complexes and/or protonated bidentate binuclear complexes) forming at $\text{pH} < 7.5$ could not be elucidated due to limitations in mid-IR range FTIR analysis. In order to identify accurate P adsorption mechanisms in this pH range, local atomic structural information (P-Fe bond distances and the coordination number) of the adsorbed P via phosphorus EXAFS analysis would be very useful to distinguish the protonated monodentate mononuclear from the protonated bidentate binuclear complexes. These analyses would also be useful in determining the formation of iron phosphate surface precipitates that could not be well evaluated by ATR-FTIR analysis.

In previous *in situ* FTIR studies on P adsorption at the goethite-water interface (Parfit and Atkinson, 1976; Tejedore and Tejedore and Anderson, 1990), peak fitting analysis on P ν^3 vibrations and deuterium exchange experiments on P surface complexes were neglected. Therefore, the P molecular symmetry of adsorption complexes with respect to protonation and surface complexation was not clearly understood. Our comprehensive *in situ* ATR-FTIR study, however, revealed not only P bonding mechanisms at the FH-water interface but also the protonation of surface complexes. Such detailed molecular scale information should greatly enhance surface complexation modeling of P adsorption reactions at the mineral-water interface. While our findings (e.g., inner-sphere bidentate binuclear complexes) provide important information on P surface speciation at the FH-water interface for reaction times of less than 48 h, longer residence time effects (months to years) on P adsorption mechanisms at the FH-water interface are not well understood. It is possible that longer contact times could result in nonsingular reactions due to chemical reconfiguration reactions, if biotic and abiotic reductive dissolution of adsorbate is inhibited. Aging effects on P surface speciation at the FH-water interface could be further investigated using time-resolved *in situ* spectroscopic techniques, such studies could provide insights on reactions in natural systems (e.g., long-term P amended soils and sediments).

2.8 References

Atkinson, R.J., R. L. Parfitt, and R.S.C. Smart. 1974. Infrared study of phosphate adsorption on goethite. *Journal of Chemical Society Faraday Transaction 1*, 70: 1472-1479.

Barron, V., N. Galvez, Jr., and J. Torrent. 1997. Epitaxial overgrowth of goethite on hematite synthesized in phosphate media: A scanning force and transmission electron microscopy study. *American Mineralogist*, 82: 1091-1100.

Barrow, N.J., J.W. Bowden, A.M. Posner, and J.P. Quirk. 1980. Describing the effects of electrolyte on adsorption of phosphate by a variable charge surface. *Australian Journal of Soil Research*, 18: 395-404.

Biber, M.V., M.D.S. Afonso, and W. Stumm. 1994. The coordination chemistry of weathering : IV. Inhibition of the dissolution of oxide minerals. *Geochimica et Cosmochimica Acta*, 58(9): 1999-2010.

Bondiatti, G., J. Sinniger and W. Stumm. 1993. The reactivity of Fe(III) (Hydr)oxides: Effects of ligands in inhibiting the dissolution. *Colloids and Surfaces*, 79: 157-167.

- Bowden, J.W., S. Nagarajah, N.J. Barrow, A.M. Posner, and J.P. Quirk. 1980. Describing the adsorption of phosphate, citrate and selenite on the variable charge mineral surface. *Australian Journal of Soil Research*, 18: 49-60.
- Chapman, A.C., and L.E. Thirlwell. 1964. Spectra of phosphorus compounds-I. The infrared spectra of orthophosphates. *Spectrochimica Acta.*, 20: 937-947.
- Edzwald, J.K., D.C. Toensing, and M.C. Leung. 1976. Phosphate adsorption reaction with clay minerals. *Environmental Science and Technology*, 10(5): 485-490.
- Fuller, C.C. and J.A. Davis. 1989. Influence of coupling of sorption and photosynthetic processes on trace element cycles in natural waters. *Nature*, 340: 52-54.
- Goldberg, S., and C.T Johnston. 2001. Mechanisms of arsenic adsorption on amorphous oxides evaluated using macroscopic measurements, vibrational spectroscopy, and surface complexation modeling. *Journal of Colloid and Interface Science*, 234(1): 204-216.
- Goldberg, S., and G. Sposito. 1984. A chemical model of phosphate adsorption by soils: 2. Nonclayey soils. *Soil Science Society of America Journal*, 48: 779-783.

Goldberg, S., and G. Sposito. 1985. On the mechanism of specific phosphate adsorption by hydroxylated mineral surfaces: A review. *Communications in Soil Science and Plant Analysis*, 16(8): 801-821.

Hansmann, D.D., and M.A. Anderson. 1985. Using electrophoresis in modeling sulfate, selenite, and phosphate adsorption onto goethite. *Environmental Science and Technology*, 19: 544-551.

Hayes, K.F., C. Papelis and J.O. Leckie. 1988. Modeling ionic strength effects of anion adsorption at hydrous oxide/solution interface. *Journal of Colloid and Interface Science*, 125(2): 717-726.

He, Z.L., V.C. Baligar, D.C. Martens, and K.D. Ritchey. 1998. Determination of soluble phosphorus in the presence of organic ligands or fluoride. *Soil Science Society of America Proceedings*, 62: 1538-1541.

Helyar, K.R., D.N. Munns, and R.G. Burau. 1976a. Adsorption of phosphate by gibbsite. I. Effects of neutral chloride salts of calcium, magnesium, sodium and potassium. *Journal of Soil Science*, 27: 307-314.

Helyar, K.R., D.N. Munns, and R.G. Burau. 1976b. Adsorption of phosphate by

gibbsite. II. Formation of a surface complex involving divalent cations. *Journal of Soil Science*, 27: 315-323.

Hiemenz, P.C., and R. Rajagopalan. 1997. Electrophoresis and other electrokinetics phenomena. *Principles of colloid and surface chemistry*. Marcel Dekker, Inc., New York, 534-555 pp.

Hug, S.J. 1997. In situ Fourier transform infrared measurements of sulfate adsorption on hematite in aqueous solutions. *Journal of Colloid and Interface Science*, 188: 415-422.

Hunter, R.J. 1981. Zeta potential in colloid science. *Principles and Applications*. Colloid science. A series of monographs. Academic press, San Diego, pp. 219-257.

Jackson, T.A. and Keller, W.D., 1970. Comparative study of the role of lichens and inorganic processes in the chemical weathering of recent Hawaiian lava flows. *American Journal of Science*, 269: 446-467.

Kafkafi, U., B. Bar-Yosef, R. Rosenberg, and G. Sposito. 1988. Competitive adsorption of P by Ca- and K-saturated kaolinite and montmorillonite: II. Organic anion competition. *Soil Science Society of America Journals*, 52: 1585-1589.

Kandori, K., S. Uchida, S. Kataoka, and T. Ishikawa. 1992. Effects of silicate and phosphate ions on the formation of ferric oxide hydroxide particles. *Journal of material science*, 27: 719-728.

Kumamoto, J. 1965. Vibrational frequencies of phosphate derivatives. *Spectrochimica Acta.*, 21: 345-350.

Lincoln, S.F. and D.R. Stranks. 1968. Phosphate complexes of cobalt(III). General structural and hydrolytic properties. *Australian Journal of Chemistry*, 21: 37-56.

McBride, M.B. 1997. A critique of diffuse double layer models applied to colloid and surface chemistry. *Clays and Clay Minerals*, 45(4): 598-608.

Murphy, J. and J.P. Riley. 1962. A modified single solution method for the determination of phosphate in natural waters. *Analytical Chimica Acta*, 27: 31-36.

Nakamoto, K. 1997. *Infrared and Raman spectra of inorganic and coordination compounds*. John Wiley and Sons, New York.

Nanzyo, M. 1986. *Infrared spectra of phosphate sorbed on iron hydroxide gel and the*

sorption products. *Soil Science and Plant Nutrition*, 32(1): 51-58.

Nanzyo, M. and Y. Watanabe. 1982. Diffuse reflectance infrared spectra and ion-adsorption properties of the phosphate surface complex on goethite. *Soil Science and Plant Nutrition*, 28(3): 359-368.

Parfitt, R.L., J. D. Russell, and V. C. Farmer, 1976. Confirmation of surface structure of goethite and phosphated goethite by infrared spectroscopy. *Journal of Chemical Society Faraday Transaction*, 172: 1082-1087.

Parfitt, R.L. 1989. Phosphate reactions with natural allophane, ferrihydrite and goethite. *Journal of Soil Science*, 40: 359-369.

Parfitt, R.L. and R.J. Atkinson. 1976. Phosphate adsorption on goethite(α -FeOOH). *Nature*, 264(30): 740-741.

Parfitt, R.L., R.J. Atkinson, and R.S.C. Smart. 1975. The mechanism of phosphate fixation by iron oxides. *Soil Science Society of America Proceedings*, 39: 837-841.

Peak, D., R.G. Ford and D.L. Sparks. 1999. An in-situ ATR-FTIR investigation of sulfate bonding mechanisms on goethite. *Journal of Colloid and Interface Science*,

218: 289-299.

Persson, P., N. Nielsson, and S. Sjöberg, 1996. Structure and bonding of orthophosphate ions at the iron oxide-aqueous interface. *Journal of Colloid and Interface Science*, 177: 263-275.

Ro, C. et al., 2001. Single-particle analysis of aerosols at Cheju Island, Korea. using low-Z electron probe X-ray microanalysis: A direct proof of nitrate formation from sea salts. *Environmental Science and Technology*, 35: 4487-4494.

Rose, J., A. Flank, A. Masion, J. Bottero, and P. Elmerich. 1997. Nucleation and growth mechanisms of Fe oxyhydroxide in the presence of PO₄ ions. 2. P K-edge EXAFS study. *Langmuir*, 13: 1827-1834.

Rose, J., A. Manceau, J. Bottero, A. Manion, and F. Garcia. 1996. Nucleation and growth mechanisms of Fe oxyhydroxide in the presence of PO₄ ions. 1. Fe K-edge EXAFS study. *Langmuir*, 12: 6701-6707.

Ryden, J.C., J.K. Syers, and R.F. Harris. 1973. Phosphorus in runoff and streams, *Advances in Agronomy*, pp. 1-45.

Ryden, J.C., J.K. Syers and J.R. Mclaughlin. 1977. Effects of ionic strength on chemisorption and potential-determining sorption of phosphate. *Journal of Soil Science*. 28: 62-71.

Ryden, K.C. and J.K. Syers. 1975. Rationalization of ionic strength and cation effects on phosphate sorption by soils. *Journal of Soil Science*. 26: 395-406.

Schecher, W.D. and D.C. McAvoy. 1998. MINEQL+. Environmental Research Software, Hallowell, ME.

Schulthess, C.P., K. Swanson, and H. Wijnja. 1998. Proton adsorption on an aluminum oxide in the presence of bicarbonate. *Soil Science Society of America Journals*. 62(1): 136-141.

Schwertmann, U., and R.M. Cornell. 1991. *Iron Oxides in the Laboratory: Preparation and Characterization*. VCH Publisher, Weinheim/New York, pp.137.

Schwertmann, U., D.G. Schulze, and E. Murad. 1982. Identification of ferrihydrite in soils by dissolution kinetics, differential X-ray diffraction and Mössbauer spectroscopy. *Soil Science Society of America Journals*, 46: 869-875.

Schwertmann, U. and R.M. Taylor. 1989. Iron oxides. In: J.B. Dixon and S.B. Weed (eds.), Minerals in soil environments. Soil Science Society of America, Madison, WI. pp. 379-438.

Snoeyink, V.L. and D. Jenkins. 1980. Precipitation and dissolution. Water Chemistry. John Wiley & Sons, Inc., New York, pp. 243-315.

Suarez, D.L., S. Goldberg, and C. Su. 1998. Evaluation of oxyanion adsorption mechanisms in oxides using FTIR spectroscopy and electrophoretic mobility. In: D.L. Sparks and T.J. Grundl (eds.), Mineral-water interfacial reactions kinetics and mechanisms. Am. Chem. Soc., Washington, DC, pp. 136-178.

Tejedor-Tejedor, M.I., and M.A. Anderson. 1990. Protonation of phosphate on the surface of goethite as studied by CIR-FTIR and electrophoretic mobility. Langmuir. 6: 602-611.

Vaithyanathan, P. and D.L. Correll. 1992. The Rode river watershed: Phosphorus distribution and export in forest and agricultural soils. Journal of Environmental Quality, 21: 280-288.

Waychunas, G.A., B.A. Rea, C.C. Fuller, and J.A. Davis. 1993. Surface chemistry of ferrihydrite: Part 1. EXAFS studies of the geometry of coprecipitated and adsorbed

arsenate. *Geochimica et Cosmochimica Acta*, 57: 2251-2264.

Wijnja, H. and C.P. Schulthess. 2000. Vibrational spectroscopy study of selenate and sulfate adsorption mechanisms on Fe and Al (Hydr) oxide surfaces. *Journal of Colloid and Interface Science*, 229: 286-297.

Wilhelmy, R.B., R.C. Patel, and E. Matijevic. 1985. Thermodynamic and kinetics of aqueous ferric phosphate complex formation. *Inorganic Chemistry*, 24: 3290-3297.

Willett, I.R., C. J. Chartres, and T.T. Nguyen. 1988. Migration of phosphate into aggregated particles of ferrihydrite. *Journal of Soil Science*, 39: 275-282.

Zelazny, L.W., L. He, and A. Vanwormhoudt. 1996. Charge analysis of soils and anion exchange. In: D.L. Sparks (Editor), *Methods of soil analysis Part 3-Chemical methods*. SSSA Book Series No.5. Soil Science Society of America, Inc., Madison, Wisconsin, pp. 1231-1254.

Chapter 3

X-RAY ABSORPTION SPECTROSCOPIC INVESTIGATION OF ARSENITE AND ARSENATE ADSORPTION AT THE ALUMINUM OXIDE– WATER INTERFACE

3.1 Abstract

Arsenite (As(III)) and Arsenate(As(V)) adsorption complexes at the γ -Al₂O₃ water interface were investigated as a function of pH and ionic strength (I), using a combination of adsorption envelopes, electrophoretic mobility(EM) measurements and X-ray absorption spectroscopy (XAS). The As adsorption envelopes show that 1) As(III) adsorption increases with increasing pH and is insensitive to I changes (0.01 M and 0.8 M NaNO₃) at pH 3-4.5, while adsorption decreases with increasing I between pH 4.5 and 9.0, and 2) As(V) adsorption decreases with increasing pH and is insensitive to I changes at pH 3.5-10. The EM measurements show that As(III) adsorption does not significantly change the EM values of γ -Al₂O₃ suspension in 0.1M NaNO₃ at pH 4-8, whereas As(V) adsorption lowered the EM values at pH 4-10. The EXAFS data indicate that both As(III) and As(V) form inner-sphere

complexes with a bidentate binuclear configuration, as evidenced by a As(III)-Al bond distance of $\approx 3.22 \text{ \AA}$ and a As(V)-Al bond distance of $\approx 3.11 \text{ \AA}$. The As(III) XANES spectra, however, show that outer-sphere complexes are formed in addition to inner-sphere complexes, and that the importance of outer-sphere As(III) complexes increases with increasing pH (5.5 to 8) and with decreasing I. In short, the data indicate for As(III) that inner- and outer sphere adsorption co-exist whereas for As(V) inner-sphere complexes are predominant under our experimental conditions.

3.2 Introduction

Arsenic (As) is an ubiquitous toxic metalloid in the soil/water environment due to natural geologic processes (volcanic eruption and weathering) and anthropogenic sources (mining, industrial processes, and agricultural practices). The average total As content in uncontaminated soils is approximately 5 ppm (Anderson et al., 1976; Raven et al., 1998; Xu et al., 1988), however, the total As levels in fields that received As containing pesticides and defoliants range from 5 to 2.553 ppm (Walsh and Keeny, 1975). In aquatic environments, typical concentrations of total As range from 1ppb to 3 ppm (Onishi, 1969; People, 1975; Westcot et al., 1993; Whitacre and Pearse, 1974).

The U.S. EPA recently lowered the maximum concentration level (MCL) for total As in drinking water from 50 ppb to 10 ppb (USEPA, 2001). This new MCL raises serious concerns about human and ecological health in many parts of the U.S where As levels currently are above 10 ppb. Inorganic As has four oxidation states:

+5, +3, 0, and -3. In the soil/water environment, it is mainly present in the +3 and +5 oxidation states. In reduced environments, arsenious acid is a common As(III) aqueous species, whereas oxidized environments contain more an As(V) aqueous species. These two aqueous species may adsorb onto inorganic and organic soil components and or precipitate in a variety of forms. The pKa values of As(III) and As(V) (As(III): $pK_1 = 9.22$ and $pK_2 = 12.13$, and As(V): $pK_1 = 2.20$, $pK_2 = 6.97$, and $pK_3 = 13.4$ (Wagman et al., 1982)), predict that the predominant solution species at typical environmental pH values (4-8) would be $As(OH)_3^0(aq)$ for As(III) and $H_2AsO_4^-$ and $HAsO_4^{2-}$ for As(V).

The environmental fate of As in subsurface environments is highly dependent on the As speciation, pH, ionic strength, and the presence of adsorbents such as metal oxides and phyllosilicates. In acid to alkaline environments, arsenic can be adsorbed onto variable-charge mineral surfaces by inner-sphere and or outer-sphere complexation. Inner-sphere complexes form via a ligand exchange reaction with a surface functional group, and as a result, no water molecules are present between surface functional groups and the adsorbate ions. Outer-sphere complexes form mainly by electrostatic interactions and contain more than one water molecule between the adsorbate and the adsorbent functional groups (Sposito, 1989). Several researchers have investigated As adsorption on soil minerals using macroscopic techniques and surface complexation models. As(V) adsorption studies on metal oxides have shown that As(V) is strongly adsorbed on amorphous $Al(OH)_3$, $\alpha-Al_2O_3$, ferrihydrite and hematite at acidic pH (pH 3-5), and that adsorption

gradually decreases with increasing pH between pH 6-10 (Anderson et al., 1976; Raven et al., 1998; Xu et al., 1988). Conversely, As(III) adsorption on ferrihydrite, goethite, kaolinite, illite, montmorillonite, and amorphous aluminum oxide has been shown to increase gradually with increasing pH from 3.5 up to 8-9 (Manning et al., 1998; Manning and Goldberg, 1997; Raven et al., 1998). An application of the triple layer model to As(V) adsorption on amorphous iron oxide at pH 4-10 suggested the formation of inner-sphere monodentate mononuclear species (Hsia et al., 1992). The constant capacitance model has been used to describe As(III) adsorption behavior on goethite, assuming the formation of bidentate binuclear surface complexes (Manning et al., 1998).

X-ray absorption fine structure spectroscopic (XAFS) studies have shown the formation of both inner-sphere bidentate binuclear and monodentate As(V) complexes on ferrihydrite and goethite at pH 6-8 (Fendorf et al., 1997; Waychunas et al., 1993). Attenuated Total Reflectance Fourier Transform Infrared spectroscopy (ATR-FTIR) studies, electrophoretic mobility (EM) measurements, and titration studies also suggested inner- sphere adsorption mechanisms of As(V) and As(III) on ferrihydrite (Suarez et al., 1998). *Ex-situ* ATR-FTIR studies indicated that both As(III) and As(V) adsorbed to the goethite surface as inner-sphere bridging bidentate complexes at pH 3-8.5 (Sun and Doner, 1996). An *in situ* EXAFS investigation of As(III) adsorption at the goethite/water interface reported a bidentate binuclear bridging configuration with an average As-Fe distance of $3.378 \pm 0.014 \text{ \AA}$ (Manning et al., 1998).

Unfortunately there are no *in-situ* spectroscopic studies of arsenic adsorption at the aluminum oxide/water interface. Aluminum oxides such as gibbsite may play an important role in As retention in soil/water environments because their aluminol functional groups serve as dynamic sinks for various oxyanions (Goldberg et al., 1995). A strong correlation between As(V) retention with ammonium oxalate extractable Al indicated the importance of As(V) fixation by amorphous aluminum oxides in soils (Jacobs et al., 1970; Livesey and Huang, 1981).

In this study, we investigated the complexation of As(III) and As(V) at the γ -Al₂O₃ / water interface as a function of pH and ionic strength using a combination of adsorption envelopes, electrophoretic mobility measurements, and X-ray absorption spectroscopy (XAS). We chose γ -Al₂O₃ (Degussa Corp., Akron, OH) as the adsorbate in this study, because the surface of well hydrated γ -Al₂O₃ (Degussa Corp., Akron, OH) is structurally similar to that of aluminum oxides (*e.g.*, bayrite) in soils. ATR-FTIR and diffuse reflectance (DR) Fourier transformed infrared (FTIR) spectroscopic investigations showed that the surface of γ -Al₂O₃ transformed into the bayerite polymorph upon aging (Dyer et al., 1993; Wijnja and Schulthess, 1999).

3.3 Materials and Reagents

Total ignition and transmission electron microscopic analysis (TEM) of the γ -Al₂O₃ showed greater than 99.6 % purity and an average particle radius of 13 nm (Degussa Corp., Akron, OH). The five-point Brunauer-Emmett-Teller (BET) surface area of the γ -Al₂O₃ was $\approx 90.1 \text{ m}^2 \text{ g}^{-1}$. The isoelectric point was ≈ 9.3 , as determined

by electrophoretic mobility measurements. ACS grade sodium arsenate, $\text{Na}_2\text{HAsO}_4 \cdot 7\text{H}_2\text{O}$ (Baker) and sodium m-arsenite, NaAsO_2 (Sigma) were used as sources of arsenic reagents. All reagents and samples were prepared with boiled DDI water in a N_2 filled glove box to minimize the competitive adsorption between As and carbonate species as well as potential As(III) oxidation by dissolved oxygen. The As(III) reagent was prepared in an acidic medium ($\text{pH} \approx 3$ HNO_3 solution) to avoid auto-oxidation at alkaline pH.

3.4 Methods

3.4.1 Adsorption Envelopes

Arsenic adsorption was studied as a function of I (0.01 M and 0.8 M NaNO_3) and pH (3-10). The concentrations of $\gamma\text{-Al}_2\text{O}_3$ and arsenic were 5 g L^{-1} and 0.7 mM, respectively. Hydration of $\gamma\text{-Al}_2\text{O}_3$ adsorbent was effected in two steps. In the first step, 100ml $\gamma\text{-Al}_2\text{O}_3$ suspensions were hydrated in 0.01M or 0.8M NaNO_3 solutions for 7d. The $\gamma\text{-Al}_2\text{O}_3$ material transformed into a bayerite polymorph during this hydration period, as was verified via ATR-FTIR analysis. Next, the pH of suspensions was adjusted to values ranging between 3.75 and 9, using either 0.1M HNO_3 or 0.1M NaOH , and equilibrated for an additional 24 h. An appropriate amount of 5mM As(III or V) stock solution was then added to achieve an initial As concentration of 0.7mM. The samples were reacted for 20 h on an orbital shaker operating at 300rpm. The final pH was measured in the N_2 filled glove box, and 30 ml of the suspension was removed and then centrifuged at 11950g for 5 min. The

supernatant was filtered through 0.2 μm filter paper. The filtrates of the arsenite reacted samples were treated with KIO_3 to induce the oxidation of As(III) to As(V). The total As(V) concentrations of the filtrates were measured by the ammonium molybdate method described in Cummings et al. (Cummings et al., 1999).

3.4.2 Electrophoretic Mobility Measurements

The electrophoretic mobility (EM) measurements were performed on a Zeta-Meter system 3.0 (Zeta Meter, Inc., NY). To assure the accuracy in EM measurements, the instrument was calibrated by measuring a constant zeta potential ($-29 \pm 1\text{mV}$) of standard colloidal silica (Min-U-Sil) in distilled water. The suspension density of $\gamma\text{-Al}_2\text{O}_3$ was 0.25g L^{-1} , and the background electrolyte was 0.1M NaNO_3 . Hydration of the $\gamma\text{-Al}_2\text{O}_3$ material was as described above. The EM measurements of the mineral suspensions were conducted at pH 4-10 for As(V), and at pH 4-8 for As(III). Measurements at each pH value were done in both the presence and absence of 0.1mM As(III) or 0.1mM As(V) . The narrower pH range for the As(III) system was chosen due to potential As(III) oxidization at $\text{pH} > 9.2$ (Manning and Goldberg, 1997). The tracking times (sec) of a total of ten particles were averaged, and the average values were used to estimate EM using the Helmholtz – Smoluchowski equation (Hiemenz and Rajagopalan, 1997). The average particle radius of 13nm and $I = 0.1\text{M}$ are within the Hückel and Helmholtz – Smoluchowski limits for estimating the EM values using the Helmholtz – Smoluchowski equation (Hiemenz and Rajagopalan, 1997).

3.4.3 Synchrotron XAS Data

All XAS samples were prepared at 25 (± 2) °C in a N₂ filled glove box using the same experimental methods as described above for preparation of the As adsorption envelopes. The arsenite samples were prepared at I = 0.8 M and 0.01M NaNO₃ and pH 5.5 and 8. The arsenate samples were prepared at pH 4, 8, and 10 at the same two I values used in the As(III) experiments. The total sample volumes were 30 ml. The γ -Al₂O₃ suspensions were centrifuged at 11950 g for 5 min and the wet paste was recovered for XAS analysis. The mass of residual As in the entrained solution represented at most 3.5 % of the total adsorbed As, and therefore the contribution of entrained (non-adsorbed) As to the XAS spectra was negligible in all samples.

In addition to the As sorption samples, XAS spectra of As solutions (10mM of sodium arsenite at pH 3.5 and sodium arsenate at pH 4.2) were collected as references for As(III) and As(V) outer-sphere complexes. According to the MINEQL+ chemical modeling speciation program (Schecher and McAvoy, 1998), the speciation of As in these solutions was 100 % As(OH)₃(aq) and 100 % H₂AsO₄⁻(aq) at these pH's. The spectra of aqueous As(V) collected at pH 4, 8 and 10 all were the same; therefore, the XANES and the EXAFS results were not sensitive to As(V) protonation. The solution and paste samples were loaded in Teflon sample holders inside the glove box, which were then sealed with Kapton tape (CHR Industries), and stored in double zip-lock bags containing a N₂ atmosphere. The samples were kept at \approx 3-5 °C without exposure to atmospheric air prior to XAS data collection.

Arsenic K-edge (11867 eV) XAS spectra were collected on beamline X-11A at the National Synchrotron Light Source (NSLS), Brookhaven National Laboratory, Upton, NY. The electron storage ring was operated at 2.528 GeV with a current range of 130 to 300 mA. The XAS spectra were collected in fluorescence mode with a Lytle detector filled with Krypton gas. The ionization chamber (I_0) was filled with 90 % N_2 and 10 % Ar. As an internal standard, the arsenic K-edge of sodium arsenate salt was run simultaneously with adsorption samples to check for potential energy shifts during the run as well as possible As(III) oxidation during data collection. No oxidation of As(III) adsorbed at the γ - Al_2O_3 surface was observed. A Ge-filter was used to remove elastically scattered radiation from the fluorescence emissions. The monochromator consisted of two parallel Si(111) crystals with a vertical entrance slit of 0.5 mm. The Teflon sample holder was oriented at 45° to the unfocused incident beam, and was attached to a cold finger cooled by liquid nitrogen ($T=77$ K). We performed data collection of the sorption samples at 77 K to minimize thermal disorder and possible oxidation of As(III) samples. For some samples, data collection was done at 298 K. Except for the signal to noise ratio, no differences were observed with the data collected at 77 K. The solution reference samples were scanned at 298K. A total of three spectra were collected for the sorption samples, and one spectrum was collected for the solution samples.

XAS data reduction and analysis were performed with WinXas 1.1 (Ressler, 1997) using the following procedures. First, three spectra (except for the solution samples) per sample were averaged. The averaged spectra were normalized with

respect to E_0 determined from the second derivative of the raw spectra, and then the total atomic cross sectional absorption was set to unity. A low-order polynomial function was fit to the pre-edge region and the post-edge region. Next, the data were converted from E-space to k -space and weighted by k^3 to compensate for dampening of the XAFS amplitude with increasing k space. Fourier transformation was then performed over the k -space range of 1.3 to 11.6 \AA^{-1} to obtain the radial structural functions (RSF). Final fitting of the spectra was done on Fourier transformed k^3 weighted spectra in R-space. The FEFF7 code reference (Zabinsky et al., 1995) was utilized to calculate single scattering theoretical spectra and phase shifts for As-O and As-Al backscatteres using an input file based on the structural refinement of scorodite ($\text{FeAsO}_4 \cdot \text{H}_2\text{O}$) (Kitahama et al., 1975) with one Fe atom at 3.3376 \AA replaced by Al. The amplitude reduction factor was 0.91. During fitting, the values of N and R of the As-O and As-Al shells were allowed to float, as well as a single E_0 for all sets of backscattering atoms. The Debye-Waller factors of the As-O shells were also allowed to float, but those of the As-Al shells were fixed at 0.01 \AA^2 for As(III) and 0.006 \AA^2 for As(V). When allowed to float, the Debye-Waller factors of the As-Al shells showed no trends for different samples (e.g. as a function of pH or I), and we therefore used the average values (0.006 \AA^2 for As(V) and 0.01 \AA^2 for As(III)) in the final fitting procedure to reduce the number of free parameters. Error estimates for the As-O shells are ± 0.02 \AA and ± 20 % for the R and N values, respectively, based on fits to the aqueous standards and the scorodite reference compound. The N and R values for the more distant Al shells will be less accurate than for the As-O shells, but

we lacked an As-Al reference compound to make an accurate estimate of the errors. Based on the As-Fe shell fitting results of the scorodite reference compound, we estimate the errors to be at least $\pm 0.03 \text{ \AA}$ and $\pm 30 \%$ for $R_{\text{As-Al}}$ and $N_{\text{As-Al}}$, respectively.

The XANES spectra of the adsorption and solution samples were normalized with respect to the step height at the edge energies, and compared to gain additional information regarding the local atomic structure of adsorbed As(III) and As(V) on the $\gamma\text{-Al}_2\text{O}_3$ surface.

3.5 Results and Discussion

3.5.1 Adsorption Envelopes

Figure 3.1 shows the effects of ionic strength (I) on As(III) and As(V) adsorption envelopes. Arsenate adsorption appears to be insensitive to changes in I between pH 3 and 9.2. Approximately 90 % of As(V) was removed at $\text{pH} \approx 5$ at both I, and the net adsorption decreased to 25 % with pH increases up to 10 (Figure-1). Adsorption of As(III), however, was dependent on both I and pH: adsorption increased from 30 % to 55 % with increasing pH from 3.2 to 8.2, and decreased with increasing I within the same pH range (Figure 3.1). Hayes and co-workers proposed an indirect macroscopic method for distinguishing inner-sphere from outer-sphere complexes by examining I effects on adsorption envelopes coupled with the generalized triple layer model (Hayes et al., 1988). According to this method, the formation of inner-sphere complexes is not greatly affected by I, whereas the

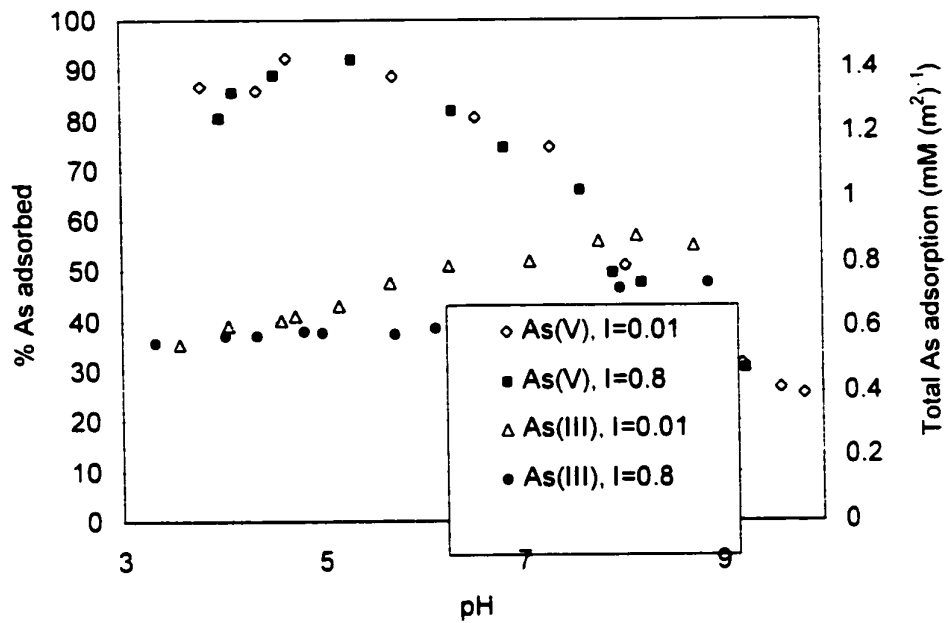


Figure 3.1 Ionic strength effects on As(III and V)/ γ -Al₂O₃ adsorption envelopes.

presence of outer-sphere complexes is indicated by changes in sorption with changing I due to competitive adsorption with counter anions. Based on this theory, our data suggest that As(III) predominantly forms inner-sphere complexes at pH 3-4, and outer-sphere complexes form in the pH range 4.5-10, whereas As(V) predominantly forms inner-sphere complexes regardless of pH and I.

It is interesting to compare this data interpretation with the adsorption mechanisms that may be expected based on the pH-dependent As solution speciation and charge properties of aluminum oxide surfaces. The dissociation constants of As(III) and As(V) indicate that the predominant solution species are negatively charged As(V) species (H_2AsO_4^- and or HAsO_4^{2-}) and uncharged As(III) species ($\text{As}(\text{OH})_3$) at pH 3-9. The surface of the aluminum oxide in this pH range has a net positive charge due to its relatively high IEP (≈ 9.3) (Figure 3.2). Therefore, As(V) might adsorb on the $\gamma\text{-Al}_2\text{O}_3$ surface at $\text{pH} < 9.3$ via electrostatic interactions (outer-sphere complexes), but at $\text{pH} > 9.3$ predominantly inner-sphere complexation would be expected to occur. Similarly, electrostatic interactions and or ligand exchange reactions between As(III) and the $\gamma\text{-Al}_2\text{O}_3$ surface may occur at pH 3-9, whereas predominant inner-sphere adsorption is expected at $\text{pH} > 9.2$ due to the development of negatively charged As(III) species ($\text{pK}_1 = 9.22$; $\text{As}(\text{OH})_3 + \text{H}_2\text{O} = \text{As}(\text{OH})_4^- + \text{H}^+$).

Based on the results of the I dependent adsorption envelopes and the surface complexes predicted by pH dependent characteristics of the adsorbents and the adsorbate, no conclusive statements on the As(III) and As(V) surface speciation can

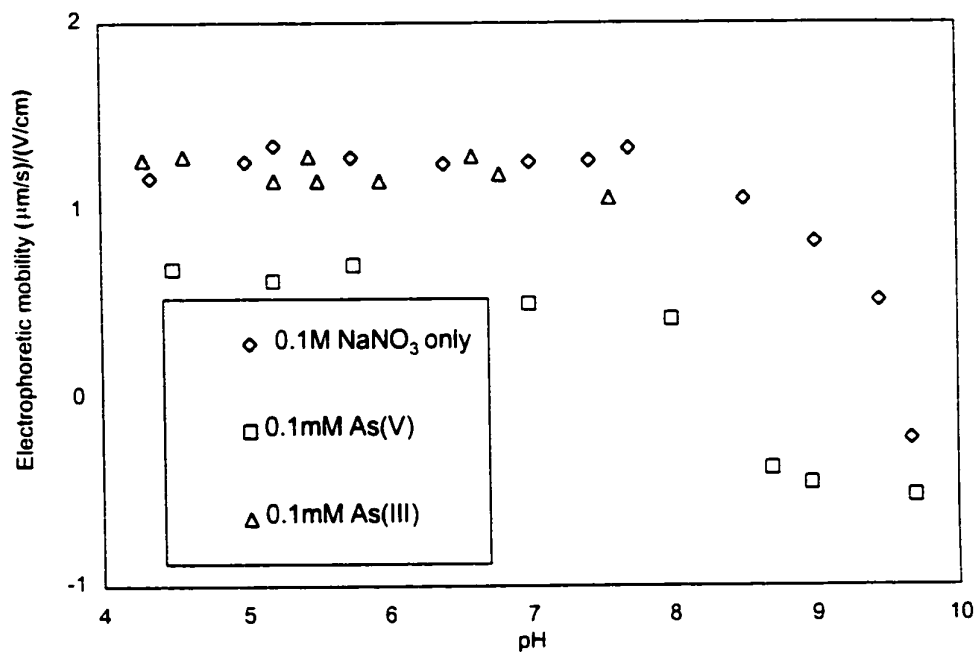


Figure 3.2 Electrophoretic mobility measurements on $\gamma\text{-Al}_2\text{O}_3$ with and without 0.1mM As(III or V). All systems contained 0.1M NaNO_3 .

be made. Recent spectroscopic studies have shown that mixtures of inner- and outer-sphere complexes may occur at metal oxide and clay mineral surfaces (Papelis and Hayes, 1996; Peak et al., 1999; Strawn and Sparks, 1999). We therefore performed EM measurements and XAS studies for further characterization of As complexation at the alumina/water interface.

3.5.2 Electrophoretic Mobility Measurements

According to Hunter (1981), electrophoretic mobility (EM) measurements are useful not only in obtaining isoelectric points (IEP) for colloidal materials, but also to indirectly distinguish inner-sphere complexes from outer-sphere complexes (Hunter, 1981). Non-specific ion adsorption of indifferent electrolytes outside of the shear plane (i.e., formation of outer-sphere complexes via van der Waals forces) generally does not affect the IEP but it could cause shifts in the value of EM if present at high concentrations of indifferent electrolyte (Hunter, 1981). The shear plane is at the outer edge of the inner part of the double layer and near the outer Helmholtz plane or the Stern layer, depending on the models to describe the interface (Hunter, 1981). Inner-sphere complexes generally cause shifts in both IEP and EM due to specific ion adsorption inside the shear plane (Hunter, 1981). In some cases, however, inner-sphere adsorption does not significantly affect the EM and IEP of the pure solid suspension (Hunter, 1981; Suarez et al, 1998).

The electrophoretic mobility (EM) measurements indicated that sorption of As(V) (in a 0.1M NaNO₃ background) lowered the EM between pH 4-10 and shifted

the isoelectric point (IEP) of the solid from ≈ 9.4 to ≈ 8.4 (Figure 3.2). Adsorption of As(III), however, resulted in no significant change in EM between pH 4 and 8 (Figure 3.2). These results agree with the EM measurements on amorphous $\text{Al}(\text{OH})_3$ reacted with As(III and V) reported by Suarez *et al.* (Suarez et al., 1998). A large shift in the point of zero charge (PZC) from pH 9.2 to 5.4 was observed in the presence of 1 mM As(V), whereas the same measurement with As(III) showed only a slight shift in PZC (Suarez et al., 1998).

Based on the information above, our EM measurements suggest the formation of inner-sphere complexes for As(V) at pH 4-10. It is true that EM can be shifted by a physically adsorbed anion such as nitrate, but the nitrate concentration is constant in all EM measurements. If physical adsorption of nitrate is outcompeting the formation of outer-sphere As(V) complexes, we should observe the same EM values for the systems containing 0.1 M NaNO_3 in the presence and absence of 0.1 mM As(V), which is not the case (Figure 3.2). Therefore, our experimental evidence (shifts in IEP and EM with 0.1 mM As(V) and 0.1 M NaNO_3) suggests that As(V) is specifically adsorbed (i.e., forms inner-sphere complexes) at the γ -aluminum oxide/water interface.

Another explanation for the observed EM shift of the As(V)- $\gamma\text{-Al}_2\text{O}_3$ samples is the formation of aluminum-arsenate (surface) precipitates, which might mask the charge properties of the $\gamma\text{-Al}_2\text{O}_3$. However, speciation calculations in MINEQL+ predict that all samples were undersaturated with respect to $\text{AlAsO}_4 \cdot 2\text{H}_2\text{O}(\text{s})$. Calculations were based on the initial $[\text{As}] = 0.7 \text{ mM}$, and total dissolved Al

concentrations < 99 μM , which was the highest Al concentration measured in the supernatants of the hydrated samples before As was added. Additionally, our EXAFS data show no indication of the formation of such precipitates, as will be shown in a later section.

The fact that we do not observe a change in the EM value of $\gamma\text{-Al}_2\text{O}_3$ upon As(III) adsorption can be explained by either the formation of outer-sphere complexes and or the formation of neutral inner-sphere complexes.

3.5.3 Arsenic XANES Analyses

The normalized XANES spectra of the As(III and V) adsorption samples and the reference arsenic solution samples are presented in Figure 3.3 and 3.4. For the As(III)/ $\gamma\text{-Al}_2\text{O}_3$ samples reacted at pH 8, there is a significant effect of ionic strength on the XANES spectra, whereas only a minor effect is observed at pH 5.5 (Figure 3.3). Comparison of the XANES spectra of the high and low I As(III) adsorption samples reacted at pH 8 to the spectrum of aqueous As(III) (Figure 3.3), shows that the low I (0.01 M) adsorption sample has a similar overall oscillation pattern to the aqueous As(III) standard between 0 and 100 eV. The highest point in both spectra (at $\approx +3\text{eV}$), is followed by a downward oscillation between 3 and 50 eV. For the other three As(III) adsorption samples, the first downward oscillation is between 3 and ≈ 40 eV (indicated by dashed line C in Figure 3.3) and contains a well resolved beat (indicated by dashed line B in Figure 3.3) at ≈ 27 eV. This beat is absent in the As(III)(aq) sample, and not well resolved in the As(III)/ $\gamma\text{-Al}_2\text{O}_3$ sample reacted at pH

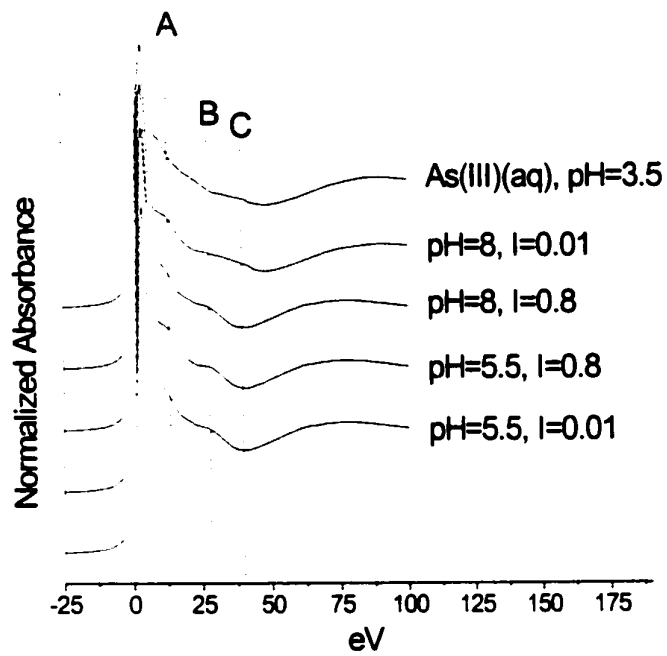


Figure 3.3 XANES spectra of the As(III)- γ -Al₂O₃ and sodium As(III) solution samples

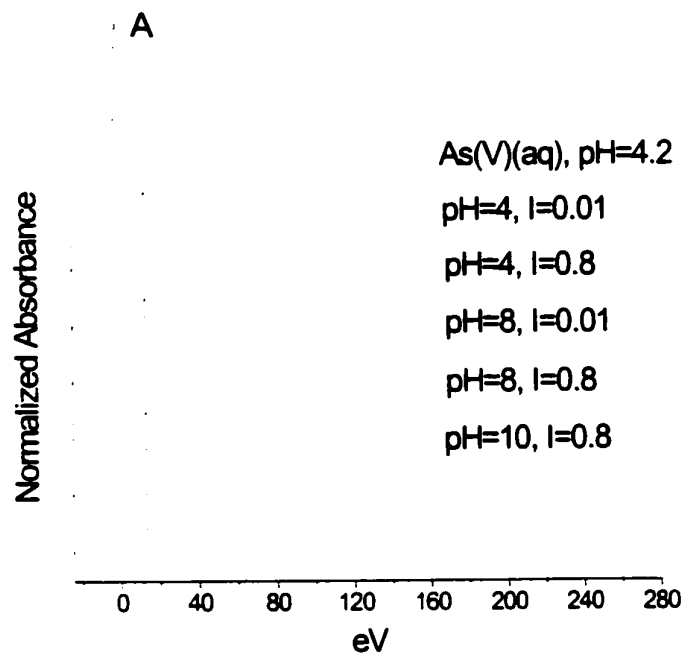


Figure 3.4 XANES spectra of the As(V)- γ -Al₂O₃ and sodium As(V) solution samples.

8 and $I = 0.01$. A shoulder also occurs at ≈ 10 eV (indicated by dashed line A in Figure 3.3), and is present in all spectra, but it is broader in the As(III) adsorption samples than in the aqueous As(III) spectrum.

Overall, the spectrum of the sample reacted at pH 8 and $I = 0.01$ M appears to be intermediate between the aqueous As(III) spectrum and the spectra of the other As(III) adsorption samples, i.e., it contains features from both spectra. This indicates that this sample contains a mixture of inner-sphere and outer-sphere As(III) complexes, whereas the other samples contain mainly As(III) sorbed in an inner-sphere fashion.

To substantiate the notion that the As(III)/ γ -Al₂O₃ samples (i.e., pH 8, $I = 0.01$) contains a mixture of outer-sphere and inner-sphere As(III) sorption complexes, XANES spectrum of the sample was fit with a linear combination of spectra representative of inner- and outer-sphere complexes As(III) complexes (Ressler, 1997). For the outer-sphere reference, we used the spectrum of a sodium arsenite solution (10mM, and pH 3.5). For the inner-sphere reference, we used the spectrum of the As(III)/ γ -Al₂O₃ sample reacted at pH 5.5 and $I = 0.8$, since it shows pronounced features of inner-sphere complexation (Figure 3.2). During the LC XANES fitting, the inner-sphere reference spectrum (pH 5.5 and $I=0.8$) accounts for this non-sorbed As(III) (< 3.5 %) complexes which also present in the adsorption sample. Therefore, the % outer-sphere complex as the result of LC XANES fitting purely represents the outer-sphere complexes form in the adsorption sample (pH 8, $I = 0.01$). An excellent fit was obtained with relative contributions of inner-sphere and

outer-sphere complexes (Figure 3.5). It is clear that the sample (pH 8 and I = 0.01M) is an intermediate (66.04 % inner-sphere and 33.96 % outer-sphere), indicating the presence of mixture. Our As(III) XANES results, which suggest the mixture of inner-sphere and outer-sphere complexes at pH 8, I = 0.01M, but the predominant formation of inner-sphere complexes at pH 5.5, are consistent with the results of the I effect on the As(III) adsorption envelopes (Figure 3.1). At pH > 5.5, lowering I resulted in increased As(III) adsorption, which indirectly suggested that outer-sphere As(III) complexation occurs in this pH range, whereas the insensitivity of As(III) adsorption to I changes at pH < 5 suggests the predominant formation of inner-sphere As(III) complexation (Figure 3.1).

The EM measurements of As(III)-reacted γ -Al₂O₃ showed no significant change in the EM values of γ -Al₂O₃ between pH 4 and 8 compared to non-reacted γ -Al₂O₃ (Figure-2). Combined with the As(III) XANES data, our EM data suggest that the As(III) inner-sphere complexes forming at the γ -Al₂O₃ are neutral, both below pH 5.5, where they predominate, as well as at pH > 5.5, where they co-exist with outer-sphere As(III) surface complexes.

Unlike the As(III) samples, there were no significant differences in the XANES features in the As(V) adsorption samples reacted under different reaction conditions (Figure 3.4). Moreover, the spectra of the sorption samples show distinct features different from the aqueous As(V) spectrum (Figure 3.4). Therefore, our As(V) XANES data suggest As(V) inner-sphere complexation in all adsorption samples, regardless of pH and I. This result is consistent with the result of the adsorption

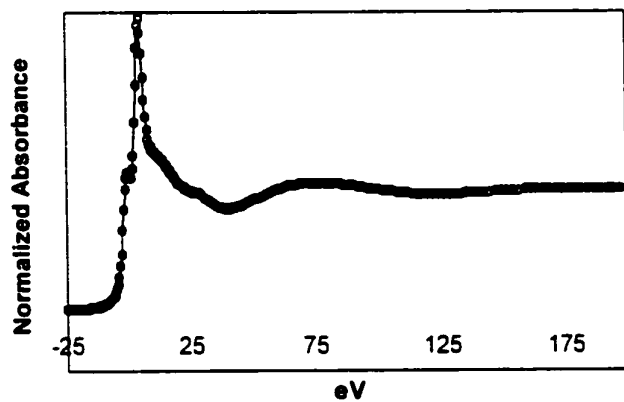


Figure 3.5 Results of linear combination (LC) of XANES profile fit for As(III)/ γ -Al₂O₃ adsorption sample (pH 8, I=0.01). The solid line is the experimental data and the open circles represent the LC fit.

envelope as a function of k and the EM measurements, which suggested the formation of As(V) inner-sphere complexes at the alumina surface (Figure 3.1 and 3.2).

3.5.4 Arsenic K-edge EXAFS Analyses

Figures 3.6 and 3.7 show the background subtracted k^3 -weighted χ -functions of the As(III and V)/ γ -Al₂O₃ samples and the As(III and V) solution samples. The spectra show strong sinusoidal oscillations resulting from O-shell backscattering. Figures 3.8 and 3.9 show the RSF's (uncorrected for phase shift) of the As(III and V) solutions and adsorption samples. The solid lines represent the Fourier Transforms of the experimental data and the dashed lines are the best fit obtained from multiple shell fitting. The vertical dashed lines A and B correspond to the As-O and As-Al shells, respectively. The structural parameters obtained from the linear least square fits of the EXAFS data are shown in Table 3.1. The radial distances of As-Al shells were ≈ 3.22 Å for As(III) and ≈ 3.11 Å for As(V). These distances can be used to determine the configuration of As(III) and As(V) inner-sphere complexes forming at the hydrated γ -Al₂O₃ surface. Using a known Al-O distance of the AlO₆ octahedral (1.85 to 1.97 Å), an O-O edge separation distance of 2.52 - 2.86 Å (Ishizawa et al., 1980), and the experimental As-O distances, the theoretical As-Al bond distances were estimated for different As adsorption configurations (e.g., monodentate, bidentate mononuclear, and bidentate binuclear), assuming that the surface structure of γ -Al₂O₃ (i.e., aluminum tetrahedral configuration) was fully converted to the aluminum octahedral configuration of the bayerite polymorph after 7 d of hydration.

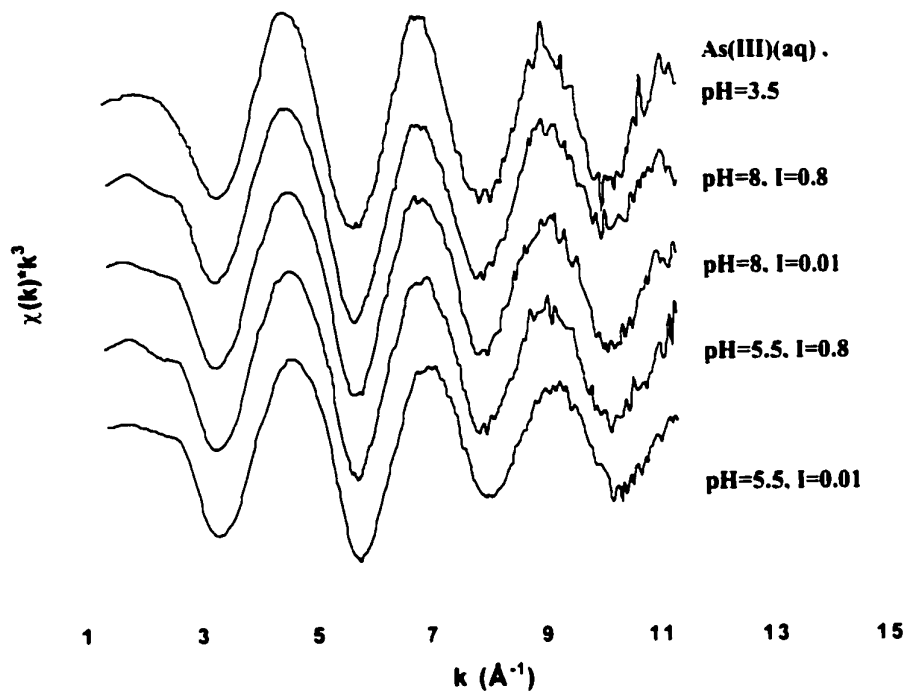


Figure 3.6 k^3 weighted normalized χ -functions for As(III)(aq) and As(III)/ γ -Al₂O₃ adsorption samples.

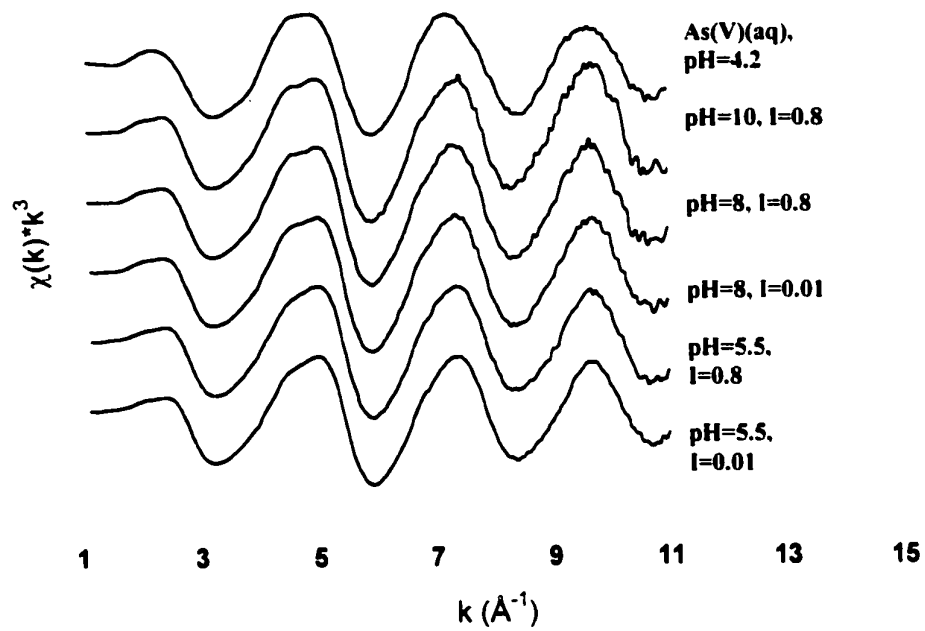


Figure 3.7 k^3 weighted normalized χ -functions for As(V)(aq) and As(V)/ γ -Al₂O₃ adsorption samples.

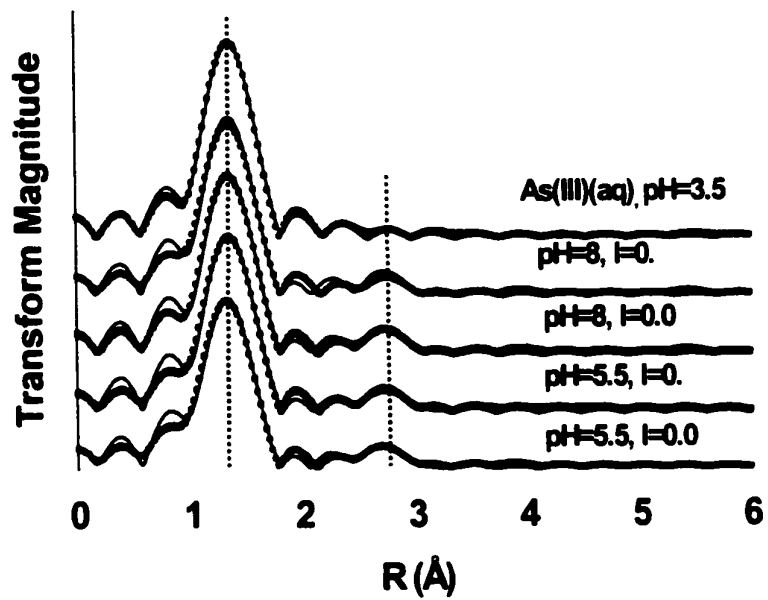


Figure 3.8 Fourier transforms (RSF) of the χ -functions of As(III)/ γ -Al₂O₃ adsorption samples. The solid lines are the experimental data and the dotted lines represent the theoretical multishell fit to the data.

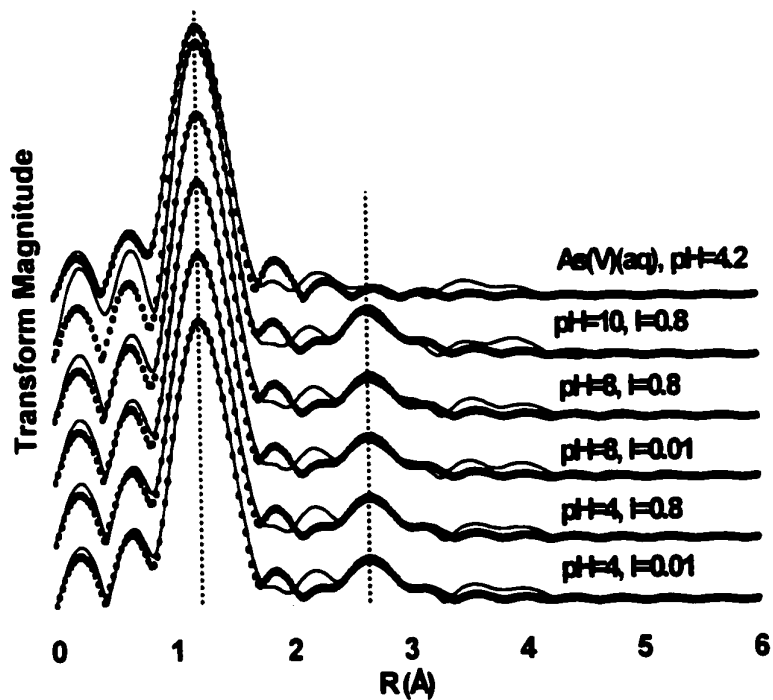


Figure 3.9 Fourier transforms (RSF) of the χ -functions of As(V) γ -Al₂O₃ adsorption samples. The solid lines are the experimental data and the dotted lines represent the theoretical multishell fit to the data.

Table 3.1 Structural parameters from EXAFS analysis for As(III and V)/ γ -Al₂O₃, adsorption and As(III and V) solution samples.

Sample	As(III)-O			As(III)-Al			E ₀ (eV) ^d
	CN ^{e,f}	R (Å) ^g	σ ² (Å ²) ^h	CN ^{e,f}	R (Å) ^g	σ ² (Å ²) ^h	
As(III)aq, pH=3.5	3.1	1.78	0.0046				5.58
pH=8, I=0.8	3.0	1.78	0.0054	0.9	3.22	0.01*	5.75
pH=8, I=0.01	3.0	1.77	0.0060	1.3	3.22	0.01*	5.61
pH=5.5, I=0.8	3.2	1.77	0.0067	1.2	3.19	0.01*	5.77
pH=5.5, I=0.01	3.2	1.75	0.0077	1.1	3.19	0.01*	5.48
				As(V)-Al			
As(V)aq, pH=4	4.0	1.68	0.0040				3.36
pH=10, I=0.8	4.0	1.69	0.0020	2.2	3.11	0.006*	3.58
pH=8, I=0.8	4.1	1.69	0.0025	2.1	3.12	0.006*	3.76
pH=8, I=0.01	4.0	1.69	0.0026	2.1	3.11	0.006*	3.58
pH=4, I=0.8	4.0	1.68	0.0030	2.1	3.11	0.006*	3.63
pH=4, I=0.01	3.9	1.68	0.0029	2.1	3.11	0.006*	3.50

^eCoordination number. ^gInteratomic distance. ^hDebye-Waller factor. Fit quality confidence limits for parameters: ^d±20%, ^e±0.02Å, ^f±30%, and ^g±0.03Å. *Fixed Parameter.

The presence of an Al shell in all samples indicates that As(III) and As(V) inner-sphere complexation occurs under all conditions studied (Figure 3.8 and 3.9). For monodentate inner-sphere complexation, the $R_{\text{As(III)-Al}}$ range is calculated to be 3.62 - 3.74 Å and the $R_{\text{As(V)-Al}}$ range 3.54 - 3.66 Å. For bidentate mononuclear bonding, the $R_{\text{As(III)-Al}}$ range is 2.21 - 2.75 Å, and the $R_{\text{As(V)-Al}}$ range is 2.07 - 2.64 Å. For bidentate binuclear complexation, the $R_{\text{As(III)-Al}}$ range is 3.16 - 3.51 Å and the $R_{\text{As(V)-Al}}$ range is 3.03 - 3.41 Å. The average As-Al distances of the experimental samples as determined by EXAFS (≈ 3.21 Å and ≈ 3.11 Å for As(III) and As(V), respectively) are therefore consistent with inner-sphere bidentate binuclear complexes for both As(III) and As(V). Although Our XANES data indicated that a mixture of inner-sphere and outer-sphere As(III) complexes was present at pH 8 and $I = 0.01$ M. We do not, however, observe the resultant lower average N_{Al} we would expect as a result of the presence of outer-sphere complexes for this sample compared to the other As(III) samples (Table 3.1). This indicates that the EXAFS data for this spectra are not very sensitive to changes with respect to the Al coordination shell, which is probably due to the weak backscattering of the light Al atom, leading to relatively high uncertainties in N_{Al} . This illustrates the usefulness of combining macroscopic techniques with XANES and EXAFS data in investigating metal/metalloid speciation at mineral/water interfaces. The XANES spectra suggest predominantly inner-sphere As(III) complexation at pH 5.5 and $I = 0.8$ M. The $N_{\text{As-Al}}$ value found for this sample, however, is significantly lower than the $N_{\text{As-Al}}$ values found for the As(V)/alumina spectra, despite the similar molecular configurations of the inner-sphere complexes of

As(V) and As(III). This suggests a higher degree of disorder in the population of inner-sphere As(III) complexes, since this leads to destructive interference and therefore an apparent decrease in second neighbor Al scattering.

3.6 Conclusion

In this study we demonstrated the effectiveness of combining macroscopic (I-dependent pH adsorption envelopes and EM measurements) and spectroscopic studies (XANES and EXAFS) in investigating surface complexation mechanisms of As(III) and As(V) at the γ -Al₂O₃/water interface.

Our results suggest that: 1) a mixture of inner-and outer-sphere As(III) complexes exist at pH > 5.5, where outer-sphere As(III) complexes become more important with decreasing I; 2) As(III) predominantly forms inner-sphere bidentate binuclear complexes at pH ≤ 5.5; and 3) As(V) predominantly forms inner-sphere bidentate binuclear complexes regardless of pH and I. The co-existence of As(III) inner-sphere and outer-sphere adsorption complexes may be important in predicting the fate and transport of As(III) in Al-oxide rich environment.

3.7 References

Anderson, M.A., Ferguson, J.F. and Gavis, J.. 1976. Arsenate adsorption on amorphous aluminum hydroxide. *Journal of Colloid and Interface Science*, 54: 391-399.

Cummings, D.E., F. Caccavo, J., Fendorf, S. and Rosenzweig, R.F.. 1999. Arsenic mobilization by the dissimilatory Fe(III)-reducing bacterium *shewanella alga* BrY. *Environmental Science and Technology*, 33(5): 723-729.

Dyer, C., Hendra, P.J., Forsling, W. and Ranheimer, M.. 1993. Surface hydration of aqueous gamma-Al₂O₃ studied by Fourier transform Raman and infrared spectroscopy. 1. Initial results. *Spectrochimica Acta Part A-Molecular and biomolecular spectroscopy*, 49(5-6): 691-705.

Fendorf, S.E., Eick, M.J., Grossl, P. and Sparks, D.L.. 1997. Arsenate and chromate retention mechanisms on goethite. 1. Surface structure. *Environmental Science and Technology*, 31(2): 315-320.

Goldberg, S., Davis, J.A. and Hem, J.D. 1995. In: G. Sposito (ed.) *The environmental chemistry of aluminum*. CRC press, Boca Raton, FL, 271-332 pp.

Hayes, K.F., Papelis, C. and Leckie, J.O., 1988. Modeling ionic strength effects of

anion adsorption at hydrous oxide/solution interface. *Journal of Colloid and Interface Science*, 125(2): 717-726.

Hiemenz, P.C. and Rajagopalan, R., 1997. Electrophoresis and other electrokinetics phenomena. *Principles of colloid and surface chemistry*. Marcel Dekker, Inc., New York. 534-555 pp.

Hsia, T.H., Lo, S.F. and Lin, C.F., 1992. As(V) Adsorption on amorphous iron oxide: Triple layer modeling. *Chemosphere*, 25(12): 1825-1837.

Hunter, R.J., 1981. Zeta potential in colloid science. *Principles and Applications*. Colloid science, A series of monographs. Academic press, San Diego. pp. 219-257.

Ishizawa, N., Miyata, T., Minato, I., Marumo, F. and Iwai, S., 1980. A structural investigation of α -Al₂O₃ at 2170K. *Acta Crystallographica*, C36: 228-230.

Jacobs, L.W., Syers, J.K. and Keeney, D.R., 1970. Arsenic sorption by soils. *Soil Science Society of America Proceedings*, 34: 750-754.

Kitahama, K., Kiriya, R. and Baba, Y., 1975. Refinement of the crystal structure of scorodite. *Acta Crystallographica*, B31: 322-324.

Livesey, N.T. and Huang, P.M., 1981. Adsorption of arsenate by soils and its relation to selected chemical properties and anions. *Soil Science*, 131(2): 88-94.

Manning, B.A., Fendorf, S.E. and Goldberg, S., 1998. Surface structure and stability of arsenic(III) on goethite: Spectroscopic evidence for Inner-sphere complexes. *Environmental Science and Technology*, 32: 2383-2388.

Manning, B.A. and Goldberg, S., 1997. Adsorption and stability of arsenic (III) at the clay mineral-water interface. *Environmental Science and Technology*, 31(7): 2005-2011.

Onishi, H., 1969. Arsenic. *Handbook of geochemistry*. Springer-Verlag, New York.

Papelis, C. and Hayes, K.F., 1996. Distinguishing between interlayer and external sorption sites of clay minerals using X-ray absorption spectroscopy. *Colloids and Surfaces A-Physicochemical and engineering aspects*, 107: 89-96.

Peak, D., Ford, R.G. and Sparks, D.L., 1999. An in-situ ATR-FTIR investigation of sulfate bonding mechanisms on goethite. *Journal of Colloid and Interface Science*, 218: 289-299.

People, S.A., 1975. Review of arsenical pesticides. In: E.A. Woolson (ed.). *American Chemical Society*, pp. 1-12.

Raven, K.P., Jain, A. and Loeppert, R.H.. 1998. Arsenite and arsenate adsorption on ferrihydrite: Kinetics, equilibrium, and adsorption envelopes. *Environmental Science and Technology*, 32: 344-349.

Ressler, T., 1997. Winxas: a program for X-ray absorption spectroscopy data analysis under MS-Windows. *Journal of Synchrotron Radiation*. 5: 118-122.

Schecher, W.D. and McAvoy, D.C.. 1998. MINEQL+. Environmental Research Software. Hallowell, ME.

Sposito, G., 1989. *The chemistry of soils*. Oxford university press, New York.

Strawn, D.G. and Sparks, D.L., 1999. The use of XAFS to distinguish between inner- and outer-sphere lead adsorption complexes on montmorillonite. *Journal of Colloid and Interface Science*. 216: 257-269.

Suarez, D.L., Goldberg, S. and Su, C., 1998. Evaluation of oxyanion adsorption mechanisms in oxides using FTIR spectroscopy and electrophoretic mobility. In: D.L. Sparks and T.J. Grundl (eds.), *Mineral-water interfacial reactions kinetics and mechanisms*. Am. Chem. Soc., Washington, DC, pp. 136-178.

Sun, X. and Doner, H.E.. 1996. An investigation of arsenate and arsenite bonding structures on goethite by FTIR. *Soil Science*. 161(12): 865-872.

United States Environmental Protection Agency. 2001. EPA To Implement 10ppb Standard for Arsenic in Drinking Water. EPA 815-F-01-010.

Wagman, D.D. et al.. 1982. *J. Phys. Chem. Ref. Data II. Suppl.*, 2: 392.

Walsh, L.M. and Keeny, D.R.. 1975. Behavior and phytotoxicity of inorganic arsenicals in soils. In: E.A. Woolson (Editor). *Arsenical pesticides*. ACS. Washington, DC., pp. 35-52.

Waychunas, G.A., Rea, B.A., Fuller, C.C. and Davis, J.A.. 1993. Surface chemistry of ferrihydrite: Part 1. EXAFS studies of the geometry of coprecipitated and adsorbed arsenate. *Geochimica et Cosmochimica Acta*. 57: 2251-2264.

Westcot, D.W., Chilcott, J.E. and Smith, G.. 1993. Pond water, sediments and crystal chemistry. ASCE National conference on irrigation and drainage engineering. ASCE, New York.

Whitacre, R.W. and Pearse, C.S.. 1974. Arsenic and the environment. *Colorado school of mines minerals industries bulletin*, 17(3).

Wijnja, H. and Schulthess, C.P., 1999. ATR-FTIR and DRIFT spectroscopy of carbonate species at the aged γ -Al₂O₃/water interface. *Spectrochimica Acta. Part A.* 55: 861-872.

Xu, H., Allard, B. and Grimvall, A., 1988. Influence of pH and organic substance on the adsorption of As(V) on geologic materials. *Water, Air, and Soil Pollution.* 40: 293-305.

Zabinsky, S.I., Rehr, J.J., Ankudinov, A., Albers, R.C. and Eller, M.J., 1995. Multiple-scattering calculations of X-ray-absorption spectra. *Physical Review B.* 52(4): 2995-3009.

Chapter 4

RESIDENCE TIME EFFECTS ON PHOSPHATE SURFACE SPECIATION AT THE FERRIHYDRITE-WATER INTERFACE

4.1 Abstract

Understanding residence time effects on phosphorus (P) retention/release in P rich soils and sediments is important to predict the environmental impact (e.g., eutrophication) in surrounding water bodies. In this study, aging (days to year) effects on P sorption/desorption reactions and the surface speciation at the ferrihydrite (FH)-water interface were investigated using batch adsorption/desorption experiments coupled with *in situ* Attenuated Total Reflectance Fourier transform infrared spectroscopy (ATR-FTIR) and *in situ* P K-edge X-ray Absorption near edge structure (XANES) analyses. Phosphate adsorption was initially rapid followed by a slow continuous uptake for 24 h at pH 4-9.5, and the rate of P adsorption increased with decreasing pH. Increased aging times (2d-1 yr) reduced the reversibility of sorbed P at pH 4 and 7.5, indicating residence time effects. ATR-FTIR analyses showed slight shifts in ν_3 vibrations (i.e., C_{2v} and/or C_1 symmetry) at pH 4 and 7.5 with aging,

indicating changes in surface speciation. In the XANES analyses, the pre-edge feature (i.e., a signature for the inner-sphere Fe(III) octahedral and P tetrahedral linkage) was enhanced with aging and the post-edge resonance feature was dissimilar from that of ferric phosphate minerals. This suggests an increase in P-O-Fe coordination environments possibly due to chemical reconfiguration of adsorption complexes from lower energy (e.g., monodentate mononuclear linkage) to higher energy binding (e.g., bidentate binuclear linkage). Overall, *in situ* spectroscopic analyses showed that the residence time might cause surface complex reconfiguration. The higher energy binding may be an important chemical factor for controlling retention and release of P at the FH-water interface.

4.2 Introduction

In the last few decades, excess P has been recognized as a nonpoint-source agricultural pollutant throughout the world due to the over-application of both inorganic and animal derived fertilizers such as poultry manure (Ryden et al., 1973; Vaithyanathan and Correll, 1992). Eutrophication, as well as the over-growth of cyanobacteria due to excessive P in recreational, industrial and drinking water could greatly threaten human and ecological health (Kotak et al., 1993; Sharpley and Rekolainen, 1997). In recent years, the nutrient (e.g., inorganic phosphorus) rich surface runoff from Atlantic Coastal Plain soils has been indirectly linked to the growth of the toxic microorganism, *psitesteria* (Burkholder and Glasgow Jr., 1997).

This microscopic organism produces a toxin killing various lower food chain marine organisms, and is also known to cause human health problems (Levin et al., 1997).

The long term fate and transport of P in soil/water environments must be well understood to propose the best remediation strategies for effectively reducing negative impacts on aquatic/terrestrial environments. Residence time effects are one of the most important abiotic factors controlling bioavailability of P. Soils and sediments are nearly always at disequilibrium with respect to ion transformations (Sparks, 1987). Therefore, the rate of bioavailability can be reduced or increased with increasing time (Pignatello and Xing, 1995). Residence time effects are often described as irreversible, hysteretic, and nonsingular reactions, and can be suggested by the observation of two slow reaction processes; 1) a continuous slow sorption of the adsorptive onto the adsorbent with increasing time and 2) a slow desorption of the adsorptive from the adsorbate with increasing time.

Continuous slow adsorption of P on soils and soil components over time scales of hours to months (i.e., amorphous $\text{Al}(\text{OH})_3$, natural allophane, ferrihydrite, hematite, goethite, $\alpha\text{-Al}_2\text{O}_3$ and kaolinite) have been reported by many researchers (Barron and Torrent, 1995; Barrow, 1974; Barrow, 1985; Beek and van Riemsdijk, 1982; Black, 1942; Colemann, 1944; Edzwald et al., 1976; Hingston et al., 1974; Hsu and Rennie, 1962; Kafkafi et al., 1967; Madrid and Posner, 1979; Okajima et al., 1983; Parfitt, 1979; Parfitt, 1989; Ryden and Syers, 1977; van Riemsdijk et al., 1977; Willett et al., 1988). In addition, P reacted Australian sandy loam soils, ferrihydrite and kaolinite have exhibited hysteresis in adsorption/desorption isotherms (Barrow,

1983b, Kafkafi et al, 1967, Ryden and Syers, 1977). Residence times can have a significant influence on P desorbability from soils and goethite (Barrow, 1979; Barrow and Shaw, 1975; Madrid and Posner, 1979).

Unfortunately, mechanisms responsible for these slow adsorption/desorption reactions have not been clearly understood based on macroscopic studies alone. Several physicochemical factors have been indirectly suggested; 1) solid-state diffusion, or intra- and inter-pore diffusion, 2) surface precipitation and 3) higher energy binding on surface structures via chemical reconfiguration (Beek and van Riemsdijk, 1982; Fendorf et al., 1992; Pignatello and Xing, 1995).

In this study, we investigated residence time effects on P surface speciation (e.g., binding mechanisms and surface precipitates) and adsorption/desorption reactions at the ferrihydrite (FH)-water interface using a combination of macroscopic techniques including batch adsorption/desorption experiments and *in situ* spectroscopic methods. Attenuated total reflectance Fourier transform infrared spectroscopy (ATR-FTIR) and P K-edge X-ray Absorption Near Edge Structure (XANES) Spectroscopy were used to understand the chemical factors (e.g., P coordination and protonation environment) responsible for the slow adsorption/desorption reactions at the FH-water interface. Two-line ferrihydrite (FH) (an amorphous hydrous ferric oxide) was chosen in this study because 1) it commonly forms in soils and sediments (Fuller and Davis, 1989; Jackson and Keller, 1970; Schwertmann and Fischer, 1973; Schwertmann et al., 1982) and; 2) it has a strong

adsorption capacity for P (Parfitt, 1989; Willett et al., 1988) which has implications for P agrochemical cycles in the environment.

4.3 Materials

Two-line ferrihydrite (FH) was synthesized according to Schwertmann and Cornell (Schwertmann and Cornell, 1991). Forty g of ferric nitrate was dissolved in 500 ml deionized water. The pH of the solution was titrated to pH 7.5, and maintained at this pH value for 45 min by addition of 1 M NaOH. The FH precipitate was washed several times by centrifugation and decantation with deionized water until the nitrate concentration was reduced to below 0.003 mM. The FH paste was then freeze-dried prior to the adsorption experiments. The five-point Brunauer-Emmett-Teller (BET) surface area was $260 \text{ m}^2 \text{ g}^{-1}$. The Point of Zero Salt Effect (PZSE) as determined by a potentiometric titration method, (Zelazny et al., 1996) was about 8. Powder X-ray diffraction (XRD) analysis revealed the diagnostic two broad peaks for two-line ferrihydrite (0.24 and 0.15 nm).

To investigate the formation of ferric phosphate precipitates, several Fe(III)-P reference minerals (strengite ($\text{Fe}^{\text{III}}(\text{PO}_4) \cdot 2\text{H}_2\text{O}$, Indian Mt. Alabama), barbosalite ($\text{Fe}^{\text{II}}\text{Fe}^{\text{III}}_2(\text{PO}_4)_2(\text{OH})_2$, Tip Top Mine, Custer County, South Dakota) and rockbridgeite ($(\text{Fe}^{\text{II}}, \text{Mn}^{\text{II}})\text{Fe}^{\text{III}}_4(\text{PO}_4)_3(\text{OH})_5$, Shady, Polk county, Arkansas) were used in P K-edge XANES analyses. Amorphous strengite was also synthesized according to the method described by Dalas (Dalas, 1991). 100 ml of 0.1 M $\text{Fe}(\text{NO}_3)_3 \cdot 9\text{H}_2\text{O}$ and 0.2 M of KH_2PO_4 solutions were prepared in 250 ml polycarbonate bottles.

The ferric nitrate solution was slowly added (10 ml per 30 s) into the potassium phosphate solution while the bottles were stirred at 400 rpm at 298 K. The suspensions were continuously stirred for an additional 2 h and the capped bottles were kept in a 100 °C (± 3) oven for 5 d. Filtered suspensions were washed and freeze-dried for further use. The amorphous structure was confirmed via XRD analyses.

4.4 Methods

4.4.1 Batch Adsorption Experiments

Adsorption kinetics experiments were performed in two steps. Firstly, mineral suspensions (1.25 g L^{-1}) were prepared in 200 ml of 0.1 M NaCl background electrolyte in six 250ml polycarbonate reaction vessels. After 2 min of ultrasonification at 60 W, pH was adjusted to 4, 4.75, 6.25, 7.5, 8.5 and 9.5 using a stirred pH-stat apparatus for 24 h with N_2 purging. Fifty ml of the P stock solutions (i.e., 5 mM sodium phosphate and 0.1M NaCl) were slowly added (10 ml addition every 30 s) to the mineral suspension at the same pH to assure an initial concentration of 1 mM and a final suspension density of 1 g L^{-1} . The mineral suspensions were stirred at 300 rpm. Periodically (i.e., 5, 10, 30 min, 1, 2, 4, 12, and 24 h), 10 ml of mineral suspensions were removed, and then passed through a 0.2 μm Gelman Supor®-200 membrane filter (Pall Corp. MI). The supernatants were analyzed for dissolved P using the molybdenum blue method (He et al., 1998; Murphy and Riley, 1962).

4.4.2 Phosphate Desorption Experiments

Aged P adsorbed FH samples (i.e., 2 d - 19 mo) at pH 4 (1 g L^{-1} , and $[\text{P}]_0 = 1 \text{ mM}$) and pH 7.5 (1 g L^{-1} , and $[\text{P}]_0 = 0.6 \text{ mM}$) were prepared using the method described in the previous adsorption kinetics section. Use of different initial P concentrations at pH 4 and 7.5 were employed to provide the same loading levels during different incubation times. 250 ml of P adsorbed FH suspensions (1 g L^{-1}) were centrifuged at 2000 rpm, and then 200 ml of the supernatants were removed to prepare concentrated mineral suspensions (i.e., 5 g L^{-1}). To reach the detection limit of the molybdate blue method during stirred-flow desorption experiments, total P levels in the mineral suspensions need to be increased using this process. The stirred-flow system is an ideal system to study desorption/dissolution behavior at realistic soil to solution ratios that better simulate field conditions. The adsorbents are exposed to a greater mass of ions than a static batch system, and the flowing solution continuously removes reaction products (desorbed species) (Sparks, 1989).

7.6 ml of the mineral suspensions were transferred into a stirred flow chamber assembled with a $0.2 \text{ }\mu\text{m}$ Gelman Supor®-200 membrane filter (Pall Corp. MI) (Sparks, 1989). Desorption experiments were carried out on samples aged for 3 d to 9 mo using the following desorptives: 1) 1 mM sodium sulfate + 1 mM sodium acetate + 0.0096 M NaCl at pH 4.5 and 2) 1 mM sodium sulfate and 1 mM MES (2-(*N*-morpholino) ethane sulfonic acid, and 0.0096 M NaCl at pH 7.5. Sulfate was used to promote P desorption, and sodium acetate and MES were used to buffer the reaction

pHs during the desorption experiments. The influents were pumped into the reaction chamber at the flow rate of 0.3 ml min^{-1} , and 9 ml effluents were collected every 30 min using a fraction collector. Filtrates were analyzed for dissolved P using the method described above.

4.4.3 ATR-FTIR Analyses

Infrared spectra of P sorbed on FH were collected as a function of pH 4 and 7.5. All samples were prepared according to methods described in the adsorption kinetics section. Subsample (30 ml) were collected over a period of 15 min to 1 year, and then centrifuged at 11750 g to recover the paste. The paste was quickly loaded on a ZnSe or Ge horizontal ATR-FTIR crystal (45° angle of incidence) trough that was continuously purged with N_2 during the FTIR analysis. The use of a Ge crystal was only necessary for acidic ($\text{pH} < 3$) samples. ATR-FTIR data were collected using a Perkin-Elmer 1720x spectrometer equipped with a Whatman FT-IR N_2 gas generator (Model 75-63, Whatman Inc, MA) to remove H_2O and CO_2 from the sample compartment and MCT detector. A total of 1000 co-added spectra were collected for the adsorption samples at a resolution of 2 cm^{-1} .

All spectra were ratioed against the spectra of an empty cell. Subtraction of the spectra was performed to obtain all final spectra. For example, the final spectra were obtained by subtracting the spectra of the entrained solution and the FH paste from the spectra of P adsorbed FH. All spectra were normalized with respect to the highest absorbance (at $\approx 1020 \text{ cm}^{-1}$) of each sample. Since ATR-FTIR spectral

subtraction was done at the slope of an absorption band of the ferrihydrite ($<1100\text{ cm}^{-1}$), it is difficult to preserve the $\text{P } \nu_1$ band at $<800\text{ cm}^{-1}$ if present. Therefore the changes in the $\text{P } \nu_3$ vibrations are mainly discussed in the Results and Discussion section.

4.4.4 Theoretical IR Vibrations of Phosphoric Acid

A tetrahedral penta-atomic P molecule (*i.e.*, PO_4^{3-}) exhibits four different vibrations; 1) the symmetric P-O stretching (A_1, ν_1), 2) the symmetric P-O-P bending (E, ν_2), 3) the asymmetric P-O stretching (F, ν_3) and 4) the asymmetric P-O-P bending (F, ν_4). The ν_1 (nondegenerate symmetric stretching) and the ν_3 (triply degenerate asymmetric stretching) vibration can be utilized to understand not only the molecular symmetry of the phosphoric acid (P) but also the coordination environments of the P adsorption complexes on metal oxide surfaces. Infrared spectra of P have been extensively investigated by several researchers (Chapman and Thirlwell, 1964; Nakamoto, 1997; Persson et al., 1996; Tejedor-Tejedor and Anderson, 1990). Phosphate has several pK_a values ($\text{pK}_1;2.20$, $\text{pK}_2;7.2$, and $\text{pK}_3;12.3$) (Snoeyink and Jenkins, 1980), and the protonation significantly affects the P molecular symmetry. In Table-4.1, we have summarized 1) the molecular symmetry and 2) the number and the position of the ν_1 and ν_3 vibrations of phosphoric acid at different pHs reported in our previous study (Chapter 2). The IR spectra of P solution species at different pH values were produced using methods reported by Tejedor-Tejedor and Anderson's research (1990).

Fully deprotonated phosphoric acid (PO_4^{3-}) at pH 12.8 has near T_d/C_{3v} symmetry. This tetrahedral molecule shows a single ν_3 asymmetrical vibration (F_2) at $\approx 1006\text{cm}^{-1}$, and there is no activation of the ν_1 vibration (Table 4.1). Monoprotonated (HPO_4^{2-}) species have C_{3v} symmetry and the ν_3 vibration splits into two (E and A_1) at ≈ 1077 and 989cm^{-1} . There is also ν_1 band activation at $\approx 850\text{cm}^{-1}$. Further protonation results in the formation of diprotonated phosphate (i.e., H_2PO_4^-), which leads to a reduction in the symmetry from C_{3v} to the C_{2v} . The ν_3 (E) vibration splits into two bands (B_1 and B_2), therefore, there are a total of three ν_3 bands (B_1 , B_2 and A_1) at ≈ 1160 , 1074 and 940cm^{-1} . The ν_1 vibration shifts to higher wavenumber at $\approx 870\text{cm}^{-1}$. At pH ≈ 1.3 , the symmetry of the dominant phosphoric acid species is H_3PO_4 (C_{3v}) and the spectrum shows doublets (E and A_1) of the ν_3 vibration at ≈ 1179 and 1006cm^{-1} . In summary, the numbers of the ν_3 vibration are two for the C_{3v} symmetry and three for the C_{2v} or lower (C_1) symmetry. The results of the P IR spectra are in good agreement with the studies by Chapman (1964) and Nakamoto (1997).

We can apply the concept of molecular symmetry as related to changes in the ν_3 and ν_1 vibrations to P adsorption complexes on metal oxide surfaces such as ferrihydrite. If orthophosphate ions (PO_4^{3-}) are coordinated with iron ion(s) of the FH surface by forming inner-sphere complexes, one should observe a reduction in symmetry with respect to the free aqueous PO_4^{3-} . As the symmetry lowers from T_d to C_{3v} or C_{2v}/C_1 , the triply degenerate ν_3 vibration splits into two or three bands (Nakamoto, 1997). In fact this was the case in the P adsorption complexes at the FH-water interface after 24 h of equilibration time. Our previous ATR-FTIR study

showed that the symmetry of inner-sphere P adsorption complexes ($\Gamma = 0.38 \mu\text{mol m}^{-2}$ and pH 4-9, $\Gamma = 2.69 \mu\text{mol m}^{-2}$ and pH 4, $\Gamma = 2.42 \mu\text{mol m}^{-2}$ and pH 7.5) are C_{2v}/C_1 as evidenced in the triply degenerate ν_3 vibrational mode (Table 4.1) (Arai and Sparks, 2001).

To investigate the changes in the P surface speciation at the FH-water interface with aging (1 d – 1 yr), we compared the IR spectra of aged adsorbed species to the spectra from the previous short-term (24 h) adsorption study shown in Table 4.1. Second, we assigned the symmetry of the adsorption complexes based on the number of ν_3 band splitting. Peak fitting using Gaussian profiles was performed to reveal the assemblage of multiple ν_3 bands using the Peaksolve™ software package version 1.05 (Galactic Industries Corp.). This molecular symmetry assignment allows us to speculate on the configurations of the surface complexes. Based on the combined information from these experiments, the final surface species can be proposed.

4.4.5 Phosphorus K-edge XANES Analyses

Phosphorus K-edge (2145.5 eV) XANES data were collected at beamline X-19A at the National Synchrotron Light Source (NSLS), Brookhaven National Laboratory, Upton, NY. The electron storage ring was operated at 2.528 GeV with a current range of 130 to 300 mA. The XANES spectra were collected in fluorescence mode with a passivated implanted planar silicon detector (Canberra Industries, Meriden, CT) and helium flight path at 298K. The spectra were taken between 2130

Table 4.1 Position of IR peak maxima of phosphoric acid and P adsorption complexes at the ferrihydrate-water interface.

Species, symmetry and reaction conditions (Reference)	Infrared active band positions (cm ⁻¹)		
	1100	1000	900
PO ₄ ³⁻ (aq), T _d (Chapter 2)		1006(v ₁)	
HPO ₄ ²⁻ (aq), C _{3v} (Chapter 2)		1077(v ₁)	989(v ₁) 850(v ₁)
H ₂ PO ₄ ⁻ (aq), C _{2v} (Chapter 2)	1160(v ₁)	1074(v ₁)	940(v ₁) 870(v ₁)
H ₃ PO ₄ (aq), C _{3v} (Chapter 2)	1179(v ₁)	1006(v ₃)	
Ferrihydrate-P (paste), 24 h reaction time (Chapter 2)			
pH 4 - 9, 0.38 μmol m ⁻²	1102-1070(v ₃)	1020-1025(v ₃)	940-920
pH 4, 2.69 μmol m ⁻²		≈1085(v ₃) 1020(v ₁)	≈950(v ₁)
pH 7.5, 2.42 μmol m ⁻²	≈1100(v ₁)	≈1020(v ₁)	≈920(v ₁)
Ferrihydrate-P (Paste) (This study)			
pH 4, 2 d, 2.70 μmol m ⁻²		1091(v ₁) 1029(v ₁)	976(v ₁)
pH 4, 1.5 mo, 2.74 μmol m ⁻²		1095(v ₁) 1015(v ₁)	932(v ₁)
pH 4, 1 yr, 2.76 μmol m ⁻²		1095(v ₁) 1035(v ₁)	970(v ₁) 944(v ₁)
pH 7.5, 2 d, 2.01 μmol m ⁻²		1082(v ₁) 1022(v ₁)	946(v ₁)
pH 7.5, 1.5 mo, 2.10 μmol m ⁻²		1089(v ₁) 1020(v ₁)	942(v ₁)
pH 7.5, 1 yr, 2.35 μmol m ⁻²		1090(v ₁) 1019(v ₁)	

and 2190 eV with a step size of 0.03eV and 0.1s integration time per step. A Si(111) crystal monochromator was used. Samples were placed in a groove cut into a polycarbonate sample holders that was oriented at 45° to the unfocused incident beam. The photon energy scale was calibrated to the energy (≈ 2159 eV) at the half-height of the P absorption K-edge of an ACS grade sodium phosphate salt ($\text{Na}_2\text{HPO}_4 \cdot \text{H}_2\text{O}$, Fisher). This calibration was repeated before and after sample analysis. Phosphorus salts and minerals were finely ground. The powder materials were directly placed on the adhesive surface of scotch tape and covered with a mylar film (Spex Industries, Edison, NJ). Phosphorus samples from adsorption kinetics studies at pH 4 and 7.5 were analyzed. The paste was collected onto a 0.2 μm Gelman glass fiber filter paper (Pall Corp., MI) by vacuum filtrating 10 ml of mineral suspensions. The filter with paste was directly loaded onto a sample holder, and the paste surface was covered with a mylar film (SPEX CertiPrep Inc. NJ) to inhibit moisture loss during the XANES measurements. A total of 2-3 spectra per sample were averaged after normalizing to unity using Winxas 2.0 (Ressler, 1997).

4.5 Results and Discussion

4.5.1 Phosphate Adsorption Envelope Kinetics

Phosphate adsorption envelope kinetics at the FH-water interface at pH 4.0-9.5 are shown in Fig.4.1. Phosphate adsorption increases with decreasing pH from 9.5 to 4 (Fig. 4.1). Whereas 98.2 % adsorption ($2.70 \mu\text{mol m}^{-2}$) at pH 4 was achieved after 24 h, slow adsorption continued at pH > 4 after 24h (Fig. 4.1). Only 58 % (1.59

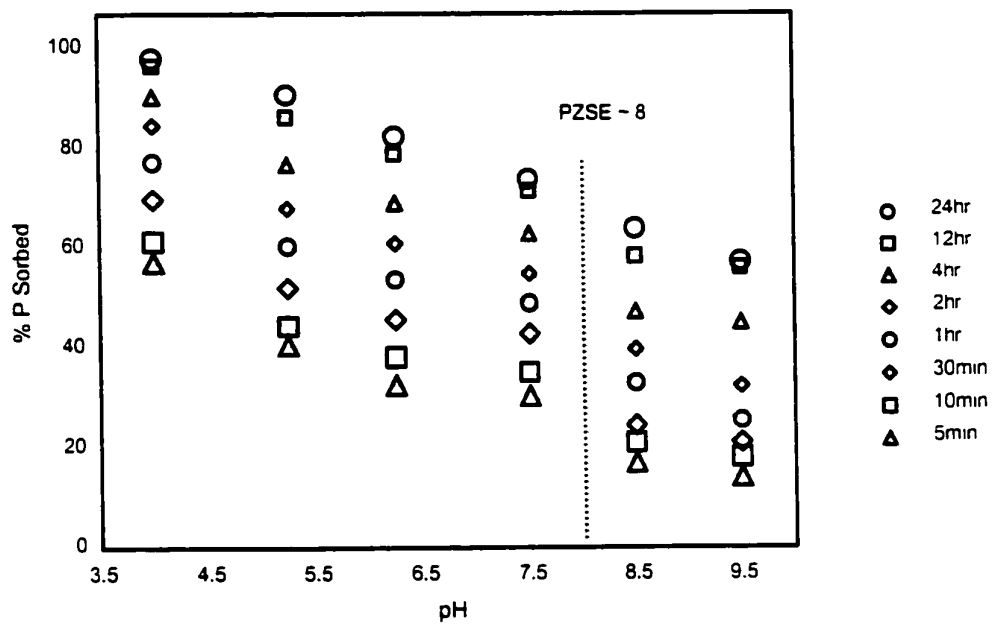


Figure 4.1 Phosphate adsorption kinetics at the ferrihydrite-water interface as a function of pH.

$\mu\text{mol m}^{-2}$) of total P uptake was achieved at pH 9.5 after 24 h and the slow P uptake continued after 1 d (Fig. 4.1). Several studies have also reported slow P adsorption on soils and other soil components (i.e., amorphous $\text{Al}(\text{OH})_3$, natural allophane, ferrihydrite, hematite, goethite, $\alpha\text{-Al}_2\text{O}_3$ and kaolinite) over different time scales (hours to months) (Barron and Torrent, 1995; Barrow, 1974; Barrow, 1985; Beek and van Riemsdijk, 1982; Black, 1942; Colemann, 1944; Edzwald et al., 1976; Hingston et al., 1974; Hsu and Rennie, 1962; Kafkafi et al., 1967; Madrid and Posner, 1979; Okajima et al., 1983; Parfitt, 1979; Parfitt, 1989; Ryden et al., 1977; van Riemsdijk et al., 1977; Willett et al., 1988).

The difference in the kinetics at different pH values could be explained by differences in the surface charge density of FH at the experimental pH values. The dissociation constants of H_3PO_4 ($\text{p}K_1$ 2.1, $\text{p}K_2$ 7.2 and $\text{p}K_3$ 12.3) would indicate that the predominant P solution species were negatively charged at our experimental pH values (i.e., H_2PO_4^- at $\text{pH} < 7.2$ and HPO_4^{2-} at $\text{pH} > 7.2$) (Snoeyink and Jenkins, 1980). The surface charge density of FH becomes more negatively charged with increasing pH from 4.0 to PZSE of the solid ($\text{pH}_{\text{PZSE}} \approx 8$). The mineral surface at $\text{pH} < 8$ is more positively charged than at $\text{pH} > 8$, and the protonated mineral surfaces at $\text{pH} < 8$ strongly attract negatively charged P solution species (e.g., H_2PO_4^-). It is interesting that the rate of P adsorption kinetics rapidly drops after $\text{pH} \approx 8$. This is probably due to changes in net surface charge density of FH from positively to negatively charged surfaces that repel HPO_4^{2-} species.

Our macroscopic evidence indicated that negatively charged P solution species significantly sorbed onto both positively/negatively charged FH surfaces at pH 4-9.5 over time, suggesting possibilities for both electrostatic interaction and ligand exchange mechanisms. Previous electrophoretic mobility (EM) measurements have shown the formation of P inner-sphere surface complexes at the FH-water interface due to shifts in the electrophoretic mobility of FH particles after P adsorption at the same pH range (Arai and Sparks, 2001). In addition, an *in situ* ATR-FTIR study (Arai and Sparks, 2001) has shown that the formation of inner-sphere complexes via ligand exchange was predominantly responsible for P adsorption (< 48 h) at the FH-water interface under similar experimental conditions.

While previous EM measurements and *in situ* spectroscopic studies on short-term (< 48 h) samples have shown formation of inner-sphere surface complexes (Chapter 2), it is still unclear that the same reaction mechanisms are taking place at the FH surface after long reaction times (2 d-1 yr). The short-term (< 48 h) adsorption kinetics data are insufficient to provide mechanistic information on 1) slow P adsorption reactions at pH > 4 after 24 h; 2) the stability of sorbed P over longer times, and 3) changes in P surface speciation > 24 h. Therefore, we performed batch desorption experiments and *in situ* spectroscopic analysis on aged P reacted FH.

4.5.2 Residence Time Effects on Phosphate Desorption

Figs. 4.2 and 4.3 show short-term (24 h) P desorption at pH 4 and 7.5 using the stirred flow method. Since nearly 100% adsorption was achieved within 2 d, the

loading levels for all aged samples were approximately equal at each pH ($\Gamma \approx 2.7$ $\mu\text{mol m}^{-2}$ at pH 4, and $\Gamma \approx 1.62$ $\mu\text{mol m}^{-2}$ at pH 7.5). Biphasic P desorption reactions were observed at both pH values (Fig. 4.2 and 4.3). At pH 4, the initial fast reaction occurred during the first 3-5 hours, and slow reactions followed up to 24 hours, and total P desorption decreased from 4.81 % to 0.92 % with increasing aging time from 2 d to 10 m, suggesting a residence time effect (Table 4.2).

Table 4.2 Phosphate desorption experimental conditions and total desorbed P after 24 h of desorption.

Sample conditions	Total P desorbed (mg kg^{-1}) after 24 h of desorption, (%)
pH 4, 2 d	1491.18, (4.81 %)
pH 4, 1 m	655.82, (2.12 %)
pH 4, 4 m	626.82, (2.02 %)
pH 4, 10 m	286.36, (0.92 %)
pH 7.5, 2 d	1873.94, (10.07 %)
pH 7.5, 1 m	968.06, (5.20 %)
pH 7.5, 9 m	944.41, (5.08 %)
pH 7.5, 19 m	713.21, (3.83 %)

Similarly, biphasic desorption behavior was observed at pH 7.5 (Fig. 4.3). Total desorbable P decreased from 10.07 % to 3.83 % with increasing aging time from 2 d to 19 m at pH 7.5 (Table 4.2). It is interesting that total desorbable P is much less at pH 4 even though the initial loading levels at pH 4 are much higher than those at pH 7.5. These results suggest that different reaction mechanisms might be responsible for differences in the irreversibility at the two different pHs.

Several researchers have reported similar irreversible P adsorption/desorption

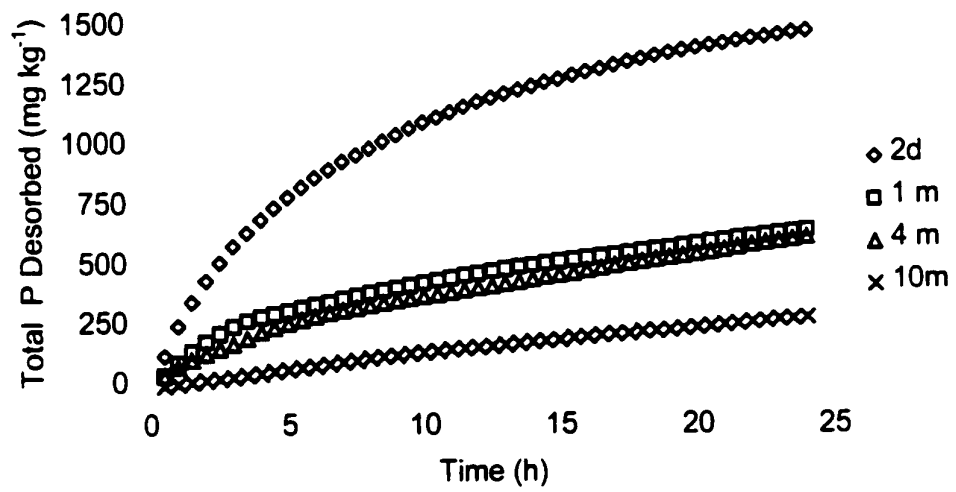


Figure 4.2 Residence time effects on P desorption from ferrihydrite at pH 4.0.

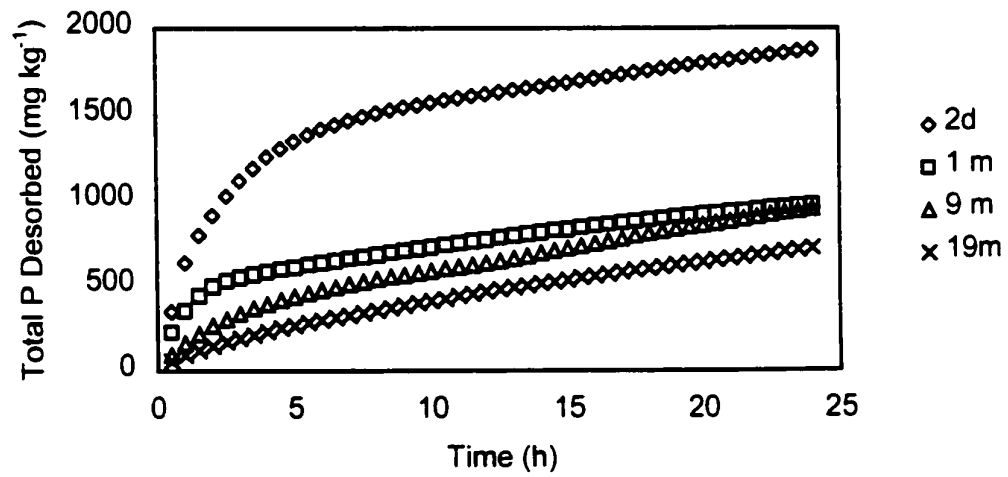


Figure 4.3 Residence time effects on P desorption from ferrihydrite at pH 7.5.

reactions. In early P research, Australian researchers compared P adsorption and desorption processes on soils and soil components, investigating the hysteresis effect, in which an adsorption isotherm curve does not coincide with a desorption isotherm curve. Using a batch equilibrium study (< 24 h), Barrow (1983b) showed slight shifts between adsorption and desorption isotherm curves on an Australian sandy loam. Ryden and Syers (1977) utilized the same experimental approaches to compare the P hysteresis effect on soils and ferrihydrite. Desorption isotherm curves on the soils and ferrihydrite were greatly shifted from adsorption isotherm curves, and ferrihydrite showed greater irreversibility than the soils. The concentration effect on hysteresis was also investigated. A wide range of initial P ($[P]_0 = 0.001\text{-}1\text{ mM}$) was reacted with kaolinite, and then desorption was investigated using isotopic exchange (Kafkafi et al., 1967). A hysteresis effect was observed over all concentration ranges. Incubation time highly influences the reversibility of adsorbed P from soils and soil components. Barrow and co-workers (1979; 1975) reported that P desorption from Australian soils was rapid when aging time was short (< 24 h), but the desorption process became much slower when aging time was longer (> 24 h). Madrid and Posner (1979) observed similar irreversible P desorption from goethite. P desorption decreased with increasing aging time from 1 h to 23 h. A similar study was also conducted on a synthetic goethite and Australian clay loam using longer desorption experiments (> 96 h) and varying incubation time. The irreversibility was enhanced with increasing aging time (Barrow, 1979; Madrid and Posner, 1979). Irreversibility could also occur after a short adsorption reaction (<15 s).

It is important to mention that the residence time effects are attributed not only to chemical factors (i.e., chemisorption and/or precipitation reactions) but also to physical factors (i.e., diffusion). Ions trapped in meso-pores (inter-particle) between aggregates and micro-pores (intra-particles) within an individual particle fissure are difficult to extract/desorb with any desorptive. Several researchers have shown the importance of diffusion (i.e., solid-state meso-pore and micro-pore diffusion) in controlling P adsorption/desorption reactions on soils and soil components (i.e., amorphous iron and aluminum oxides) using Barrow's mechanistic models (Barrow, 1983a; Bolan et al., 1985; Enfield et al., 1981; Ryden et al., 1977; van Riemsdijk et al., 1984). Temperature dependent P desorption kinetic studies from desert soils and kaolinite also showed that slow P release could depend on diffusion processes due to estimated activation energies of less than 42 kJ mole⁻¹ (Bar-Yosef and Kafkafi, 1978; Evans and Jurinak, 1976). Other researchers have indicated that enhanced slow reaction and irreversibility on iron oxides (i.e., goethite, ferrihydrite, and lepidocrocite) were attributed to micro-pore diffusion into amorphous particles and/or specific particle morphologies (thin, multidomainic laths and slit-shaped macropores of multidomainic laths) (Cabrea et al., 1981; Parfitt, 1989; Torrent et al., 1992; Willett et al., 1988).

The chemical mechanisms responsible for the irreversible adsorption/desorption reactions are difficult to elucidate based on macroscopic data alone. We, therefore, performed *in situ* ATR-FTIR and XANES analysis on the aged P reacted FH samples to reveal the changes that might take place in surface speciation

over time.

4.5.3 ATR-FTIR Analyses

ATR-FTIR spectra of aged P adsorbed FH with Gaussian profile fits are shown in Fig. 4.4a and 4.4b. In pH 4 and pH 7.5 samples (Figs. 4.4a and 4.4b), the fitted Gaussian peaks show triply degenerate ν_3 vibrations except for those in 1.5 mo and 1 yr samples at pH 7.5, suggesting that the symmetry of the surface species is C_{2v} and/or C_1 . Since the positions of triply degenerate peaks of the sorption samples are shifted from those of solution species at the same pH values ($H_2PO_4^-$ at pH 4 or HPO_4^{2-} at pH 7.5) (Table 4.1), ν_3 vibration splitting can be ascribed to inner-sphere complexation onto the iron octahedra of the FH. Interestingly the peak positions of the ν_3 vibrations are similar to those in the previous short-term adsorption study (Table 4.1), indicating that similar surface complexes might be forming. In chapter 2, I reported that effects of deuterium exchange did not cause any significant peak shift at pH 7.5 but some shifts occurred at pH 4 at the loading levels $\leq 2.42 \mu\text{mol m}^{-2}$. Therefore, the predominant surface complexes of the 2 d aged pH 7.5 sample can be assigned to nonprotonated bidentate binuclear complexes. Determination of exact bonding environments at pH 4 is difficult based on the FTIR information alone because several different molecular configurations (e.g., monoprotonated bidentate binuclear and/or bidentate binuclear with hydrogen bonding to mineral surfaces) could satisfy C_{2v} and/or C_1 symmetry with proton associations.

It is interesting that peak broadness is consistently present in all samples at

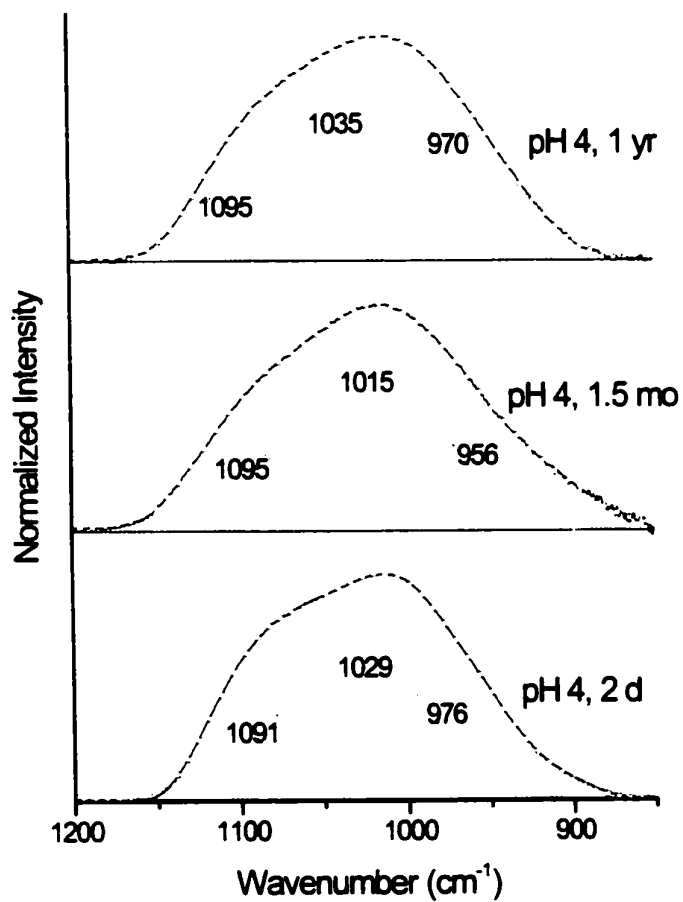


Figure 4.4a ATR-FTIR spectra of P adsorbed ferrihydrite at pH 4 as a function of residence time. The raw spectra are shown with solid lines, the deconvoluted peaks with dotted lines, and the fitted curve with open circles.

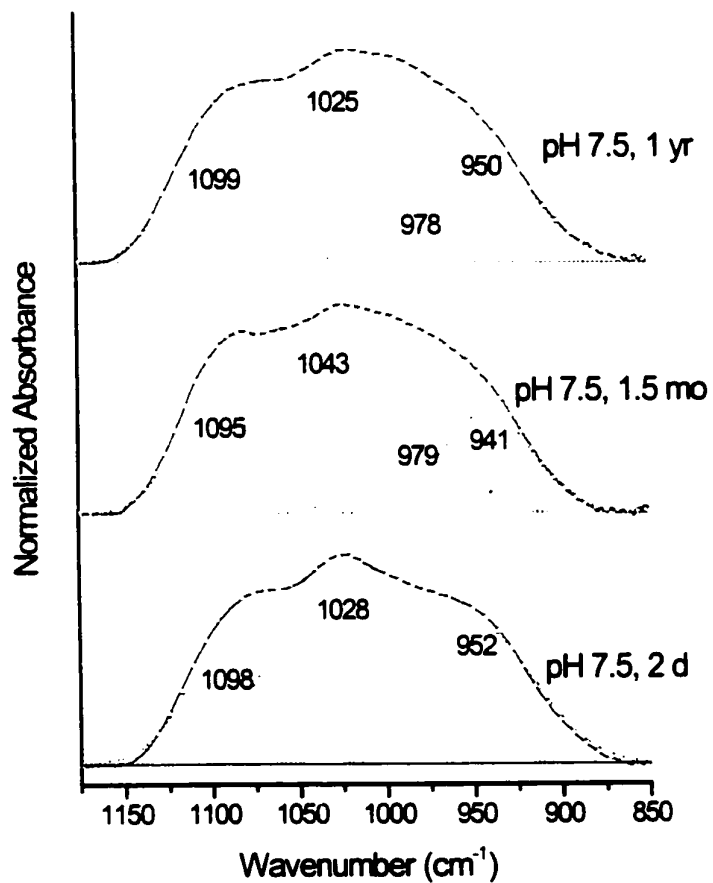


Figure 4.4b ATR-FTIR spectra of P adsorbed ferrihydrite at pH 7.5 as a function of residence time. The raw spectra shown with solid lines and the deconvoluted peaks with dotted lines, and the fitted curve with open circles.

both pH values, which might suggest mixtures of different surface complexes can co-exist at the FH surfaces (e.g., non-protonated bidentate binuclear complexes (C_2) and monoprotonated monodentate mononuclear complexes (C_1)). Additional Gaussian peak fit analyses revealed that 1) shifts in ν_3 band peak positions in pH 4 and 7.5 with aging, and 2) the presence of an additional ν_3 band ($\approx 979 \text{ cm}^{-1}$) in 1.5 mo and 1 yr aged pH 7.5 samples (Fig. 4.4b), suggesting changes in surface speciation (e.g., surface complex reconfiguration) were occurring with aging. To explain the surface complex reconfiguration theory, the adsorption reaction steps are schematically illustrated in Fig. 4.5 assuming the reaction condition of $\text{pH}_{\text{bulk}} \leq \text{PZSE}$. At step I, the negatively charged HPO_4^{2-} molecule is forming an outer-sphere complex via van der Waals forces at the FH-water interface, and the complex can undergo several reaction paths to form different inner-sphere complexes (e.g., monodentate mononuclear complex (Step II), monodentate mononuclear complex with hydrogen bonding (Step III), bidentate binuclear complex (Step IV), and bidentate mononuclear complex (Step V)). Based on our previous IR and electrophoretic mobility measurement study (Chapter 2), inner-sphere adsorption reactions are already taking place in less than 24 h. Therefore, if one argues that there is a slow chemical reconfiguration with aging, the rate limiting reaction steps after the initial inner-sphere complexation (i.e., formation of monodentate mononuclear complexes in Steps II and III) become important.. For instance, the chemical transformation from lower to higher energy binding (e.g., from Step II: monodentate mononuclear to Step IV: bidentate binuclear complexes) is expected to be rate limited due to the formation of new covalent bonds.

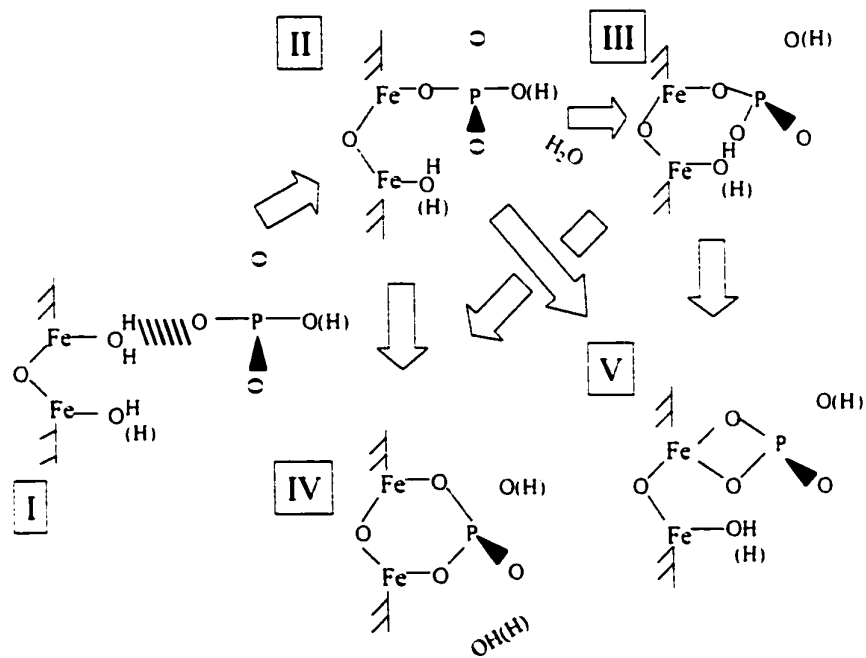


Figure 4.5 Phosphorus adsorption reaction steps at the ferrihydrite-water interface at $\text{pH}_{\text{bulk}} \leq \text{PZSE}$, Step I = Formation of outer-sphere complex, Step II = Formation of monodentate mononuclear complex, Step III = Formation of monodentate mononuclear hydrogen bonded with the hydroxyl group of the FH, Step IV = Formation of bidentate binuclear complex, and Step V = Formation of bidentate mononuclear complex.

It is likely that simultaneous parallel reaction steps (Step II-III, Steps II-IV, and Steps III-IV) are occurring at the FH-water interface, and these slow chemical reconfiguration mechanisms can be speculated on based on the IR data from the pH 7.5 systems (Fig 4.4b). An appearance of a new peak at 979 cm^{-1} after 1.5 mo indicates the formation of new surface complexes (e.g., monodentate mononuclear complexes (Step II) and /or formation of a monodentate mononuclear hydrogen bonded complex with OH(H) functional groups of the FH (Step III)) in addition to non-protonated bidentate binuclear complexes in the 2 d aged sample (Chapter 2). With increasing aging time from 1.5 mo to 1 yr, distribution of triply degenerate ν_3 vibrations (1099 , 1025 , and 950 cm^{-1}) becomes similar to those in 2 d, indicating re-establishment of non-protonated bidentate binuclear complexes after 1 yr.

In summary, the FTIR analyses showed changes in surface speciation with respect to adsorption surface species with aging, however, formation of Fe(III)-P like precipitates via Ostwald ripening mechanisms cannot be excluded. Therefore, we performed *in situ* XANES analyses to investigate the formation of Fe(III)-P precipitate phases in the adsorption kinetic samples.

4.5.4 Phosphorus K-edge XANES Analysis

In Figs. 4.6a, b, and c, XANES spectra of Fe-P minerals (predominantly ferric ion(s) based minerals) and P adsorption samples are shown. Phosphorus K-edge XANES spectra of reference iron phosphate minerals, strengite ($\text{Fe}^{\text{III}}(\text{PO}_4)_2 \cdot 2\text{H}_2\text{O}$), barbosalite ($\text{Fe}^{\text{II}}\text{Fe}^{\text{III}}_2(\text{PO}_4)_2(\text{OH})_2$) and rockbridgeite ($(\text{Fe}^{\text{II}}, \text{Mn}^{\text{II}})\text{Fe}^{\text{III}}_4(\text{PO}_4)_3(\text{OH})_5$),

are compared in Fig 4.6a. Strong whiteness peaks can be observed in all spectra as the result of a P 1s electron transition into an unoccupied valence state of PO_4 sp^3 hybridized orbitals. Distinctive post edge resonance features at 5-25 relative energy (eV) are similar in crystalline and amorphous strengite but barbosalite and rockbridgeite show different features. The relative energy region of pre-edge features (indicated by dotted lines between -6 and -3 eV) are similar in strengite, barbosalite, and rockbridgeite. The pre-edge region of P K-edge XANES spectra includes a sharp whiteness peak resulting from electronic transitions of the core electronic states in the conduction band (Behrens, 1992; Fendorf and Sparks, 1996). The electronegativity, number of nearest neighbors, and coordination environment (i.e., molecular symmetry) of the absorbing atoms could influence the intensity of the position of the pre-edge features (Behrens, 1992; Behrens et al., 1991; Wong et al., 1984). Based on the P XANES study on several transition-metal phosphates by Okude and co-workers (1999), the pre-edge features in the Fe(III)-P salt (i.e., $\text{Fe}_4(\text{PO}_4)_3(\text{OH})_3$) were attributed to interactions between P 3p states (i.e., sp^3 hybridization of the phosphate (PO_4) tetrahedral molecule) and the $3d^5$ electronic state of Fe(III), however relations between the features and specific binding mechanisms are not clearly understood. Therefore, we further investigated the relation between the pre-edge feature and the specific P tetrahedral attachment on iron octahedra (e.g., bidentate binuclear configuration) in different Fe(III)-P minerals.

Phosphate tetrahedra and Fe octahedra coordination environments in barbosalite, rockbridgeite, and strengite were previously studied by Rose and co-

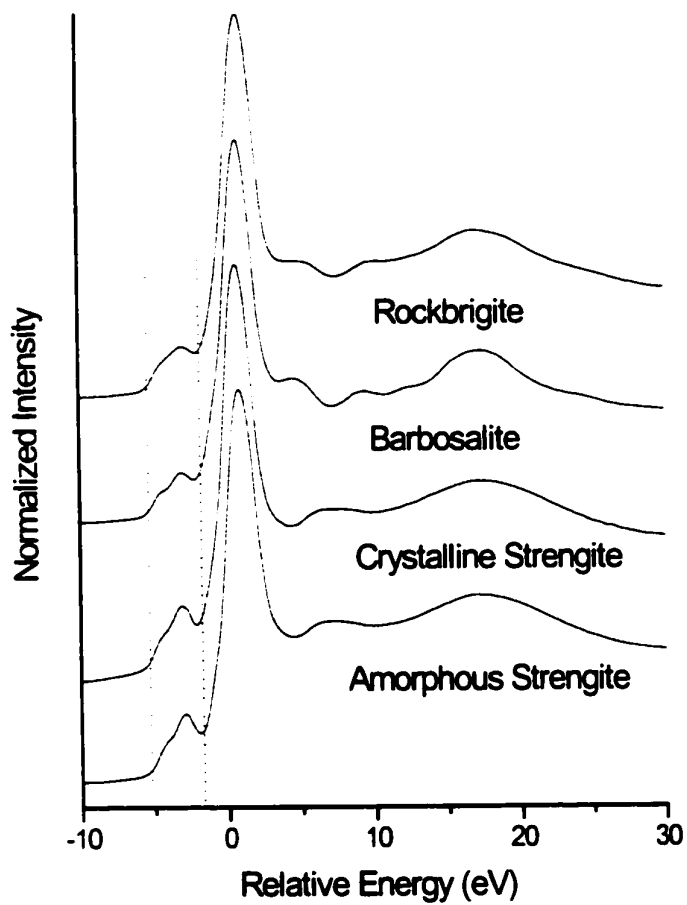


Figure 4.6a P K-edge XANES spectra of synthetic amorphous strengite, crystalline strengite, barbosalite and rockbrigitte.

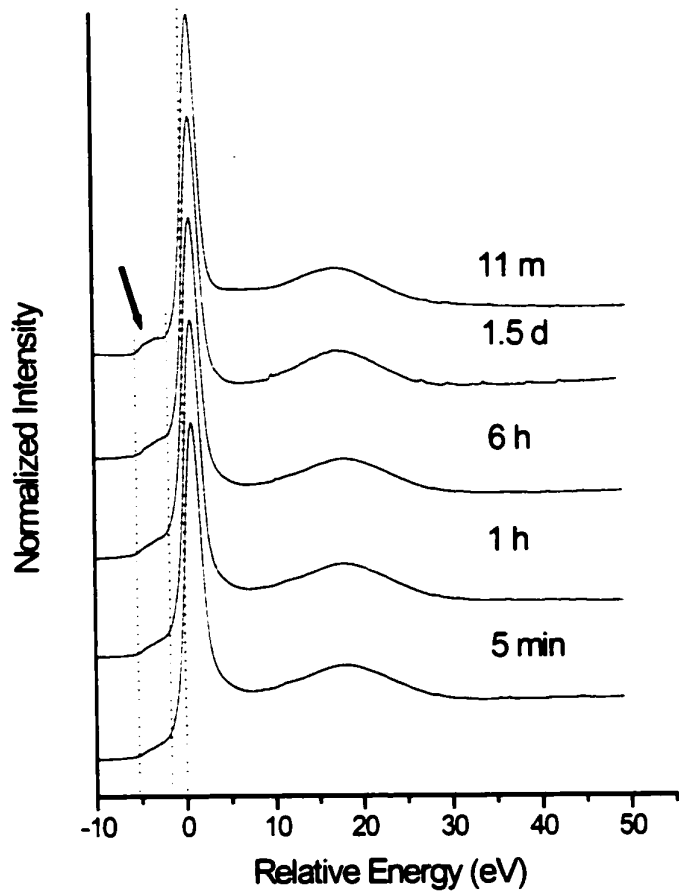


Figure 4.6b P K-edge XANES spectra of P reacted ferrihydrite at pH 4.0 as a function of residence time.

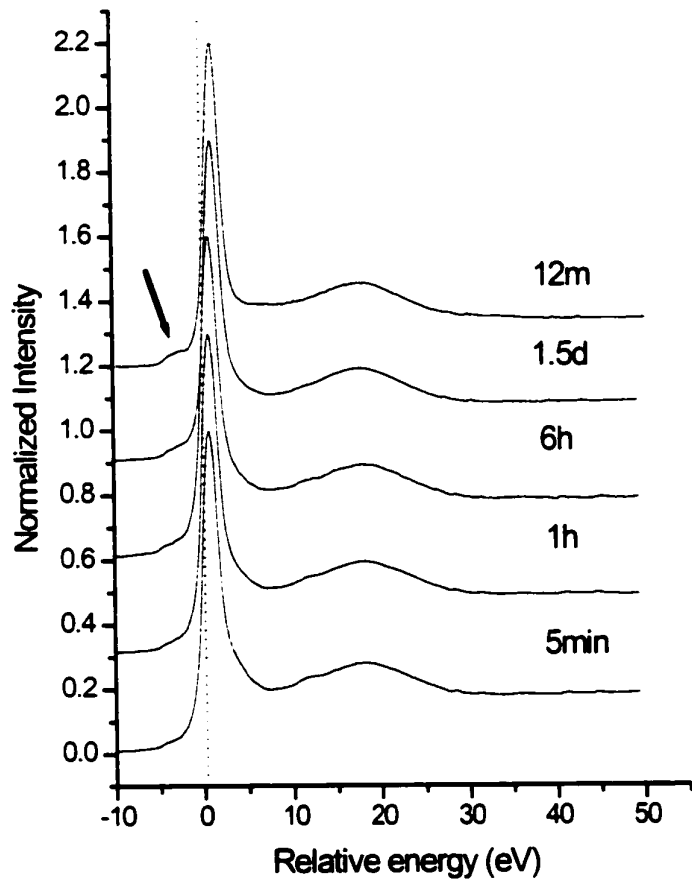


Figure 4.6c P K-edge XANES spectra of P reacted ferrihydrite at pH 7.5 as a function of residence time.

workers (Rose et al, 1997). They described the coordination environments using a notation (NXM^Y) based on the number of corners of the P tetrahedron in association with the Fe(III) octahedron and the number of Fe atoms in the second coordination sphere. The notation NXM^Y was used to describe the different linkages: N is the number of corners of the P tetrahedron involved in the linkage, X is the type of linkage between the polyhedra (i.e., C for corner and E for edge), M stands for the number of iron atoms in the second coordination sphere of P (for one linkage), and Y is the type of linkage between iron octahedra (C for corner and F for face), when more than one Fe(III) octahedra is in the second coordination sphere (Rose et al, 1997). The linkages are $1C1$ (monodentate mononuclear corner attachment on a iron octahedron) for strengite, and $1C2^F$ (monodentate binuclear corner attachment on the center of the face sharing two iron octahedra) for both barbosalite and rockbridgeite and $2C2^C$ (bidentate binuclear corner attachment on two corner sharing iron octahedra) for both barbosalite and rockbridgeite (Rose et al, 1997). Since the similar pre-edge features are consistently present in all of these Fe(III) minerals regardless of the different types of Fe(III)-O-P linkages (Rose et al, 1997), it is difficult to conclude the origin of the pre-edge feature is attributed to the specific coordination environments between P tetrahedra and Fe octahedra. However, it is safe to say that the pre-edge feature is indicative of inner-sphere complexation between P tetrahedral and Fe octahedra structures.

In Figs. 4.6 b and c, XANES spectra of adsorption kinetic samples at pH 4 and 7.5 are shown. The distinctive post edge resonance features seen in the Fe(III)-P

reference minerals at 0-30 eV are absent in all of the sorption kinetic samples, indicating there is no predominant fraction of Fe(III)-P bulk/surface precipitates forming (Fig. 4.6 b and c). This is probably due to destructive interferences of the outgoing multiple scattered photoelectron wave function from predominant two dimensional adsorption complexes which overwhelm weak resonance features of Fe(III)-P precipitates, if any form. Interestingly, very weak pre-edge features (indicated by two dotted lines and an arrow) appear after 5 min of P adsorption on FH at both pH values (Fig. 4.6 b and c). The features are consistently present after 11 mo at both pHs, however the intensity of the pre-edge features in the adsorption samples are much weaker than that of the Fe(III)-P reference minerals. This is probably due to different P/Fe ratio and/or P loading level. For instance, the P/Fe of the adsorption complexes (11 mo aged pH 4 sample) is approximately five times lower than the strengite. The peak positions are similar (between -6 and -3 eV) to those in the ferric phosphate minerals, indicating the inner-sphere P tetrahedral linkages on the Fe(III) octahedral structure are forming after 5 min. This is good agreement with the results of ATR-FTIR analyses and electrophoretic mobility measurements (Chapter 2). In Fig. 4.7, the first derivative of the spectra in Fig. 4.6 a, b, and c also confirm the presence of pre-edge features (indicated by an arrow) in all sorption samples. It is interesting that these double pre-edge features become more pronounced with increasing aging time from 1 h to >11 mo samples at both pH values (indicated by open circles in Fig. 4.7). The intensity of peaks seems to increase with increasing aging time from 1.5 d to 11-12 mo at both pHs, indicating the P-O-Fe(III) linkage

increased over time. In the pH 4 systems, it is true that the amount of P adsorption (i.e., P/Fe ratio) significantly increased between 1 h and 1.5 d, therefore the feature becomes more pronounced. However the surface loading levels were near equal ($\approx 2.73 \pm 0.03 \mu\text{mol m}^{-2}$) between 1.5 d and 11 mo samples. The intensification in the pre-edge feature with aging from 1.5 d to 11 mo might be attributed to an increase in Fe-O-P linkages via the surface complex reconfiguration mechanism as discussed in the previous ATR-FTIR section. In Fig. 4.5, reaction steps from II/III to IV clearly indicate an increase in Fe-O-P linkages by transforming a monodentate mononuclear complex into a bidentate binuclear complex. It is possible that minor fractions of monodentate mononuclear complexes are slowly transforming into bidentate binuclear complexes at the FH-water interface. In similar fashion, the enhancement of the pre-edge features in the pH 7.5 system (Fig. 4.6c) can be explained by the surface complex rearrangement theory, however the surface loading level might have contributed some to the pre-edge feature since it was continuously increasing after 1.5 d.

In the past, several researchers have suggested the formation of aluminum and iron phosphate precipitates at mineral surfaces (i.e., gibbsite, amorphous $\text{Al}(\text{OH})_3$, α - Al_2O_3 , natural goethite, and hematite) upon P sorption using various microscopic and spectroscopic techniques (Jonasson et al., 1988; McCammon and Burn, 1980; Nanzyo, 1984; Nanzyo, 1986; van Riemsdijk and Lyklema, 1980; Wang, 1987; Wang and Tzou, 1995). However these research findings were later questioned because: 1) high ($>1 \text{ mM}$) P concentration might cause a supersaturated condition

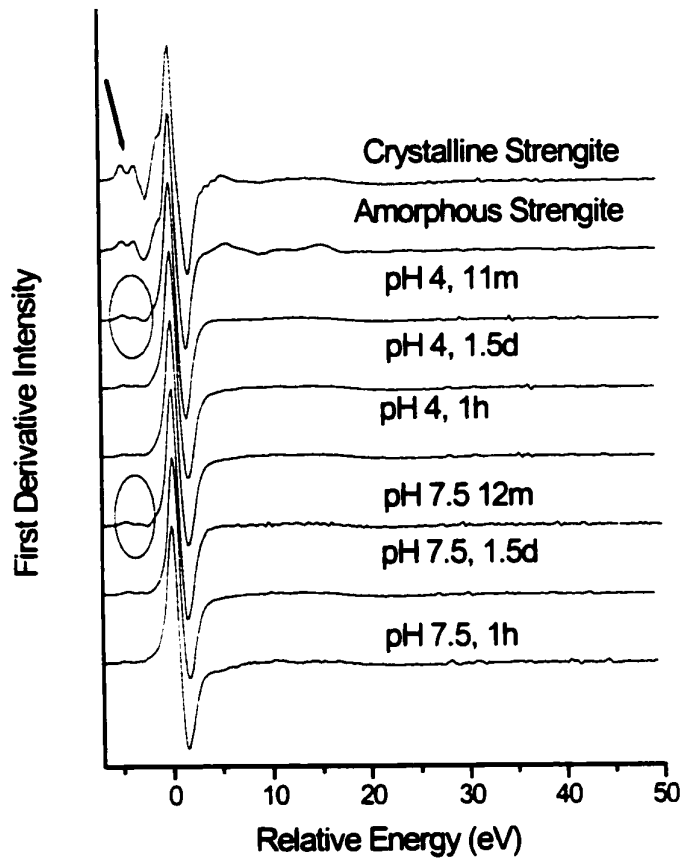


Figure 4.7 First derivative of P XANES spectra in Fig 4.6a-c.

with respect to bulk precipitates; and 2) *ex situ* conditions in XRD, XPS, SEM, and TEM analyses might create artifacts with residual P in the samples.

Our *in situ* XANES and ATR-FTIR spectroscopic studies have shown that adsorption complex predominates regardless of aging time and pH, and there is no evidence for the formation of ferric phosphate precipitates at the FH-water interface after 11 mo of aging time at pH 4 and 7.5.

4.6 Conclusions

In this study, we observed slow P adsorption on FH, and the rate of P adsorption increased with decreasing pH from 9 to 4. The reversibility in sorbed P was slightly decreased with increasing aging time from 2 d to 1 yr at pH 4 and 7.5. *In situ* ATR-FTIR and P K-edge XANES analyses showed that inner-sphere adsorption complexes predominated, and the surface rearrangement of adsorption complexes from lower to higher energy binding might be an important aging mechanism responsible for P retention and release at the FH-water interface.

Natural soil environments are far from equilibrium and undergo a continuum of slow chemical changes (Koskinen and Harper, 1990; Steinfield et al., 1989). As the sorption complexes become more stable (i.e., less soluble and/or result in multidentate complexes) with increasing aging time via chemical transformations, the release of the adsorbate becomes slower, as evidenced by slow desorption phenomena. It is possible that this slow reaction can be accelerated or decelerated due to other biogeochemical factors in the environment. Therefore, our research findings

should be applied to natural systems (e.g., P rich agricultural soils resulting from long term animal derived fertilizer amendments) to provide strategies for remediation, nutrient management, and environmental monitoring.

4.7 Reference

Anderson, M.A., J. F. Ferguson, and J. Gavis. 1976. Arsenate adsorption on amorphous aluminum hydroxide. *Journal of Colloid Interface Science*. 54: 391-399.

Arai, Y., E. J. Elzinga, and D. L. Sparks. 2001. X-ray absorption spectroscopic investigation of arsenite and arsenate adsorption at the aluminum oxide-water interface. *Journal of Colloid Interface Science* 235: 80-88.

Barron, E.A.V., and J. Torrent. 1995. Organic matter delays but does not prevent phosphate sorption by cerrado soils from Brazil. *Soil Science*. 159(3): 207-211.

Barrow, N.J. 1974. The slow reactions between soil and anions. 1. Effects of time, temperature, and water content of a soil on the decrease in effectiveness of phosphate for plant growth. *Soil Science*. 118: 380-386.

Barrow, N.J. 1979. The description of desorption of phosphate from soil. *Journal of Soil Science*. 30: 259-270.

Barrow, N.J. 1983a. A mechanistic model for describing the sorption and desorption of phosphate by soil. *Journal of Soil Science*. 34: 773-750.

Barrow, N.J. 1983b. On the reversibility of phosphate sorption by soils. *Journal of Soil Science*. 34: 751-758.

Barrow, N.J. 1985. Reactions of anions and cations with variable-charge soils. *In Advances in Agronomy*, pp. 183-230.

Barrow, N.J., and T. C. Shaw. 1975. The slow reactions between soils and anions: 2. Effect of time and temperature on the decrease in phosphate concentration in the soil solution. *Soil Science*. 119(2): 167-177.

Bar-Yosef, B., and U. Kafkafi. 1978. Phosphate desorption from kaolinite suspensions. *Soil Science Society of America Journal*. 42: 570-574.

Beek, J., and W. H. van Riemsdijk. 1982. Interactions of orthophosphate ion with soil. *In Soil chemistry B, Physico-chemical models*. G.H. Bolt (ed.) Elsevier Science Publisher Co., Amsterdam, pp. 259-284.

Behrens, P. 1992. X-ray absorption spectroscopy in chemistry. 2. X-ray absorption near edge structure. *Trends in Analytical Chemistry*. 11(7): 237-244.

Behrens, P., J. Felsche, S. Vetter, G. Schulzekloff, N. I. Jaeger, and W. Miemann. 1991. A XANES and EXAFS investigation of titanium silicalite. *Journal of Chemical Society-Chemical Communication*. 10: 678-680.

Black, C.A. 1942. Phosphate fixation by kaolinite and other clays as affected by pH, phosphate concentration, and time of contact. *Soil Science Society of America Proceedings*. 123-133.

Bolan, N.S., N. J. Barrow, and A. M. Posner. 1985. Describing the effect of time on sorption of phosphate by iron and aluminium hydroxides. *Journal of Soil Science*. 36: 187-197.

Burkholder, J.M., and G. B. Glasgow Jr. 1997. *Pfiesteria piscicida* and other *Pfiesteria*-like dinoflagellates: Behavior, impacts, and environmental controls. *Limnology and Oceanography*. 42(5): 1052-1075.

Cabrea, F., P. D. Arambarri, L. Madrid, and C. G. Toca. 1981. Desorption of phosphate from iron oxides in relation to equilibrium pH and porosity. *Geoderma*. 26: 203-216.

Chapman, A.C., and L. E. Thirlwell. 1964. Spectra of phosphorus compounds-I The infra-red spectra of orthophosphates. *Spectrochim. Acta*. 20: 937-947.

Colemann, R. 1944. The mechanism of phosphate fixation by montmorillonitic and kaolinitic clays. *Soil Science Society of America Proceedings*. 9: 72-78.

Dalas, E. 1991. The crystallization of iron(III) phosphate on polymeric substrates. *Journal of Colloid Interface Science*. 144, 468-472.

Edzwald, J.K., D. C. Toensing, and M. C. Leung. 1976. Phosphate adsorption reaction with clay minerals. *Environmental Science and Technology*. 10(5): 485-490.

Enfield, C.G., T. Phan, D. M. Wolters, and R. Ellis, Jr. 1981. Kinetic model for phosphate transport and transformation in calcareous soils I. and II. *Soil Science Society of America Journal*. 45: 1059-1064.

Evans, R.L., and J. J. Jurinak. 1976. Kinetics of phosphate release from a desert soil. *Soil Science*. 121(4): 205-211.

Fendorf, S., D. L. Sparks, and M. Fendorf. 1992. Surface precipitation reactions on oxide surfaces. *Journal of Colloid Interface Science*. 148: 295-298.

Fendorf, S.E., and D. L. Sparks. 1996. X-ray absorption fine structure spectroscopy. *In* *Methods of soil analysis*. D.L. Sparks (ed.). Soil Science Society of America

Madison, WI, pp. 377-416.

Fuller, C.C., and J. A. Davis. 1989. Influence of coupling of sorption and photosynthetic processes on trace element cycles in natural waters. *Nature*. 340: 52-54.

Fuller, C.C., J. A. Davis, and G. A. Waychunas. 1993. Surface chemistry of ferrihydrite: Part 2. Kinetics of arsenate adsorption and coprecipitation. *Geochimica Cosmochimica Acta*. 57: 2271-2282.

He, Z.L., V. C. Baligar, D. C. Martens, and K. D. Ritchey. 1998. Determination of soluble phosphorus in the presence of organic ligands or fluoride. *Soil Science Society of America Proceedings*. 62: 1538-1541.

Hingston, F.J., A. M. Posner and J. P. Quirk. 1974. Anion adsorption by goethite and gibbsite. *Journal of Soil Science*. 25: 16-26.

Hsu, P.H., and D. A. Rennie. 1962. Reactions of phosphate in aluminum systems. I. Adsorption of phosphate by x-ray amorphous aluminum hydroxide. *Canadian Journal of Soil Science*. 42: 197-209.

Jackson, T.A., and W. D. Keller. 1970. Comparative study of the role of lichens and

inorganic processes in the chemical weathering of recent Hawaiian lava flows.

American Journal of Science. 269: 446-467.

Jonasson, R.G., R. R. Martin, M. E. Giuliacci, and K. Tazaki. 1988. Surface reactions of goethite with phosphate. *Journal of Chemical Society Faraday Transaction 1*, 84(7): 2311-2315.

Kafkafi, U., A. M. Posner, and J. P. Quirk. 1967. Desorption of phosphate from kaolinite. *Soil Science Society Proceedings*. 31: 348-353.

Koskinen, W.C., and S. S. Harper. 1990. The retention process: Mechanisms. *In Pesticides in the soil environment: Processes, Impacts, and modeling*. H.H. Cheng (ed.). Soil Science Society of America Inc., Madison, WI, pp. 51-77.

Kotak, B.G., S. L. Kenefick, D. L. Fritz, C. G. Rousseau, E. E. Prepas, and S. E. Hrudely. 1993. Occurrence and toxicological evaluation of cyanobacterial toxins in Alberta lakes and farm dugouts. *Water Research*. 27: 495-506.

Levin, E.D., D. E. Schmechel, J. M. Burkholder, H. B. Glasgow, Jr., N. J. Deamer-Melia, V. C. Moser, and G. J. Harry. 1997. Persisting learning deflects in rats after exposure to *Pfiesteria piscida*. *Environmental Health Perspective*. 105(12): 1320-1325.

Madrid, L., and A. M. Posner. 1979. Desorption of phosphate from goethite. *Journal of Soil Science*. 30: 697-707.

McCammon, C.A., and R. G. Burn. 1980. The oxidation mechanism of vivianite as studied by Mössbauer spectroscopy. *American Mineralogists*. 65: 361-366.

Murphy, J., and J. P. Riley. 1962. A modified single solution method for the determination of phosphate in natural waters. *Analytical Chemica Acta*. 27: 31-36.

Nakamoto, K. 1997. *Infrared and Raman spectra of inorganic and coordination compounds*. John Wiley and Sons, New York.

Nanzyo, M. 1984. Diffused reflectance infrared spectra of phosphate sorbed on alumina gel. *Journal of Soil Science*. 35: 63-69.

Nanzyo, M. 1986. Infrared spectra of phosphate sorbed on iron hydroxide gel and the sorption products. *Soil Science and Plant Nutrition*. 32(1): 51-58.

Okajima, H., H. Kubota, and T. Sakuma. 1983. Hysteresis in the phosphorus sorption and desorption processes of soils. *Soil Science and Plant. Nutrition*. 29(3): 271-283.

Okude, N., H. Noro, M. Nagoshi, H. Yamamoto, Y. Baba, and T. A. Sasaki. 1999. P and S K-edge XANES of transition-metal phosphates and sulfates. *Journal of Electron Spectroscopy and Related Phenomenon*. 101-103: 607-610.

O'Reilly, S.E., D. G. Strawn, and D. L. Sparks. 2001. Residence time effects on arsenate adsorption/desorption mechanisms on goethite. *Soil Science Society of America Journal*. 65(1): 67-77.

Parfitt, R.L. 1979. The nature of the phosphate goethite (α -FeOOH) complex formed with $\text{Ca}(\text{H}_2\text{PO}_4)_2$ at different surface coverage. *Soil Science Society of America Journal*. 43: 623-625.

Parfitt, R.L. 1989. Phosphate reactions with natural allophane, ferrihydrite and goethite. *Journal of Soil Science*. 40: 359-369.

Persson, P., Nielsson, N., and Sjöberg, S., 1996. Structure and bonding of orthophosphate ions at the iron oxide-aqueous interface. *Journal of Colloid Interface Science*. 177: 263-275.

Pignatello, J.J., and B. Xing. 1995. Mechanisms of slow sorption of organic chemicals to natural particles. *Environ. Science and Technology*. 30(1): 1-11.

Ressler, T. 1997. Winxas: a program for X-ray absorption spectroscopy data analysis under MS-Windows. *Journal of Synchrotron Radiation*, 5: 118-122.

Rose J., Manceau A., Bottero J., Manion A., and Garcia F. 1997. Nucleation and growth mechanisms of Fe oxyhydroxide in the presence of PO₄ ions. 2. P K-edge EXAFS study. *Langmuir*. 13, 1827-1834.

Ryden, J.C., J. R. McLaughlin, and J. K. Syers. 1977. Time-dependent sorption of phosphate by soils and hydrous ferric oxides. *Journal of Soil Science*. 28: 585-595.

Ryden, J.C., and J. K. Syers. 1977. Desorption and isotopic exchange relationship of phosphate sorbed by soils and hydrous ferric oxide. *Journal of Soil Science*. 28: 596-609.

Ryden, J.C., J. K. Syers, and R. F. Harris. 1973. Phosphorus in runoff and streams. *Advances in Agronomy*, pp. 1-45.

Schwertmann, U., and R. M. Cornell. 1991. *Iron Oxides in the Laboratory: Preparation and Characterization*. VCH Publisher. p.p.137.

Schwertmann, U., and W. R. Fischer. 1973. Natural "amorphous" ferric hydroxide. *Geoderma*. 10: 237-247.

Schwertmann, U., D. G. Schulze, and E. Murad. 1982. Identification of ferrihydrite in soils by dissolution kinetics, differential X-ray diffraction and Mössbaure spectroscopy. *Soil Science Society of America Journal*. 46: 869-875.

Sharpley, A. N. and S. Rekolainen. 1997. Phosphorus in Agriculture and its environmental implications. In *Phosphorus loss from soil to water*. H. Tunney, O.T. Carton, P. C. Brookes, and A. E. Johnston (eds.). Cab International, New York, NY. pp. 1-54.

Snoeyink, V.L., and Jenkins, D., 1980. Precipitation and dissolution. *In Water Chemistry*. John Wiley & Sons, Inc., New York, pp. 243-315.

Sparks, D.L. 1987. Dynamics of soil potassium. *Advances in Soil Science*, 6: 1-63.

Sparks, D.L. 1989. *Kinetics of Soil Chemical Processes*. Academic Press, Inc., San Diego.

Steinfeld, J.I., J. S. Francisco, and W. L. Hase. 1989. *Chemical kinetics and dynamics*. Englewood Cliffs, Prentice Hall.

Stumm, W., and J. J. Morgan. 1995. *Aquatic chemistry, Chemical equilibria and rates*

in natural water. John Wiley & Sons. Inc. New York.

Suarez, D.L., S. Goldberg, and C. Su. 1998. Evaluation of oxyanion adsorption mechanisms in oxides using FTIR spectroscopy and electrophoretic mobility. *In* Mineral-water interfacial reactions kinetics and mechanisms. D.L. Sparks and T.J. Grundl (eds.). American Chemical Society. Washington, DC, pp. 136-178.

Tejedor-Tejedor, M.I., and M. A. Anderson. 1990. Protonation of phosphate on the surface of goethite as studied by CIR-FTIR and electrophoretic mobility. *Langmuir*. 6: 602-611.

Torrent, J., U. Schwertmann, and V. Barron. 1992. Fast and slow phosphate sorption by goethite-rich natural materials. *Clays and Clay Minerals*. 40(1): 14-21.

Vaithyanathan, P., and D. L. Correll. 1992. The Rode river watershed: Phosphorus distribution and export in forest and agricultural soils. *Journal of Environmental Quality*. 21: 280-288.

van Riemsdijk, W.H., L. J. M. Boumans, and F. A. M. de Haan. 1984. Phosphate sorption by soils I. A model for phosphate reaction with metal-oxides in soil. *Soil Science Society of America Journal*. 48: 537-541.

van Riemsdijk, W.H., and J. Lyklema. 1980. Reaction of phosphate with gibbsite ($\text{Al}(\text{OH})_3$) beyond the adsorption maximum. *Journal of Colloid Interface Science* 76(1): 55-66.

van Riemsdijk, W.H., F. A. Weststrate, and J. Beek. 1977. Phosphate in soils treated with sewage water: III. Kinetics studies on the reaction of phosphate with aluminum compounds. *Journal of Environmental Quality*. 6(1): 26-29.

Wang, M.K. 1987. Synthetic and characterization of iron phosphate and aluminum-substituted iron phosphate compounds. *Journal of Chinese Agricultural Chemical Society*. 25: 398-411.

Wang, M.K., and Y. M. Tzou. 1995. Phosphate sorption by calcite, and iron-rich calcareous soils. *Geoderma*. 65: 249-261.

Willett, I.R., C. J. Chartres, and T. T. Nguyen. 1988. Migration of phosphate into aggregated particles of ferrihydrite. *Journal of Soil Science*. 39: 275-282.

Wong, J., F. W. Lytle, R. P. Messmer, and D. H. Maylotte. 1984. K-edge absorption spectra of selected vanadium compounds. *Physical review B-condensed matter*. 30(10): 5596-5610.

Zelazny, L.W., L. He, and A. Vanwormhoudt. 1996. Charge analysis of soils and anion exchange. In: *Methods of soil analysis Part 3-Chemical methods*. D.L. Sparks (ed.). SSSA Book Series No.5. Soil Science Society of America, Inc., Madison, Wisconsin, pp. 1231-1254.

Chapter 5

RESIDENCE TIME EFFECTS ON ARSENATE SURFACE SPECIATION AT THE ALUMINUM OXIDE-WATER INTERFACE

5.1 Abstract

Bioavailability of metals/metalloids is often rate limited by contact time (i.e., residence time) in soils and sediments resulting in irreversible reactions. The fate and transport of the contaminants must be predicted/modeled not only based on short-term (< 48 h) adsorption/desorption studies but also long-term (months-years) reactions. However, there is very little information on the long-term effects of metal/metalloid partitioning reactions in soils and soil components. In this study, residence time effects (3 d -1 yr) on As(V) adsorption/desorption reactions and As(V) surface speciation at the aluminum oxide-water interface were investigated using batch adsorption/desorption experiments coupled with time-resolved Extended X-ray Absorption Fine Structure spectroscopy (EXAFS). Biphaseic As(V) adsorption kinetics were observed at pH 4.5 and 7.8. Whereas the reaction at pH 4.5 was nearly completed after 3d, slow adsorption continued at pH 7.8 after 1 yr. The longer

residence time (3 d-1 yr), the greater the decrease in As(V) desorption at both pH values, suggesting nonsingular reactions. EXAFS analyses on aged As(V) reacted aluminum oxide at both pH values showed that As-Al interatomic distances were 3.11 - 3.14 Å (± 0.13 Å) in all of the aged samples (3 d to 1yr) at pH 4.5 and 7.8, suggesting predominantly bidentate binuclear bonding environments were present. Interestingly, X-ray Absorption Near Edge Structure spectroscopy (XANES) features suggested some changes in the local chemical structure of adsorbed As(V) with aging. The surface transformations (such as: 1) a rearrangement of surface complexes, and/or 2) a conversion of surface complexes into aluminum arsenate-like precipitates) might be important chemical factors responsible for the decrease in As(V) reversibility with aging.

5.2 Introduction

Soils and sediments are nearly always at disequilibrium with respect to ion transformations (Sparks, 1987). The rate of bioavailability of contaminants can be reduced in the environment with increasing time (Pignatello and Xing, 1995).

The observation that less sorbate is released with increasing contact time between the sorbent and sorbate is referred to as a residence time/aging effect (Pignatello and Xing, 1995; Sparks, 1995). Even in the absence of a residence time effect, one often observes biphasic reaction processes for both sorption and desorption of metals, metalloids and organic chemicals (Sparks, 1989). The biphasic behavior is characterized by a relatively rapid reaction followed by a slow reaction(s). The slow

reactions have been ascribed to diffusion phenomena, differing sites of reactivity, and surface precipitation (Scheidegger et al., 1996), however, without molecular scale investigations, the mechanism for sorption/desorption reactions cannot be verified.

Several *in situ* spectroscopic studies (Extended X-ray absorption fine structure spectroscopy (EXAFS), Attenuated total reflectance Fourier Transform infrared (ATR-FTIR) spectroscopy, and Raman spectroscopy) have shown different metal/metalloid chemical speciation at metal oxide/phyllsilicate-water interfaces. The formation of outer-sphere selenate complexes (Hayes et al., 1987), a mixture of inner-sphere and outer-sphere As(III), Co(II) and Pb(II) complexes (Arai et al., 2001; Papelis and Hayes, 1996; Strawn et al., 1998), inner-sphere As(III and V), Cu(II), Pb(II) and Zn(II) surface complexes (Arai et al., 2001; Bargar et al., 1997; Cheah et al., 1998; Fendorf et al., 1997; Goldberg and Johnston, 2001; O'Reilly et al., 2001; Waychunas et al., 1993), and mixed metal (Ni(II) and Zn(II))-aluminum surface precipitates (Ford and Sparks, 2000; Scheidegger et al., 1997) have been determined. While many spectroscopic studies provided important information on chemical speciation for reaction processes of less than 48 h, the mechanisms for longer reaction times (days to months) have not been extensively investigated. Changes in the surface speciation of Co(II)/Ni(II)-Al surface precipitates on kaolinite and pyrophyllite were reported for one to several month(s) of reaction time (Ford et al., 1999; O'Day et al., 1994; Scheckel et al., 2000; Thompson et al., 1999). Some researchers have shown that metals/metalloids (i.e., As(V), Ni(II) and Pb(II)) reacted with metal oxides and pyrophyllite over longer times resulted in either irreversible or reversible retention

mechanisms (Ford et al., 1999; O'Reilly et al., 2001; Strawn et al., 1998). For example, with one year aged Ni(II) reacted pyrophyllite, there was little Ni(II) release by HNO₃ and EDTA (Ford et al., 1999; Scheckel et al., 2000). Conversely, O'Reilly et al. (2001) found that 200 d aging time did not cause a decrease in As(V) release from aged As(V) reacted goethite samples when phosphate was the desorbing ligand (O'Reilly et al., 2001). Accordingly, long-term metal/metalloid ion partitioning reactions can/cannot become significant factors in controlling the contaminant bioavailability in soils and sediments.

In this study, we investigated the effect of residence time (3 d to 1 yr) on As(V) surface speciation at the aluminum-oxide water interface. To better understand chemical processes responsible for the residence time effect, macroscopic batch adsorption/desorption experiments were coupled with molecular scale time-resolved EXAFS analysis. Arsenate, derived from indigenous sources and anthropogenic inputs, was chosen as the adsorbate because it is a toxic metalloid in oxic terrestrial-water environments. There are great concerns about the impact of As on human/ecological health in the USA (Allen et al, 1995). Interest in As has been recently heightened by the controversy over setting the maximum concentration level of As in drinking water, which was recently set at 10 ppb (USEPA, 2001). Aluminum oxide was chosen as an adsorbent because 1) it is a commonly found soil mineral that has high adsorption capacity for various oxyanions (e.g., arsenate) and 2) it is a potential adsorbent (e.g., activated alumina) for As at water treatment plants.

5.3 Materials

The γ -Al₂O₃ (Degussa Inc., Akron, OH) was chosen as an adsorbate because well hydrated γ -Al₂O₃ (bayerite polymorph) contains aluminum octahedral sheets similar to aluminum oxides in soils (e.g., gibbsite) (Dyer et al, 1993, Wijnja and Schulthess, 1999). Total ignition and transmission electron microscopic analyses showed greater than 99.6 % purity and an average particle radius of 13 nm (Degussa Inc., Akron, OH). The five-point Brunauer-Emmett-Teller surface area was 90.1 (\pm 0.2) m² g⁻¹. The isoelectric point was 9.3 (\pm 0.1), as determined by electrophoretic mobility measurements (Arai et al., 2001). ACS grade sodium arsenate, Na₂HAsO₄·7H₂O (Baker) and NaCl (Fisher) were used as reagent sources. A mansfieldite (Al₂O₃·AsO₅·4H₂O, South Bedford mining, Gawton, near River Tamar, England) was used in the EXAFS analyses to extract theoretical phases-shift and amplitude reduction factors using the structural refinement data and the ab initio computer code FEFF702. The mansfieldite contains a corner-sharing three-dimensional network of cis-AlO₄·2H₂O octahedra and AsO₄ tetrahedra structures similar to other members of the variscite group such as scorodite (FeAsO₄·2H₂O).

5.4 Methods

5.4.1 Batch Adsorption Experiments

The adsorption kinetic experiments were performed in two steps. Firstly, the γ -Al₂O₃ suspension (5g L⁻¹) was hydrated in 200ml of 0.1M NaCl background electrolyte solutions for approximately 1 month. This hydration time was employed to

assure the transformation of γ - Al_2O_3 into a bayerite polymorph, hereafter referred to an aluminum oxide (Dyer et al., 1993; Wijnja and Schulthess, 1999). Secondly, the pH of the mineral suspensions was adjusted to pH 4.5 and 7.8 for 24 h using a stirred pH-stat apparatus, and these pHs were maintained during the first 48 h of the kinetic experiments as described below. The MINEQL+ chemical speciation program predicted that the experimental systems were undersaturated with respect to boehmite, gibbsite and amorphous Al_2O_3 during hydration and pH adjustments. Fifty ml of a 5 mM sodium arsenate stock solution (5 mM sodium arsenate and 0.1 M NaCl) were slowly added (10 ml additions every 30 s) to assure an initial As(V) concentration of 1 mM. The mineral suspensions were stirred at 300 rpm at 298 K. Samples (10 ml) of the mineral suspensions were periodically taken (i.e., 5, 15, 30 min., 1, 2, 4, 6, 12 and 24 h), and then passed through a 0.2 μm Gelman Supor®-200 membrane filter (Pall Corp. MI). The filtrates were analyzed for total As and Al by ICP-AES and or dissolved As(V) by the colorimetric method described by Cummings et al. (Cummings et al., 1999). After 48h of reaction using the pH-stat apparatus, the reaction vessels were placed on an orbital shaker and continuously shaken at 300 rpm for up to 12 months. pH was manually adjusted every 15-30 d with the addition of 0.1M HCl or 0.1M NaOH over the adsorption reaction period of 48 h-12 m. As(V) uptake from the bulk solution was continuously monitored at 5, 15 d, 1, 4.5, 7, and 12 m. Total As in the filtrate was analyzed using the methods described above.

5.4.2 Batch Desorption Experiments

Arsenate reversibility from aged (3 d, 1, 4.5, and 12 mo) As(V) reacted aluminum oxide samples at pH 4.5 and 7.8 was investigated using a replenishment technique. The replenishment method was chosen over a flow-method (e.g., miscible displacement and stirred flow methods) because the fine particle size of the γ -Al₂O₃ (average particle radius of 13 nm, Degussa Inc., Akron, OH) caused clogging of the filter when flow-methods were used. The aged samples were prepared according to the method described in the previous section. Thirty ml of duplicate aged suspensions were transferred into 50 ml polycarbonate high-speed centrifuge tubes, and they were centrifuged at 11,950 g for 10 min. The supernatant was decanted to recover the paste. The samples were re-suspended in 30 ml of desorption solutions containing 0.096 M NaCl, 1 mM sodium sulfate and 2 mM organic buffer (sodium acetate (Na-Ac) or 4-(2-hydroxyethyl)-1-piperazine-ethanesulfonic acid (HEPS)). The organic buffers Na-Ac and HEPS were used to maintain pH (i.e., 4.5 and 7.8 ± 0.2, respectively) during the desorption experiments. Tubes were shaken at 300 rpm at 298 K for 24 h. Then the suspensions were centrifuged and the supernatant was analyzed for As(V) using the methods described in the adsorption kinetics section. The replenishment procedure was repeated 25 times (i.e., 25 d).

5.4.3 Arsenic K edge EXAFS Analysis

XAS samples (3 d, 4, 7, and 11 m at pH 4.5 and 3d, 1, 8, and 12 mo at pH 7.8) were prepared according to the methods described in the adsorption kinetics section above. Paste samples were recovered by centrifuging 30 ml of As(V) reacted

aluminum oxide suspensions in 50ml polycarbonate high-speed centrifuge tubes at 11,950 g for 10 min, and the supernatant was decanted. All paste samples were loaded on openings (70 mm x 250 mm) of Teflon sample holders (250 mm x 400 mm), and the openings were sealed with a Type K-104 Kapton tape (SPEX CertiPrep Inc. NJ). Arsenic K-edge (11867 eV) XAS spectra were collected on beamline X-11A at the National Synchrotron Light Source (NSLS), Brookhaven National Laboratory, Upton, NY. The electron storage ring was operated at 2.528 GeV with a current range of 130 to 300 mA. The XAS spectra were collected in fluorescence mode with a Lytle detector filled with krypton gas. The ionization chamber (I_0) was filled with 90 % N_2 and 10 % Ar. As an internal standard, the arsenic K-edge of sodium arsenate salt (1% by weight in boron nitride) was run simultaneously with adsorption samples to check for potential energy shifts during the run. A Ge-filter was used to remove elastically scattered radiation from the fluorescence emissions. The monochromator consisted of two parallel Si(111) crystals with a vertical entrance slit of 0.5 mm. The Teflon sample holder was oriented at 45° to the unfocused incident beam. All samples were scanned at 298 K. A total of three to four spectra were collected for the adsorption samples, and one spectrum was collected for reference minerals such as mansfieldite which was diluted to 1% by weight in ACS grade boron nitride for the XAS measurements.

XAS data reduction and analysis were performed using WinXas 2.0 (Ressler, 1997) using the following procedures. First, three spectra per sample were averaged. The averaged spectra were normalized with respect to E_0 determined from the second

derivative of the raw spectra, and then the total atomic cross sectional absorption was set to unity. A low-order polynomial function was fit to the pre-edge region and the post-edge region. Next, the data were converted from E-space to k -space and weighted by k^3 to compensate for dampening of the XAFS amplitude with increasing k space. Fourier transformation was then performed over the k -space range of 1.8 to 11.6 \AA^{-1} to obtain the radial structural functions (RSF). Final fitting of the spectra was done on Fourier transformed k^3 weighted spectra in R-space. The FEFF702 code reference (Zabinsky et al., 1995) was utilized to calculate single scattering theoretical spectra and phase shifts for As-O and As-Al backscatters using an input file based on the structural refinement of mansfieldite ($\text{AlAsO}_4 \cdot 2\text{H}_2\text{O}$). During fitting, the values of N and R of the As-O and As-Al shells were allowed to vary, as well as a single E_0 for all sets of backscattering atoms. The Debye-Waller factors of the As-O shells were also allowed to vary, but those of the As-Al shells were fixed at 0.006 \AA^2 . When allowed to vary, the Debye-Waller factors of the As-Al shells showed no trends for different aged samples, and we therefore used the average values (i.e., 0.006 \AA^2) in the final fitting procedure to reduce the number of free parameters.

5.5 Results and Discussion

5.5.1 Arsenate Adsorption Kinetics

Arsenate adsorption kinetics at the aluminum oxide-water interface at pH 4.5 and 7.8 are shown in Fig. 5.1. The initial fast adsorption was followed by a continuous slow adsorption with increasing time at both pHs. A similar biphasic

reaction phenomenon has been well documented for tetrahedral oxyanion (i.e., phosphate and arsenate) reactions on soils and soil components (i.e., amorphous $\text{Al}(\text{OH})_3$, natural allophane, ferrihydrite, hematite, goethite, $\alpha\text{-Al}_2\text{O}_3$ and kaolinite) over different time scales (hours to months) (Anderson et al., 1976; Barron and Torrent, 1995; Barrow, 1974; Barrow, 1985; Beek and van Riemsdijk, 1982; Black, 1942; Colemann, 1944; Edzwald et al., 1976; Fuller et al., 1993; Hingston et al., 1974; Hsu and Rennie, 1962; Kafkafi et al., 1967; Madrid and Posner, 1979; Okajima et al., 1983; O'Reilly et al., 2001; Parfitt, 1979; Parfitt, 1989; Ryden et al., 1977; van Riemsdijk et al., 1977; Willett et al., 1988). While As(V) adsorption at pH 4.5 was nearly completed after 750 h, only 46 % of total As(V) uptake was achieved at pH 7.8 and the reaction continued after 1 yr (8640 h).

The difference in the kinetics at the two pH values could be explained by differences in the surface charge density of the aluminum oxide at the experimental pH values (4.5 and 7.8). The dissociation constants of H_3AsO_4 ($\text{p}K_1$ 2.20, $\text{p}K_2$ 6.97 and $\text{p}K_3$ 13.4) would indicate that the predominant As(V) solution speciation consisted of negatively charged species at our experimental pHs (i.e., H_2AsO_4^- at pH 4.5 and HAsO_4^{2-} at pH 7.8) (Schecher and McAvoy, 1998). The surface charge density of the aluminum oxide becomes more negatively charged with increasing pH_{bulk} from 4.5 to the IEP of the solid (≈ 9.3) (Arai et al., 2001). Therefore, the mineral surface at pH 4.5 is more positively charged than at pH 7.8, and the protonated mineral surfaces at pH 4.5 may strongly attract negatively charged As(V) solution species (e.g., H_2AsO_4^-). Our macroscopic evidence that negatively charged

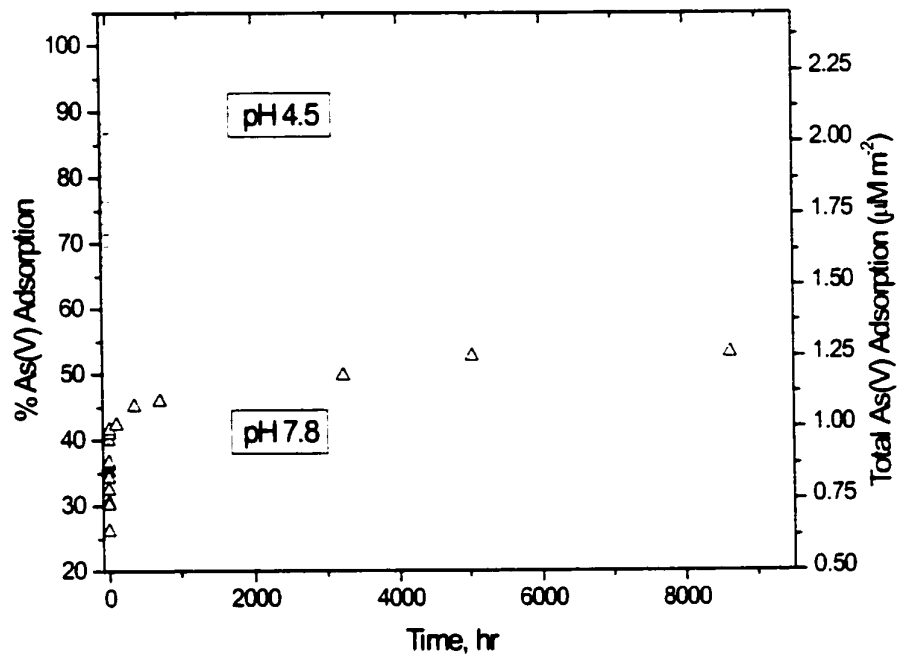


Figure 5.1 Arsenate adsorption kinetics at the aluminum oxide-water interface at pH 4.5 and 7.8.

As solution species significantly sorbed onto positively charged aluminum oxide surfaces over time suggest possibilities for both electrostatic interaction and ligand exchange mechanisms. However, previous electrophoretic mobility measurements have shown the formation of As(V) inner-sphere surface complexes at the aluminum oxide-water interface due to shifts in the electrophoretic mobility of aluminum oxide particles after As(V) adsorption (Arai et al., 2001; Suarez et al., 1998). In addition, our previous EXAFS study (Arai et al., 2001) and the *in situ* vibrational spectroscopic study of Goldberg and Johnston (Goldberg and Johnston, 2001) have shown that the formation of inner-sphere complexes via ligand exchange was predominantly responsible for As(V) adsorption (< 48 h) at the aluminum oxide-water interface.

Differences in the initial (< 48 h) adsorption kinetics at pH 4.5 and 7.8 might be largely attributed to the charge property of the mineral surface and the adsorbate solution speciation discussed above. However the chemical factors responsible for the slow As(V) adsorption kinetics after 48 h are difficult to determine based on the macroscopic data alone, since changes in the charge properties of the mineral surface, the surface area, and the aluminum oxide structure are probably occurring with aging. Therefore, we used the EXAFS technique to investigate the changes in As(V) surface speciation as a function of time. Additionally, the stability of aged As(V) reacted aluminum oxide was tested via batch desorption experiments to provide some insights on As bioavailability.

5.5.2 Arsenate Desorption

Figure 5.2 and 5.3 show total As(V) desorption from aged As(V) reacted aluminum oxide. Since the adsorption kinetics at pH 4.5 were much faster than at pH 7.8 (Fig. 5.1), the loading levels of the aged samples depended on pH and time (Table 5.1). Therefore the amount of desorbed As(V) was normalized with respect to the initial loading levels in Fig. 5.2 and 5.3. Continuous As(V) release was observed in all samples at both pH values (Fig. 5.2 and 5.3), however the extent of As(V) desorption after 25 replenishment cycles was different in each aged sample. At pH 4.5, total As(V) desorption decreased with increasing aging time from 3 d to 1 yr, suggesting a residence time effect (Fig. 5.2). The extent of As(V) release in 3 d and 1 mo aged samples after 15-25 d of desorption was much greater than for 4.5 mo-1 yr aged samples. Similar residence time effects (i.e., irreversibility) were also observed at pH 7.8 (Fig. 5.3). In the 3 d and 1 mo aged samples, total As(V) release was approximately 80-85 % after 25 d of desorption, however, only 51-56 % of As(V) was released from 4.5 mo-1 yr aged samples (Fig. 5.3). Overall, as aging time increased from 3 d to 1 yr, the relative amount of As(V) remaining on the mineral surface increased from 54.81 to 23.46 % at pH 4.5 and 48.9 to 15.43 % at pH 7.8 (Table 5.1). It appears that a stabilization of adsorbed As(V) occurred after a residence of 4.5 mo at both pH values. Similar research findings (i.e., irreversible As(V) desorption from soils and clay minerals) have been reported by several researchers. Woolson and co-workers investigated the aging effects on As(V) extractability from three different Maryland soils (silty clay loam, sandy loam, and fine sand) (Woolson et al., 1971). 1M NH₄Cl extractable As(V) decreased with

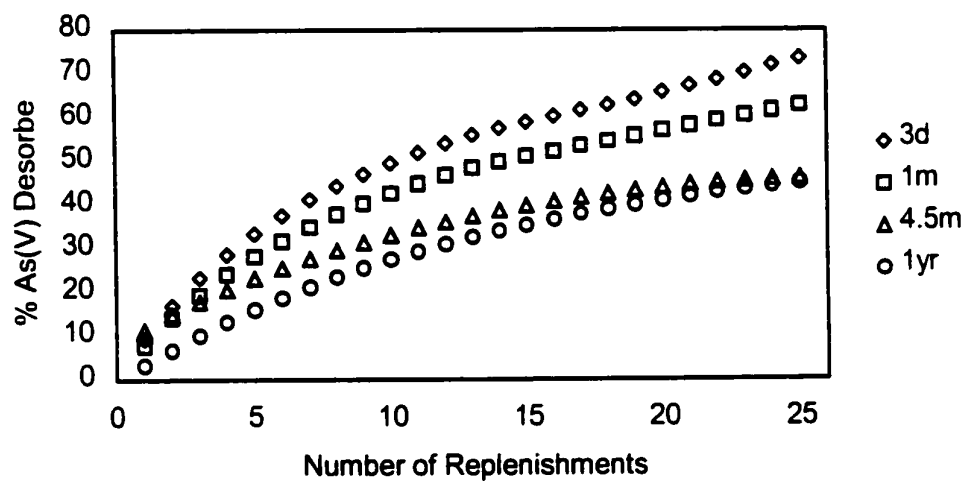


Figure 5.2 Residence time effects on As(V) desorption from aged As(V) reacted aluminum oxide at pH 4.5.

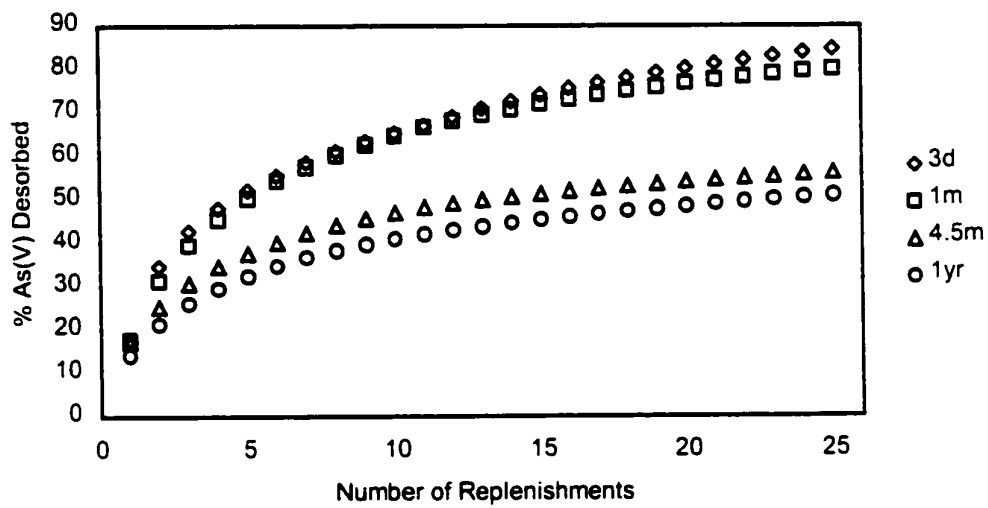


Figure 5.3 Residence time effects on As(V) desorption from aged As(V) reacted aluminum oxide at pH 7.8.

Table 5.1 As(V) desorption experimental conditions and As(V) remaining after 25 d of desorption.

Sample	Initial loading levels ($\mu\text{mol m}^{-2}$)	Total As(V) remaining ($\mu\text{mol m}^{-2}$) after 25 replenishment cycles of desorption. (%)
pH 4.5, 3d	2.11	0.56, (23.46 %)
pH 4.5, 1mo	2.25	0.84, (37.16 %)
pH 4.5, 4.5mo	2.26	1.24, (54.79 %)
pH 4.5, 1yr	2.27	1.24, (54.81 %)
pH 7.8, 3d	1.04	0.16, (15.43 %)
pH 7.8, 1mo	1.13	0.23, (19.98 %)
pH 7.8, 4.5mo	1.18	0.51, (43.63 %)
pH 7.8, 1yr	1.26	0.62, (48.90 %)

increasing aging time up to 36 wks in all soils. Lin and Puls also reported irreversible As(V) sorption on clay mineral surfaces (halloysite, kaolinite, illite, montmorillonite, and chlorite) (Lin and Puls, 2000). Their As(V) recovery decreased with increasing aging time from 1 to 75 d, and the effects were most pronounced in halloysite and kaolinite. Since the changes in surface speciation cannot be elucidated by

macroscopic data alone, we therefore performed *in situ* EXAFS analysis on the aged As(V) reacted aluminum oxide samples.

5.5.3 Arsenic K-edge EXAFS Analysis

Figure 5.4a shows the background subtracted k^3 -weighted χ -functions of aged As(V)/aluminum oxide samples and the aluminum arsenate reference compound, mansfieldite. The spectra show strong sinusoidal oscillations resulting from O-shell backscattering in all samples. Peak dampening and/or additive amplitude effects in the χ function are also observed due to second shell backscattering. However, different experimental conditions (i.e., aging time, loading levels and pH) did not produce any distinctive patterns and shapes in oscillations. We therefore, used the Fourier transformed χ functions to isolate the contribution of neighboring atoms (i.e., As-O and As-Al interatomic distances).

Figure 5.4b shows the RSF's (uncorrected for phase shift) of aged As(V) adsorption samples at pH 4.5 and 7.8 and mansfieldite. The vertical dashed lines correspond to the As-O and As-Al shells, respectively. The solid lines represent the Fourier Transforms of the experimental data and the open circles are the theoretical spectra derived from multiple shell fitting. The structural parameters (coordination number (CN), the interatomic distance (R), and the Debye-Waller factor (σ^2)), obtained from the EXAFS data fitting are presented in Table-2. Error estimates of R and N for the As-O shells are $\pm 0.02 \text{ \AA}$ and $\pm 20 \%$, respectively, based on EXAFS fits on the aluminum arsenate (mansfieldite) reference compound and the values

derived from XRD analyses using ATOMS and FEFF702 (Harrison, 2000).

For the first coordination shells, there is a good agreement between data derived from EXAFS and X-ray structural refinements. However, slightly larger errors exist in $R_{\text{As-Al}}$ ($\pm 0.13 \text{ \AA}$) and $N_{\text{As-Al}}$ ($\pm 31\%$), based on the mansfieldite reference compound. The interatomic distances of As-Al derived from EXAFS measurements were much shorter (3.15 \AA (EXAFS) vs 3.28 \AA (XRD/FEFF)). Similar errors have been reported in the case of Zn minerals (O'Day et al. 1998; Ziegler et al. 2001). This observation was explained by 1) the presence of impurities and amorphous compounds (strong disorder neighboring atoms) which strongly influenced the EXAFS analysis, and 2) different matrices and crystallinity between our materials and the materials used in X-ray analysis (Ziegler et al. 2001).

The As-O radial distances of adsorption samples at both pH values are between 1.68 and 1.70 \AA (Table 5.2), indicating the predominant As (+5) oxidation state (i.e., arsenic tetrahedral; AsO_4) was present at the surface of aluminum oxide regardless of aging time.

The presence of an As-Al shell in all aged samples indicates that As(V) inner-sphere complexation occurs over a residence time of 3 d to 12 mo (Fig 5.4b and Table 5.2). The radial distances of As-Al shells ranged from $\approx 3.11 \text{ \AA}$ to 3.14 \AA . These radial distances can be used to determine the configuration of As(V) inner-sphere complexes forming at the aluminum oxide-water interface. Using a known Al-O distance of the AlO_6 octahedral (1.85 to 1.97 \AA), an O-O edge separation distance of 2.52 - 2.86 \AA (Ishizawa et al., 1980), and the experimental As-O distances, the

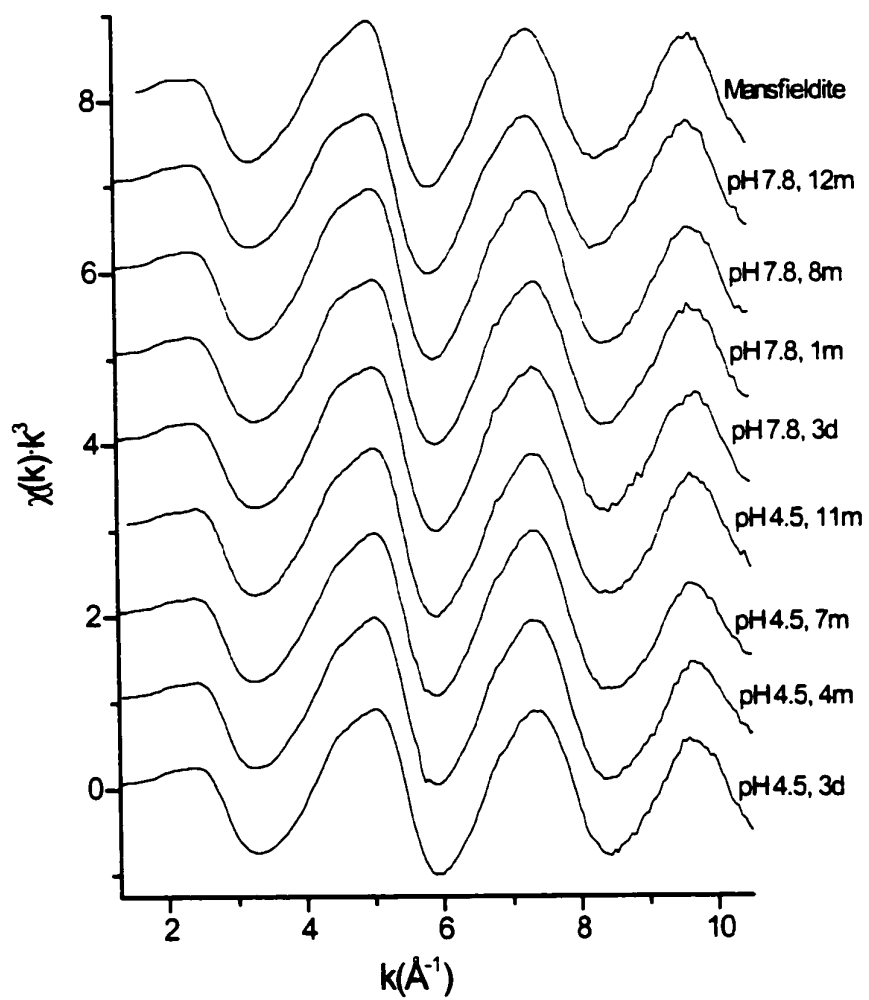


Figure 5.4a k^3 -weighted normalized χ functions for aged As(V) reacted Aluminum oxide and reference Al-As(V) compounds.

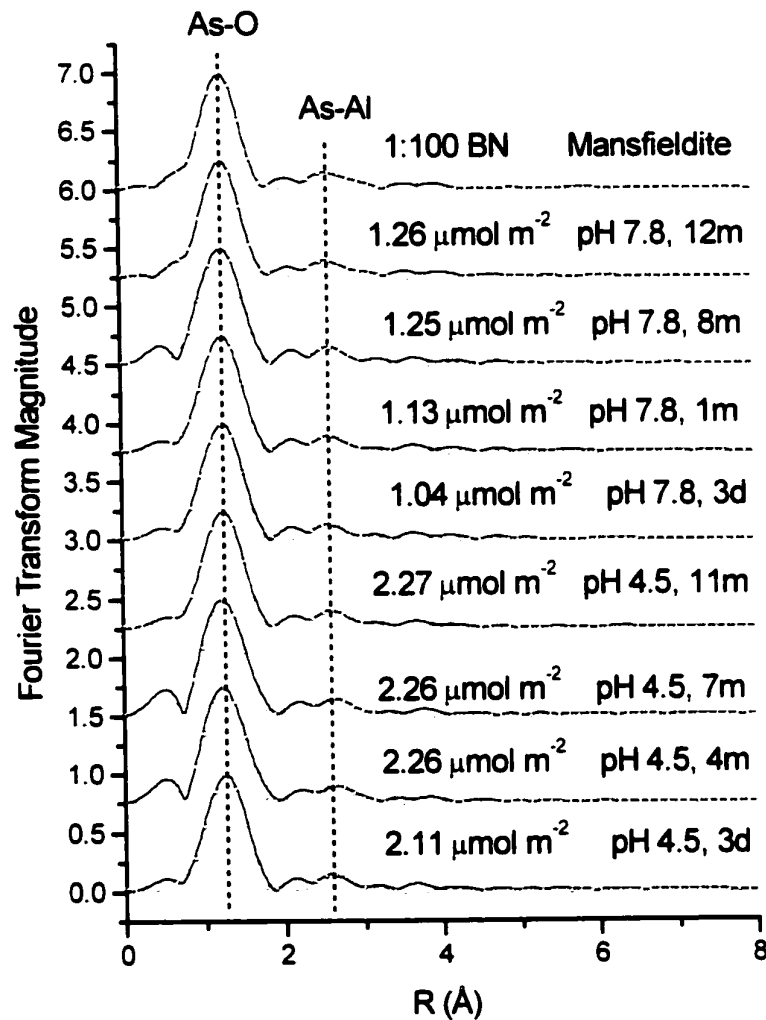


Figure 5.4b Fourier transforms of the χ functions (uncorrected for phase shift) for aged As(V) reacted aluminum oxide and reference Al-As(V) compounds. The solid lines are the experimental data and the opened circles represent the theoretical fit to the data.

Table 5.2 Structural parameters from EXAFS and XRD analysis for aged As(V) reacted aluminum oxide and aluminum arsenate reference compounds.

Sample	As(V)-O			As(V)-Al			E_a (eV) ^b
	CN ^a	R (Å) ^a	σ^2 (Å ²) ^a	CN ^a	R (Å) ^a	σ^2 (Å ²) ^a	
Mansfieldite (AlAsO ₄ ·2H ₂ O)	5.07	1.68	0.0031	2.95	3.15	0.006*	3.67 (XRD/FEFF)
	4	1.68-1.69		4	3.28-3.31		(XRD/FEFF)
Berlinite-like (AlAsO ₄)	4	1.55-1.56		2	3.15		(XRD/FEFF)
Quartz-like (AlAsO ₄)	4	1.67		2	3.15-3.16		(XRD/FEFF)
pH 4.5, 3d	5.38	1.68	0.0040	2.60	3.11	0.006*	3.89
pH 4.5, 4m	5.10	1.68	0.0033	2.90	3.12	0.006*	3.22
pH 4.5, 7m	5.14	1.68	0.0037	2.80	3.12	0.006*	3.23
pH 4.5, 11m	5.03	1.68	0.0038	2.71	3.13	0.006*	3.98
pH 7.8, 3d	5.47	1.69	0.0038	2.52	3.11	0.006*	4.05
pH 7.8, 1m	5.51	1.69	0.0040	2.62	3.11	0.006*	4.21
pH 7.8, 7m	5.51	1.69	0.0042	2.78	3.12	0.006*	4.10
pH 7.8, 1yr	5.10	1.70	0.0033	2.65	3.14	0.006*	3.73

theoretical As-Al bond distances were estimated for different As adsorption configurations (e.g., monodentate mononuclear, bidentate mononuclear, and bidentate binuclear), assuming that the surface structure of γ -Al₂O₃ (i.e., aluminum tetrahedral configuration) was fully converted to the aluminum octahedral configuration of the bayerite polymorph over 1 m of hydration. For monodentate mononuclear inner-sphere complexation, the $R_{\text{As(V)-Al}}$ range is calculated to be 3.54 - 3.66 Å. For bidentate mononuclear bonding, the $R_{\text{As(V)-Al}}$ range is 2.07 - 2.64 Å. For bidentate binuclear complexation, the $R_{\text{As(V)-Al}}$ range is 3.03 - 3.41 Å (Arai et al. 2001). The average As-Al distances of the experimental samples (\approx 3.11-3.14 Å) therefore are consistent with inner-sphere bidentate binuclear As(V) complexes. This configuration is in good agreement with previous equilibrium (< 48 h) studies (Arai et al., 2001; Foster et al., 1998).

It is interesting that the As-Al radial distances slightly increase from 3.11 to 3.14 Å with increasing residence time at both pH values (Table 5.2). This phenomenon could be attributed to following two different aging mechanisms; 1) a rearrangement of surface complexes, and/or 2) a conversion of surface complexes into aluminum arsenate precipitates.

An increase in the As-Al interatomic distances with aging could occur via a rearrangement of the surface complexes. If a small percentage of bidentate mononuclear complexes (As-Al: 2.07-2.64 Å) were initially present, and were gradually converted into bidentate binuclear complexes (As-Al: 3.03-3.41 Å) over time, this would result in an increase in the average As-Al distances.

Additionally, the conversion of the surface complexes into aluminum arsenate-like precipitates could result in an increase in the average As-Al radial distance, since the increased As-Al radial distances (i.e., 3.12-3.14 Å) are at between those of equilibrium (< 48 h) adsorption complexes (3.11 Å) (Arai et al., 2001) and aluminum arsenate minerals (3.15 Å)(Table 5.2).

The As-Al distances of As bearing berlinite-like (AlAsO_4) and quartz-like (AlAsO_4) minerals were estimated using ATOMS and FEFF702 based on X-ray structural refinements (Baumgartner et al., 1989; Thong and Schwarzenbach, 1979). The As-Al distances were the same (i.e., 3.15 Å) in the aluminum tetrahedral minerals (i.e., berlinite-like and quartz-like minerals), but the aluminum octahedral mineral, mansfieldite gave much longer As-Al distances (3.28-3.31 Å) (Table 5.2). It is possible that residual aluminum tetrahedral molecules of $\gamma\text{-Al}_2\text{O}_3$ could react with arsenate ions to form As bearing berlinite/quartz-like precipitate over time. The intermediate bond distances (3.12-3.14 Å) can be explained if mixtures of adsorption complexes and aluminum arsenate precipitates are present simultaneously. The surface transformation of adsorption complexes to aluminum arsenate precipitate phases might occur over time, assuming an increase in As-Al radial distances.

As is mentioned above, errors in the As-Al shell in mansfieldite between EXAFS and XRD/FEFF analysis were slightly large ($R_{\text{As-Al}} (\pm 0.13 \text{ \AA})$ and $N_{\text{As-Al}} (\pm 31 \%)$). In the case of berlinite-like and quartz-like minerals, we do not have As-Al distance comparisons between EXAFS and XRD/FEFF analysis. Therefore it is difficult to make a clear case for the formation of the mansfieldite/berlinite-

like/quartz-like precipitate in our aged samples based on the parameters derived via EXAFS and XRD analysis alone.

We further investigated the aging mechanisms by comparing XANES spectra of aged adsorption samples and mansfieldite assuming a three dimensional surface transformation occurred. In Fig. 5.5a, magnified XANES features occurring at the highest point (≈ 11.88 keV) after the edge jump show differences between aged samples and mansfieldite. The features (indicted by arrows in Fig. 5.5a) at pH 4.5 and 7.8 changed with increasing aging time (≥ 11 mo) at each pH, indicating changes in the local structure. The XANES features in aged (≥ 11 mo) samples seem to be a mixture of mansfieldite and 3 d sorption samples at each pH (Fig 5.5a). We, therefore, performed linear combination (LC) analyses of the XANES profile fit on aged (≥ 11 mo) samples between 11.8 and 12.20 keV using XANES spectra of 3 d samples (i.e., bidentate binuclear reference spectra) at each pH and mansfieldite (i.e., an aluminum arsenate precipitate reference spectrum), using the procedure of Pickering et al (1995). This analysis was done under the assumption that mansfieldite is a good representative of aluminum arsenate precipitates that may form on the aluminum oxide surfaces with aging. Results of the LC fit on ≥ 11 mo samples are shown in Fig. 5.5b. The percent contribution of mansfieldite was over 80 % in the ≥ 11 mo samples at both pHs. Similarly good fits were obtained in the other intermediate time spectra (1-8 mo) (data not shown). The percent contribution of mansfieldite increased from 37 % (4 mo) to 58 % (7 mo) at pH 4.5 and 2 % (1 mo) to 97 % (8 mo) at pH 7.8. The trend in increasing contribution of mansfieldite with

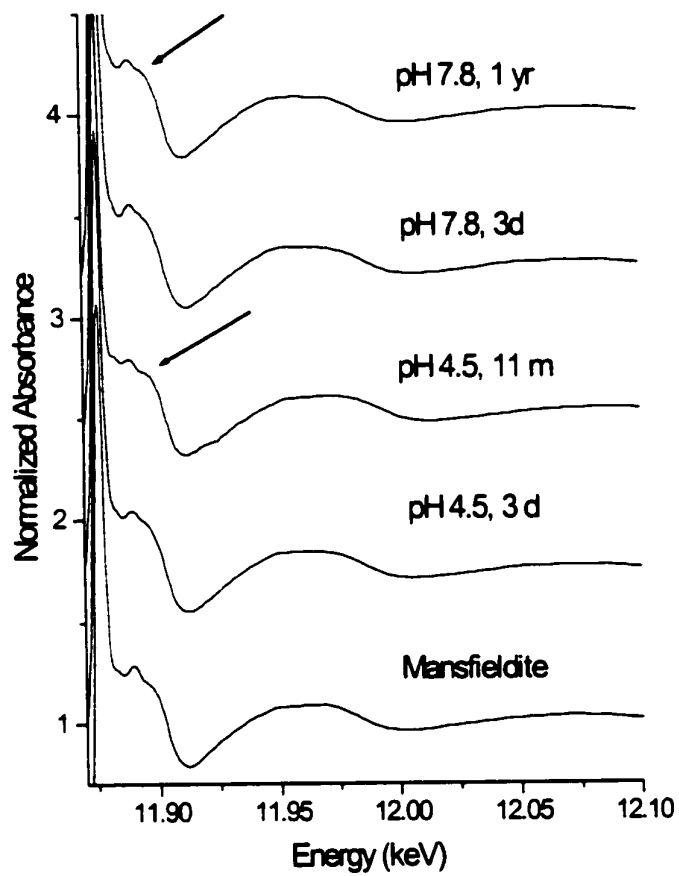


Figure 5.5a. Magnified XANES spectra of aged As(V) sorption samples and mansfieldite.

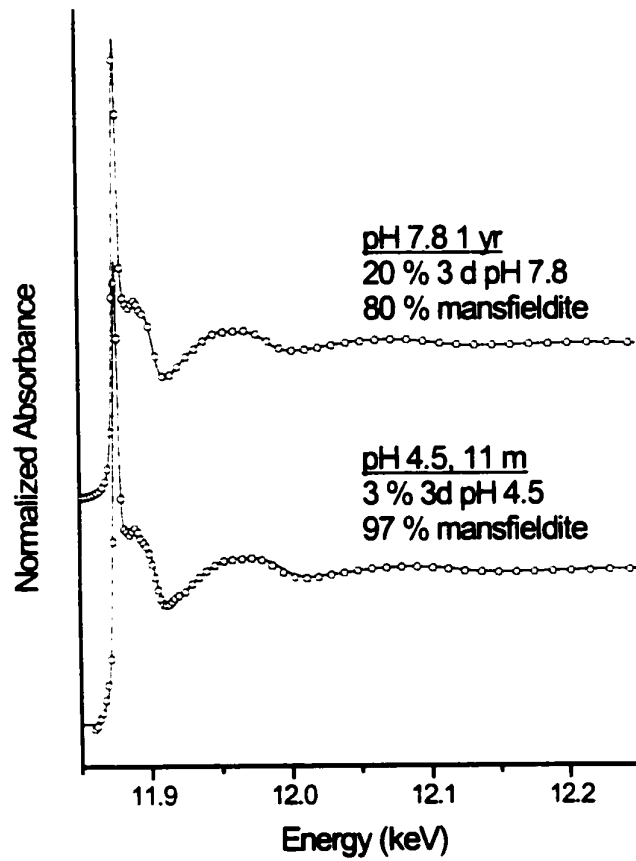


Figure 5.5b Results of linear combination (LC) of XANES profile fit for a 11 m aged sample at pH 4.5 and a 1 yr aged sample at pH 7.8. The solid lines are the experimental spectra and the open circles represent the LC fit in which 3d at pH 4.5 or pH 7.8 and mansfieldite spectra were used as components.

aging might suggest a surface transformation to aluminum arsenate-like precipitates with aging. However, other aluminum arsenate reference compounds (i.e., As bearing berlinite-like and quartz-like mineral) are not available for XANES analyses, so we cannot exclude the possibility of berlinite/quartz-like precipitate formation.

During the long-term As(V) adsorption reactions, the total aluminum concentration was less than 100 μmol and no trends in Al dissolution occurred. The MINEQL⁺ chemical speciation program (Schecher and McAvoy, 1998) predicted that the system was undersaturated with respect to boehmite, gibbsite, amorphous Al_2O_3 , and aluminum arsenate bulk precipitates. Therefore, the aluminum arsenate precipitate can be categorized as a surface precipitate if any formed.

Three possible mechanisms can be suggested to explain the surface transformation of adsorption complexes to Al-As(V) surface precipitates. James and Healy suggested that the activity of ions at the mineral-water interface increased due to the changes in the dielectric constant properties of the bulk solution (James and Healy, 1972). Surface precipitation processes can be facilitated by increased ion activity at the interface via decreased dielectric constant of the interface and/or increased ion density near charged surfaces. A second mechanism is that dissolved cations from adsorbents and adsorbate ions in the bulk fluid could form co-precipitates at the mineral-water interface (Chisholm-Brause et al., 1990; Farley et al., 1985). Under our experimental conditions at pH 4.5 and 7.8, it is possible that ligands (i.e., protons and hydroxyl) promoted aluminum dissolution over time, and the dissolved aluminum ions interacted with non-adsorbed and/or adsorbed arsenate. Ostwald

ripening nucleation processes gradually result in three-dimensional structures over time. It is true that specific adsorption of inorganic anions (e.g., phosphate and arsenate) can inhibit dissolution of metal oxides (Biber et al., 1994; Bondietti et al., 1993). However, slow dissolution of adsorbents still occurs over time since the mineral/water interface is in disequilibrium with respect to ion transformation. We monitored total Al dissolution during the long term As(V) adsorption. However, there was no trend in dissolved aluminum with increasing As(V) adsorption at both pH values. The final possible mechanism for transformation from adsorption complexes to surface precipitates could be physical entrapment due to Al oxide particle agglomeration. One could speculate that an initial charge interaction between As(V) non-reacted and reacted aluminum oxide particles can occur with increasing residence time. Since our experimental pH values (4.5 and 7.8) are below the IEP of the aluminum oxide (≈ 9.3), the surface charge density of As(V) unreacted aluminum oxide particles is positively charged. These positively charged particles could electrostatically be attracted to As(V) adsorbed aluminum oxide surfaces which are negatively charged due to specific As(V) adsorption. Previous electrophoretic mobility measurements have shown that charge reversal can occur via inner-sphere As(V) surface complexation on aluminum oxides (Arai et al 2001 and Suarez et al, 1999). The particle interaction could eventually lead to the formation of multi-aluminum oxide layers/clusters, entrapping adsorption complexes within the structure. Unfortunately, these surface precipitation mechanisms are still speculative since changes in interfacial physicochemical properties are analytically difficult to

measure.

5.6 Conclusion

Biphasic As(V) adsorption was observed at pH 4.5 and 7.8. The kinetics of As(V) adsorption at pH 4.5 was nearly complete in less than 3 d, however, the reaction at pH 7.8 continued over 1 yr. As(V) desorption decreased with increasing aging time (3 d – 1 yr) at both pH values. Our EXAFS results suggested that the presence of inner-sphere bidentate binuclear bonding environments regardless of aging time, however changes in the local chemical structure were suggested based on alternations in XANES features upon aging. The increased irreversibility of adsorbed As(V) might be due the changes in the As surface speciation, such as a rearrangement of surface complexes and/or a transformation of surface complexes into aluminum arsenate-like surface precipitates. Residence time effects (i.e., irreversible As(V) adsorption/desorption) could also be ascribed to physicochemical processes. Intra-particle diffusion, sorption reactions on higher energy binding sites (structural defects), and structural entrapment of sorbed As during particle growth also cannot be excluded (Papelis, 1995; Papelis et al., 1995).

Our experimental results can be useful in understanding actual environmental processes (e.g., As reactions in aluminum oxide rich fly coal ash settling ponds) and/or evaluating remediation methods (e.g., alumina as an As(V) uptake coagulant at water treatment plants). Further research on more complex model systems (e.g., competitive organic acid and anion reactions) and in heterogeneous systems (e.g.,

aluminum oxide rich soils and sediments) is needed to better understand the role of aluminum oxide with respect to As(V) partitioning reactions in soils and sediments.

5.7 References

- Allen, H. E., C. P. Huang, G. W. Brailley, and A. R. Bowers. 1995. Metal speciation and contamination of soil. Lewis Publisher. Co. Ann Arbor, MI, pp. 384.
- Anderson, M.A., J.F. Ferguson. and J. Gavis. 1976. Arsenate adsorption on amorphous aluminum hydroxide. *Journal of Colloid and Interface Science*. 54: 391-399.
- Arai, Y., E.J. Elzinga. and D.L. Sparks. 2001. X-ray absorption spectroscopic investigation of arsenite and arsenate adsorption at the aluminum oxide-water interface. *Journal of Colloid and Interface Science*. 235: 80-88.
- Bargar, J.R., G.E. Brown Jr. and G.A. Parks. 1997. Surface complexation of Pb(II) at oxide-water interfaces: I. XAFS and bond-valence determination of mononuclear and polynuclear Pb(II) sorption products on aluminum oxides. *Geochimica et Cosmochimica Acta*. 61(13): 2617-2637.
- Barron, E.A.V. and J. Torrent. 1995. Organic matter delays but does not prevent phosphate sorption by cerrado soils from Brazil. *Soil Science*. 159(3): 207-211.
- Barrow, N.J., 1974. The slow reactions between soil and anions. 1. Effects of time, temperature, and water content of a soil on the decrease in effectiveness of phosphate

for plant growth. *Soil Science*. 118: 380-386.

Barrow, N.J., 1985. Reactions of anions and cations with variable-charge soils. *Advances in Agronomy*, pp. 183-230.

Baumgartner, O., M. Behmer and A. Preisinger. 1989. The crystal-structure of AlAsO_4 at 2 °C, 500 °C and 750 °C. *Zeitschrift fur kristallographie*. 187: 125-131.

Beek, J. and W.H. van Riemsdijk. 1982. Interactions of orthophosphate ion with soil. In: G.H. Bolt (Editor), *Soil chemistry B, Physico-chemical models*. Elsevier Science Publ. Co., Amsterdam, pp. 259-284.

Biber, M.V., M.D.S. Afonso and W. Stumm. 1994. The coordination chemistry of weathering : IV. Inhibition of the dissolution of oxide minerals. *Geochimica et Cosmochimica Acta*. 58(9): 1999-2010.

Black, C.A., 1942. Phosphate fixation by kaolinite and other clays as affected by pH, phosphate concentration, and time of contact. *Soil Science Society of America Proceedings*: 123-133.

Bondiatti, G., J. Sinniger and W. Stumm. 1993. The reactivity of Fe(III) (Hydr)oxides: Effects of ligands in inhibiting the dissolution. *Colloids Surfaces*, 79:

157-167.

Cheah, S.-F., G. E. Brown Jr. and G.A. Parks. 1998. XAFS Spectroscopy Study of Cu(II) sorption and amorphous SiO₂ and γ -Al₂O₃: Effect of substrate and time on sorption complexes. *Journal of Colloid and Interface Science*. 208: 110-128.

Chisholm-Brause, K.F. Hayes, C.J., A.L. Roe, G.E. Brown Jr., G.A. Parks, J.O. Leckie. 1990. Spectroscopic investigation of Pb(II) complexes at the γ -Al₂O₃/water interface. *Geochimica et Cosmochimica Acta*. 54: 1897-1909.

Colemann, R. 1944. The mechanism of phosphorus fixation by montmorillonitic and kaolinitic clays. *Soil Science Society of America Proceedings*. 9: 72-78.

Cummings, D.E., F. Caccavo Jr., S. Fendorf and R.F. Rosenzweig. 1999. Arsenic mobilization by the dissimilatory Fe(III)-reducing bacterium *shewanella alga* BrY. *Environmental Science and Technology*. 33(5): 723-729.

Dyer, C., P.J. Hendra, W. Forsling, and M. Ranheimer. 1993. Surface hydration of aqueous gamma-Al₂O₃ studied by Fourier transform raman and infrared spectroscopy. 1. Initial results. *Spectrochim. Acta Part A-Molecular and biomolecular spectroscopy*, 49(5-6): 691-705.

Edzwald, J.K., D.C. Toensing and M.C. Leung. 1976. Phosphate adsorption reaction with clay minerals. *Environmental Science and Technology*. 10(5): 485-490.

Farley, K.J., D.A. Dzombak and F.M.M. Morel. 1985. A surface precipitation model for the sorption of cations on metal oxides. *Journal of Colloid and Interface Science*. 106: 226-242.

Fendorf, S.E., M.J. Eick, P. Grossl, and D.L. Sparks. 1997. Arsenate and chromate retention mechanisms on goethite. 1. Surface structure. *Environmental Science and Technology*. 31(2): 315-320.

Ford, R.G., A.C. Scheinost, K.G. Scheckel and D.L. Sparks. 1999. The link between clay mineral weathering and the stabilization of Ni surface precipitates. *Environmental Science and Technology*. 33: 3140-3144.

Ford, R.G. and D.L. Sparks. 2000. The nature of Zn precipitates formed in the presence of pyrophyllite. *Environmental Science and Technology*. 34: 2479-2483.

Foster, A.L., G.E. Brown Jr., T.N. Tingle and G.A. Parks. 1998. Quantitative arsenic speciation in mine tailing using X-ray absorption spectroscopy. *American Mineralogists*, 83(5-6): 553-568.

Fuller, C.C., J.A. Davis and G.A. Waychunas. 1993. Surface chemistry of ferrihydrite: Part 2. Kinetics of arsenate adsorption and coprecipitation. *Geochimica et Cosmochimica Acta*, 57: 2271-2282.

Goldberg, S. and C.T. Johnston. 2001. Mechanisms of arsenic adsorption on amorphous oxides evaluated using macroscopic measurements, vibrational spectroscopy, and surface complexation modeling. *Journal of Colloid and Interface Science*. 234(1): 204-216.

Harrison, W.T.A., 2000. Synthetic mansfieldite, $AlASO_4 \cdot 2H_2O$. *Acta Crystallographica C*56: E421 part10.

Hayes, K.F. A.L. Roe, G.E. brown Jr., K.O. Hodgson, J. O. Leckie and G.A. Parks. 1987. In situ x-ray absorption study of surface complexes: Selenium oxyanions on α -FeOOH. *Science*. 238: 783-786.

Hingston, F.J., A.M. Posner and J.P. Quirk. 1974. Anion adsorption by goethite and gibbsite. *Journal of Soil Science*. 25: 16-26.

Hsu, P.H. and D.A. Rennie. 1962. Reactions of phosphate in aluminum systems. I. Adsorption of phosphate by x-ray amorphous aluminum hydroxide. *Canadian Journal*

of Soil Science. 42: 197-209.

Ishizawa, N., T. Miyata, I. Minato, F. Marumo, and S. Iwai. 1980. A structural investigation of α -Al₂O₃ at 2170 K. *Acta crystallographica*, C36: 228-230.

James, R.O. and T.W. Healy. 1972. Adsorption of hydrolyzable metal ions at the oxide-water interface II. Charge reversal of SiO₂ and TiO₂ colloids by adsorbed Co(II), La(III), and Th(IV) as model systems. *Journal of Colloid and Interface Science*. 40(1): 53-64.

Kafkafi, U., A.M. Posner and J.P. Quirk. 1967. Desorption of phosphate from kaolinite. *Soil Science Society Proceedings*. 31: 348-353.

Lin, Z. and R.W. Puls. 2000. Adsorption, desorption and oxidation of arsenic affected by clay minerals and aging process. *Environmental Geology*. 39(7): 753-759.

Madrid, L. and A.M. Posner. 1979. Desorption of phosphate from goethite. *Journal of Soil Science*. 30: 697-707.

O'Day, P., G.A. Parks and G.E. Brown Jr. 1994. X-ray absorption spectroscopy of cobalt (II) multinuclear surface complexes and surface precipitates on kaolinite. *Journal of and Interface Science*. 165: 269-289.

Okajima, H., H. Kubota and T. Sakuma. 1983. Hysteresis in the phosphorus sorption and desorption processes of soils. *Soil Science and Plant Nutrition*. 29(3): 271-283.

O'Reilly, S.E., D.G. Strawn and D.L. Sparks. 2001. Residence time effects on arsenate adsorption/desorption mechanisms on goethite. *Soil Science Society of America Journal*. 65(1): 67-77.

O'Day, P.A., S.A. Carroll and G.A. Waychunas. 1998. Rock-water interactions controlling Zinc, Cadmium, and lead concentrations in surface waters and sediments. U.S. Tri-state mining district. 1. Molecular identification using X-ray absorption spectroscopy. *Environmental Science and Technology*. 32: 943-955.

Papelis, C., 1995. X-ray Photoelectron spectroscopic studies of cadmium and selenite adsorption on aluminum oxides. *Environmental Science and Technology*. 29: 1526-1533.

Papelis, C. and K.F. Hayes. 1996. Distinguishing between interlayer and external sorption sites of clay minerals using X-ray absorption spectroscopy. *Colloid and Surfaces A-Physicochemical and engineering aspects*, 107: 89-96.

Papelis, C., P.V. Roberts and J.O. Leckie. 1995. Modeling the rate of cadmium and

selenite adsorption on micro- and mesoporous transition aluminas. *Environmental Science and Technology*. 29: 1099-1108.

Parfitt, R.L., 1979. The nature of the phosphate goethite (α -FeOOH) complex formed with $\text{Ca}(\text{H}_2\text{PO}_4)_2$ at different surface coverage. *Soil Science Society of America Journal*. 43: 623-625.

Parfitt, R.L., 1989. Phosphate reactions with natural allophane, ferrihydrite and goethite. *Journal of Soil Science*. 40: 359-369.

Pickering, I.J., G.E. Brown Jr. and T.K. Tokunaga. 1995. Quantitative speciation of selenium in soils using X-ray absorption spectroscopy. *Environmental Science and Technology*. 29(9): 2456-2458.

Pignatello, J.J. and B. Xing. 1995. Mechanisms of slow sorption of organic chemicals to natural particles. *Environmental Science and Technology*. 30(1): 1-11.

Ressler, T., 1997. Winxas: a program for X-ray absorption spectroscopy data analysis under MS-windows. *Journal of Synchrotron Radiation*. 5: 118-122.

Ryden, J.C., J.R. Mclaughlin and J.K. Syers. 1977. Time-dependent sorption of phosphate by soils and hydrous ferric oxides. *Journal of Soil Science*. 28: 585-595.

Schecher, W.D. and D.C. McAvoy. 1998. MINEQL+. Environmental Research Software. Hallowell, ME.

Scheckel, K.G., A.C. Scheinost, R.G. Ford and D.L. Sparks. 2000. Stability of layered Ni hydroxide surface precipitates-a dissolution kinetics study. *Geochimica et Cosmochimica Acta*, 64(16): 2727-2735.

Scheidegger, A.M., M. Fendorf and D.L. Sparks. 1996. Mechanisms of nickel sorption on pyrophyllite: macroscopic and microscopic approaches. *Soil Science Society of America Journal*. 60: 1763-1772.

Scheidegger, A.M., G.M. Lamble and D.L. Sparks. 1997. Spectroscopic evidence for the formation of mixed-cation hydroxide phases upon metal sorption on clays and aluminum oxides. *Journal of Colloid and Interface Science*. 62: 2233-2245.

Sparks, D.L. 1987. Dynamics of soil potassium. *Advances in Soil Science*. 6: 1-63.

Sparks, D.L., 1989. *Kinetics of soil chemical processes*. Academic Press, San Diego, CA.

Sparks, D.L., 1995. *Sorption phenomena on soils*, Environmental soil chemistry.

Academic press. San Diego, CA, pp. 99-139.

Strawn, D.G., A.M. Sheidegger and D.L. Sparks. 1998. Kinetics and mechanisms of Pb(II) sorption and desorption at the aluminum oxide-water interface. *Environmental Science and Technology*. 32: 2596-2601.

Suarez, D.L., S. Goldberg and C. Su. 1998. Evaluation of oxyanion adsorption mechanisms in oxides using FTIR spectroscopy and electrophoretic mobility. In: D.L. Sparks and T.J. Grundl (eds.), *Mineral-water interfacial reactions kinetics and mechanisms*. Am. Chem. Soc., Washington, DC, pp. 136-178.

Thompson, H.A., G.A. Parks and G.E. Brown, Jr. 1999. Dynamic interactions of dissolution, surface adsorption, and precipitation in an aging cobalt(II)-clay-water system. *Geochimica et Cosmochimica Acta*, 63(11/12): 1767-1779.

Thong, N.G.O. and D. Schwarzenbach. 1979. Use of electric-field gradient calculations in charge-density refinements .2. Charge-density refinement of the low-quartz structure of aluminum phosphate. *Acta crystallographica section A*, 35: 658-664.

United States Environmental Protection Agency. 2001. EPA To Implement 10ppb Standard for Arsenic in Drinking Water. EPA 815-F-01-010.

van Riemsdijk, W.H., F.A. Weststrate and J. Beek. 1977. Phosphate in soils treated with sewage water: III. Kinetics studies on the reaction of phosphate with aluminum compounds. *Journal of Environmental Quality*. 6(1): 26-29.

Waychunas, G.A., B.A. Rea, C.C. Fuller and J.A. Davis. 1993. Surface chemistry of ferrihydrite: Part 1. EXAFS studies of the geometry of coprecipitated and adsorbed arsenate. *Geochimica et Cosmochimica Acta*, 57: 2251-2264.

Wijnja, H. and C.P. Schulthess. 1999. ATR-FTIR and DRIFT spectroscopy of carbonate species at the aged γ -Al₂O₃/water interface. *Spectrochimica Acta. Part A*. 55: 861-872.

Willett, I.R., C.J. Chartres and T.T. Nguyen. 1988. Migration of phosphate into aggregated particles of ferrihydrite. *Journal of Soil Science*. 39: 275-282.

Woolson, E.A., J.H. Axley and P.C. Kearney. 1971. Correlation between available soil arsenic, estimated by six methods, and response of corn (*Zea Mays L.*). *Soil Science Society of America Proceedings*. 35: 101-105.

Zabinsky, S.I., J.J. Rehr, A. Ankudinov, R.C. Albers and M.I. Eller. 1995. Multiple-scattering calculations of X-ray-absorption spectra. *Physical Review B*, 52(4): 2995-

3009.

Ziegler, F., A.M. Scheidegger, C.A. Johnson, R. Dähn and E. Wieland. 2001.

Sorption mechanisms of zinc to calcium silicate hydrate: X-ray absorption fine structure (XAFS) investigation. *Environmental Science and Technology*. 35. 1550-1555.

Chapter 6

MULTI-SCALE SPECTROSCOPIC INVESTIGATION ON ARSENIC SOLID STATE SPECIATION IN INDUSTRIALLY CONTAMINATED SOILS

6.1 Abstract

Solid-state speciation (i.e., oxidation state, precipitates, and adsorption complexes) of arsenic (As) is one of the most important factors controlling its bioavailability in soils and sediments. In this study, the direct chemical speciation of As in industrially contaminated soils from oxidized and reduced sites was investigated using multi-scale spectroscopic techniques. Synchrotron based *in situ* microfocused (μ) X-ray fluorescence spectroscopy (μ -SXRF), μ -X-ray Absorption Near Edge Structure spectroscopy (μ -XANES), and X-ray powder diffraction (XRD) were combined to facilitate the final bulk extended X-ray absorption fine structure spectroscopic (bulk-EXAFS) analyses on the natural materials. In the reduced sample, simultaneous μ -XANES and μ -SXRF analyses revealed that As(V) was highly associated with Ba, Ca, and Fe, and As(III) was not strongly distributed with these elements. Similarly the oxidized sample also contained both As (III and V) oxidation

states, and the As(V) species was predominant at the region where Fe concentration was elevated. Final bulk EXAFS analyses of the reduced sample suggested the formation of As(V) bidentate binuclear/bidentate mononuclear adsorption complexes on amorphous iron oxyhydroxides and amorphous realgar (AsS) like precipitates. In addition, the presence of As(V)-Ba/Ca shells in the radial structural functions indicated that 1) As(V) formed sorption complexes on barite (BaSO_4)/gypsum (CaSO_4) and/or 2) AsO_4 substituting for SO_4 in these minerals. On the contrary, the oxidized sample contained the predominant As(V)-Fe shell at $\approx 3.25 \text{ \AA}$, suggesting the formation of As(V) bidentate binuclear surface species on amorphous iron oxyhydroxides and/or As/Fe coprecipitates.

In this study, novel *in situ* μ -SXRF, μ -XANES, bulk-EXAFS were effectively utilized to elucidate the average As solid-state speciation in natural materials (i.e., soils and sediments). The presence of mixed As (III and V) phases raises serious concerns about the current environmental risk assessment that is based on “operationally defined total As values” via chemical extraction/digestion. Since the mobility and toxicity of As are highly dependent on the solid speciation, bulk characterization of solid-state species should be considered to develop better risk assessment methods for future remediation and monitoring efforts at metal/metalloid contaminated sites.

6.2 Introduction

Recent controversy over setting the maximum concentration level of total As at 10 ppb in U.S. drinking water has created great interest in understanding the fate and transport of As in soils and sediments. Current risk assessment of As in aquatic/terrestrial environments must improve to propose environmentally safe limits for the protection of human and ecological health. Bulk chemical analyses (i.e., chemical extraction/digestion (e.g., EPA3050 and Toxicity Characteristic Leaching Protocol)) are traditional approaches used by the U.S. Environmental Protection Agency to understand the total As levels and volume-averaged leachability in heterogeneous materials. While these methods are useful in measuring operationally defined extractable/leachable As, the results often underestimate or overestimate As bioavailability because of the complex reactivity of mixed As solid phases (e.g., adsorption complexes and precipitates) in soil matrices. To accurately predict the bioavailability of As in natural materials, solid-state speciation of As must be well understood. Bulk X-ray absorption spectroscopy (XAS) has been applied to investigate solid state speciation of As in soils and sediments (e.g., mine waste) (Bertsch and Hunter, 2001; Foster et al., 1998; Savage et al., 2000), however, the heterogeneous nature of the natural materials makes the bulk XAS analyses extremely difficult and problematic.

To accurately understand As solid state speciation (i.e., oxidation state, and structure) in natural materials, bulk XAS analyses can be augmented with spatially resolved micron-scale surface probing techniques. Since micron-scale techniques significantly reduce the variability of chemical speciation in heterogeneous materials,

the XANES/EXAFS data analyses are simplified. In the case of a toxic metalloid like As, detection of residual As(III) phases are extremely important because of the higher toxicity and mobility of As(III) compared to As(V). Therefore, spatially variable information on As(III and V) is critically needed.

Synchrotron based micro X-ray fluorescence spectroscopy provides spatially resolved elemental distribution maps (resolution as low as 0.5-1 μm for hard X-rays (>3 eV)) with high sensitivity (50-100 ng g^{-1}) for transitional metals (Bertsch and Hunter, 2001) under *in situ* conditions. Microfocused-XAS measurements can then be performed at a specific region of interest based on the elemental distribution data generated by μ -SXRF. Spatially resolved XAS measurements can provide valence state and bonding environments at the region where the targeted element is localized or elevated.

In this study, *in situ* bulk- (beam size ≈ 2.5 mm^2) and μ - (beam size ≈ 18 -100 μm^2) XANES, bulk-EXAFS and XRF, and *ex situ* bulk-XRD were coupled to investigate detailed As solid state speciation (*i.e.*, oxidation state, adsorption complexes, and precipitates) in industrially contaminated soils. Chemical digestion/extraction were also used to aid in the final bulk-EXAFS analyses. The materials used in this study were collected from sites which have had long term (over 3 decades) storage/disposal history of the industrial byproducts from sulfuric acid and As based pesticides derived from manufacturing processes. High levels of total As (> 50 ppb) were detected in adjacent groundwater wells. Therefore it is important to understand the distribution and fixation mechanisms of As at the sites.

6.3 Materials and Site History

A geoprobes™ was used to collect two As contaminated subsurface soil samples (sample A(A): 1.6-2.4 m and sample B(B): 0.6-1.2 m) from a former commodity, specialty, and agricultural chemicals manufacturing site located in the northeastern United States. The samples were immediately sealed in N₂ filled acetate tube liners, and kept at 5°C in a N₂ filled environment prior to further analyses.

Samples A and B represent the highest total As concentration (284 mg kg⁻¹ and 76mg kg⁻¹, respectively) from reduced and oxidized sites, and redox potentials were -143 mV for sample A and +76 mV for sample B. Since mixed redox couples were always present in the soils, the redox potential values cannot be used for quantitative data interpretation. However the values are still useful in understanding the intensity of oxidation/reduction in natural materials.

During its 96-year history, the plant manufactured and sold an array of products, including inorganic and organic herbicides, fungicides, and insecticides, sulfuric acid, and Lithopone white pigment. Production of the inorganic arsenical, lead arsenate, for many years was the primary source of arsenic contamination of groundwater and soils at the site. Our preliminary research showed near neutral soil pH (A: 7.07 and B: 6.97), organic matter content by Walkley-Black method (Nelson and Sommers, 1996) was 2.43 % for Sample A and 3.04 % for Sample B, and significant amounts of total Ba (A: 2280 mg kg⁻¹ and B: 8804 mg kg⁻¹), Ca (A: 12680 mg kg⁻¹ and B: 16820 mg kg⁻¹), and S (A: 2070 mg kg⁻¹ and B: 46300 mg kg⁻¹) were determined via the microwave digestion method. Barium in the soil originates from

the manufacture of Lithopone (BaSO_4) as a white pigment in paints, paper, and rubber products decades ago. The main source of calcium and sulfur in the soil is waste gypsum ($\text{CaSO}_4 \cdot 2\text{H}_2\text{O}$) that was generated from the use of lime to neutralize waste sulfuric acid and to remove sulfate impurities from a major herbicide produced at the site. The waste gypsum “muds” were landfilled on the site, which was an accepted practice at the time. Due to lead arsenate inputs, the total Pb levels in sample A and B were 781 and 230 mg kg^{-1} , respectively. Both samples were rich in Al, Fe, and Si (7.0, 3.14, and 20.46 wt % in sample A, and, 5.62, 7.70, and 17.55 wt % in sample B), indicating metal oxides and aluminosilicate minerals in the soils might serve as sinks for dissolved As (Anderson et al., 1976; Fendorf et al., 1997; Goldberg and Glaubig, 1988; Lumsdon et al., 1984; O'Reilly et al., 2001; Xu et al., 1988). According to the results of ammonium oxalate extraction, samples A and B contained 3253.92 and 16368.96 mg kg^{-1} of iron, respectively, suggesting the presence of amorphous iron oxyhydroxide like precipitates. Amorphous iron oxyhydroxide is known to strongly react with dissolved As(III and V)(Fuller et al., 1993; Jain et al., 1999; Raven et al., 1998). Total Ti and Mn levels were not significant (< 0.07 and < 0.04 wt %) in both samples.

Over the years, the original tidal meadows at the site were gradually filled in as the plant expanded. The exact composition of the blocky and gravelly fill materials employed over the years is not known, however, limestone shale was used as a surface cover in the production areas to neutralize sulfuric acid spills. In recent years, a wetlands area was constructed in an area directly adjacent to the landfilled gypsum

muds. Efforts have been focused on minimizing dissolution of the gypsum muds due to tidal action and on preventing contaminated groundwater from seeping into the wetlands area.

For XAS analyses, several As reference compounds were prepared. As(III and V) adsorption samples on iron and aluminum oxides were prepared according to the method described by Arai et al. (2001). Dussertite ($\text{BaFe}_3\text{AsO}_4$, Tecoma, Elko Co., Nevada), conichalcite (CaCuAsO_4 , Gold Chain Mine, Mammoth, Juab Co., Utah), and orpiment (As_2S_3 , Getchell Mine, near Golconda, Nevada) were manually ground using a mortar and pestle. Minerals were diluted down to 1 % wt with boron nitride for XAS analyses.

6.4 Methods

6.4.1 Bulk-X-ray Diffraction Analyses

Freeze-dried samples were finely ground using a mortar and pestle, and passed through a 0.64 mm sieve. Powder XRD data were collected from 5 to 95° 2 θ with a Philips X-ray powder diffractometer (graphite monochromatized Cu K α radiation, 0.05° 2 θ step size, and 4 sec count time per step). All samples were analyzed as random mount using the back-packed procedure. The detection limit for crystalline phases by bulk XRD under these conditions is approximately 2 wt %. Mineral identifications were conducted using the JCPDS reference files.

6.4.2 *In situ* Microfocused SXRF Analyses

In situ μ -SXRF measurements on the soil sample were performed at beamline X26A at the National Synchrotron Light Source (Brookhaven National Laboratory, Upton, NY). The paste samples were sealed between 8 micron Kapton films (SPEX CertiPrep Inc. NJ) using X-ray solution cells (SPEX CertiPrep Inc. NJ) in a N_2 filled glove box. The samples were mounted on an automated x-y-z stage at 45° . A Si(Li) energy-dispersive detector was used to measure fluorescent X-rays. An approximately $18 \mu m^2$ monochromatic beam was used with the aid of microfocusing optics (Channel-cut Si(111) monochromator and double elliptical Au coated Kirkpatrick-Baez mirror). Elemental mappings were performed on $100 \times 100 - 300 \times 300 \mu m^2$ areas under 300 s live counts and 5 – 10 μm increment steps in the x-y plane. Elemental maps for most of the elements below the As fluorescence energy (e.g., Zn, Cu, Ni, Fe, Mn, Cr, Ti, and Ca) were performed at slightly above the As K edge absorption energy (11.88 keV). Since K emission lines of light elements (e.g., Al and S) are typically strongly absorbed by the air path between a fluorescence detector and samples, Al, Si, and S SXRF analyses were not performed. It is important to monitor the elemental distribution relation between As and Pb since As was originally introduced as a lead arsenate compound. However, simultaneous measurements of fluorescence signals for As and Pb were difficult since fluorescence energies of As $K\alpha$ (10.543 keV) and Pb $L\alpha$ (10.549 keV) are close to each other. We therefore monitored Pb $L\beta$ (12.611 keV) and As $K\beta$ (11.725 keV) signals by adjusting the monochromator energy above the As $K\beta$ (11.725 keV) energy.

6.4.3 *In situ* Microfocused XANES Analyses

In situ μ -XANES measurements were carried out at beamline X26A at the National Synchrotron Light Source (Brookhaven National Laboratory, Upton, NY) and at sector 13-ID/GeoSoilEnviroCARS (GSECARS) (Advanced Photon Source (APS), Argonne, IL). Sample preparation was as described in the μ -XRF analyses section. At beamline X26A, As K edge μ ($\approx 18 \mu\text{m}^2$)-XANES measurements were performed at regions selected from the elemental maps, and spectra were collected up to 50 eV above the As K edge absorption energy in fluorescent mode using a solid state Ge detector.

Similarly, As K edge μ ($\approx 100 \mu\text{m}^2$)-XANES spectra were collected at GSECARS. This 3rd generation synchrotron source was used to take advantage of the higher flux of the microfocused beam which enhanced the resolution of the post edge resonance features of the XANES spectra. A channel-cut Si(220) monochromator and a double elliptical Rh-coated Kirkpatrick-Baez mirror system were used to produce a microfocused ($\approx 100 \mu\text{m}^2$) X-ray beam, and 5-7 spectra were collected using a Ge 9-element detector. A resolution of $100 \mu\text{m}^2$ was chosen at the GSECARS to inhibit beam induced oxidation of As(III) in the samples by reducing the flux per square micron area. ACS grade $\text{Na}_2\text{HAsO}_4 \cdot 7\text{H}_2\text{O}$ (Baker) (1 % by weight in boron nitride) was used for energy calibration at both the X26A and GSECARS beamline. It was also run between samples to check for potential energy shifts during the run at beamline X26A.

6.4.4 *In situ* bulk-EXAFS Analyses

Bulk ($\approx 2.5 \text{ mm}^2$)- EXAFS analyses were performed on beamline X11A at the NSLS. The electron storage ring was operated at 7 GeV with a current range of >100 mA. The XAS spectra were collected in fluorescence mode with a 13-element Ge array detector. The monochromator consists of two parallel Si(111) crystals with a vertical entrance slit of 0.5 mm. The sample was loaded on a Teflon sample holder in a N_2 -filled glove box. As an internal standard, the arsenic K-edge of sodium arsenate salt was run simultaneously with the soil samples to check for potential energy shifts during the run as well as possible As(III) oxidation during data collection. The sample holder was oriented at 45° to the unfocused incident beam, and a total of five to eight spectra were collected at room temperature. Two spectra were collected via transmission mode for dussertite and conichalcite (1% dilution with boron nitride).

The XAS data reduction and analysis were performed with WinXas 2.0 using the following procedures (Ressler, 1997). First, the spectra (except for the solution samples) per sample were averaged. The averaged spectra were normalized with respect to E_0 determined from the second derivative of the raw spectra, and then the total atomic cross sectional absorption was set to unity. A low-order polynomial function was fit to the pre-edge region and the post-edge region. Second, the data were converted from E-space to k -space and weighted by k^3 to compensate for dampening of the EXAFS amplitude with increasing k space. Third, Fourier transformation was performed to obtain the radial structural functions (RSF). The code FEFF7.02 was utilized to calculate single scattering theoretical spectra and

phase shifts for different As paths (Rehr et al., 1992). Dussertite ($\text{BaFe}_2\text{AsO}_4(\text{OH})_2 \cdot \text{H}_2\text{O}$) and conichalcite ($\text{CaCuAsO}_4 \cdot \text{OH}$) spectra were fit with the theoretical phase-shift and the amplitude reduction factors estimated from the multiple-scattering computer code FEFF7.02 (Rehr et al., 1992) using atomic clusters generated from structural refinement data of dussertite and conichalcite (Qurashi and Barnes, 1953; Qurashi and Barnes, 1954; Szymanski, 1988). Individual peaks of the EXAFS spectra of the reference materials were initially fitted in the radial structural functions (RSF) with FEFF7.02 reference functions to estimate the interatomic distances. Coordination numbers (N) for reference compounds were held constant but the R (interatomic distances) and σ^2 (Debye-Waller factors) were allowed to vary. In the soil samples, σ^2 for only As-O shells were allowed to float during the fit. To facilitate overall fitting processes, the reported values (N, R and σ^2) of reference materials (i.e., minerals and adsorption complexes) were initially given for other shells, and then only σ^2 values were fixed.

6.5 Results and Discussion

6.5.1 Bulk XRD Analyses

Figure 6.1 shows the bulk X-ray diffractograms of samples A and B. Quartz is predominant in sample B with a small amount of albite ($\text{K/Na (AlSi}_3\text{O}_8)$), calcite (CaCO_3) and hematite (Fe_2O_3). Bricks mixed with fill materials in site B sample (0-8') are probably an origin of hematite in sample B as evidence by visual observation. A mixture of three mineral components (barite (BaSO_4), gypsum(CaSO_4), and quartz

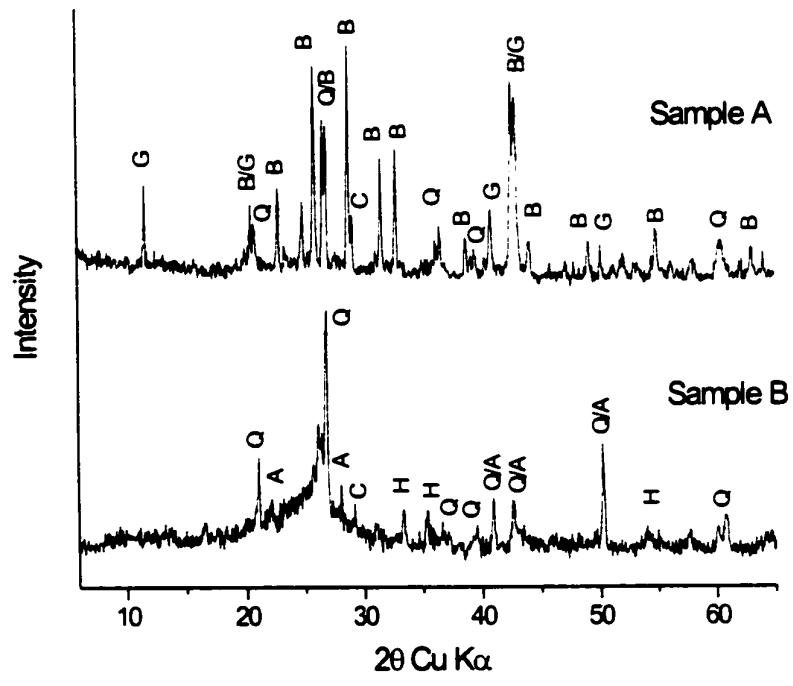


Figure 6.1 X-ray diffraction pattern of sample A and B. Peak labels: A = albite, B = barite, C = calcite, G = gypsum, H = hematite, and Q = quartz.

(SiO₂) was found in sample A. The XRD data were consistent with a large amount of total Ba, Ca, and S values mentioned in the material section.

6.5.2 Bulk XANES Analyses

Bulk XANES analyses, based on the absorption edge energy positions, provide the important information of averaged As oxidation states. Whereas the energy position of As(V) sorbed on minerals and As(V) minerals/salts exhibit ≈ 11874 eV, the As absorption energy position of As(II/III) sulfide minerals (i.e., orpiment (As₂S₃) and realgar (AsS)) further decreases to ≈ 11869 eV (Foster et al., 1998; La Force et al., 2000). Based on the absorption edge energy positions, these As valence states can be suggested.

Fig. 6.2a shows bulk XANES spectra for sample A and B. A shoulder feature of a wide whiteness peak seen in sample A spectrum (indicated by an arrow) indicates the presence of multi-oxidation states in both samples. The post edge resonance features indicated by dotted circles are different in each sample, suggesting the presence of different As solid state speciation. Well split first derivatives of these spectra (Fig. 6.2b) clearly show the presence of mixed oxidation states in both samples. The highest inflection points at about 11.874 keV (indicated by arrow A and B) indicate an As(V) oxidation state in both samples. Whereas first derivative peaks are clearly split in the sample A, the peak splitting is much weaker in sample B. The vertical dotted line at 11.869 keV might indicate the presence of As(II/III)-S species in sample A, but the first absorption energy position in sample B is slightly shifted to

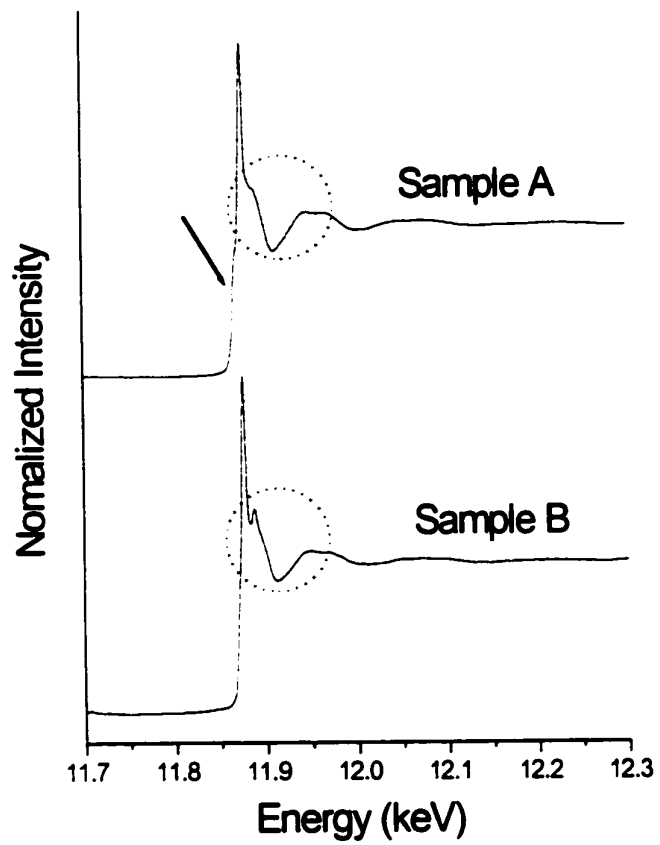


Figure 6.2a Bulk XANES spectra of sample A and B.

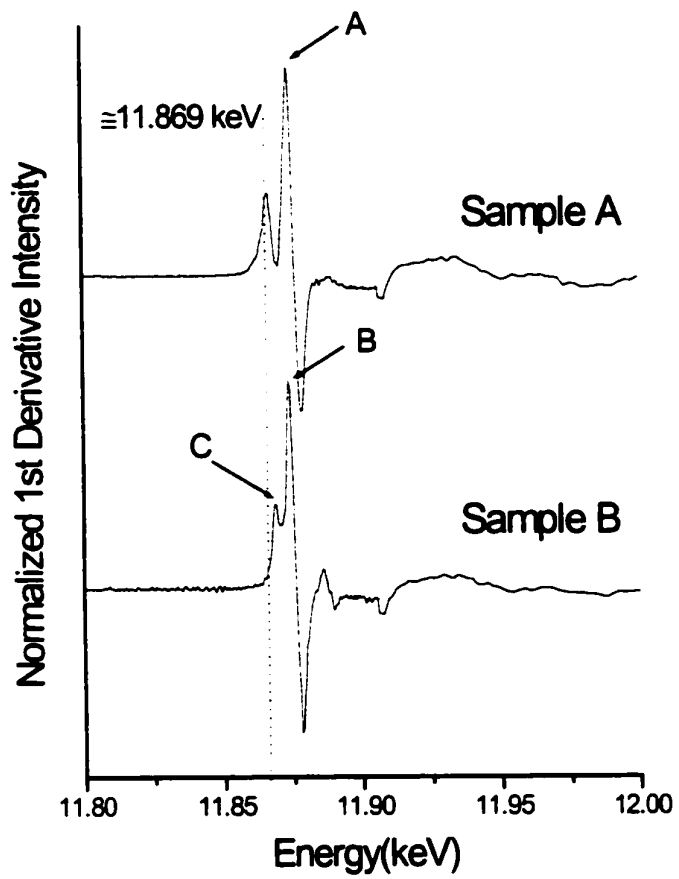


Figure 6.2b First derivative of the bulk XANES spectra shown in Fig 6.1a.

a higher level (indicated by arrow C). As(III) is probably associated with different adsorbents like iron and aluminum oxides rather than forming complexes with sulfides.

It is likely that different solid phases are associated with mixed oxidation states, therefore it is difficult to assign the predominant species (i.e., reference compounds/ surface complexes) based on the XANES analyses alone.

In order to accurately perform bulk EXAFS analyses on the materials, we further studied the samples using synchrotron based microfocused X-ray techniques. Simultaneous measurements of synchrotron based μ -XRF and μ -XANES provide micron scale elemental associations, valence states, and possibly discrete predominant phases. We therefore performed *in situ* μ -XRF/XANES using different resolutions.

6.5.3 *In situ* μ -SXRF Analyses

Elemental maps of selected areas on sample A and B are shown in Figure 6.3a and 6.3b. Fluorescence signals (counts) of each element are indicated by color contour bars (high in yellow and low in black) on the left side of each map. It is important to mention that the bar is arbitrary scaled with respect to each element. In Fig 6.3a, a μ -SXRF spectrum of region 1 of the As map (indicated by an open circle), where the As concentration is elevated, is highly associated with Ba, Ca, and Fe, and to a much lesser extent with Pb, Mn, Ni, Ti, and Zn (data not shown), suggesting the original $Pb_3(AsO_4)_2$ speciation has changed over time. Regions 2 and 3 of the As map

do not have elevated As concentration, and As does not seem to be associated with other elements including Ni, Mn, Pb, Ti, and Zn (data not shown). Fig. 6.3b shows elemental maps of sample B. It appears that As is not as strongly associated with Ba, Ca, and Fe as seen in sample A. Additionally we did not find a correlation between As and Ni, Mn, Pb, Ti, and Zn. (data not shown). As we observed in the sample A, Fe covers most of the area in sample B, and elevated As concentration in region 5 is included within the Fe rich area.

Based on the elemental maps, it is difficult to elucidate As binding mechanisms in heterogeneous soils, however the information on the elemental correlations assists in the final bulk-EXAFS analyses by suggesting possible As adsorption complexes and/or precipitates that might be present. To gain insights on the chemical speciation such as As valence state, μ -XANES analyses were performed on regions 1-6 of sample A and B.

6.5.4 *In Situ* Microfocused-XANES Analyses

The microfocused ($\approx 18 \mu\text{m}^2$) normalized XANES spectra of regions 1-6 are shown in Figure 6.4. These XANES spectra were collected with the previous μ -XRF measurements at beamline X26A at NSLS, so that the As valence state and the elemental correlation could be related. The two vertical dotted lines A and B, are positioned at $\approx 11.869 \text{ keV}$ and at $\approx 11.874 \text{ keV}$, respectively, indicating As(II/III)-S and As(V), respectively, as shown in the previous bulk XANES analyses section. In the stagnant sample A (regions 1-3 in Figure 6.3a), the single whiteline peak present

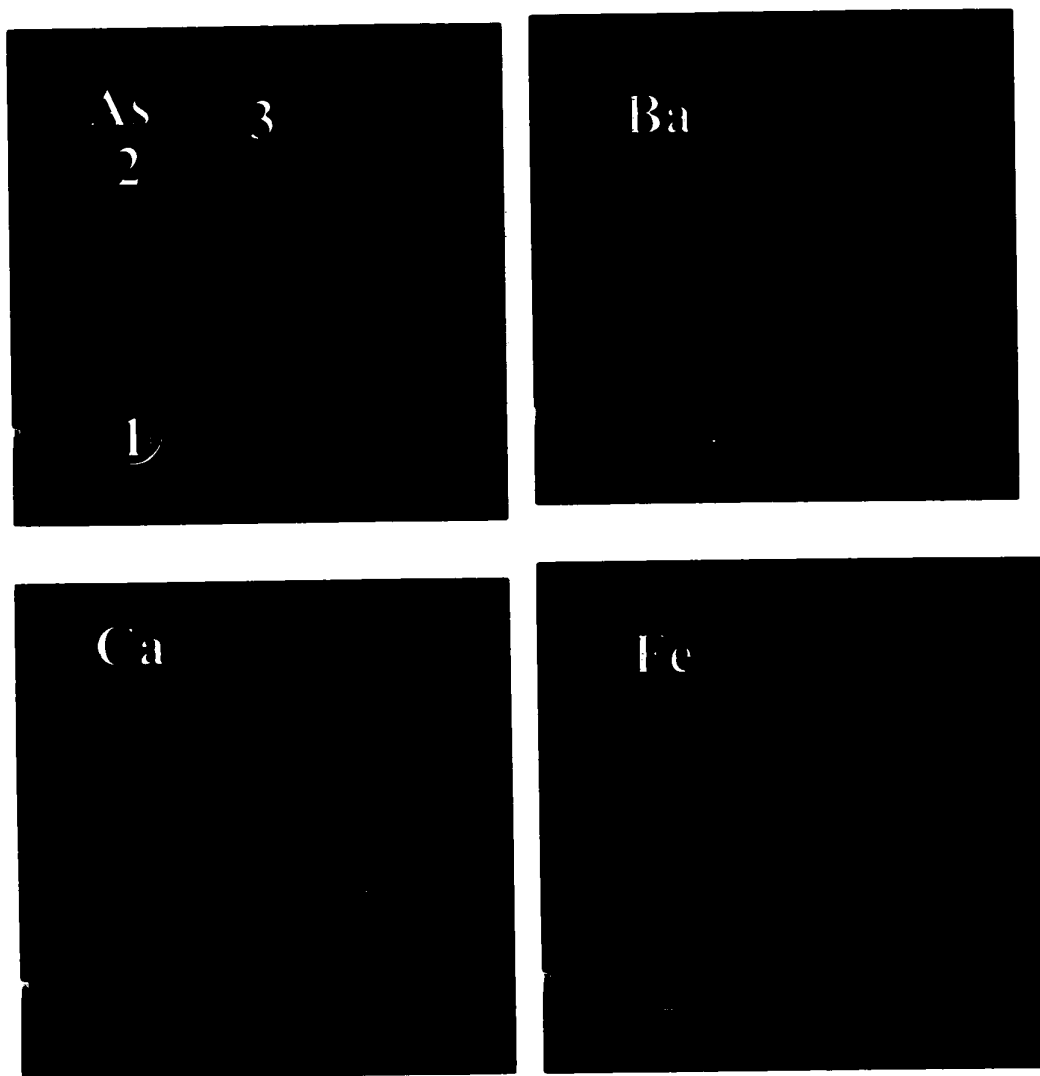


Figure 6.3a Microfocused SXRF elemental map images of sample A (300 μm x 300 μm).

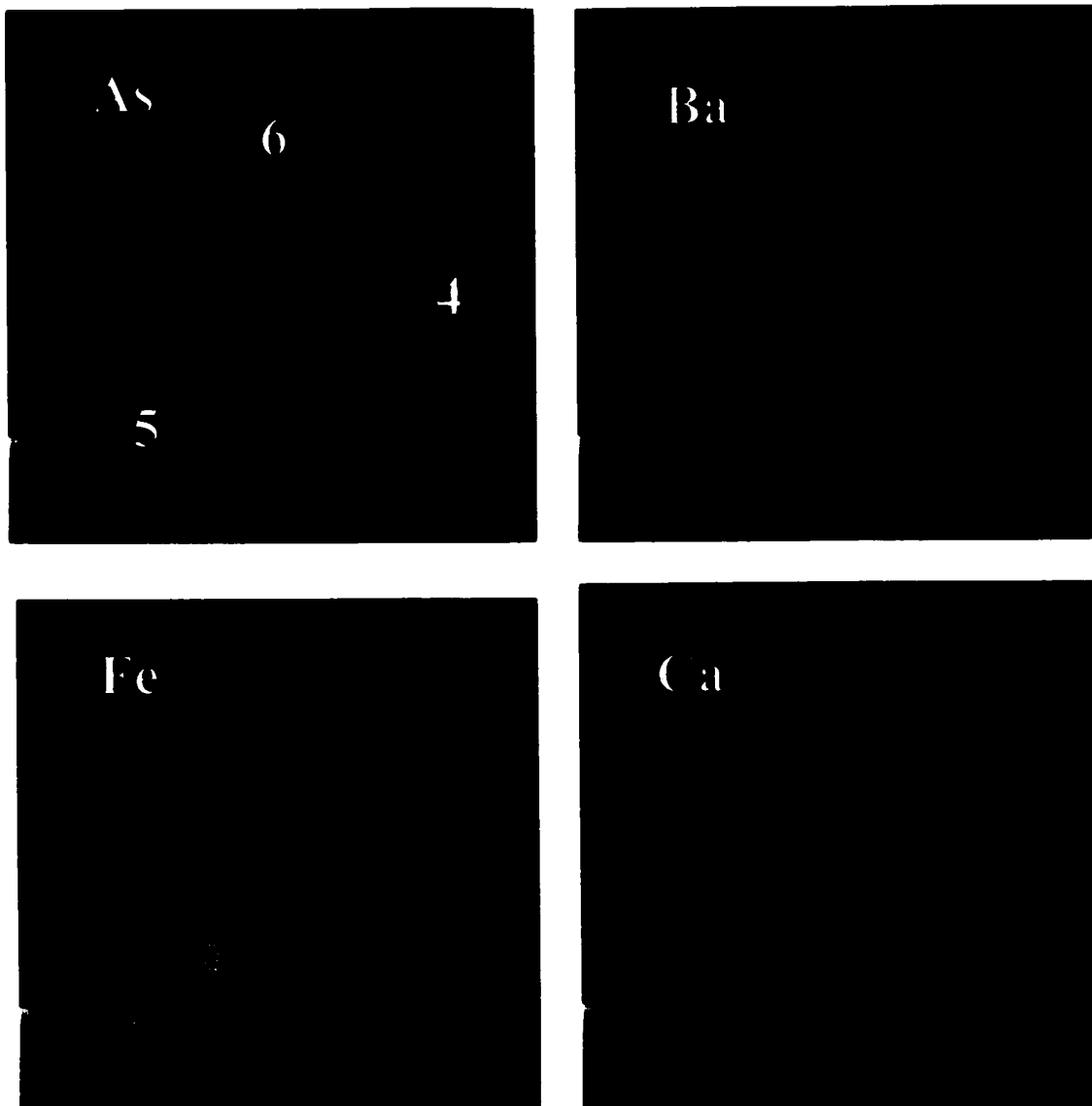


Figure 6.3b Microfocused SXRF elemental map images of sample B (300 μm x 300 μm).

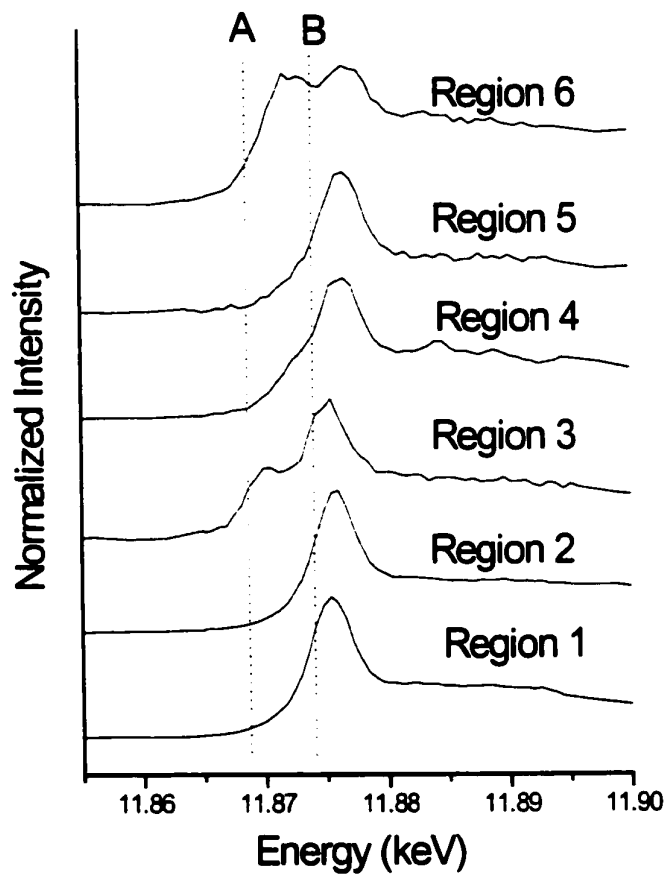


Figure 6.4 Microfocused (18 μm resolution) XANES spectra at region 1-6 of sample A and B shown in Fig 6.3a and 6.3b.

in region 1 where As is highly associated with Ca, Ba and Fe, and the absorption edge energy position indicates a predominant As(V) oxidation state. Region 2 also shows a predominant As(V) valence state, but this region did not have significant contributions from the Ba, Ca, and Fe as seen in region 1. Interestingly, the whiteness peak of the XANES spectrum from region 3 is split. Based on the second derivative of the spectrum (data not shown), the peak was attributed to be an assemblage of As(V) (≈ 11.874 keV) and As(II/III)-S (≈ 11.869 keV) species. Arsenite is probably associated with sulfide like electron withdrawing groups. This may indirectly support the contention that As is not strongly associated with Ba and Fe in region 3.

In the tidal sample B (region 4-6 in Figure 6.3b), the As valence state is also different at the different regions. Whereas the As(V) species predominate in regions 4 and 5 where Fe concentrations are elevated, mixed oxidation states are present in region 6 as evidenced by a wide whiteness peak (Figure 6.4). In region 6, the lower As absorption energy position is slightly shifted from the vertical dotted line A (≈ 11.869 keV) to a higher energy (≈ 11.871 keV). This suggests that As(III) is unlikely to be associated with sulfides.

To better resolve the As XANES spectra at the post edge region (up to 150 eV), additional μ -XANES measurements were performed at the third generation synchrotron source (i.e., GSECARS). The higher flux within the transition metal absorption energy range offers significant advantages (i.e., better detection limit) in making the As K edge XANES measurements. The μ ($\approx 100 \mu\text{m}^2$)-XANES spectra of samples A (1-3) and B (1-3) are shown in Figure 6.5. The two vertical dotted lines A

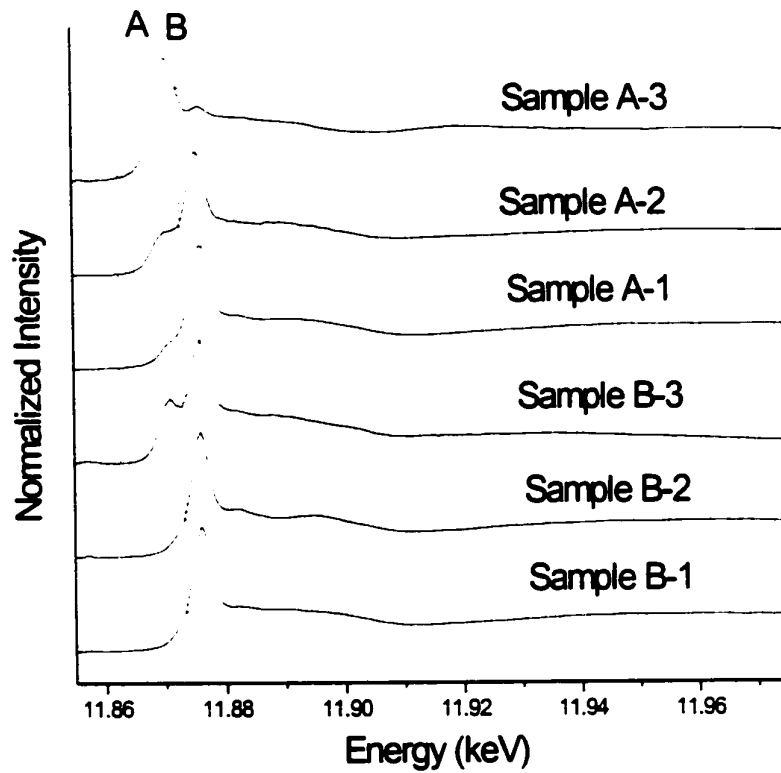


Figure 6.5 Microfocused ($100 \mu\text{m}^2$ resolution) XANES spectra of sample A and B shown in Figure 6.3a and 6.3b.

and B are positioned at energies of 11.869 and 11.874 keV to distinguish As(II/III)-S from As(V) species. The use of the larger resolution ($\approx 100 \mu\text{m}^2$) at the GSECARS beamline was to inhibit the beam induced As(III) oxidation effects by defocusing the beam size, therefore the flux per square micron area was reduced. Because of this large spatial resolution, elemental maps were not generated. To facilitate As speciation via fingerprinting, bulk XANES spectra of reference compounds and the first derivative spectra are also presented in Figure 6.6 and 6.7, respectively. In the reduced sample A (Figure 6.5), the lowest As absorption edge jump (indicated by the dotted line A at 11.869 keV) occurs in both samples A-2 and A-3, indicating the presence of As(II/III)-S speciation (e.g., orpiment like). This is also supported by 1) the first derivative of the A-2 and A-3 spectra (Figure 6.7) and 2) the resemblance of the XANES spectra for the A-3 (Figure 6.5) and orpiment (Figure 6.6). In sample A-1 and 2, the predominant As valence state is As(V), however the presence of the shoulder features (indicated by arrows) also indicates an additional As(III) species. The first derivative of the A-1 spectra and that of the reference compounds (Figure 6.7) indicates that the As(III) species in sample A-1 is likely to be sorption complexes on Fe/Al oxides if these adsorbents are present.

In oxidized sample B, the predominant As(V) oxidation state is observed in samples B-1, 2 and 3. These results were consistent with the additional three measurements taken for sample-B (data not shown). As observed in sample A-1, a similar As(III) species is also present in sample B-3. Since the first whiteline peak is between line A (11.869 keV) and B (11.874 keV), As(III) is unlikely to be associated

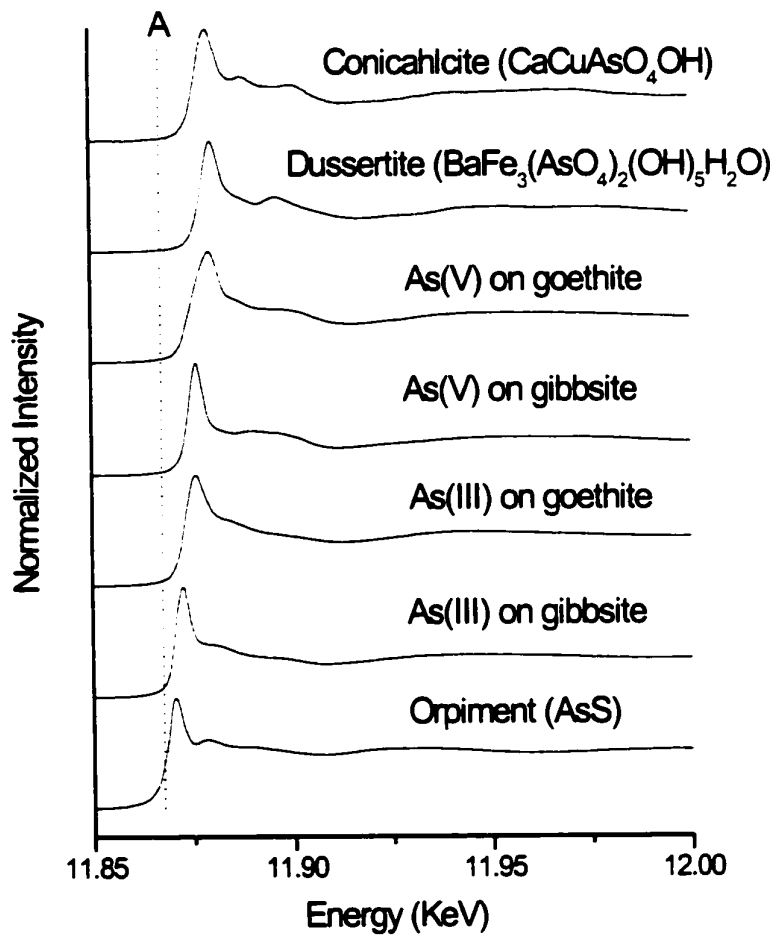


Figure 6.6 Bulk XANES spectra of reference minerals and As adsorption complexes.

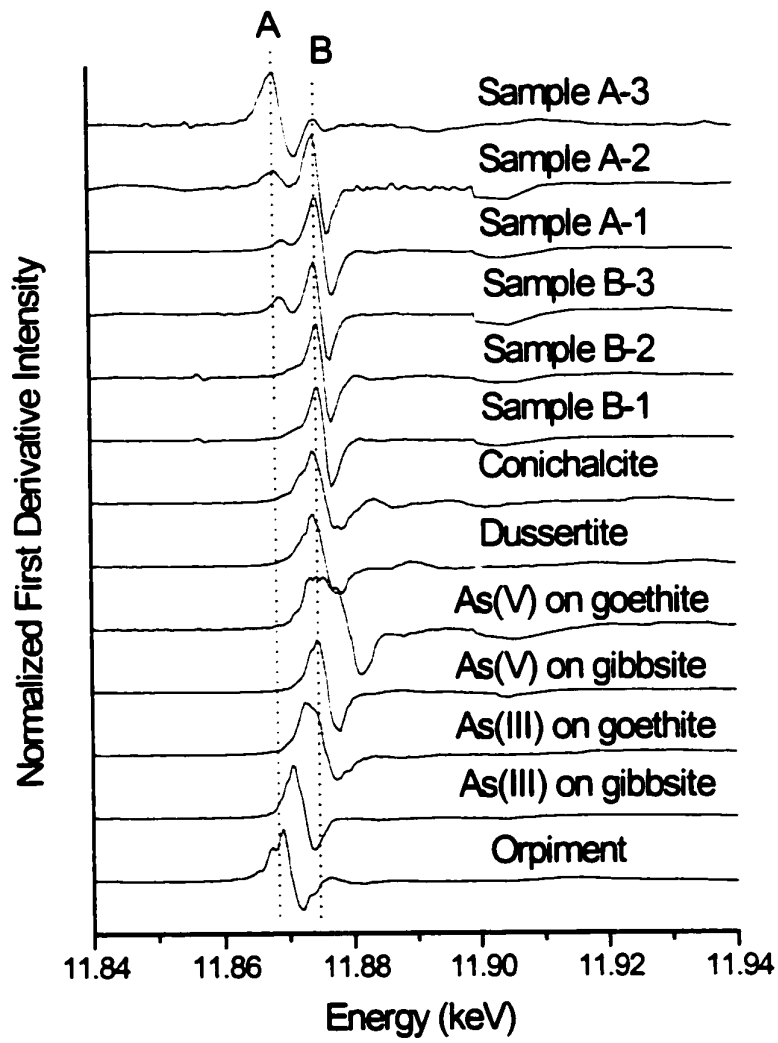


Figure 6.7 First derivative of the XANES spectra shown in Fig. 6.5 and 6.6.

with sulfides. This can be clearly seen in the first derivative of these spectra (Figure 6.7).

To further elucidate the As solid state speciation, the normalized XANES spectra were compared with the reference compounds in energy (eV) and k (\AA^{-1}) units, however the contribution of different As (III and V) solid state species makes the fingerprinting analyses extremely difficult except for the A-3 sample (i.e., orpiment like). Therefore, linear combination XANES profile fits and/or principle component analysis were not performed to estimate the % contribution of specific As species in the samples.

Overall, the presence of the predominant As(V) species is seen in both samples A and B via *in situ* (≈ 18 and $100 \mu\text{m}^2$) μ -XANES analyses. Simultaneous *in situ* μ -SXRF measurements showed that the As(V) was strongly associated with the regions where Ba, Ca, and Fe concentrations were elevated. Whereas the presence of As(II/III)-S species are suspected in the reduced sample A, As(III) is unlikely to be associated with sulfide in the oxidized sample B.

6.5.5 *In Situ* Bulk-EXAFS Analyses

Non-linear least-square fits of normalized k^3 -weighted EXAFS and FT spectra of the reference compounds and samples A and B are shown in Figure 6.8a and 6.8b. Fit parameters are summarized in Table 6.1. In the dussertite least-square fit (Figure 6.8b top), the first shell fit indicates four nearest oxygen neighbor oxygen atoms (i.e., As(V)-O), but the second shell ($\approx 2.65 \text{\AA}$ when corrected for phase shift) does not

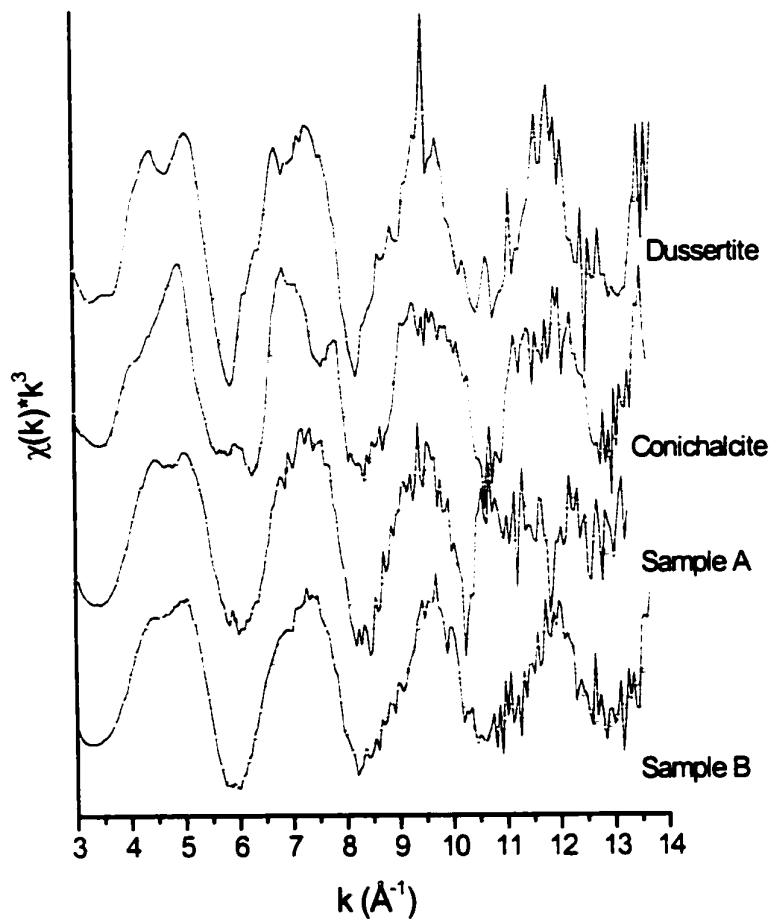


Figure 6.8a Non-linear least-square fits to normalized k^3 -weighted EXAFS spectra of the reference compounds and the sample A and B. Raw data and fits are shown in solid lines and open circles, respectively. See Table 1 and 2 for fit parameters.

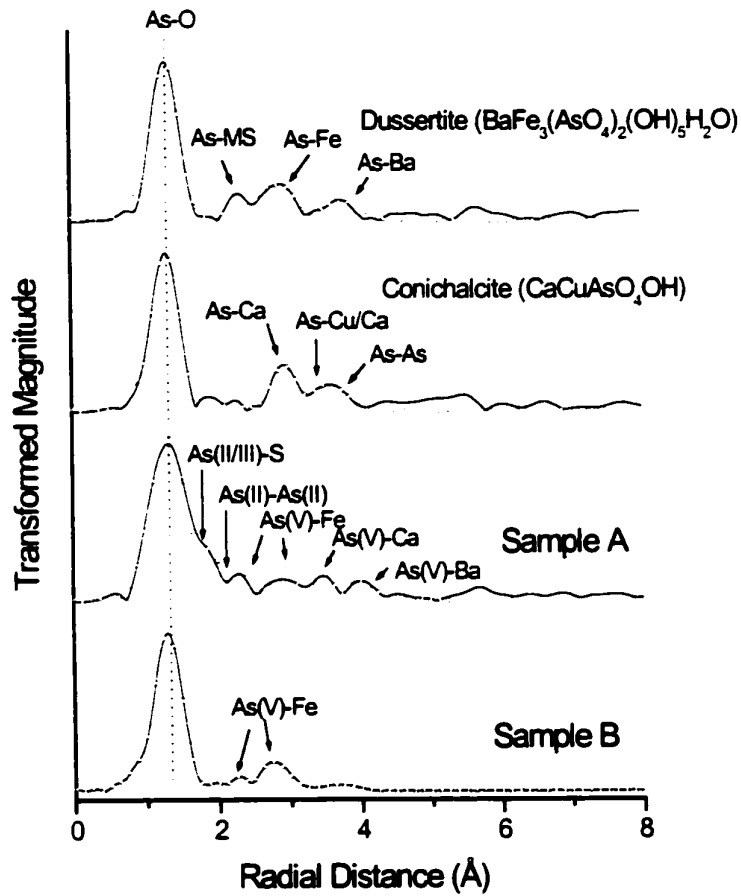


Figure 6.8b Non-linear least-square fits to Fourier transforms (FT) of the reference compounds and the sample A and B. Raw data and fits are shown in solid lines and open circles, respectively. See Table 1 and 2 for fit parameters.

Table 6.1 Structural parameters for dussertite and conichalcite derived from the best-fit results of EXAFS experimental data.

Sample	XRD/FEFF		Least-square fit			ΔE_0 (eV)
	N	R(Å)	N	R(Å)	$\sigma^2(\text{Å}^2)$	
Dussertite (BaFe ₃ AsO ₄)						
As-O	4	1.68	4*	1.70	0.002	2.55
As-MS	6	2.96	-----	-----	-----	-----
As-Fe	2	3.36	2*	3.30	0.001	-----
As-Ba	2	4.28	2*	4.09	0.007	-----
As-As	2	4.32	-----	-----	-----	-----
Conichalcite (CaCuAsO ₄)						
As-O	4	1.69	4*	1.70	0.002	3.16
As-Ca	2	3.19-3.27	2*	3.23	0.006	-----
As-Cu	4	3.42-3.55	4*	3.53	0.008	-----
As-Ca	3	3.63-3.76	-----	-----	-----	-----
As-As	1	3.99	1*	3.98	0.005	-----

*Assumed value fit, As-MS: multiple scattering paths

seem to correspond to As-Fe, As-Ba and As-As interatomic distances (3.36, 4.28, and 4.34 Å, respectively) generated from the FEFF/XRD calculation. Since the calculation indicates that six multiple scattering paths are present at ≈ 2.96 Å, it likely has risen from a multi-scattering effect. The rest of the two shells (As-Fe and As- Ba) were fit at 3.30 and 4.09 Å.

In the conicalcrite least-square fit (Figure 6.8a), the first shell (≈ 1.70 Å) also suggests a tetrahedral linkage between a As(V) atom and four oxygen atoms. The second and third shells were assemblages of three shells (As-Ca, As-Cu, and As-As) and they were fit at 3.23, 3.53, and 3.98 Å (Table 6.1). We attempted to fit conicalcrite with one more As-Ca at 3.63 Å as the XRD/FEFF calculation indicated (Table 6.1). However, a best fit was not obtained. Alternatively, we fit this second As-Ca distance by replacing the As-Cu contribution. The EXAFS fit resulted in a second As-Ca interatomic distance at 3.59 Å (Debye-Waller factor: 0.006), and the distances for the As-O, As-Ca, and As-As shells were the same as the previous fit with the As-Cu contribution.

Bulk EXAFS analyses on natural materials are difficult due to backscattering signals from multi-neighboring atoms and background iron fluorescence. In the case of As contaminated natural materials, the EXAFS analysis becomes more complex because of the presence of two oxidation states. Therefore the results from the XRD, chemical extraction, μ -SXRF maps, and bulk- and μ -XANES analyses were used to facilitate analysis of adsorption complexes and/or precipitates. In this section, radial distances are mainly discussed to elucidate the As solid state speciation rather than

comparing spectral features in k (\AA^{-1}) or R (\AA) space. Since the mixed As(III and V) phases are present in the samples, as evidenced from the XANES analyses, the spectral feature comparison between natural samples and reference materials or simulated EXAFS spectra cannot be strongly relied on to suggest As solid-state speciation.

In the oxidized sample B, As(V) with a fraction of As(III) species are considered for the first shell fit in the FT spectrum (Figure 6.8b bottom) based on the results of the bulk-XANES analyses (Figure 6.2a and 6.2b). Accordingly, we have attempted to fit both As(V)-O (1.69 \AA) and As(III)-O (1.77 \AA) distances (Arai et al., 2001; Manning et al., 1998), however only the As(V)-O interatomic distance (1.69 \AA) could be fit, indicating the predominant As(V) valence state in sample B. Next a two-shell fit (2.7 and 3.3 \AA when corrected for phase shift) was performed based on the results of XRD, chemical extraction and μ -SXRF analyses. We speculated that iron oxides, aluminum oxides and quartz were the major adsorbents, and Ba and Fe to be elements of interest. First, the interatomic distance for the As(V) bidentate binuclear configuration on aluminum oxides (As(V)-Al: 3.19 \AA) (Table 6.3) was used to fit either the second or third shell (2.7 and 3.3 \AA when corrected for phase shift). However, a best fit was not attainable even if the error for the As(V)-O distances (at most ± 0.05 \AA) (Foster et al., 1998; Ladeira et al., 2001) was considered. In similar fashion, we could not fit the bidentate binuclear configuration for an As(V) tetrahedron linkage on a silica tetrahedron (2.6 \AA) (Foster et al., 1998). Since quartz is a poor adsorbent for arsenate at near neutral pH (Xu et al., 1988), no As(V)

Table 6.2 Structural parameters for sample A and B derived from the best-fit results of EXAFS experimental data.

Sample A	N	R (Å)	σ^2 (Å ²)	ΔE_0 (eV)
As(V)-O	5.90	1.71	0.007	6.70
As(III/III)-S	2.71	2.25	0.0025*	
As(II)-As(II)	2.55	2.60	0.0075*	
As(V)-Fe	3.27	2.80	0.01*	
As(V)-Fe	1.81	3.35	0.01*	
As(V)-Ca	2.55	3.68	0.006*	
As(V)-Ba	2.72	4.26	0.007*	
Sample B				
As(V)-O	4.75	1.70	0.003	
As(V)-Fe	0.78	2.69	0.01*	
As(V)-Fe	3.20	3.28	0.01*	

Table 6.3 Reported structural parameters for As adsorption complexes on aluminum and iron oxides and orpiment from the best-fit results of EXAFS experimental data.

Sample	N	R (Å)	σ^2 (Å ²)	Reference
Orpiment, As ₂ S ₃				Foster et al. 1998
As(III)-S	3.0	2.28	0.004	
As(III)-As(III)	1.0	3.19	0.007	
As(III)-As(III)	3.0	3.54	0.012	
Realgar, AsS				Helz et al. 1995
As(II)-S	2.1	2.23	0.0025	
As(II)-As(II)	1.7	2.56	0.0075	
As(II)-As(II)	2.5	3.46	0.0045	
As(II)-S	1.0	3.59	0.021	
As(II)-As(II)	1.3	3.55	0.036	
Scorodite, FeAsO ₄ ·2H ₂ O				Foster et al. 1998
As(V)-O	6.4	1.68	0.003	
As(V)-Fe	4	3.36	0.004	
As(V)-As(V)	1	4.20	0.006	
As(V)-ferrihydrite (As/Fe: 0.001-0.1, pH 7.7, 1 wk)				Waychunas et al. 1993
As(V)-O	3.79	1.67	0.0035	
As(V)-Fe	2.02-3.03	3.26	0.0098	
As(V)-Fe	0.49-1.72	3.60-3.62	0.0098	
A(V)/Fe coprecipitate (As/Fe: 0.01-0.6, pH 8, 1 wk)				Waychunas et al. 1993
As(V)-O	4.70	1.66	0.0035	
As(V)-Fe	2.06-2.54	3.23-3.27	0.01	
As(V)-Fe	0.35-0.48	3.57-3.63	0.01	
As(V) on goethite				O'Reilly et al. 2001
As(V)-O	4.2-4.9	1.69-1.70	0.0015-0.0024	
As(V)-Fe	1.76-2.54	3.29-3.30	0.0028-0.0068	
As(V) on gibbsite				Foster et al. 1998 Ladeira et al. 2001
As(V)-O	4.1	1.68	0.0005-0.002	
As(V)-Al	1.3	3.19	0.0009-0.007	

adsorption complexes on quartz were expected. Third, the second and third shell distances (2.8-3.3 Å when corrected for phase shift) were both too short for the As-Ba distance (4.09 Å via EXAFS analyses) reported for the dussertite EXAFS fit (Table 6.1). Finally, two As-Fe distances seem to give the best fit for the second and third shells at 2.69 Å and 3.28 Å. Considering the error for the As(V)-Fe distance ($\pm 0.3\%$) reported by O'Reilly et al. (2001), the 3.28 Å interatomic distance corresponds well to the As(V) bidentate binuclear configuration on iron oxides (e.g., hematite). As the ammonium oxalate extraction indicated that sample B contains a large amount of oxalate extractable iron (0.16 wt %), ferrihydrite like precipitates are likely to be a predominant adsorbent. Waychunas et al. (1993) reported that the As(V)-Fe linkage at ≈ 3.25 Å distance was in both As(V) adsorption complexes on ferrihydrite and the As(V)/Fe coprecipitate phases (Table 6.3). Since both phases give an identical interatomic distance, the possibility for As(V)/Fe coprecipitate phases cannot be excluded. One of the second shells at 2.69 Å seems to be too short to be any As(V) adsorbed species and/or precipitates. Even though we were unable to fit the first shell with the As(III)-O distance, a fraction of As(III) species could be present in sample B as adsorbed and/or precipitate phases. A theoretically estimated As(III)-Al bidentate mononuclear configuration of 2.21-2.75 Å (Arai et al, 2001) and/or As(III) coordination with organic soil components are possible, however there is no clear explanation to support the FT feature at 2.69 Å. This may be simply due to the fitting difficulty in the overlapped first and second shells.

In the reduced sample A, we first considered fitting the first shell with two

distances (i.e., As(V)-O As(II/III)-S) (Figure 6.8b). The presence of As(V) and As(II/III)-S species are supported by not only the results of bulk- and μ -XANES analyses but also a wide first shell feature (at 0.8-2.2 Å, uncorrected for phase shift) in the FT spectrum (Figure 6.8b). The As(V)-O and As(II/III)-S interatomic distances (1.71 and 2.25 Å) were successfully fit in the first shell, and the fit results were in good agreement with the data reported by other researchers (Table 6.3). Considering As(II/III)-As(II/III) interatomic distance errors for realgar (AsS) and orpiment (As₂S₃) reported by Helz et al (± 0.03 Å, and ± 0.02 Å, respectively), it is possible that either As(II)-S or As(III)-S species are present. Since there was clear evidence for the presence of As(II/III)-S species, a As(II)-As(II) or As(III)-As(III) contributions must be considered at the 2.56 and 3.19 Å distances seen in the EXAFS analyses for orpiment and realgar (Table 6.3). A next four-shell (at 2.2-4.3 Å uncorrected for phase shift) fit was performed, based on the results of the bulk-XRD, chemical digestion/extraction, and μ -SXRF analyses. We speculated that iron oxides, aluminum oxides and quartz were major adsorbents, and Ba, Ca and Fe were elements of interest.

We were able to fit two As-Fe distances at 2.80 and 3.35 Å (Table 6.2). These two As(V)-Fe distances correspond to two different As(V) coordination environments (i.e., bidentate mononuclear and bidentate binuclear configurations). Interestingly, a As(II)-As(II) distance in realgar like mineral seems to provide best fit at 2.60 Å. This distance is slightly longer than the reported value (2.56 Å) in realgar via EXAFS analyses (Table 6.3), however it is within the error (± 0.002 Å) based on our

FEFF/XRD calculation and the EXAFS analyses by Helz and co-workers(1995). Helz and co-workers reported that crystalline realgar has a strong As(II)-As(II) contribution at 3.46 Å, but we were unable to fit this shell in our sample A spectrum (Figure 6.8b). This suggest that the structure of the As(II)-S realgar like mineral could be amorphous if present. Similar to the case in sample B, the As(V)-Al and As(V)-Si interatomic distances could not be fit in sample A, indicating the absence of As(V) adsorption complexes on the aluminum oxides and other phyllosilicate minerals.

The final two shells beyond 3.3 Å (corrected for phase shift) were considered with As(V)-cation interatomic distances. The As(V)-As(V) interatomic distance at 4.20 Å observed in scorodite is unlikely. Since the soil pH is near neutral pH, the presence of crystalline scorodite, which is stable at acidic conditions (Dove and Rimstidt, 1985), is thermodynamically unfavorable. Therefore the As(V)-Ca and As(V)-Ba interactions were mainly considered based on the results of μ -SXRF and XANES analyses which clearly showed a strong As(V) correlation with Ba and Ca. The As(V)-Ca distance in the conichalcite at 3.68 Å and the As(V)-Ba distance at 4.26 Å were successfully fit. The possible explanation for the presence of As(V)-Ba and -Ca shells may be the AsO₄-cation(s) ternary complexes on iron oxides and/or As(V) adsorption complexes on barite/gypsum surfaces and/or amorphous Ba/Ca coprecipitates with other anions (e.g., arsenate). Arsenate could be substituted into the structure of gypsum (CaSO₄) and/or barite (BaSO₄) that were identified via XRD and micropetrographic analyses (data not shown). Foster et al. (1998) previously reported that a FEFF generated model of arsenate substituted gypsum has As(V)-Ca distances

of ≈ 3.1 and ≈ 3.7 Å and the latter value seems to match with our As(V)-Ca interatomic distance of 3.68 Å.

6.6 Conclusion

In this study, As solid-state speciation (*i.e.*, oxidation state, adsorption complexes, and precipitates) was investigated using multi-scale spectroscopic techniques (*in situ* bulk- and μ - XANES and μ -SXRF, *ex situ* bulk- XRD) in subsurface samples of oxidized and reduced sites contaminated with As. Mixed valence states were present in both samples, but As(V) species seemed to predominate as evidenced from the bulk- and μ -XANES analyses. Simultaneous *in situ* μ -SXRF measurements showed that As(V) was elevated at regions where Ba and Fe concentrations were elevated, and Ca was also only associated with As(V) in the reduced sample A. Interestingly, a mixture of As(II/III and V) were present at regions where these cations were not elevated, and the absorption energy position of the reduced sample indicated the presence of As(II/III)-S species. The bulk EXAFS analyses showed that As(V) species are likely to be present as bidentate binuclear and monodentate binuclear surface complexes on amorphous iron oxyhydroxides in both samples. The reduced sample might also contain amorphous Ba/Ca/Fe-As(V) coprecipitates and/or As(V) sorption complexes on barite/gypsum and or Ba/Ca-As(V) ternary complexes on amorphous iron oxide surfaces, and amorphous realgar like precipitates may be controlling the solubility of As(II/III) in the adjacent ground water.

Detailed As speciation has future implication for assessing the environmental risk at contaminated sites with regards to the toxicity and bioavailability of As. Based on complex As solid state species suggested in this study, several suggestions can be made to facilitate selection of the environmental monitoring methods and/or remediation strategies with respect to As(III and V) species.

As_2S_3 and AsS like precipitates have relatively high solubility and are easily oxidized. Kim and co-workers (2000) reported that carbonation of arsenic sulfides minerals (e.g., realgar) is important As(II/III) dissolution processes in anaerobic conditions. The redox potential and alkalinity with respect to carbonate in the ground water might be important factors controlling dissolved As(III) species at the reduced site. Seasonal phosphate release could also become a serious concern for As(V) bioavailability because P is known to displace inner-sphere As(V) surface complexes on goethite surfaces regardless of aging time (O'Reilly et al., 2001). At both sites that were examined in this study, there were significant amounts of dissolved phosphorus ($\approx 1000 \text{ mg kg}^{-1}$) throughout the soil profiles. This suggests the instability in As(V) adsorption complexes on iron oxides which we proposed. Gao and co-workers (1997) reported that calcium arsenate could decrease the dissolved As(V) concentration at high pH as long as an excess amount of lime is available. However the instability of calcium arsenate phases was pointed out at $\text{pH} > 8$ where calcium carbonate can compete and precipitate out in open systems (Gao et al., 1997). This suggests that pH and dissolved Ca could be key parameters in predicting dissolved As(V), assuming $Ca_3(AsO_4)_2$ like precipitates are present.

Federal agencies currently use total ion concentrations in solid materials as a basis for metal/metalloid remediation decisions. Our findings (i.e., various As(II/III/V) solid-state species) showed that 1) the presence of various species which cannot be elucidated by total As levels and 2) the different mobility and bioavailability of these mixed species could have a significant impact on As levels in the groundwater with seasonal changes in geochemistry. The current environmental risk assessment with respect to the total As levels must be reevaluated to protect human and ecological health.

6.7 References

Amacher, M.C., 1996. Nickel, cadmium, and lead. In: D.L. Sparks (ed.), *Methods of soil analysis: Chemical methods, Part 3*. SSSA and ASA, Madison, WI, pp. 739-768.

Anderson, M.A., Ferguson, J.F. and Gavis, J., 1976. Arsenate adsorption on amorphous aluminum hydroxide. *Journal of Colloid and Interface Science*, 54: 391-399.

Arai, Y., Elzinga, E.J. and Sparks, D.L., 2001. X-ray absorption spectroscopic investigation of arsenite and arsenate adsorption at the aluminum oxide-water interface. *Journal of Colloid and Interface Science*, 235: 80-88.

Bertsch, P.M. and Hunter, D.B., 2001. Application of synchrotron-based X-ray microprobes. *Chemical Reviews*, 101: 1809-1842.

Dove, P.M. and Rimstidt, J.D., 1985. The solubility and stability of scorodite, $\text{FeAsO}_4 \cdot 2\text{H}_2\text{O}$. *American Mineralogist*, 70: 838-844.

Essington, M.E., 1988. Solubility of barium arsenate. *Soil Science Society of America Proceedings*, 52: 1566-1570.

Fendorf, S.E., Eick, M.J., Grossl, P. and Sparks, D.L., 1997. Arsenate and chromate retention mechanisms on goethite. 1. Surface structure. *Environmental Science and Technology*, 31(2): 315-320.

Foster, A.L., Brown Jr., G.E., Tingle, T.N. and Parks, G.A., 1998. Quantitative arsenic speciation in mine tailing using X-ray absorption spectroscopy. *American Mineralogist*, 83(5-6): 553-568.

Fuller, C.C., Davis, J.A. and Waychunas, G.A., 1993. Surface chemistry of ferrihydrite: Part 2. Kinetics of arsenate adsorption and coprecipitation. *Geochimica et Cosmochimica Acta*, 57: 2271-2282.

Gao, S., Tanji, K.K. and Goldberg, S., 1997. Session 1: Potentially toxic trace elements in soils and sediments Paper 4: Reactivity and transformation of arsenic. In *Agroecosystems: Sources, control, and remediation of oxyanions*. In: L.M. Dudley and J. Guitjens (eds.), *Symposium on sources, control, and remediation of oxyanions in agroecosystems*. Proc. Symp., Pacific Div., Am. Assoc. Adv. Sci., San Francisco.

Goldberg, S. and Glaubig, R.A., 1988. Anion sorption on a calcareous, montmorillonitic soil-arsenic. *Soil Science Society of America Journal*, 52: 1297-1300.

- Helz, G. R., Tossell, J. A., Charnock, J. M., Patrick, R. A., Vaughan, D. J., and Gardner, C. D. 1995. Oligomerization in As(III) sulfide solution: Theoretical constraints and spectroscopic evidence. *Geochimica et Cosmochimica Acta*, 59: 4591-4604.
- Jain, A., Raven, K.P. and Loppert, R.H., 1999. Arsenite and arsenate adsorption on ferrihydrite: surface charge reduction and net OH⁻ release stoichiometry. *Environmental Science and Technology*, 33: 1179-1184.
- Kim, M., Nriagu, J., and Haack, S. 2000. Carbonate ions and arsenic dissolution by groundwater. *Environmental Science and Technology*, 34: 3094-3100.
- La Force, M.J., Hansel, C.M. and Fendorf, S., 2000. Arsenic speciation, seasonal transformations, and co-distribution with iron in a mine waste-influenced palustrine emergent wetland. *Environmental Science and Technology*, 34: 3937-3943.
- Ladeira, A.C.Q., Ciminelli, V.S.T., Duarte, H.A., Alves, M.C.M. and Ramos, A.Y., 2001. Mechanism of anion retention from EXAFS and density functional calculation: Arsenic (V) adsorbed on gibbsite. *Geochimica et Cosmochimica Acta*, 65: 1211-1217.
- Loeppert, R.H. and Inskeep, W.O., 1996. Iron. In: D.L. Sparks (ed.), *Method of soil analysis, Part 3, Chemical methods*. Soil Science Society of America, Inc.

American Society of Agronomy, Inc., Madison, WI, pp. 649-650.

Lumsdon, D.G., Fraser, A.R., Russell, J.D. and Livesey, N.T., 1984. New infrared band assignments for the arsenate ion adsorbed on synthetic goethite (α -FeOOH). *Journal of Soil Science*. 35: 381-386.

Manning, B.A., Fendorf, S.E. and Goldberg, S., 1998. Surface structure and stability of arsenic(III) on goethite: Spectroscopic evidence for Inner-sphere complexes. *Environmental Science and Technology*, 32: 2383-2388.

Nelson, D.W. and Sommers, L.E., 1996. Total carbon, organic carbon, and organic matter. In: D.L. Sparks (ed.), *Methods of soil analysis: Chemical methods, Part 3*. SSSA and ASA, Madison, WI, pp. 961-1010.

O'Reilly, S.E., Strawn, D.G. and Sparks, D.L., 2001. Residence time effects on arsenate adsorption/desorption mechanisms on goethite. *Soil Science Society of America Journal*, 65(1): 67-77.

Qurashi, M.M. and Barnes, W.H., 1953. The space group of conichalcite. *American Mineralogists*, 38: 557-559.

Qurashi, M.M. and Barnes, W.H., 1954. The structure of the minerals of the Des-

Cloizite and Adelite groups. 1. Descloizite and conichalcite. *American Mineralogists*, 39: 416-435.

Raven, K.P., Jain, A. and Loeppert, R.H., 1998. Arsenite and arsenate adsorption on ferrihydrite: Kinetics, equilibrium, and adsorption envelopes. *Environmental Science and Technology*, 32: 344-349.

Rehr, J.J., Albers, R.C. and Zabinsky, S.I., 1992. High-order multiplescattering calculations of x-ray absorption fine structure. *Physical review letters*, 69: 3379-3400.

Ressler, T., 1997. Winxas: a program for X-ray absorption spectroscopy data analysis under MS-Windows. *Journal of Synchrotron Radiation*, 5: 118-122.

Sadiq, M., Zaidi, T.H. and Mian, A.A., 1983. Environmental behavior of arsenic in soils: Theoretical. *Water, Air, Soil Pollution*, 20: 1126-1130.

Savage, K.S., Tingle, T.N., O'Day, P.A., Waychuna, G.A. and Bird, D.K., 2000. Arsenic speciation in pyrite and secondary weathering phases, Mother Lode Gold District, Tuolumne county, California. *Applied Geochemistry*, 15: 1219-1244.

Szymanski, J.T., 1988. The Crystal-structure of Beudantite, $\text{Pb}(\text{Fe},\text{Al})_3 [(\text{As},\text{S})\text{O}_4]_2(\text{OH})_6$. *Canadian Mineralogist*, 26: 923-932.

Xu, H., Allard, B. and Grimvall, A.. 1988. Influence of pH and organic substance on the adsorption of As(V) on geologic materials. *Water, Air, and Soil Pollution*, 40: 293-305.

Chapter 7

SUMMARY AND CONCLUSIONS

There are major concerns about point/non-point pollution of arsenic(As) and phosphorus(P) in aquatic-terrestrial environments due to widely distributed indigenous sources and continuous anthropogenic inputs. Since soils and sediments act as finite and dynamic sinks for hazardous metalloids and nutrients, understanding oxyanion reactivity and speciation is critical to accurately predict their environmental fate. The research presented in this dissertation illustrates the application of novel *in situ* spectroscopic techniques in understanding the oxyanion surface speciation and reaction mechanisms in model and heterogeneous systems (i.e., soil components and soils, respectively). Arsenite, arsenate, and phosphate speciation and adsorption/desorption reactions at the metal oxide-water interface in soils were ascertained using a combination of macroscopic, microscopic and spectroscopic techniques as a function of various reaction conditions (i.e., pH, ionic strength, loading level, and reaction time). To elucidate kinetic reaction mechanisms, unique time resolved *in situ* spectroscopic techniques were used to monitor changes in molecular scale chemical speciation at the soil mineral-water interface. Furthermore,

novel *in situ* microfocused X-ray fluorescence and X-ray absorption spectroscopic techniques were applied to investigate arsenic solid-state speciation in natural materials. Identification of labile solid-state species could significantly enhance the development of more effective remediation strategies, risk assessment methods, and monitoring systems to reduce the negative impact of hazardous oxyanions in soil and water environments.

Short-term (≈ 24 h) equilibrium and kinetic studies, coupled with *in situ* spectroscopy showed that As (III and V) and P surface speciation and their reactivity at iron and aluminum oxide-water interfaces were influenced by pH, ionic strength, loading level, and reaction time. The equilibrium studies showed that phosphate and arsenate adsorption reactions on the metal oxide surfaces were similar. Adsorption decreased with increasing pH from 3 to 9 and was insensitive to changes in ionic strength. However, arsenite adsorption on bayerite was sensitive to ionic strength at $\text{pH} > 4.5$, and sorption increased up to $\text{pH} 4.5$ and gradually decreased from $\text{pH} 4.5$ to 9.0. *In situ* ATR-FTIR and XAS spectroscopic investigations and EM measurements, that indicated the formation of inner-sphere bidentate binuclear surface complexes via ligand exchange reactions, were the primary adsorption mechanisms for phosphate and arsenate on ferrihydrite and bayerite, respectively, but the presence of outer-sphere complexes were suggested in the case of As(III) adsorption on bayerite.

The study findings suggested that the reactivity of As (III and V) and P is significantly affected by reaction conditions, and that the valence state of As is an important factor influencing As chemical speciation (i.e., outer-sphere vs inner-sphere

complexes) and reactivity at the aluminum oxide-water interface. Subsequent studies on As(V) and P adsorption kinetics on bayerite and ferrihydrite, respectively, showed that the oxyanion uptake was initially fast, followed by slow reactions with increasing time. A novel time resolved ATR-FTIR and EXAFS spectroscopic investigation suggested that As(V) and P bidentate binuclear bonding environments were predominant regardless of residence time (1 h - 1 yr), however reversibility decreased with aging. Additional XANES analyses indicated that changes in the local chemical structure were occurring with aging. Surface transformations, such as a rearrangement of As(V)/P surface complexes and/or a conversion of surface complexes into aluminum arsenate-like precipitates on bayerite, could be important chemical factors responsible for the increased oxyanion irreversibility.

Overall results from the short-term equilibrium and kinetic model studies showed that reaction conditions (e.g., time, pH, and ionic strength) highly influenced As(III and V) and P reactivity (i.e., adsorption/desorption) and surface speciation at the metal oxides-water interfaces. These findings suggest that reaction conditions relevant to natural systems must be carefully considered in current environmental modeling programs for predicting the long-term fate and transport of these oxyanions and in selecting best remediation strategies and environmental monitoring methods. While these basic research findings, based on single adsorbate/adsorbent systems, provided significant insight into oxyanion retention/release mechanisms, difficulties still remain predicting the fate and transport of oxyanions in soils and sediments because natural systems typically contain more variables such as multi-adsorbents

(e.g., phyllosilicates and humic substances) and adsorbates (e.g., cations and organic ligands), resulting in the formation of complex co- and bulk- precipitates as well as adsorbed/chelated complexes. The latter are of great interest in understanding complex contaminant speciation in heterogeneous materials so that the rate-limiting factor (i.e., labile solid-state species) can be identified.

Taking further steps to expand our knowledge of more complex systems. arsenic speciation of subsurface landfill materials was investigated using novel microfocused *in situ* XRF, XANES spectroscopies, and bulk EXAFS spectroscopy. Mixed As solid-state speciation was indeed found in the landfill materials suggesting the presence of complex speciation and reaction dynamics in this real world system. While As(V) formed bidentate binuclear adsorption complexes on the amorphous iron oxide in the oxygenated system, As(V) adsorption complexes on iron oxides. AsO₄/SO₄ co-precipitates with Ba and Ca and/or AsO₄ adsorption complexes on barite and gypsum, and As(II/III)-sulfide species might co-exist in the reduced environment.

Unfortunately, complex chemical speciation that is present in inherently heterogeneous soils and sediments is generally neglected in current risk assessments (i.e., based on total chemical extraction/digestion analyses) used by environmental federal agencies. This raises serious concerns with regard to protecting environmental health because a small fraction of labile solid-state species could have a significant impact on contaminant mobility and bioavailability in soil-water environments. Further use of synchrotron based X-ray and other optical microscopic techniques to

understand molecular scale chemical speciation of contaminants in heterogeneous materials is recommended to aid in accurate current risk assessments. Molecular and atomic scale resolution information not only helps one to understand specific rate-limiting reaction mechanisms occurring in natural systems but also enable one to develop more precise chemical speciation and transport models that can predict contaminant fate and transport at the landscape scale. While these spectroscopic techniques can provide significant insights in studying contaminant speciation in heterogeneous materials, analytical limitations are often questioned by environmental scientists. Synchrotron based spectroscopic techniques generally require a long time for data acquisition and analysis for only a small number of samples. Therefore, statistical data with respect to contaminant distribution/speciation at the landscape scale is significantly lacking. Combined techniques can be suggested to compensate for limitations in traditional bulk chemical extraction/digestion and advanced molecular scale techniques. It is likely that total metal/metalloid levels based on current extraction procedures overestimate or underestimate contaminant bioavailability due to inaccurate data interpretation arising from complex contaminant species. Molecular scale techniques can be used for analyzing pre- and post-extracted reference mineral samples and/or series of contaminated soils and sediments to test the extractability of these methods, so that 1) different extraction procedures can be developed/recommended for specific soils (e.g., calcareous soils and limed land fill materials) and 2) additional safety factors can be considered for assessing environmental risks if any non-extractable phases are persistently present. In addition,

improved bulk extraction/digestion procedures can be effectively used to obtain statistical contaminant distribution data at the field scale and to screen samples for further spectroscopic studies to gain detailed knowledge on contaminant speciation. Continuous research efforts are needed using traditional and advanced techniques to better understand the fundamental chemistry of oxyanion speciation and reactivity in complex model systems as well as heterogeneous systems.